OCS Study
BOEM 2020-011

A Parametric Analysis and Sensitivity Study of the Acoustic Propagation for Renewable Energy

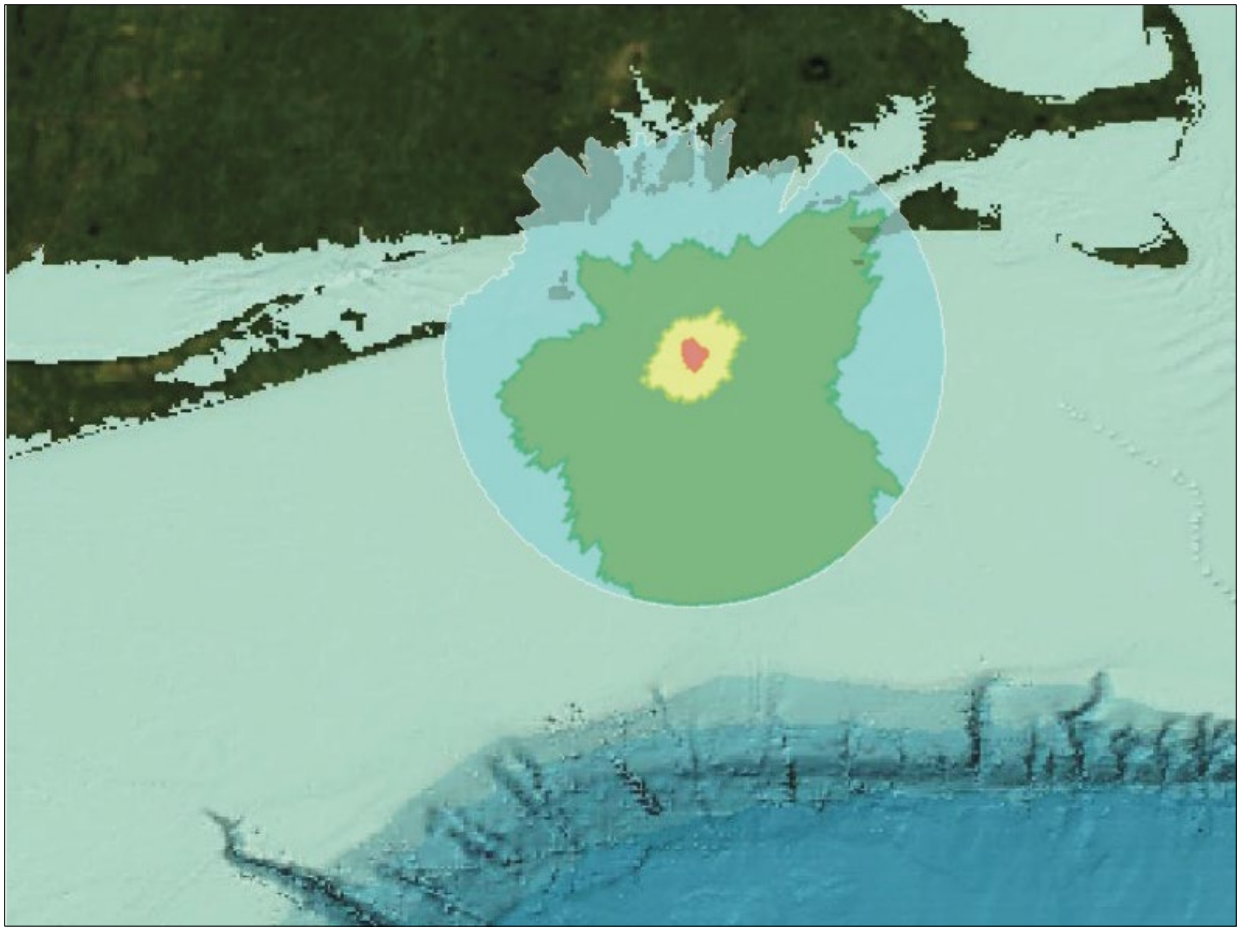

US Department of the Interior
Bureau of Ocean Energy Management
Office of Renewable Energy Programs

BOEM
Bureau of Ocean Energy Management

OCS Study
BOEM 2020-011

A Parametric Analysis and Sensitivity Study of the Acoustic Propagation for Renewable Energy Sources

10 February 2020

Authors:

Kevin D. Heaney, Michael A. Ainslie, Michele B. Halvorsen, Kerri D. Seger, Roel A.J. Müller, Marten J.J. Nijhof, Tristan Lippert

Prepared under BOEM Award M17PD00003

Submitted by:
CSA Ocean Sciences Inc.
8502 SW Kansas Avenue
Stuart, Florida 34997
Telephone: 772-219-3000

US Department of the Interior
Bureau of Ocean Energy Management
Office of Renewable Energy Programs

BOEM
Bureau of Ocean Energy Management

DISCLAIMER

Study concept, oversight, and funding were provided by the U.S. Department of the Interior, Bureau of Ocean Energy Management (BOEM), Environmental Studies Program, Washington, D.C., under Contract Number M15PC00011. This report has been technically reviewed by BOEM, and it has been approved for publication. The views and conclusions contained in this document are those of the authors and should not be interpreted as representing the opinions or policies of the U.S. Government, nor does mention of trade names or commercial products constitute endorsement or recommendation for use.

REPORT AVAILABILITY

To download a PDF file of this report, go to the U.S. Department of the Interior, Bureau of Ocean Energy Management Data and Information Systems webpage (http://www.boem.gov/Environmental-Studies-EnvData/), click on the link for the Environmental Studies Program Information System (ESPIS), and search on 2020-011. The report is also available at the National Technical Reports Library at https://ntrl.ntis.gov/NTRL/.

CITATION

Heaney KD, MA Ainslie, MB Halvorsen, KD Seger, RAJ Müller, MJJ Nijhof, T Lippert. 2020. A Parametric Analysis and Sensitivity Study of the Acoustic Propagation for Renewable Energy Sources. Sterling (VA): U.S. Department of the Interior, Bureau of Ocean Energy Management. Prepared by CSA Ocean Sciences Inc. OCS Study BOEM 2020-011. 165 p.

ABOUT THE COVER

Cover graphic by Kerri Seger and Kevin Heaney, based on Figure 6-22. Propagation modeling performed by Peregrine software of Applied Ocean Sciences, LLC. Plotting performed through Jupyter notebooks with Python environment in Miniconda 4.7.10.

ACKNOWLEDGMENTS

We thank Dr. Stephan Lippert (Hamburg University of Technology) for providing data from the 2014 COMPILE workshop (Lippert et al., 2016). We thank Dr. Martine Graafland (Directorate-General for Public Works and Water Management) for permission to use the TNO report TNO 2016 R11338 (Binnerts et al., 2016) describing a validation study for the Gemini and Luchterduinen wind farms. We thank Dr. Luuk Folkerts (Ecofys) and Dr. Sytske van den Akker (ENECO) for permission to use data from the Gemini and Luchterduinen wind farms. We thank the CSA document production team for their attention to fine details.

Contents

List of Figures

List of Tables

List of Acronyms, Symbols, and Abbreviations

10logR	cylindrical spreading
20logR	spherical spreading
2D	two dimensional
µPa	micropascal
τ_{90}	90% energy signal duration
τ_{eff}	effective signal duration
ϕ	phi (grain size)
AOS	Applied Ocean Sciences, LLC
BO1	BARD Offshore 1 wind farm (German)
BOEM	Bureau of Ocean Energy Management
BR1	Borkum Riffgrund 1 wind farm (German)
Caltrans	California Department of Transportation
CASS/GRAB	comprehensive acoustic simulation system/gaussian ray bundle
CDF	cumulative density function
CMST	Curtin University (Australia), Centre for Marine Science and Technology
COMPILE	a portmanteau combining computation, comparison, and pile
CSA	CSA Ocean Sciences Inc.
dB	decibel
DCS	damped cylindrical spreading
ECMWF	European Commission Medium Weather Forecast
EMODnet	European Marine Observation and Data Network
EUSeaMap	EMODnet broadband seabed habitat map (for Europe)
f	frequency
faSEL	frequency-accumulated sound exposure level
FD	finite difference
FE	finite element
FHWG	Fisheries Hydroacoustic Working Group
$g(t)$	forcing function
GARFO	Greater Atlantic Regional Fisheries Office
GEBCO	general bathymetric chart of the oceans
GFS	global forecasting system
GT1	Global Tech I wind farm (German)
HF	high frequency
Hz	hertz
IEC	International Electrotechnical Commission
IFFT	inverse fast Fourier transform
ISO	International Organization for Standardization
ITAP	Institut für technische und angewandte Physik
JASCO	Jasco Applied Sciences
kHz	kilohertz
km	kilometer
LF	low-frequency

L_E	sound exposure level
$L_{E,12\mathrm{h}}$	cumulative 12-hour sound exposure level
$L_{E,\mathrm{ss}}$	single-strike sound exposure level
$L_{E,\mathrm{w}}$	weighted sound exposure level
$L_{E,\mathrm{w},24\mathrm{h}}$	broadband weighted sound exposure level cumulated for 24 hours
L_p	sound pressure level
$L_{p,90\%}$	90% root-mean-square sound pressure level
$L_{p,\mathrm{eff}}$	effective sound pressure level
$L_{p,\mathrm{pk}}$	zero to peak sound pressure level
$L_{p,\mathrm{pk-pk}}$	peak to peak sound pressure level
$L_{p,\mathrm{rms}}$	root-mean-square sound pressure level
L_{pk}	peak sound pressure level
m	meter
MF	mid frequency
MMPA	Marine Mammal Protection Act
MN	meganewton
MP	measurement position
MSP	mean-square sound pressure
NCEI	NOAA's National Centers for Environmental Information
NCOM	US Navy Coastal Ocean Model
$N_{24\mathrm{h}}$	Number of pile strikes in a 24-hour period
NM	normal mode
NMFS	National Marine Fisheries Service
NOAA	National Oceanic and Atmospheric Administration
Np	neper
NPL	National Physical Laboratory (United Kingdom)
$p(t)$	sound pressure time series
PDF	probability density function
PE	parabolic equation
PL	propagation loss
PML	perfectly matched layer
PSLM	practical spreading loss model
PTS	permanent (hearing) threshold shift
RAM	range-dependent acoustic model
re	with reference to
rms	root-mean-square
s	second
SEL	sound exposure level
$SEL_{\#n}$	cumulative sound exposure level caused by n pile strikes
SEL_{12h}	12-hour sound exposure level
SEL_{ss}	single-strike sound exposure level
SEL_{w}	weighted sound exposure level
$SEL_{w,24h}$	broadband weighted sound exposure level cumulated for 24 hours
SL	source level

SNU	Seoul National University (South Korea)
SOFAR	sound fixing and ranging
SPL	sound pressure level
SSP	sound speed profile
TL	transmission loss
TNO	Netherlands Organisation for Applied Scientific Research (Nederlandse Organisatie voor Toegepast Natuurwetenschappelijk Onderzoek)
TTS	temporary (hearing) threshold shift
TUHH	Hamburg University of Technology (Germany)
U.S.	United States
UoS	University of Southampton (United Kingdom)
USGS	US Geological Survey
WOA	World Ocean Atlas
WTD71	Bundeswehr Technical Centre for Ships and Naval Weapons (Germany)

Extended Abstract

As countries explore renewable energy opportunities, offshore wind farms are being developed along coastlines. To construct these wind farms, piles are driven into the seafloor as foundational structures for the turbines. Pile driving involves risk of noise pollution that can affect marine fauna. To mitigate these risks, risk assessments and permits are required and are based on the best oceanographic understanding and acoustic modeling available at the time of the permitting process. This project aims to facilitate improved risk prediction by recommending the most efficient acoustic models and ranking the most influential environmental parameters at two representative sites.

Many underwater sound sources, like sonar transmitters, appear point-like from a distance when they have a maximum dimension that is small enough. That is, they radiate sound in all directions into their far field, where sound propagates spherically away from the source, as if it originated from a point. Even large sources (e.g., ships, airgun arrays) have this far-field property because the ocean is deeper than the wavelengths these sources emit. If the water is deep enough, it is possible to get far enough away from these sources for them to behave as if they were point sources—the basic requirement for a far field. A sound source with this salient property of having a far field can be characterized in terms of its source level (SL). The SL typically is obtained from the far-field sound pressure level (SPL, i.e., L_p) and is scaled depending on the propagation pathway and distance the sound travels from the source to the receiving location. When the SL value is derived based on spherical spreading, only the distance in which the sound travels to the far field is needed (not the direction).

Pile driving involves a source (the monopile) that extends from the surface to the seafloor and into the sediment. Being a large, cylindrical source in shallow water, the requirement for attaining a far field will never be met. There is no position anywhere in the water column to which the sound arrives after some propagation loss (PL) as if from a point source. This means that a pile driver does not have a SL, which also means that traditional methods of calculating the SPL using the sonar equation (SPL = SL - PL) cannot be applied.

Methods

To address the issue of a pile not having an SL, the quantitative characterization of the sound field radiated by the pile needs to be estimated in some other way. The method applied in this project is to simulate the sound field around the source (up to a 5 m distance from the pile axis of symmetry) using a specialized finite element (FE) model of the hammer, pile, and surrounding media (air, water, and sediment). For this project, such an FE model was created, and its field computationally propagated to assumed receiver positions at least 60 km from the pile using a parabolic equation (PE) model. The sea surface was assumed to be perfectly smooth. This procedure provided the sound pressure time series as a function of receiver position. Each time series was then processed for the metrics root-mean-square sound pressure level ($L_{p,\mathrm{rms}}$), peak sound pressure level ($L_{p,\mathrm{pk}}$), and single strike sound exposure level ($L_{E,ss}$).

The complexity of the FE and PE resulted in a practical upper frequency limit for application to the pile-driving problem of approximately 2 kHz. Although most of the acoustic energy radiated by pile driving is in the range of 100 to 200 Hz, the relatively weak contribution in the 2 to 20 kHz band creates a potential risk to some marine fauna, especially mid-frequency (MF) and high-frequency (HF) cetaceans.

Therefore, frequencies above 2 kHz were accounted for by weighting the strength of sounds according to their frequency and the available weighting functions for animal groups. This was achieved by extrapolating the field at 2 kHz to higher frequencies using a frequency-dependent scaling of the volume attenuation within the PE. This procedure was followed to calculate the weighted sound exposure level ($L_{E,\mathrm{w}}$), using weighting functions published by the National Marine Fisheries Service. Cumulative sound exposure level ($L_{E,\mathrm{cum}}$) (weighted or unweighted) was calculated from $L_{E,\mathrm{w}}$ by assuming 3,500 identical hammer strikes in 24 hours for a stationary receiver (animal).

Model sensitivity to environmental parameters was evaluated across season, site, bearing, and grain size. These parameters were proxies for sound speed profile (SSP), water column depth, range-dependent bathymetry, and sediment type variation, respectively. The validated model was used to compute the sound pressure time series and subsequent L_E, $L_{p,\mathrm{pk}}$, and $L_{p,\mathrm{rms}}$ metrics, and to investigate the overall impact on modeling predictions from varying environmental parameters. Impact volumes were then computed based on acoustic thresholds for various marine faunal groups and compared across environmental variables.

Results

As proxies for water depth and oceanography, two sites off the United States Atlantic Coast, Rhode Island (RIsland)and Virginia Beach (VAbeach), were chosen for modeling. The environmental variable with the greatest impact on acoustic propagation, and thereby on impact volume, was site. Although site was intended as a proxy for water column depth, the sites also differed by distance to shore and had unique bathymetries. RIsland was closer to land and deeper than VAbeach, leading to differences of 40 dB at ranges beyond 20 km. Changes in sediment type exerted the next largest influence on impact volume. Hard sediments reflect sound more than soft sediments, leading to larger impact volumes over harder sediments. The environmental driver with comparatively less impact was season (the proxy for SSP), with better propagation in winter than in summer, which led to higher received levels at all ranges and, therefore, larger impact volumes in winter. Summer impact volumes were smaller because warm surface waters lead to increased refraction towards the seafloor and thus more absorption of sound into the seafloor.

There was substantial variability in the impact volumes. Marine mammal impact volumes were as small as 0.0001 km^3 (permanent threshold shift [PTS] in MF cetaceans; **Table 6-1**) and as large as 218 km^3 (temporary threshold shift [TTS] for 24-hour exposure in low-frequency [LF] cetaceans; **Table 6-3**). In fishes, with application of the Greater Atlantic Regional Fisheries Office (2016) criteria, impact volumes varied between 17 km^3 (injury, large fish; **Table 6-9**) and 221 km^3 (behavior, any fish; **Table 6-11**). For comparison, application of the Popper et al. (2014) guidelines resulted in volumes between 0.04 km^3 (recoverable injury, fishes with no swim bladder; **Table 6-6**) and 127 km^3 (TTS, fishes with a swim bladder involved in hearing; **Table 6-8**). On average for fishes with and without a swim bladder, the calculated impact volumes for injury based on the criteria of Stadler and Woodbury (2009) (**Table 6-9**) were 30x and 1,600x larger than for recoverable injury based on the criteria of Popper et al. (2014) (**Table 6-6**), respectively. In sea turtles, the impact volume spread was between 0.5 km^3 (physiological; **Table 6-12**) and 25 km^3 (behavior; **Table 6-12**).

Recommendations

The following suggestions about the important features of the project results provide guidance for future projects modeling pile driving in the coastal ocean. A very specific starter field based on a pile size and forcing function, among other parameters, was used for this project and this starter field may not apply to future modeling efforts. However, the results from this project provide the basis for recommendations on the degree of difference between two sites that is needed for additional modeling efforts to be desirable. The environmental aspects that were considered include water depth, season, latitude along the U. S. Atlantic Coast, sediment type, bathymetry, and distance from shore. Each of these aspects must be considered when deciding how much one pile-driving site's model can represent other sites.

Most pile-driving sites will not occur in water deeper than 50 m, but variation in sound propagation exists across water columns from 0 to 50 m deep. For identical propagation conditions a change of 50% in water depth should change the impact volume by 50%. Therefore, it is recommended that pile-driving sites that differ by 50% deeper or shallower (e.g., 5, 7, 11, 16, 23, 34, or 50 m deep) should be modeled separately and those results can be extrapolated to the depths between.

The extremes of SSPs that exist between Virginia and Rhode Island during opposite seasons were represented in the models, but seasonality may be more pronounced farther north and less pronounced farther south. Therefore, models should be run for the month of a proposed pile driving to adequately capture the most likely SSP for that site.

Pile driving likely will occur in areas where the seafloor is mud or soft sand instead of rocky, and the models in this project incorporated the span of these grain sizes. Uniform sediment type over the extent of the modeled environment was assumed. To address this model assumption in the future, three potential recommendations are made. If no new high-resolution sediment data are available and a uniform sediment type needs to be assumed, then (1) new models should be run when grain size (in "phi" ϕ units) differs between piles by 1 ϕ, or (2) incorporate Monte Carlo simulations of grain size into the model(s). If new or higher-resolution data on sediment type are available for a site, then run new models using the known ϕ values at each range step.

Distance from shore can drastically alter impact volumes. Sites that shallow quickly at one or more bearings will have smaller impact volumes than sites where bearings either follow the same isobath or get deeper. When water depth increases, it enables sound to propagate farther. The 30 km difference in distance to shore between the two sites (VAbeach's closest distance to shore was 56 km while RIsland's was 26 km) could also have contributed to the impact volumes of VAbeach being 2 to 3 times larger than those at RIsland. This would suggest that two sites whose closest distances to shore are 15 km different, could have impact volumes different by 1 to 1.5 times each other. Therefore, sites that have distances at least 15 km farther or closer from shore than this study's sites (i.e., closest distances of 11, 41, 71, 86 km etc. to shore) should be re-evaluated to understand the specific bathymetrical effect on propagation.

In general, if a pile site differs by more than 50% in depth, more than 1 ϕ in grain size, may be installed during different seasons, or at intervals of 15 km farther away or closer to shore, then new models should be generated during the month of proposed activity to understand how sound may travel through the environment.

1 Introduction

1.1 Background

Environmental compliance documents are prepared for offshore renewable energy projects located throughout federal waters of the United States (U.S.) Outer Continental Shelf. Preparation and analysis of acoustic fields for these documents are conducted by numerous contractors who often use different models, databases, and approaches, resulting in varying estimations of predicted acoustic fields produced by renewable energy activities. This variability makes it difficult to determine if the calculations were overly conservative, and if so, to what degree. Overly conservative calculations could unnecessarily restrict a proposed activity.

Activities performed during renewable energy projects have common noise sources and occur in similar environmental conditions. Some commonalities include limited: (1) numbers of sources (e.g., pile driving for a meteorological tower, wind turbine, or servicing platform); (2) range of pile diameters and hammer energies; (3) locations (typically on the continental shelf, in waters <50 m deep with similar acoustic propagation modes); (4) substrate types (e.g., sand, gravel, rock areas) with relatively strong acoustic reflection characteristics; and (5) oceanographic conditions (e.g., low sea states or wind speeds) within which the activity can be completed.

Modern acoustic propagation models make generalized assumptions that are partially inapplicable to pile driving. The main assumption that does not hold is that a far field exists for pile driving. For a far field to exist, there must be a region far enough from a source that the sound spreads spherically, therefore appearing to radiate from a single point. The non-existence of a far field for pile driving means that the concept of source level (SL) is undefined, which in turn means the concept of propagation loss (PL) is undefined, making widely used models such as the range-dependent acoustic model (RAM) or SCOOTER inapplicable unless the model is coupled to a known starting field close to the pile. The approach using a known starter field was applied first by Reinhall and Dahl (2011), who constructed a field close to the source by treating it as a compound source with a vertical array of phase-delayed monopoles. It was applied later by Zampolli et al. (2013), who used a finite element (FE) model of the hammer and pile to generate the starter field. The main point is that the concepts of SL and PL only exist for a source if that source has a far field. A pile driver has no far field, and therefore no SL or PL (Ainslie et al., 2012).

1.1.1 Project Team

The project team comprised Dr. Michele Halvorsen (Project Manager, CSA Ocean Sciences Inc. [CSA]), Dr. Kevin Heaney (Lead Principle Investigator, formerly OASIS, currently Applied Ocean Sciences, LLC [AOS]), Dr. Kerri Seger (AOS), Dr. Michael Ainslie (formerly Netherlands Organisation for Applied Scientific Research [TNO], currently Jasco Applied Sciences [JASCO]), Dr. Marten Nijhof (TNO), and Dr. Roel Müller (TNO). Dr. Tristan Lippert (AqustiX) contributed by providing advice and regression analyses. The core expertise is provided by Drs. Halvorsen, Heaney, and Ainslie, all three of whom have previously worked together successfully on projects and proposals. Dr. Halvorsen is an experienced Project Manager who understands the U.S. regulatory requirements for environmental impact statement (EIS)-related projects, is familiar with the peer-reviewed scientific literature leading to the regulatory

requirements (e.g., National Oceanic and Atmospheric Administration [NOAA], California Department of Transportation [Caltrans]), and has contributed extensively to that literature. Dr. Heaney regularly provides acoustic propagation expertise to customers such as the U.S. Navy, the Preparatory Commission for the Comprehensive Nuclear-Test-Ban Treaty Organization, and the Bureau of Ocean Energy Management. Dr. Seger is a biological acoustician trained in soundscape mapping and cetacean response to anthropogenic noise with experience in recording and analyzing baseline acoustic conditions along coastlines of multiple continents to compare to subsequent environmental states. Dr. Ainslie is a founding member of the expert group that advises European Union (EU) member states on the implementation of the EU's Marine Strategy Framework Directive and works with international colleagues on solving propagation issues associated with sound radiated by percussively driven piles. Notably, he is the originator of the damped cylindrical spreading rule described by Zampolli et al. (2013) and validated by Lippert et al. (2018). Dr. Nijhof developed a state-of-the-art FE source model for a hammer-driven pile, coupled this FE model to a normal mode (NM) program to enable computation of the sound field at long range from the pile, and demonstrated the model's accuracy by verification at an international pile-driving modeling workshop (co-organized by Dr. Nijhof himself) and by validation against pile-driving measurements in the North Sea. Drs. Ainslie, Müller, and Nijhof have worked together on a series of projects for the Netherlands Government involving the development, testing, and validation of a modeling capability to predict the sound radiated by pile driving in the context of North Sea wind farm development.

1.1.2 Project Scope, Objectives, and Framework

The objective of this project was to improve understanding of shallow-water acoustic propagation characteristics and the sound field created by activities associated with the construction of renewable energy facilities as well as understanding of the potential risk to marine fauna. This involved specifically addressing pile-driving sources and predicting effects on marine life from the sound radiated by these activities.

A technical analysis of acoustic propagation modeling of pile driving for wind turbine installations on the U.S. Atlantic continental shelf was performed to (1) provide recommendations for a consistent underwater acoustic modeling approach across renewable energy projects, including recommendations for models, databases, and methodologies that address pile driving; (2) provide a baseline range of expected modeling results, including impact volumes around typical sources; (3) identify a baseline of variability for acoustic modeling results based on ranges of critical environmental input parameters; (4) perform a sensitivity study of critical environmental parameter influences; and (5) validate and apply the damped cylindrical spreading method, including its implementation in the form of an Excel spreadsheet. Data from wind farm construction and other measured-at-sea sources were used to validate the recommended modeling approach.

Confusion arises from inconsistent use of underwater acoustical terminology (see Ainslie, 2015; Hawkins et al., 2015; National Marine Fisheries Services [NMFS], 2018a,b). To minimize the risk of such confusion in this report, and more generally throughout this project, the project will follow the International Organization for Standardization (ISO) 18405:2017 "Underwater Acoustics – Terminology" standard (ISO, 2017).

This report has many mathematical formulas and complex analyses; therefore, to avoid confusion of acoustic terms, the mathematical symbols are used instead of the abbreviations usually seen in text (**Table 1-1**; **Appendix A**).

Table 1-1. Acoustic metrics

Symbol	Abbreviation	Metric Name	Units
L_E	SEL	Sound exposure level	dB re 1 µPa^2 s
$L_{E,12\mathrm{h}}$	SEL_{12h}	Cumulative 12-hour sound exposure level	dB re 1 µPa^2 s
$L_{E,\mathrm{ss}}$	SEL_{ss}	Single-strike sound exposure level	dB re 1 µPa^2 s
$L_{E,\mathrm{w}}$	SEL_{w}	Weighted sound exposure level	dB re 1 µPa^2 s
$L_{E,\mathrm{w},24\mathrm{h}}$	$\mathrm{SEL}_{w,24h}$	Broadband weighted, cumulative 24-hour sound exposure level	dB re 1 µPa^2 s
$L_{p,\mathrm{pk}}$	SPL_{pk}	Peak sound pressure level	dB re 1 µPa
$L_{p,\mathrm{pk-pk}}$	$\mathrm{SPL}_{pk\text{-}pk}$	Peak to peak sound pressure level	dB re 1 µPa
$L_{p,\mathrm{rms}}$	SPL_{rms}	Root-mean-square sound pressure level	dB re 1 µPa
$L_{p,\mathrm{eff}}$	L_{eff}	Effective sound pressure level	dB re 1 µPa
$L_{p,90\%}$	L_{90}	90% energy sound pressure level	dB re 1 µPa

µPa = micropascal; dB = decibel; L = level; L_p = sound pressure level; re = with reference to.

1.1.3 Technical Foundation

The sound field radiated by complicated sources (e.g., a driven pile), in principle, can be computed by summing the contributions of multiple point sources distributed around the source's acoustically active surface. However, doing so requires knowledge of the SL of each individual point source. The challenge lies in how to obtain values for these individual point source SLs, which remains an open research question, especially for impact pile driving. An alternative approach (e.g., Zampolli et al., 2013) is to sidestep the uncertainty of SLs and instead calculate the acoustic field radiated from the pile by constructing an FE model of the source combined with a given forcing function (i.e., the time-dependent force imparted by the hammer). Research on this alternative approach is ongoing, and the best method for computing a nearby sound field has yet to be determined. This uncertainty led to an international workshop, called COMPILE, in June 2014, organized by the Hamburg University of Technology (TUHH) and the TNO. One of the key findings of the COMPILE workshop was a comparison that led to increased confidence in modeling techniques for impact-driven piles (Lippert et al., 2016), including the FE source model used in this project (Zampolli et al., 2013).

The output of an FE source model is a representation of the acoustic field at a small distance (i.e., a few centimeters or meters) from the pile, within the near field of the source. This acoustic near field can be coupled to an acoustic propagation model without knowledge of the SL, but it requires an interface be developed between the FE source model and the acoustic propagation model. The construction of a pile model is labor intensive, and consequently, FE model predictions were produced and processed for a single pile only, with the sensitivity assessed by considering variants around that single pile.

The Mach cone, a conical wave radiated by a compressional wave traveling down the pile wall (as explained further in **Section 1.4**), propagates out to approximately 10 kilometers (km), depending on water depth, after which it is replaced by some other contribution, the nature of which is an open research question. Measurements of the sound exposure level (SEL, i.e., L_E) at close range (approximately 10 m) can be used to estimate the total acoustic energy put into the water. However, an extrapolation of range from this measurement, via the 15logR rule described below (NMFS, 2018b), or some other propagation model, is difficult because most models assume a point source. The concept of a point source is incompatible with the presence of a Mach cone. One of the goals of this project is to develop a clear understanding of the range-evolution of the Mach cone within the first few kilometers of the source. In the region dominated by the Mach cone, propagation follows a modified (exponentially damped) version of the cylindrical spreading rule, referred to as damped cylindrical spreading (DCS) (**Section 3**). In the DCS region, the acoustic field varies as defined by **Equation 1.1** (Zampolli et al., 2013; Lippert et al., 2018):

$$L(r) = L(r_1) - 10\log_{10}\frac{r}{r_1}\ \mathrm{dB} - \alpha(r - r_1) \qquad \textit{Equation 1.1}$$

where:

$L(r) =$ sound exposure level at distance r
$L(r_1) =$ sound exposure level at distance r_1
$\alpha =$ attenuation coefficient
$\mathrm{dB} =$ decibel.

The following is a brief discussion regarding two equations currently used by regulatory agencies to assess disturbance to marine mammals and fish. A NMFS memo issued in January 2012 (NMFS, 2012a) provided guidance for evaluating the effects of pile driving on marine mammals under the Marine Mammal Protection Act (MMPA). The memo provided risk thresholds of the root-mean-square sound pressure level ($L_{p,\mathrm{rms}}$) for disturbance and injury and advised how to extrapolate a measurement made at distance r_1 of an acoustic received level $L(r_1)$ to that at some other distance r. Specifically, NMFS (2012a) advised the use of **Equation 1.2**:

$$L(r) = L(r_1) - 15\log_{10}\frac{r}{r_1}\mathrm{dB}, \qquad \textit{Equation 1.2}$$

to estimate the received level $L(r)$ at distance *r*. This formula (**Equation 1.2**), henceforth referred to as the 15logR rule, was made available in the form of an Excel spreadsheet by NMFS (2012b). Since publication of NMFS (2012a), NMFS (2018a) prepared comprehensive guidelines for marine mammals in the form of dual risk thresholds of the peak sound pressure level ($L_{p,\mathrm{pk}}$) and L_E.

For fish, potential adverse effects are addressed via protective measures (for listed species and Essential Fish Habitat) included in the Endangered Species Act and Magnuson-Stevens Fishery Conservation and Management Act. Acoustic impacts initially were covered by an "Agreement in Principle" published by the Fisheries Hydroacoustic Working Group (FHWG, 2008), which suggested risk thresholds for L_E and $L_{p,\mathrm{pk}}$. Little or no scientific research had been published at that time on the effects of pile driving on fish, and the "Agreement in Principle" was precautionary.

A comprehensive set of guidelines for fishes and sea turtles subsequently was published by Popper et al. (2014). Based on the pioneering research of Halvorsen and her colleagues (Halvorsen et al., 2011, 2012a,b; Casper et al., 2012, 2013), the Popper et al. (2014) guidelines recommended L_E risk thresholds for fish that were between 16 and 33 dB higher than those of the FHWG (2008). Subsequently, a report published by Caltrans (2015) acknowledged the Popper et al. (2014) guidelines, but did not adopt the recommendations, advising instead to continue using the precautionary risk thresholds from the FHWG (2008).

The Caltrans (2015) report further recommended use of **Equation 1.3**:

$$L(r) = L(r_1) - F \log_{10} \frac{r}{r_1} \text{ dB}, \qquad \textit{Equation 1.3}$$

where F is a "site-specific (sound) attenuation factor based on several conditions, including water depth, pile type, pile length, substrate type, and other factors" (Caltrans, 2015). **Equation 1.2** commonly is used with r_1 = 10 m to calculate $L(r)$ at distances r >10 m, but the absence of an attenuation term (αr) limits its applicability to interpolation between measured data points. Predictions based on extrapolation (outside the region between measurement points on which interpolation is based) are prone to error.

To summarize, use of the 15logR rule (**Equation 1.2**), or the site-specific version (**Equation 1.3**), for transmission loss (TL) leads to errors in acoustic predictions for sound radiation from impulsive pile-driving activities because these equations do not account for the exponential decay of the Mach cone arising from multiple seafloor reflections. For impulsive pile driving, to avoid error in propagation predictions caused by the influence of the Mach cone, it is recommended to first compute the immediate near field using an FE source model for the pile, and then propagate the predicted near field (i.e., starter field) to long range using a suitable propagation model.

1.2 Overview of Acoustic Propagation Models

1.2.1 State-of-the-art Underwater Acoustic Models

Most modeling is used to predict the propagation of sound energy, sound intensity, or sound pressure. The appropriateness of different propagation modeling solutions is determined largely by three general characteristics of the source and propagation medium: (1) frequency characteristics of the source output; (2) environmental dependence (e.g., range-dependent bathymetry, seafloor type, sound speed) of the propagation region; and (3) water depth. Propagation environments generally are categorized as either range-independent, for which the input parameters are constant with propagation range, or range-dependent, for which any of the environmental parameters (e.g., water depth, sound speed) vary with distance from the source. The most suitable propagation model can be selected given a particular frequency band and environment.

A variety of models are available; some are free to download and others are publicly available. State-of-the-art models are archived and distributed by the Ocean Acoustics Library (http://hlsresearch.com/oalib). These state-of-the-art models are complex and require an experienced user in order to generate reasonable results.

Available propagation models were categorized according to their underlying computational solution approach. The following model groups capture the most common methods:

- Ray tracing;
- Normal mode (NM);
- Parabolic equation (PE);
- Wavenumber integration;
- Energy flux; and
- Finite difference (FD)/FE (least common).

Ray Tracing Models

Ray tracing models are efficient and address range-dependent environments but are high-frequency (HF) approximations to the wave equation, requiring special attention to properly address sediment propagation, focusing (of the acoustic signal), and wave diffraction (Tindle, 1983; Westwood and Tindle, 1987). The most popular ray tracing model is BELLHOP, developed by Porter (2011). The U.S. Navy standard model is the Comprehensive Acoustic Simulation System/Gaussian Ray Bundle (CASS/GRAB).

Normal Mode Models

NM models compute a solution to the range-independent wave equation, providing local NMs in the vertical. This solution naturally includes effects of refraction and diffraction as well as sound penetration into the seafloor. The number of propagating modes increases with water depth and frequency, so the NM solution approach is most efficient at low frequencies or in shallow water. NM models include KRAKEN and ORCA. Range-dependent environments can be addressed by coupled mode models; however, there are high computational costs associated with this approach, making them unpopular.

Parabolic Equation Models

The PE model solves the wave equation using a paraxial approximation. This modeling approach is computationally efficient and can address range-dependent environments. The computational time of the PE model increases linearly with water depth and frequency squared; therefore, the PE often is avoided for HF modeling in deep water. The PE model is the industry standard for full-wave propagation of lower-frequency sound (usually up to 1 kilohertz [kHz]). The U.S. Navy uses the PE model for frequencies below 600 hertz (Hz). Within the acoustics community, the primary PE model used is RAM, developed by Collins (1993, 1996). PE models are limited in vertical angle support, making them problematic where steep angles tend to prevail (i.e., at ranges less than the water depth). In this project, results generated using the PE model were extrapolated from 2,380 Hz to 20 kHz using an effective attenuation scaling.

Wavenumber Integration Models

Wavenumber integration models are analytic solutions to the wave equation and cover very high-angle energy. This mathematical solution is only accurate for a range-independent environment, and therefore is used primarily for short-range propagation or for benchmarking other models.

Energy Flux Models

Energy flux models have become popular among acoustic modelers, permitting rapid computation of the incoherent energy in range-dependent environments. These models are a hybrid of the ray tracing model and NM model methodologies, numerically solving the wave equation for a bundle of modes that follow a ray-like trajectory.

Finite Difference/Finite Element Models

FD/FE models offer a complete full-wave solution on a very high-resolution grid. FE modeling was used in this project for the source model (hammer and pile). FE models also can be used for scattering from submerged objects. FD/FE models do not handle long-range propagation (>100 m) because of the demands of the dense computational grid.

Image and Multipath Models

Other methods such as the image method model (Brekhovskikh, 1980) and the multipath expansion model (Weinberg, 1975) are not considered here because they only work for iso-velocity sound speed profiles (SSPs) and point sources. Neither of these features exist in this project and thus are not applicable to the modeling of pile-driving sources out to distance in shallow water.

The common propagation models and their general characteristics are provided in **Table 1-2**.

Table 1-2. List of common propagation models and general characteristics.

Model Name	Method	Class Frequency	Class Water Depth
Range-dependent			
Peregrine	Parabolic equation	10 Hz – 3.5 kHz*	All depths
Range-dependent Acoustic Model (RAM)	Parabolic equation	5 Hz – 3.5 kHz	All depths
KRAKEN	Normal mode	5 Hz – 1 kHz	All depths
ORCA	Normal mode	5 Hz – 1 kHz	All depths
BELLHOP	Ray	200 Hz – 200 kHz	All depths
CASS/GRAB	Ray	600 Hz – 200 kHz	All depths
Aquarius	Energy flux	100 Hz – 200 kHz	All depths
--	Finite difference/finite element	5 Hz – 200 kHz	Shallow water (≤100 m)
Range-independent			
--	Image/multipath	200 Hz – 200 kHz	Shallow water
OASES	Wavenumber integration	5 Hz – 200 kHz	All depths

CASS/GRAB = Comprehensive Acoustic Simulation System/Gaussian Ray Bundle; Hz = hertz; kHz = kilohertz; m = meter.
* Peregrine results were extrapolated to high frequencies up to 20 kHz using ray methods.

1.2.2 Recommended Project Model: Peregrine PE-RAM model

To address the project goals and objectives, a full-wave RAM was needed that could efficiently handle 10 to 2,000 Hz in shallow water (<60 m) at high-resolution range stepping (meters). For this project, the PE method was recommended because of its ability to address propagation within the sediment, range-dependent bathymetry, high-angle support, and frequency range.

OASIS Inc. developed a new version of RAM, named Peregrine, that has increased efficiency. The first major improvement in the writing of Peregrine was to the interfaces between the central processing unit and memory access that increased speed of processing; no changes were made to the physics algorithms. The second major improvement in Peregrine was an increase in efficiency in the environmental databases, enabling rapid computation of the sound field as a function of three-dimensional position around a single point source. A third benefit, developed for this project, was the accommodation of HFs up to 20 kHz using the PE model using a scaling of the frequency-dependent volume attenuation. Peregrine was recommended for and used in this project.

1.3 Environmental and Source Parameters

Underwater sound propagation is influenced by the local propagation medium (the "environment"), which may vary spatially and temporally. As such, the accuracy of a propagation model's output relies on representative environmental inputs for the time and place of interest. Changes in environmental variables such as bathymetry, seafloor properties, and SSP influence the propagating sound. Other more specific model input parameters, such as wind speed, can be used as a proxy input if surface scattering requires consideration.

Sensitivity to key environmental and source parameters that influence sound propagation depends on distance from the source (i.e., the pile). At "short range", the most influential parameters are those associated with the propagation of the Mach cone, typically up to 5 to 10 km. At "long range", defined for this project as the region after the Mach cone has died away (less than approximately 10 km), the propagation is dominated by sound paths traveling horizontally. Environmental parameters that influence the short and long ranges are discussed in this section.

During this project, the degree of influence on sound propagation by environmental parameters was investigated with a sensitivity study. The study evaluated changes in PL as environmental parameters were changed. In order to highlight some of the most common sources of uncertainty, attention was given to environmental model inputs for bathymetry, sound speed, and geoacoustical seafloor properties. In addition, publicly accessible environmental data were reviewed and provided bounds for water depths, sediment types, and sound speeds.

A sensitivity study of the influence on sound propagation by environmental parameters was carried out by TNO in 2016 (Binnerts et al., 2016) for the Netherlands Government. Where appropriate, conclusions of that work are included and summarized herein.

1.3.1 Water Depth and Bathymetry

1.3.1.1 Sensitivity to Water Depth and Bathymetry

Bathymetry is particularly important for shallow-water propagation. Seafloor shape and local water depth influence acoustic propagation. Near continental shelves, a sloping seafloor can substantially influence sound propagation. High-resolution bathymetry data may capture small-scale seafloor features such as sand waves and ripples; however, these features are dynamic and expected to change over time.

In addition to the resolution and accuracy of bathymetric data, the accuracy of modeled outputs also may be influenced by water depth. Water depth typically is based on mean sea level or the lowest astronomical tide. While tidal changes usually are less important in deep water, they can have a notable effect on the assumed water depth in shallow coastal regions. At the two sites considered (Rhode Island [RIsland] and Virginia Beach [VAbeach]), the tidal variation is only 1.5 m at both sites. Therefore, tidal variation is not a factor that required consideration in this project. However, where tidal variation is a substantial ratio of the water depth (e.g., the Bay of Fundy), it should be included in environmental sensitivity considerations.

Very high-resolution bathymetric survey data may be available in some cases, generally in relation to a local site with specific stakeholder interest. Global bathymetric data, or bathymetric data from another source, may be used for adjacent areas, outside the spatial extent of the site-specific survey data. Such global bathymetric data may be obtained from the General Bathymetric Chart of the Oceans (GEBCO, http://www.gebco.net/); these data are available at an angular resolution of "30 seconds of arc" (an angular, not temporal, unit equivalent to 1/120 of one degree). High-resolution bathymetric databases will be used in coastal regions of the U.S. In particular, the NOAA Coastal Relief Map database can be used off the U.S. East Coast.

1.3.2 Sediment Type

1.3.2.1 Sensitivity to Sediment Properties

Knowledge of the geoacoustic properties of the seafloor is essential for shallow-water acoustic propagation modeling. In general, these properties determine how much sound is reflected from the seafloor, and of the sound that was transmitted into the seafloor, how much sound re-enters the water column. For example, a stratified seafloor bends sound waves, while a hard seafloor layer, such as rock, reflects sound waves. Both mechanisms result in sound energy being retransmitted into the water column.

Acoustic properties of the sediment, and in some cases the stratification of the seafloor, often can be incorporated into an acoustic propagation model. However, the accuracy of this process is limited by the availability of data at a sufficient spatial scale and with the necessary resolution, such that the data are representative of the actual environment. It can be challenging, and in some cases impossible, to incorporate the necessary spatial variations of the seafloor into a RAM. Core measurements of the seafloor can provide information of the underlying geology, although the specific sediment types might be localized, and it might not be correct to extrapolate those characteristics across a broad region.

Binnerts et al. (2016) described measurements of pile driving from two operations: during the construction of an offshore wind farm in the Dutch North Sea (Luchterduinen), and at a nearby Dutch site (Gemini), in one-third octave bands. (A one-third octave band is a unit of logarithmic frequency interval equal to one third of an octave.) A comparison between measured and modeled L_E values was made for the Gemini wind farm (Binnerts et al., 2016). The analysis examined the sensitivity of L_E to sediment type, as shown in **Figure 1-1** (left). Sediment type varied from very fine to coarse sand. The chosen sediment parameters represented a uniform fluid sediment with an attenuation coefficient (α) proportional to frequency (*f*) (i.e., $\alpha \propto f$). These sediment parameters are valid in the frequency range of 1 to 10 kHz (i.e., 1 kHz $< f <$ 10 kHz). Below 1 kHz, frequency dependence of the attenuation coefficient is thought to depart from simple proportionality, leading to an attenuation coefficient that varies with frequency according to $\alpha \propto f^x$, with $x > 1$. Binnerts et al. (2016) applied a $f^{1.8}$ power law ($x = 1.8$ instead of $x = 1.0$) at frequencies below 1 kHz, the result of which is shown in **Figure 1-1** (right). The dashed lines in this graph were calculated using non-linear frequency dependence, making for less attenuation at low frequencies, showing an increasingly larger effect with frequency below approximately 500 Hz. From these results, it was concluded that the value of the exponent x would require consideration in the sensitivity study (**Section 6**). However, it was determined during the validation study (**Section 4.2**) that the associated frequency dependence could be modeled instead by using a layered sediment model (i.e., one with a sound speed gradient).

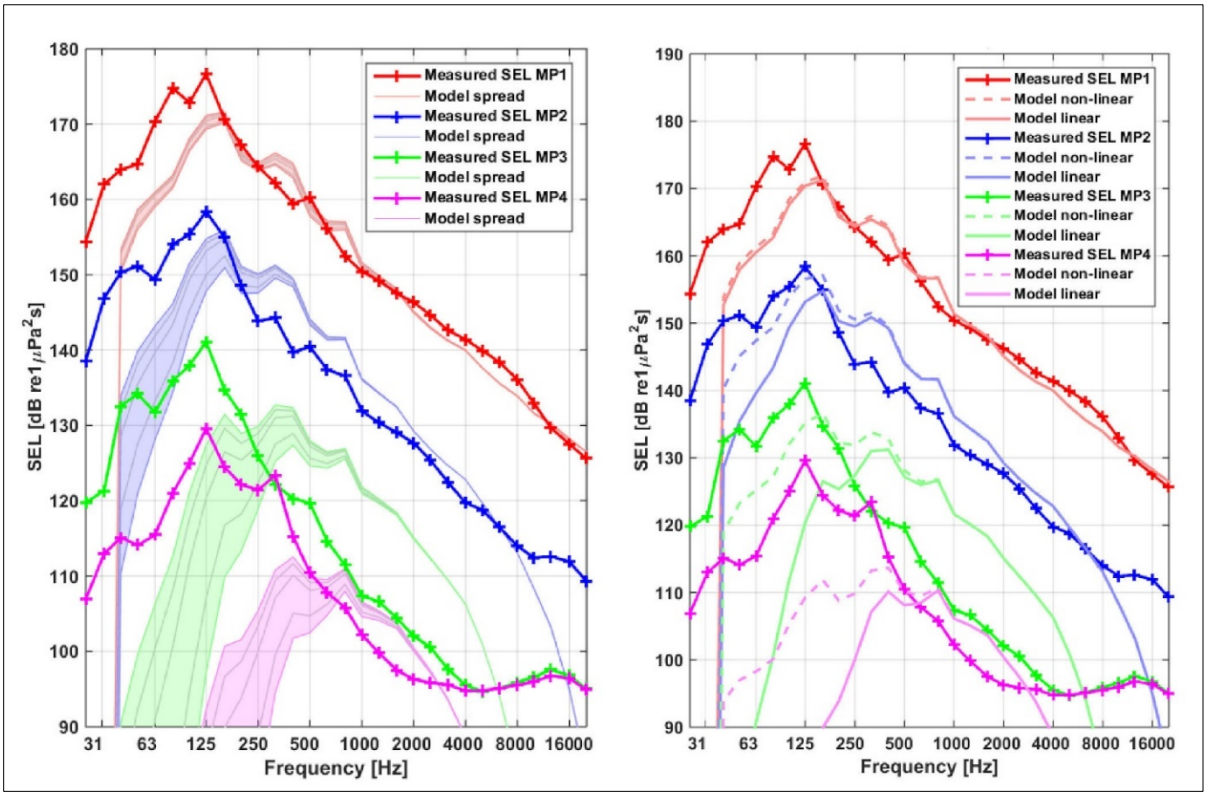

Figure 1-1. Dependence of one-third octave band SEL on sediment properties.
Left: SEL sensitivity to sediment type. Sediments range from very fine sand (pink; lowermost curve in each shaded group) to coarse sand (red; uppermost curve). Right: The effect of non-linear sediment attenuation on frequencies <1 kHz (From: Binnerts et al., 2016). µPa = micropascal; dB = decibel; re = with reference to; SEL = L_E = sound exposure level.

1.3.2.2 Sediment Properties Database

Seafloor survey data may provide information about the upper sediment layer, such as that provided by the European Marine Observation and Data Network (EMODnet) and the EMODnet broadband seabed habitat map for Europe (EUSeaMap) (http://jncc.defra.gov.uk/page-5040). However, this sediment information needs to be converted into acoustic properties for the seafloor before it can be used in modeling. Unfortunately, sufficient information is not always available in order to correlate with published acoustics properties of various sediment types (e.g., Hamilton, 1980; Hamilton and Bachman, 1982; Bachman, 1985; Lurton, 2002; Ainslie, 2010).

For regions of proposed wind farms on the U.S. Outer Continental Shelf, a comprehensive understanding of the seafloor type (particularly geotechnical information) is expected to be available. Often surficial sediment types (e.g., sand, mud, rock, clay) can be extracted from navigational charts. Other potential sources may include the NOAA Coast Survey; the National Centers for Coastal Ocean Science; the NOAA National Environmental Satellite, Data, and Information Service; and region- or site-specific studies.

1.3.3 Sound Speed Profile in Water

1.3.3.1 Sensitivity to Sound Speed Profile

The underwater SSP can substantially influence how sound propagates, especially in deep water. The SSP is determined by changes in water temperature, pressure, and salinity, with depth. Variation in sound speed with depth can bend and trap sound, which in some cases can lead to sound traveling substantially farther due to reduced spreading and less interaction with the seafloor and sea surface. A well-known example in deep water (>2,000 m) is that of sound trapped in the sound fixing and ranging (SOFAR) channel. In shallow water (<100 m), while the SSP may influence acoustic propagation through bending of sound, bathymetry and sediment acoustic properties generally are more influential propagation parameters.

In shallow water (<100 m) during the winter months, wind mixing results in an approximately isothermal water column. In these circumstances, sound speed increases gradually with increasing depth (small but positive sound speed gradient) due to increasing pressure, resulting in a slightly upward refracting SSP and more interaction with the sea surface. Solar heating during the summer results in a negative temperature gradient, and hence a strongly downward refracting (large negative sound speed gradient) SSP that results in increased interaction with the seafloor and more absorption.

1.3.3.2 Sound Speed Profile Database

In principle, the SSP may be measured *in situ* or obtained from global data sets such as those available from the World Ocean Atlas (WOA) database (http://www.nodc.noaa.gov/OC5/indprod.html). The WOA provides information about SSP geographic and seasonal variability. Within select U.S. coastal waters, the U.S. Navy Coastal Ocean Model (NCOM) is available for some periods of time and can show variability on a daily scale (www.ftp.ncep.noa.gov/data/nccf/com/ncom/proc/).

1.3.4 Wind Speed

1.3.4.1 Sensitivity to Wind Speed

Measurements of surface reflection loss are negligible for frequencies around 1 to 4 kHz and wind speeds less than 5 meters per second (m s^{-1}) (**Figure 1-2**; Weston and Ching, 1989). The losses increase with increasing frequency, suggesting that losses at lower frequencies should be lower still, and as predicted by theoretical considerations (Ainslie, 2005). Nevertheless, Binnerts et al. (2016) predicted some sensitivity to wind speed, possibly caused by extrapolation of empirical surface loss models outside their region of validity.

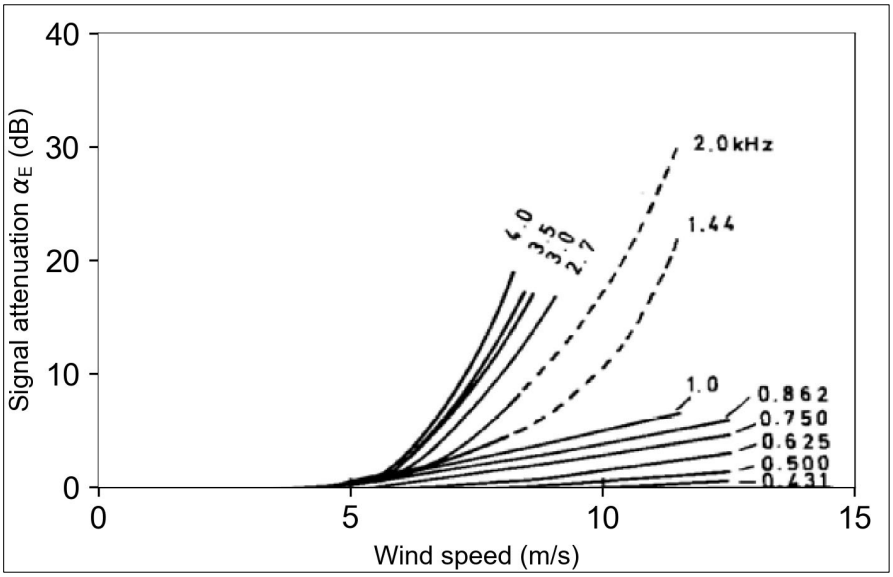

Figure 1-2. Total signal attenuation after multiple surface reflections in the Bristol Channel between May and June 1969.

Measured surface loss was negligible for wind speeds less than 5 m s^{-1} (From: Weston and Ching, 1989).

1.3.4.2 Wind Speed Database

Wind speed data sets can be obtained from NOAA/National Centers for Environmental Information (NCEI), which provides the Global Forecasting System (GFS) model (https://www.ncdc.noaa.gov/data-access/model-data/model-datasets/global-forcast-system-gfs), a global wind weather forecasting model. The European Commission Medium Weather Forecast (ECMWF) (https://www.ecmwf.int/en/forecasts/datasets) also includes wind data sets.

1.3.5 Source Parameters

1.3.5.1 Pile Penetration Depth

Binnerts et al. (2016) predicted the effects of varying the pile penetration depth between 11 and 26 m (**Figure 1-3**). At short range (<10 km), the L_E was predicted to decrease with increasing penetration depth, with the largest reductions occurring at a few tens of hertz. Similar reductions in low-frequency (LF) L_E were predicted at distances of a few tens of kilometers. At frequencies above 200 Hz, the effect reversed and L_E increased with increasing penetrating depth.

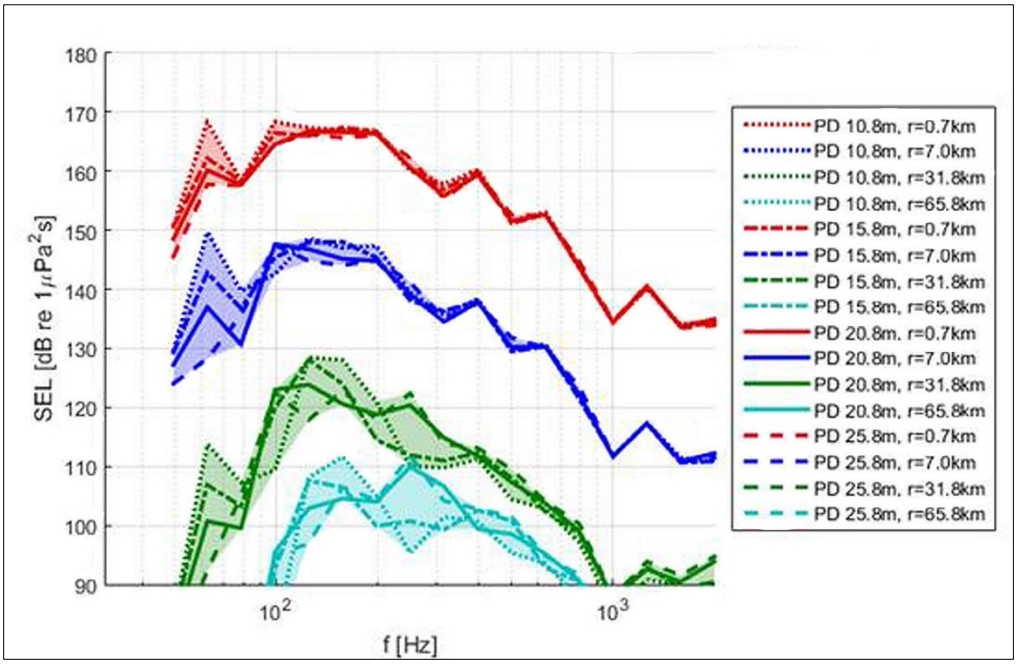

Figure 1-3. Dependence of one-third octave band single strike SEL on pile penetration depth.
μPa = micropascal; dB = decibel; f = frequency; Hz = hertz; re = with reference to; SEL = L_E= sound exposure level (From: Binnerts et al., 2016).

1.3.5.2 Pile Diameter

Binnerts et al. (2016) considered piles of two similar lengths with different diameters – U8 (7.0 m) and B3 (2.4 m) – from the Gemini wind farm, with the anvil scaled accordingly. The predicted difference in L_E between these piles is shown in **Figure 1-3**. The broadband L_E for the 7.0 m pile was about 7 to 8 dB higher than for the 2.4 m pile. The largest effects in any one-third octave band occurred at LF ($f < 30$ Hz). For **Figure 1-4** and subsequent figures showing results from Binnerts et al. (2016), the penetration depth of the pile was 21 m.

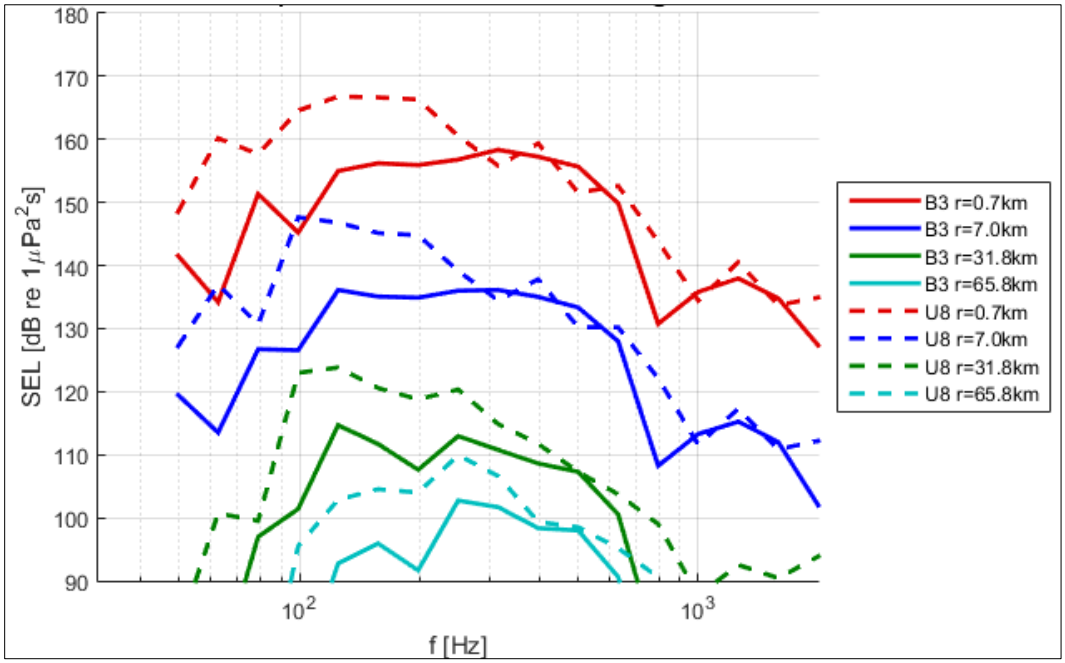

Figure 1-4. Dependence of one-third octave band single strike SEL on pile diameter, based on U8 (7 m) and B3 (2.4 m) data.

µPa = micropascal; dB = decibel; f = frequency; Hz = hertz; re = with reference to; SEL = L_E = sound exposure level (From: Binnerts et al., 2016).

1.3.6 Summary of Environmental Parameters

In summary, the most important short-range environmental parameters that influence acoustic propagation were expected to be water depth and sediment type (e.g., grain size) at the pile. At long distances, bathymetry, sediment distribution, and SSP were expected to be influential also.

1.4 Propagation Physics

1.4.1 Short-range Propagation

1.4.1.1 Mach Cone and Damped Cylindrical Spreading

When a pile is struck with a hammer, a compressional wave travels down the pile's steel wall, radiating sound into the water (**Figure 1-5**). There is a delay in the compressional wave from top to bottom of the pile, which results in the sound radiating from the pile at an angle of approximately 15° to 17° off the horizontal, depending on the properties of the pile wall. The resulting conical wavefront is known as a "Mach cone."

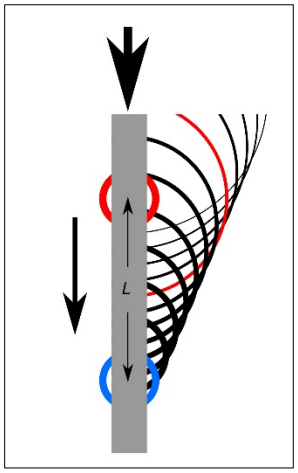

Figure 1-5. Illustration of a Mach cone (From: Dahl et al., 2015).

For a highly directional source (such as a driven pile) that radiates sound close to the horizontal angle, the energy in the radiated sound is attenuated (damped) due to multiple interactions with the seafloor. Because sound energy decays exponentially, this type of propagation is referred to as damped cylindrical spreading (DCS). The steeper the ray path, the heavier the expected dampening. The concept of DCS was introduced by Zampolli et al. (2013) and was developed further by Ainslie et al. (2014).

Undamped cylindrical spreading a few tens of meters from the pile was demonstrated by Dahl et al. (2012). Farther from the pile, after several seafloor interactions, an exponential decay is superimposed on the cylindrical spreading behavior, as demonstrated to distances of several kilometers by Binnerts et al. (2016) and Lippert et al. (2018). DCS applies to L_E, but not to $L_{p,\mathrm{pk}}$ or $L_{p,\mathrm{rms}}$. However, statistical techniques were used to bridge this gap through identification of empirical correlations between L_E and other parameters of interest (e.g., $L_{p,\mathrm{pk}}$, $L_{p,\mathrm{rms}}$).

Initially, most of the radiated energy is contained in the Mach cone, which therefore dominates the short-range propagation. The field associated with the Mach cone depends on two key parameters: the ray cycle distance (the horizontal distance between successive interactions of a ray with the seafloor), and the seafloor reflection loss per cycle. The cycle distance, r_c, depends on the water depth H and Mach cone angle θ, and is given by:

$$r_\mathrm{c} = 2H \cot\theta \, . \qquad \textit{Equation 1.4}$$

The reflection loss per cycle, L_c, is given by:

$$L_\mathrm{c} = -20 \log_{10}|R(\theta)| \ \mathrm{dB}. \qquad \textit{Equation 1.5}$$

The decay rate $= L_\mathrm{c}/r_\mathrm{c}$, expressed in units of decibels per meter (dB m^{-1}) (see Zampolli et al., 2013; Lippert et al., 2018), is given by:

$$\frac{\alpha}{\mathrm{dB/m}} = -10 \log_{10}|R(\theta)| \, \frac{\tan\theta}{H/\mathrm{m}} \qquad \textit{Equation 1.6}$$

where three key parameters control the decay rate: the water depth H; reflection coefficient R, which depends on the sediment type (especially grain size); and the Mach cone angle θ, which depends on the properties of the pile wall.

1.4.1.2 Water Depth

Water depth influences propagation due to its influence on the cycle distance, resulting in a decay rate that is inversely proportional to water depth (**Equation 1.6**). Thus, the greater the water depth, the higher the acoustic signal decay rate.

1.4.1.3 Sediment Type

Sediment type influences propagation due to its influence on the reflection loss, and is given by:

$$L_c \equiv -\log_e R = -20 \log_{10}|R(\theta)| \text{ dB} \qquad \textit{Equation 1.7}$$

which results in a decay rate directly proportional to reflection loss.

The sediment type was characterized by grain size. Coarse sediments (e.g., gravel, coarse sand) are acoustically hard, meaning they have a high sound speed (large impedance contrast) relative to water, and therefore a low reflection loss. This low reflection loss means the sound signal will travel farther (with a lower decay rate) than would be the case for an acoustically soft sediment such as silt or fine sand, for which (though less relevant for this project) sound would travel less far.

1.4.1.4 Mach Cone Angle

The Mach cone angle influences propagation due to its influence on the cycle distance and reflection coefficient, resulting in an increased rate of decay rate with increasing Mach cone angle θ. In practice, however, this angle does not vary much from its nominal value of 15° to 17° because the Mach cone angle is determined by the properties of water and steel, which are mostly fixed. This angle is steep enough to be unaffected by refraction in shallow water.

1.4.2 Long-range Propagation

The Mach cone propagation angle of approximately 17° causes multiple lossy interactions with the seafloor, resulting in exponential decay. By contrast ray paths traveling close to the horizontal direction, though initially weaker in amplitude, decay more slowly and can be expected to dominate the sound field at long range.

The precise distance at which the Mach cone decays depends on water depth and sediment type. Based on a sand-sediment and 30 m water depth scenario, the Mach cone dies away after approximately 10 km (Lippert et al., 2018) and is replaced by horizontally traveling sound energy. At greater distances, the SSP in the water column and long-range bathymetry become important. While surface scattering might become an issue at long range, it is considered less important than the effects of SSP or bathymetry.

1.4.2.1 Bathymetry

At long ranges, the effects of changing water depth, however gradual, become important. For example, a decrease in water depth for a fixed amount of sound power means that power is compressed into a smaller

area, resulting in a higher intensity. On the other hand, a decrease in water depth also leads to an increase in ray grazing angle (Weston, 1976) that results in an increased rate of decay and lower intensity (see **Equation 1.6**). In summary, this means the signal travels less distance. This increase in decay rate is further strengthened by an increase in duct cut-off frequency with decreasing water depth, which filters out LF sound. Thus, the travel range of the signal is even shorter. In extreme cases, where water depth decreases significantly in the first few kilometers, the angle of the Mach cone would increase with a corresponding increase in the decay rate.

1.4.2.2 Sound Speed Profile

The effect of the SSP on acoustic signals is to create acoustical waveguides, which means horizontally traveling sound can be trapped as if in a tunnel. Steeper paths are not trapped and decay more quickly due to multiple lossy interactions with the seafloor and sea surface. To function effectively, these waveguides require the acoustic frequency to exceed a minimum value, known as the "cut-off frequency" of the waveguide (Ainslie, 2010). The SSP is most likely to have an effect on HF sound and at long range, where the sound is traveling horizontally. The most likely consequence of the SSP is refraction of the sound in one of two directions, either (1) towards the sea surface (in upward refracting conditions, most likely in winter because of wind mixing and reduced solar heating), resulting in reduced decay rate in calm conditions (sound travels farther); or (2) towards the seafloor (in downward refracting conditions, most likely in summer), resulting in increased decay rate (sound travels less far).

1.4.2.3 Wind Speed

Wind roughens the sea surface and generates near-surface air bubbles. The roughness causes surface scattering (Weston and Ching, 1989), which increases attenuation. Scattering is enhanced by the presence of near-surface bubbles, which further increases attenuation (Ainslie, 2005). As a result, the presence of wind is most likely to influence (i.e., decrease) the propagation of HFs, in upward refracting conditions and at long ranges.

1.5 Acoustic Threshold Criteria

1.5.1 Marine Mammals

The acoustic criteria and metrics used for marine mammals (i.e., cetaceans and pinnipeds) were based on the NMFS (2018a) criteria for impulsive and non-impulsive sounds pertinent to auditory impacts, and the older behavioral impacts by NOAA (*Federal Register*, 2005). The acoustic criteria are shown in **Table 1-3** for impulsive sounds and **Table 1-4** for non-impulsive sounds. For marine mammals, the relevant metrics for auditory impacts of permanent threshold shift (PTS) and temporary threshold shift (TTS), are both weighted sound exposure level (SEL_w, i.e., $L_{E,\mathrm{w}}$) and $L_{p,\mathrm{pk}}$. The relevant metric for the behavioral criteria is $L_{p,\mathrm{rms}}$.

Table 1-3. Project-specific acoustic criteria and metrics on impulsive sounds (From: NMFS, 2018a; *Federal Register*, 2005).

Hearing Group	Impulsive Signals				
	PTS onset		TTS onset		Behavior
	$L_{E,\mathrm{w},24\mathrm{h}}$ dB re 1 µPa^2 s	$L_{p,\mathrm{pk}}$ dB re 1 µPa (unweighted)	$L_{E,\mathrm{w},24\mathrm{h}}$ dB re 1 µPa^2 s	$L_{p,\mathrm{pk}}$ dB re 1 µPa (unweighted)	$L_{p,\mathrm{rms}}$ dB re 1 µPa (unweighted)
Low-frequency cetaceans	183	219	168	213	160
Mid-frequency cetaceans	185	230	170	224	160
High-frequency cetaceans	155	202	140	196	160
Phocid pinnipeds underwater	185	218	170	212	160
Otariid pinnipeds underwater	203	232	188	226	160

µPa = micropascal; dB = decibel; $L_{p,\mathrm{pk}}$ = peak sound pressure level; $L_{p,\mathrm{rms}}$= 90% energy root-mean-square sound pressure level; PTS = permanent threshold shift; re = with reference to; $\mathrm{SEL}_{\mathrm{w},24\mathrm{h}}$ = $L_{E,\mathrm{w},24\mathrm{h}}$ = weighted sound exposure level over 24 hours; TTS = temporary threshold shift.

Table 1-4. Project-specific acoustic criteria and metrics for non-impulsive sounds (From: NMFS, 2018a; *Federal Register*, 2005).

Hearing Group	Non-Impulsive Signals		
	PTS onset	TTS onset	Behavior
	$L_{E,\mathrm{w},24\mathrm{h}}$ dB re 1 µPa^2 s	$L_{E,\mathrm{w},24\mathrm{h}}$ dB re 1 µPa^2 s	$L_{p,\mathrm{rms}}$ dB re 1 µPa (unweighted)
Low-frequency cetaceans	199	179	120
Mid-frequency cetaceans	198	178	120
High-frequency cetaceans	173	153	120
Phocid pinnipeds	201	181	120
Otariid pinnipeds	219	199	120

µPa = micropascal; dB = decibel; $L_{p,\mathrm{rms}}$ = root-mean-square sound pressure level; PTS = permanent threshold shift; re = with reference to; $\mathrm{SEL}_{\mathrm{w},24\mathrm{h}}$ = $L_{E,\mathrm{w},24\mathrm{h}}$ = weighted sound exposure level over 24 hours; TTS = temporary threshold shift.

The weighting functions for cetaceans and pinnipeds are shown in **Figure 1-6** (otariids currently do not reside along the U.S. Atlantic Coast so were not included in this project).

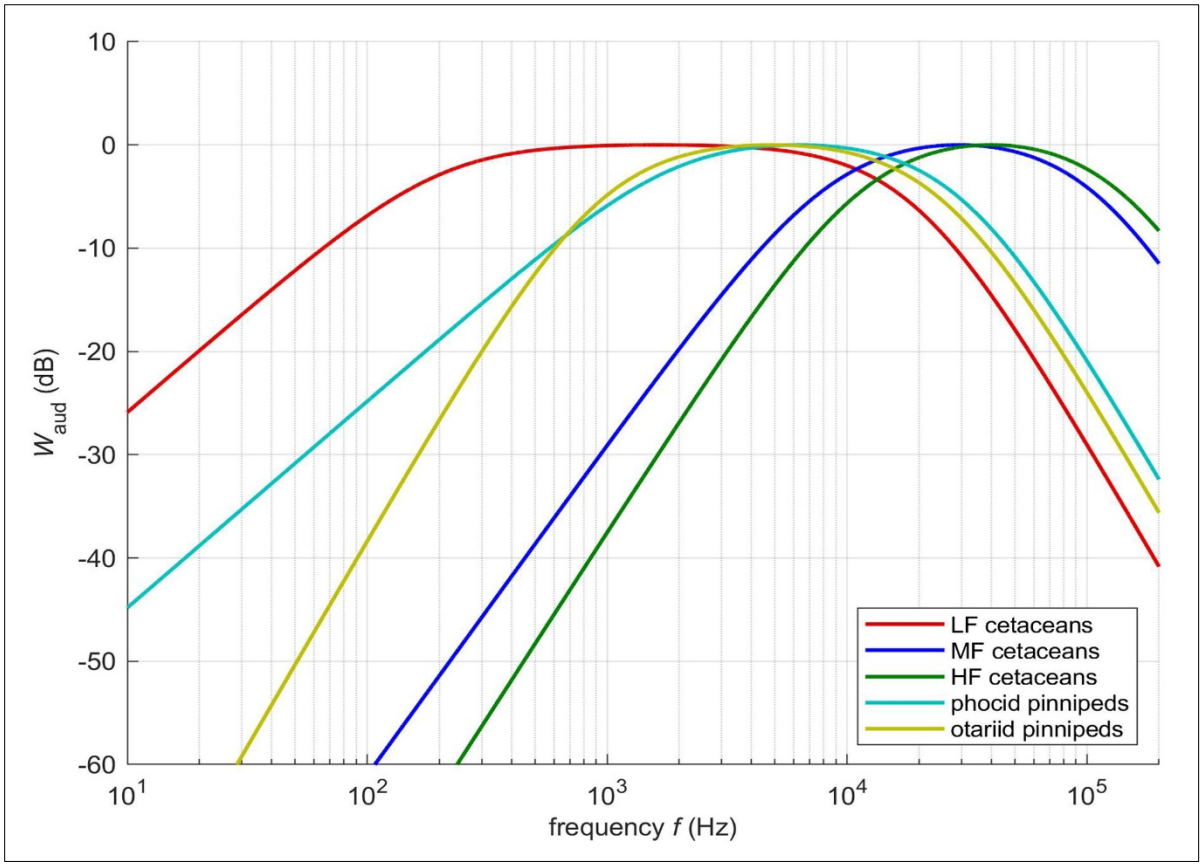

Figure 1-6. Auditory frequency weighting functions.
From the NMFS (2018a) parametrization. dB = decibel; Hz = hertz; HF = high-frequency; LF = low-frequency; MF = mid-frequency; $W_{aud}(f)$ = logarithmic auditory weighting function.

1.5.2 Fishes and Sea Turtles

The acoustic criteria and metrics for fishes and sea turtles were based on the sound exposure guidelines developed by Popper et al. (2014) for impulsive and non-impulsive sounds (**Table 1-5**) with an inclusion to address the Stadler and Woodbury (2009) criteria as well. The criteria recommendations made by Popper et al. (2014) are based on the most recent science available at the time of their publication and are widely cited (Sabet et al., 2015; Borger et al., 2016; Farcas et al., 2016; Hawkins and Popper, 2016; Lucke et al., 2016; Roberts et al., 2016a,b; de Jong et al., 2018; Taormina et al., 2018; Davidsen et al., 2019; Higgs and Humphrey, 2019). Most of the criteria recommendations for impulsive sounds from pile driving and airgun use are based on a series of publications by Halvorsen et al. (2011, 2012a,b) and Casper et al. (2012, 2013).

Table 1-5. Project-specific acoustic criteria and metrics for fishes (From: Popper et al., 2014).

Fish Group	Impulsive Signals			Non-impulsive Signals	
	Recoverable injury		TTS	Recoverable injury	TTS
	$L_{E,\#960}$ dB re 1 µPa² s (unweighted)	$L_{p,\mathrm{pk}}$ dB re 1 µPa (unweighted)	$L_{E,\#5}$ dB re 1 µPa² s (unweighted)	$L_{p,\mathrm{rms},48\mathrm{h}}$ dB re 1 µPa (unweighted)	$L_{p,\mathrm{rms},12\mathrm{h}}$ dB re 1 µPa (unweighted)
Fish without swim bladder	>216	>213	>>186	--	--
Fish with swim bladder not involved in hearing	203	>207	>186	--	--
Fish with swim bladder involved in hearing	203	>207	186	170	158

µPa = micropascal; dB = decibel; $L_{p,\mathrm{pk}}$ = peak sound pressure level; $L_{p,\mathrm{rms},12\mathrm{h}}$ = root-mean-square sound pressure level for 12 hours continuous exposure; $L_{p,\mathrm{rms},48\mathrm{h}}$ = root-mean-square sound pressure level for 48 hours continuous exposure; $SEL_{\#5} = L_{E,\#5}$ = sound exposure level from 5 airgun shots (Popper et al., 2005); $SEL_{\#960} = L_{E,\#960}$ = sound exposure level from 960 pile strikes; PTS = permanent threshold shift; re = with reference to; TTS = temporary threshold shift.

The current criteria used by NOAA for fishes are presented in **Table 1-6** (Stadler and Woodbury, 2009; Greater Atlantic Regional Fisheries Office [GARFO], 2016), and the proposed criteria for sea turtles from Popper et al. (2014) and GARFO (2016) are presented in **Table 1-7**.

Table 1-6. Project-specific acoustic criteria and metrics for fishes (From: Stadler and Woodbury, 2009; GARFO, 2016).

Fish Group	Injury		Physiological	Behavior
	$L_{E,12\mathrm{h}}$ dB re 1 µPa² s (unweighted)	$L_{p,\mathrm{pk}}$ dB re 1 µPa (unweighted)	$L_{p,\mathrm{rms}}$ dB re 1 µPa (unweighted)	$L_{p,\mathrm{rms}}$ dB re 1 µPa (unweighted)
Small fish (mass <2 g)	183 [a]	206 [a]	--	150 [b]
Large fish (mass ≥2 g)	187 [a]	206 [a]	--	150 [b]

-- = not applicable; µPa = micropascal; dB = decibel; $SEL_{12h} = L_{E,12\mathrm{h}}$ = cumulative sound exposure level, over 12 hours; $L_{p,\mathrm{pk}}$ = peak sound pressure level; $L_{p,\mathrm{rms}}$ = root-mean-square sound pressure level; PTS = permanent threshold shift; re = with reference to; TTS = temporary threshold shift.
[a] Stadler and Woodbury (2009).
[b] GARFO (2016).

Table 1-7. Acoustic criteria and metrics for sea turtles (From: Popper et al., 2014; GARFO, 2016).

Animal Group	Mortal Injury		Physiological	Behavior
	$L_{E,12\mathrm{h}}$ dB re 1 µPa² s (unweighted)	$L_{p,\mathrm{pk}}$ dB re 1 µPa (unweighted)	$L_{p,\mathrm{rms}}$ dB re 1 µPa (unweighted)	$L_{p,\mathrm{rms}}$ dB re 1 µPa (unweighted)
Sea turtles	210 [a]	>207 [a]	180 [b]	166 [b]

µPa = micropascal; dB = decibel $SEL_{12h} = L_{E,12\mathrm{h}}$ = sound exposure level for 12 hours continuous exposure; $L_{p,\mathrm{pk}}$ = peak sound pressure level; $L_{p,\mathrm{rms}}$ = root-mean-square sound pressure level; re = with reference to.
[a] Popper et al. (2014).
[b] GARFO (2016). *The GARFO criteria were updated in 2019. However, the 2016 criteria were applied for this project because the 2019 update could not be accommodated by the project schedule.

2 Metrics

The metrics L_E, $L_{p,\mathrm{pk}}$, and $L_{p,\mathrm{rms}}$ are broadband quantities for which the frequency band needs to be specified (**Appendix B**). To ensure comparability between predictions comparing like with like, the same frequency bands should be used for both/all measurements. Furthermore, it is desirable to consider a sufficiently wide range of frequencies to avoid omitting bands that contribute significantly to the total acoustic energy, particularly the main spectral peak, after weighting.

For Gemini and Luchterduinen, measurements were available in the approximate frequency band of 20 Hz to 20 kHz, with the unweighted one-third octave spectrum peaking in the bands with a center frequency between 100 and 200 Hz. Weighting for mid-frequency (MF) and (especially) HF cetaceans has the effect of emphasizing frequencies above 200 Hz relative to those below 100 Hz. Therefore, in the MF and HF cetacean hearing groups, the weighted main spectral peaks occurred at a higher frequency than the unweighted main spectral peaks. The goal was to model up to this main weighted spectral peak to include the frequency contributing the most to the acoustic energy as perceived by the HF cetacean hearing group. This approach avoided omission of any frequency band that is biologically important. For computational reasons, the maximum acoustic frequency used for FE and PE modeling was approximately 2.2 kHz. The higher frequencies required for MF and HF cetacean hearing group impact volumes were extrapolated by adjusting the 2.2 kHz sound field according to the known frequency dependence of the absorption coefficient in seawater.

Sound pressure level and related quantities are sometimes presented with logarithmic frequency spacing, such as in octave bands (i.e., in the band f_{min} to $2f_{\mathrm{min}}$, where f_{min} is the LF limit of the band) or in decade bands (i.e., in the band f_{min} to $10f_{\mathrm{min}}$). Such bands are typically subdivided into smaller bands such as one-third of an octave (i.e., one-third octave or 1/3 octave) or one-tenth of a decade (i.e., one-tenth decade, decidecade, or 1/10 decade). The frequency band corresponding to a decidecade is approximately equal to one-third of an octave, and for historical reasons, the difference between these two bands is sometimes neglected, with both occasionally referred to as a "one-third octave". This project used base 10 bands (decidecades), as required for compliance with the international standard IEC 61260-1, also followed by the COMPILE (2014) workshop.

While the standard IEC 61260-1 requires use of base 10 (decidecade) bands, the measurements by Institut für technische und angewandte Physik (ITAP, 2015a,b) used base 2 (one-third octave) bands, which results in a small discrepancy. However, the difference in bandwidth between base 2 and base 10 "one-third octave" bands is about 0.3% (amounting to less than 0.1 dB difference in band level for white broadband noise). This means the discrepancy was negligible for this project and should be determined for each project independently to make such determinations. Lower and upper frequency bands and the size of sub-bands, whether base 10 (decidecades) or base 2 (one-third octaves) are summarized in **Table 2-1**. The value of f_{max}shown in parentheses is the upper frequency limit used for FE and PE modeling work. Extrapolation to 20 kHz was carried out using the HF model.

Table 2-1. Summary of frequency bands and sub-bands for COMPILE, Gemini, and Luchterduinen data sets.

Test Case	$f_{\min}$	$f_{\max}$	Base 2 or Base 10 (measurement)	Base 2 or Base 10 (model)
COMPILE	0	2.5 kHz (2.5 kHz)	10	10
Gemini U8, Z2	20 Hz	20 kHz (2 kHz)	2	10
Luchterduinen EL39, EL42	20 Hz	20 kHz (2 kHz)	2	10

base 2 = one-third octave; base 10 = one-tenth decade (decidecade); $f_{\max}$ = maximum frequency; $f_{\min}$ = minimum frequency; Hz = hertz; kHz = kilohertz.

From the available data set options (Gemini and Luchterduinen), two piles were chosen from the Luchterduinen data set. The measured pile data from Luchterduinen were combined with data from three German sites (introduced in **Section 1.3.2**). These data were used to carry out a regression analysis between L_E and other parameters of interest ($L_{p,\mathrm{pk}}$ and $L_{p,\mathrm{rms}}$). Measurements from Gemini were used for validation of the regression formulas obtained.

2.1 Accumulation of Sound Exposure

The cumulative sound exposure level ($\mathrm{SEL_{cum}}$, i.e., $L_{E,\mathrm{cum}}$) is calculated from the single strike sound exposure level ($\mathrm{SEL_{ss}}$, i.e., $L_{E,\mathrm{ss}}$) using

$$L_{E,\mathrm{cum}} = L_{E,\mathrm{ss}} + 10\log_{10} N_{24\mathrm{h}}\ \mathrm{dB} \qquad \textit{Equation 2.1}$$

where $N_{24\mathrm{h}}$ is the number of pile strikes in a 24-hour period. The choice of $N_{24\mathrm{h}}$ is determined by estimating the maximum number of pile strikes that could occur in the 12-hour period of daylight available for work to be carried out. It was assumed that no construction work would take place during the night. The total number of strikes during a 24-hour period (day and night) for the construction of Gemini pile U8 was 6,921 strikes (ITAP, 2015b). Dividing this number by two and rounding up results in 3,500 strikes in 12 hours, which can also represent the total daily 24 hours of working and non-working time. Therefore, for this project, 3,500 strikes was the value used throughout for $N_{24\mathrm{h}}$. Substituting $N_{24\mathrm{h}}$ with 3,500 into the ($L_{E,\mathrm{cum}}$) equation above leads to a value of 35.4 dB, which is then added to the $L_{E,\mathrm{ss}}$value.

2.2 Applicability of Frequency Weighting

The GARFO (2016) spreadsheet is not applicable for $L_{E,\mathrm{w}}$; it addresses cetaceans for behavior with an unweighted $L_{p,\mathrm{rms}}$ threshold and for physiology by advising its user to consult NMFS (2018a) for the weighted thresholds. This project developed a DCS spreadsheet calculator (named Damped Cylindrical Spreading in Excel [DCSiE], pronounced “Dixie”), which evaluates the marine mammal frequency weighting functions at a frequency of 2 kHz, as specified by NMFS (2018a), Appendix D.

One way to compute $L_{E,\mathrm{w}}$ is from the spectrum of the unweighted sound exposure, which can be attained with the sound pressure time series [p(t)].

The applied weighting functions were from the NMFS (2018a) technical guidance report and have the following functional form:

$$w_{\text{aud}}(f) = \frac{v(f)}{\max v(f)} \qquad \textit{Equation 2.2}$$

$$v(f) = \frac{f_2^{2b} f^{2a}}{(f_1^2 + f^2)^a (f_2^2 + f^2)^b} \qquad \textit{Equation 2.3}$$

Here, the f_1 and f_2 cutoffs are defined specifically for each hearing group (**Figure 1-6**).

The logarithmic auditory weighting function $W_{\text{aud}}(f)$ defined by NMFS (2018a; **Table 2-2**), is related to the auditory frequency weighting function $w_{\text{aud}}(f)$ (with a lower-case w) according to

$$W_{\text{aud}}(f) = 10 \log_{10} w_{\text{aud}}(f) \text{ dB}, \qquad \textit{Equation 2.4}$$

which corresponds to NMFS (2018a) Eq. (1):

$$W_{\text{aud}}(f) = C + 10 \log_{10} v(f) \text{ dB} \qquad \textit{Equation 2.5}$$

with C defined as:

$$C = -10 \log_{10} \max v(f) \text{ dB}. \qquad \textit{Equation 2.6}$$

Where:

$w_{\text{aud}}(f)$ = auditory frequency weighting function
$W_{\text{aud}}(f)$ = logarithmic auditory frequency weighting function
$v(f)$ = function of frequency used in NMFS auditory frequency weighting function

C = weighting function gain, a constant offset to ensure the logarithmic auditory frequency weighting function has a maximum value of 0 dB

Table 2-2. Auditory weighting parameters for weighting functions, and estimated lower and upper functional hearing limits (From: NMFS, 2018a).

Hearing Group	a	b	f_1 (kHz)	f_2 (kHz)	C (dB)
Low-frequency cetaceans	1.0	2	0.2	19	0.13
Mid-frequency cetaceans	1.6	2	8.8	110	1.20
High-frequency cetaceans	1.8	2	12	140	1.36
Phocid pinnipeds (underwater)	1.0	2	1.9	30	0.75
Otariid pinnipeds (underwater)	2.0	2	0.94	25	0.64

a = low-frequency exponent in equation for $v(f)$; b = high-frequency exponent in equation for $v(f)$; C = weighting function gain, a constant offset in equation for $W_{\text{aud}}(f)$; dB = decibel; f_1 = low-frequency cutoff; f_2 = high-frequency cutoff; kHz = kilohertz; NMFS = National Marine Fisheries Service; $v(f)$ = quantity proportional to the auditory frequency weighting function.

3 Damped Cylindrical Spreading in Excel

The purpose of this section is to describe the development of a simple tool to model propagation for impact pile driving. The tool provides an alternative to the Practical Spreading Loss Model (PSLM), as found in the GARFO (2016) and NMFS (2018b) spreadsheet. The PSLM uses an empirical extrapolation to predict L_E and $L_{p,\mathrm{pk}}$. Methods used to replace the empirical extrapolations for L_E and $L_{p,\mathrm{pk}}$ are described in this section. $L_{p,\mathrm{rms}}$ was also considered. The tool is applicable to marine mammals, fishes and sea turtles. For fishes the criteria of Stadler and Woodbury (2009) are supplemented by the more recent guidelines of Popper et al. (2014).

The updated DCS calculator spreadsheet model, DCSiE, is based on the DCS model (Lippert et al., 2018), which is most accurate near the pile, where injury is the primary concern and the metrics L_E and $L_{p,\mathrm{pk}}$ are most relevant. By contrast, $L_{p,\mathrm{rms}}$ is mainly of interest at long range from the pile, where the DCS model is not applicable. L_E is calculated directly using DCS. $L_{p,\mathrm{pk}}$ and $L_{p,\mathrm{rms}}$ are then estimated from L_E using empirical correlations with L_E (Lippert et al., 2015).

The PSLM method used in the NMFS (2018b) spreadsheet is described in **Section 3.2.1**. This is followed by a description of the DCS (**Section 3.2.2**), the correlations used to obtain $L_{p,\mathrm{pk}}$ and $L_{p,\mathrm{rms}}$ (**Section 3.3**), and recommendations for calculating all three quantities (**Section 3.4**). Conclusions are drawn in **Section 3.6**.

3.1 Practical Spreading Loss Model

The latest NMFS technical guidance for acoustic assessment on marine mammals was published in June 2018 (NMFS, 2018a). The NMFS (2018b) acoustic spreadsheet prompts the user to enter source-level information for an impact pile driver (**Figure 3-22**). The user is prompted for "Source Level (RMS SPL)" and "Source Level (PK SPL)". As described in **Section 1.1**, the SL is not a well-defined concept for pile driving (Ainslie et al., 2012), making the NMFS (2018b) spreadsheet difficult to interpret. There is no need for, and no benefit derived from, the use of SL in this context. One possible interpretation is that the authors of the NMFS (2018b) spreadsheet intend the user to calculate this entry by taking the measured level at range r_1 and subtracting from it the quantity $F \log_{10}\left(\frac{r_1}{r_0}\right)$ dB, where $r_0 = 1$ m. It is suggested that the calculation method be made explicit and to avoid using the term "source level" with regard to pile driving.

The PSLM method used in the NMFS spreadsheet (NMFS, 2012b, 2018b; Caltrans, 2015; GARFO, 2016) involves extrapolation of measurements for L_E, $L_{p,\mathrm{pk}}$, or $L_{p,\mathrm{rms}}$ at a known range from the pile (r_1) to some other range (r) at which the value of the level is required. The PSLM extrapolation is carried out using the TL estimation. However, to understand the limitations of the PSLM approach, an understanding of TL and PL is required.

3.2 Transmission Loss and Propagation Loss

TL often is used interchangeably with PL; however, in underwater acoustics, it is important to distinguish between the two concepts. Some of the confusion stems from conflict in definitions between ANSI and

ISO standards. Following the most recent ISO 18405:2017 standard, the following definitions are important.

> *TL is a "reduction in … level between two specified points …"*

Specifically, TL usually is a difference in L_p or L_E between two positions at different ranges from the source, which can be measured or calculated in given conditions (e.g., for a specified site and season). This difference is used to interpolate between the two positions, thus providing intermediate values of TL for the specified conditions.

> *PL is the "difference between source level … and … sound pressure level …"*

PL at range *r* from a source is the difference between a measure of source power (its SL) and the sound pressure level at that range.

> *"note 7 to entry: the term propagation loss is sometimes used as a synonym of transmission loss (3.4.1.3). This use is deprecated."*

In other words, PL is not synonymous with TL, and it is not calculated the same way as TL.

The distinction between TL and PL is important because sometimes the acoustic field at range *r* is estimated by extrapolating from a sound pressure level measurement at some distance close to the source (in pile driving, this distance often is 10 m). The extrapolation is most appropriately performed by estimating the TL between the two locations. It is appropriate to use TL, not PL, in these circumstances because TL is the difference in level between two positions, whereas PL requires knowledge of the SL, which is unknown for pile driving (Ainslie et al., 2012; **Section 1.1**). The concept of SL is fundamental to the sonar equation and is a measure of the sound power radiated to a source's far field (Ainslie, 2010). No method has been developed to measure or define the SL of a pile driver (Ainslie et al., 2012), making the concepts of PL and SL inapplicable to pile driving.

3.2.1 Practical Spreading Loss Model

The NMFS (2018b) spreadsheet's PSLM extrapolation is carried out using the TL estimation described in **Figure 3-1**.

Equation 4-1

*Transmission loss (dB) = F*log(D_1/D_2)*

Where:

D_1 = The distance from which transmission loss is calculated (usually 10 meters).

D_2 = The distance at which the targeted transmission loss occurs.

F = A site-specific attenuation factor based on several conditions, including water depth, pile type, pile length, substrate type, and other factors.

Transmission loss (TL) = The initial sound pressure level (dB) produced by a sound source (i.e., pile driving) *minus* the ambient sound pressure level or a target sound pressure level (e.g., the injury threshold for salmon). TL also can be thought of as the change in sound pressure level between D_1 and D_2. As applied here TL is a negative number.

Figure 3-1. Equation for transmission loss used by the Practical Spreading Loss Model (From: Caltrans, 2015).

Incorporating the TL estimation results in the following expressions for L_E, $L_{p,\mathrm{pk}}$, and $L_{p,\mathrm{rms}}$ respectively:

$$L_E(r) = L_E(r_1) - F \log_{10}\frac{r}{r_1} \text{ dB} \qquad \textit{Equation 3.1}$$

$$L_{p,\mathrm{pk}}(r) = L_{p,\mathrm{pk}}(r_1) - F \log_{10}\frac{r}{r_1} \text{ dB} \qquad \textit{Equation 3.2}$$

$$L_{p,\mathrm{rms}}(r) = L_{p,\mathrm{rms}}(r_1) - F \log_{10}\frac{r}{r_1} \text{ dB} \qquad \textit{Equation 3.3}$$

Where:

L_E = sound exposure level
$L_{p,\mathrm{pk}}$ = peak sound pressure level
$L_{p,\mathrm{rms}}$ = root-mean-square sound pressure level
r_1 = range at which $L(r_1)$ is known, usually near the source (typically 10 m for pile driving)
r = range at which $L(r)$ is to be estimated (for determining impact volume)
F = attenuation factor, site specific; commonly seen as 10logR ($F = 10$), 15logR ($F = 15$), 20logR ($F = 20$)

NMFS recommends $F = 15$, i.e., 15logR (NMFS, 2012b; GARFO, 2016). A constant value of F (independent of range) implies a power law variation of energy flux density, $\sim r^{-\frac{F}{10}}$. For example, 10logR corresponds to cylindrical spreading and 20logR corresponds to spherical spreading. **Figure 3-2** shows a comparison of results from the PSLM as $F = 5, 10, 15$ for the COMPILE workshop and a North Sea wind farm construction event.

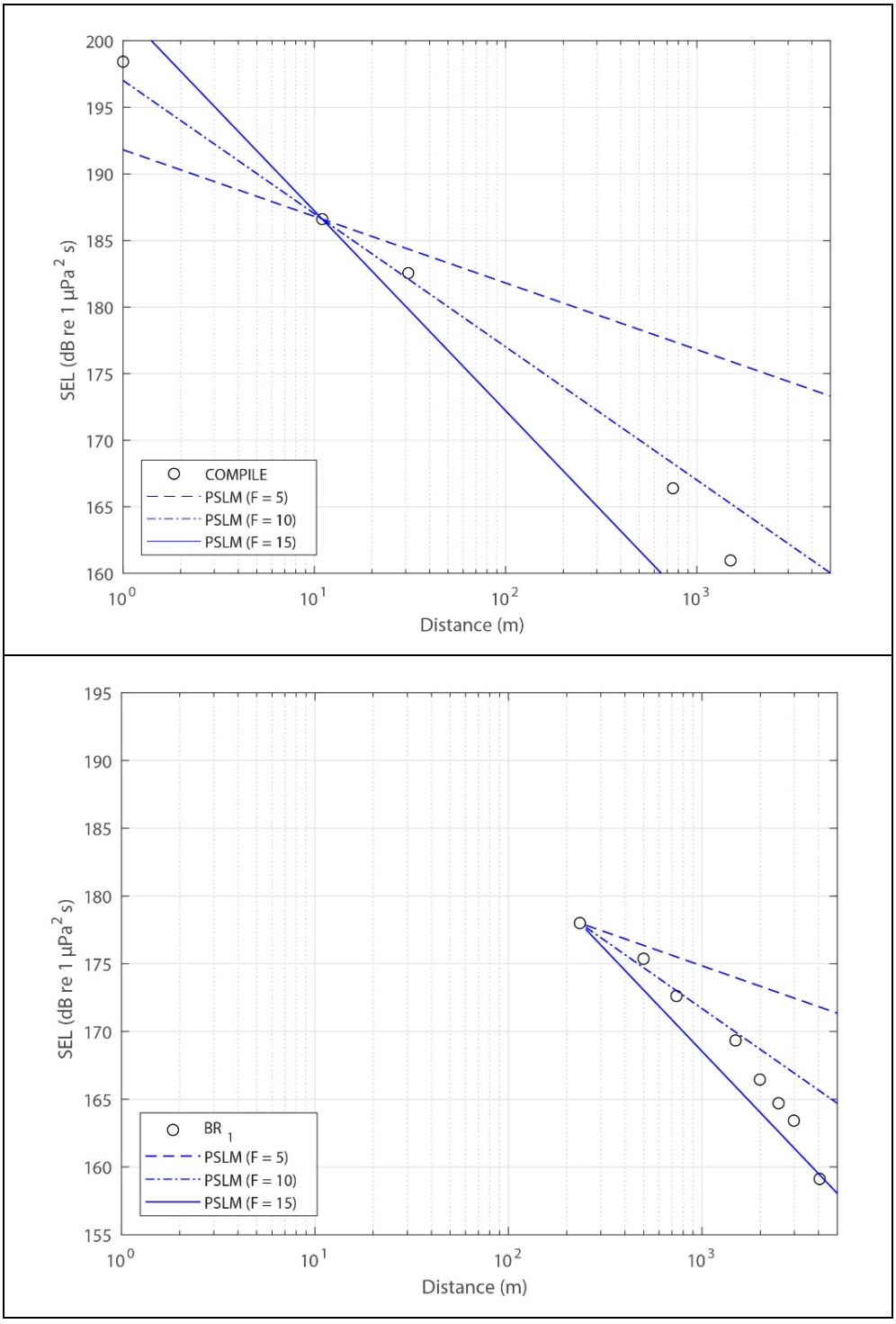

Figure 3-2. SEL versus range using the PSLM

Top: Comparison with simulated measurements for the COMPILE workshop (Lippert et al., 2016), using r_1 = 11 m as the intercept point. Bottom: Comparison with measurements from Borkum Riffgrund 1 (Lippert et al., 2018), using r_1 = 234 m as the intercept point. Straight lines are the Practical Spreading Loss Model based on F = 5, 10, 15. Circles represent real or simulated measurements. µPa = micropascal; dB = decibel; DCS = damped cylindrical spreading; PSLM = Practical Spreading Loss Model; re = with reference to; SEL = L_E = sound exposure level.

The top graph in **Figure 3-2** plots a simulation from the COMPILE workshop (Lippert et al., 2016). The advantage of this situation is that it is a well-specified synthetic scenario. The environment, hammer, and pile parameters were known precisely (because they were specified by the workshop organizers) and there was high confidence in the theoretical prediction (Lippert et al., 2016). A (simulated) measurement at $r_1 = 11$ m was used, which resulted in $L_E(r_1) = 187$ dB; this was the point where all three PSLM lines (F = 5, 10, and 15) were forced to intersect. The PSLM line that worked best out to 1 km was $F = 10$. The PSLM line based on $F = 15$ overestimated L_E at short ranges (<11 m; specifically, $r < r_1$) and underestimated L_E at longer ranges (>11 m; specifically, $r > r_1$). The opposite was true for the PSLM line based on $F = 5$.

The bottom graph in **Figure 3-2** plots the measurements made during construction of the Borkum Riffgrund 1 (BR1) wind farm in the German North Sea (**Figure 3-3**) (Bellmann et al., 2016; ITAP, 2015c). The first measurement position from Lippert et al. (2018), is r_1 at 234 m; this was the point where all three PSLM lines (F = 5, 10, and 15) were forced to intersect. The PSLM line that worked best out to 1 km was $F = 10$. At ranges greater than 234 m (specifically, $r > r_1$), the PSLM lines based on $F = 15$ underestimated the L_E while those based on $F = 5$ overestimated the L_E.

In both graphs, the symbols (representing synthesized or actual measurements) fall below the PSLM lines based on $F = 10$ (i.e., cylindrical spreading) at ranges exceeding 1 km. The deviation increases with increasing range, indicating the received levels were exponentially damped beyond 1 km and did not follow a power law, as is implicitly assumed when using the PSLM.

The PSLM lines based on $F = 10$ (i.e., cylindrical spreading), corresponding to the energy flux density (J) being proportional to the inverse of range ($J \sim r^{-1}$) are expected to work best near the pile. This behavior was predicted theoretically by Zampolli et al. (2013) and demonstrated by Dahl et al. (2012). The cylindrical spreading model proposed by Zampolli et al. (2013) included an exponential damping term (Ainslie et al., 2014; Lippert et al., 2018), which is the DCS model.

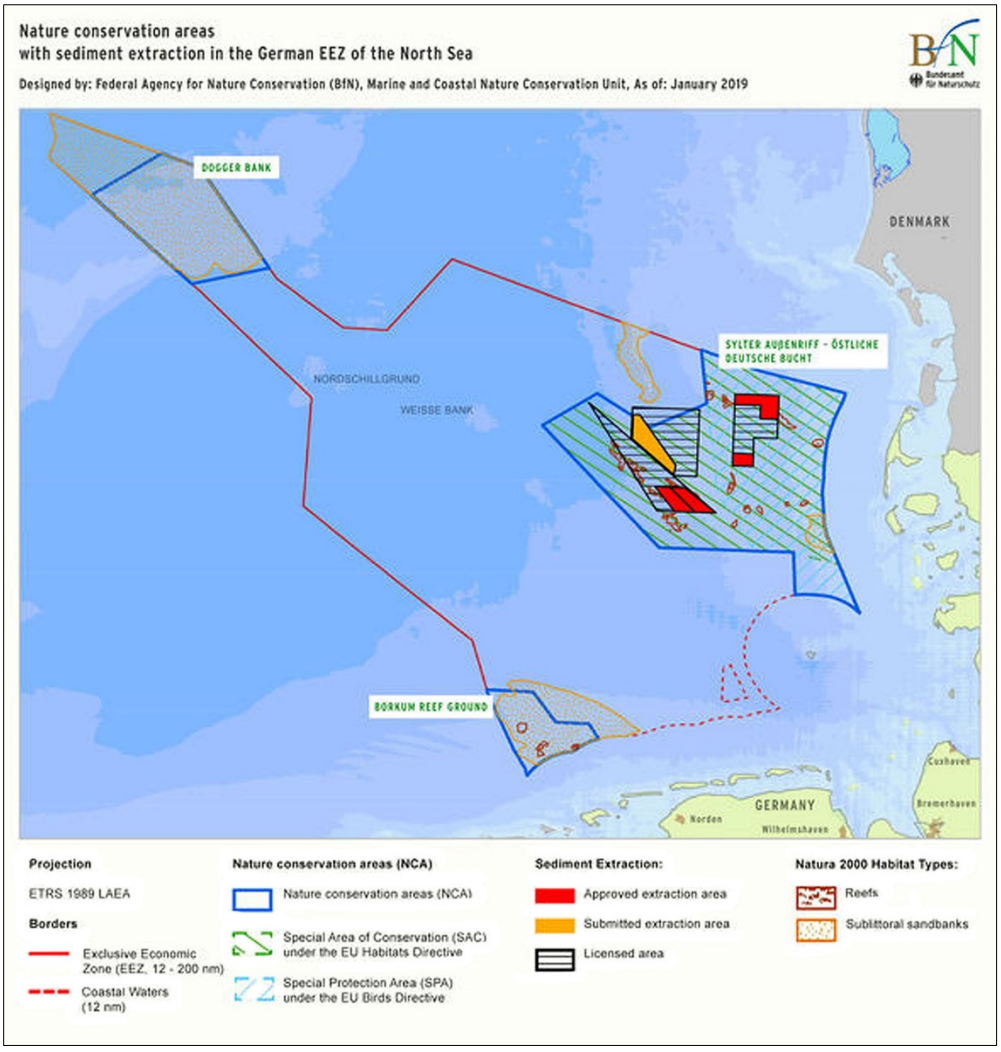

Figure 3-3. Geographical location of the Borkum Riffgrund 1 wind farm in the German North Sea.

3.2.2 Damped Cylindrical Spreading Model for L_E

Close to the pile, the radiated sound field is dominated by the Mach cone (Reinhall and Dahl, 2011; Zampolli et al., 2013; **Section 1.4.1.1**). The Mach cone carries a certain amount of energy, G_0, from the pile. At range r, this energy is spread into area $A = 2\pi rH$, where H = water depth. Ignoring boundary losses, the energy flux density is $J = \frac{G_0}{2\pi rH}$, which corresponds to cylindrical spreading. The attenuation due to multiple boundary reflections needs to be accounted for, where the energy reaching range r can be written as:

$$G = G_0 \exp(-2\alpha r) \qquad \textit{Equation 3.4}$$

Where:

α = attenuation coefficient
r = range from the pile axis of symmetry
G_0 = Mach cone energy

Cylindrical spreading corresponds to using $J = \frac{G}{A}$ for the energy flux density, but it is modified in **Equation 3.4** by exponential decay. The resulting DCS model by Lippert et al. (2018) is:

$$L_E(r) = L_E(r_1) - 10\log_{10}\frac{r}{r_1}\,\text{dB} - \alpha(r - r_1) \qquad \textit{Equation 3.5}$$

Where:

L_E = sound exposure level
r_1 = range at which $L(r_1)$ is known, usually near the source
r = range at which L(r) is to be estimated (for determining impact volume)
α = attenuation coefficient, related to the plane wave reflection coefficient (R) and cycle distance (r_c) according to:

$$\alpha = -\frac{\log_e|R|}{r_c} = -\frac{\log_{10}|R|^2\,\text{dB}}{r_c} \qquad \textit{Equation 3.6}$$

Equation 3.5 has a similar form to **Equation 3.1**, but with three important differences:

- The F coefficient of the $\log_{10}\frac{r}{r_1}$ term in **Equation 3.1** is no longer a variable because the geometry leads naturally to $F = 10$, corresponding to cylindrical spreading.
- The extra αr term provides exponential damping at long ranges.
- The derivation of **Equation 3.5** relies on the energy conservation principle and thus applies only to L_E [calculation of $L_{p,\text{pk}}$ or $L_{p,\text{rms}}$ is addressed in **Section 3.3**]).

The DCS is plotted in **Figure 3-4** for the COMPILE workshop and a BR1 event. The DCS prediction neatly explains the 10logR behavior at short range and the exponential damping beyond 1 km. The DCS follows the shape of the COMPILE simulated values (top graph) and the BR1 field measurements (bottom graph). By contrast, there is no constant value of F for the PSLM that aligns with the observed acoustic behavior. In addition to BR1, the suitability of DCS has been demonstrated by Lippert et al. (2018) for two other German sites: BARD Offshore 1 (BO1) and Global Tech I (GT1). The water depths and attenuation coefficients calculated by Lippert et al. (2018) for COMPILE and the three German sites are listed in **Table 3-1**.

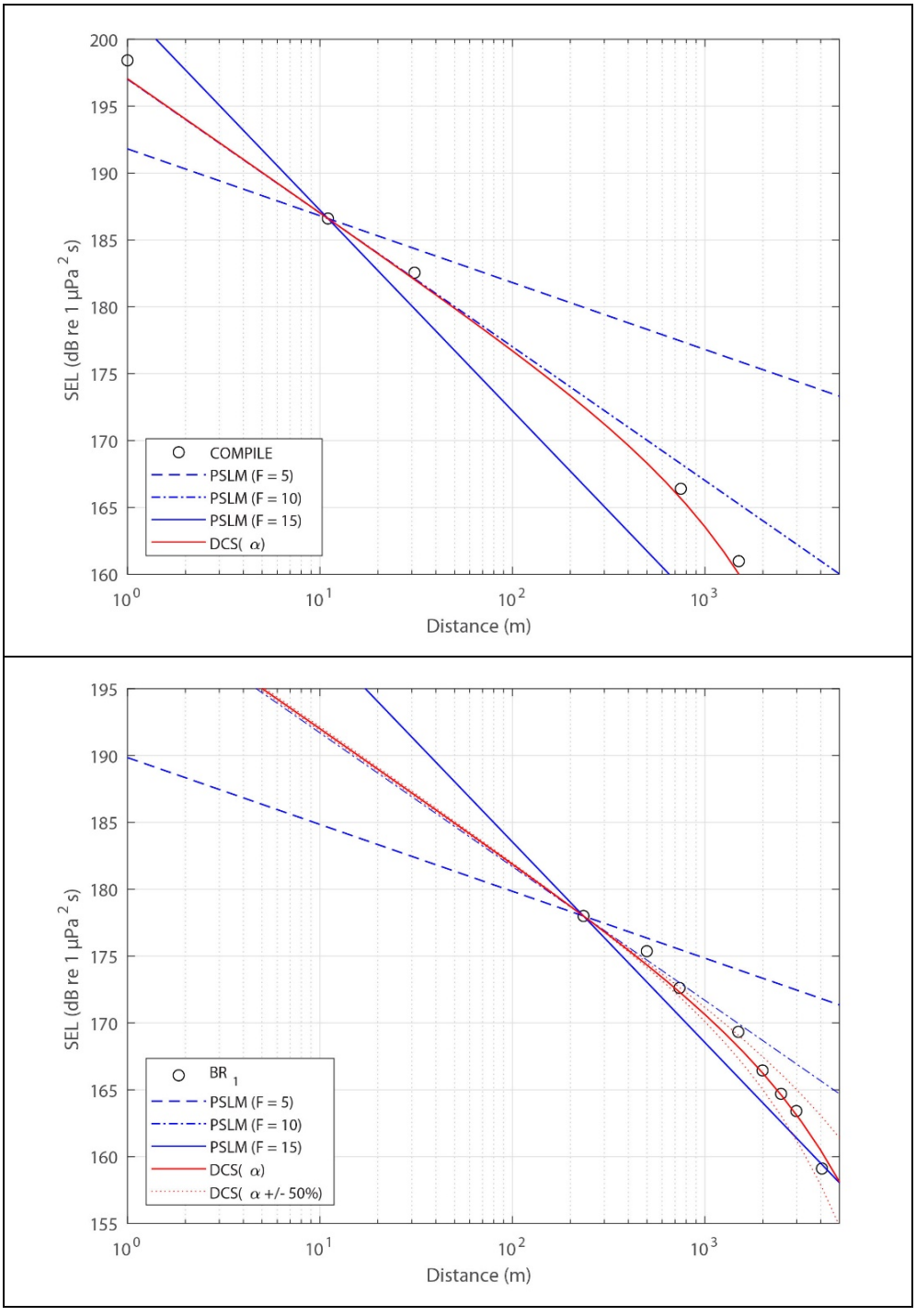

Figure 3-4. SEL versus range using the DCS model

Top: Comparison with simulated measurements from the COMPILE workshop (Lippert et al., 2016), using r_1 = 11 m as the intercept point. Bottom: Comparison with measurements from Borkum Riffgrund 1 (Lippert et al., 2018), using r_1 = 234 m as the intercept point. Straight blue lines are the PSLM based on F = 5, 10, and 15. Circles represent measurements. Red dotted lines illustrate the uncertainty in the DCS curve resulting from a spread of ±50 percent in the attenuation coefficient (α). µPa = micropascal; BR1 = Borkum Riffgrund 1; dB = decibel; DCS = damped cylindrical spreading; PSLM = Practical Spreading Loss Model; re = with reference to; SEL =L_E= sound exposure level.

Table 3-1. Water depth attenuation coefficient for four scenarios.

Scenarios	Water depth (m)	α (dB km^{-1})
COMPILE (simulated site)	10	3.5
BARD Offshore 1 (BO1)[1]	40	1.41
Global Tech I (GT1)[1]	39.5	0.94
Borkum Riffgrund 1 (BR1)[1]	27	1.38

α = attenuation coefficient; dB = decibel; km = kilometer; m = meter.
[1] Lippert et al. (2018).

For the αr term, α is a constant and r is range (variable); the product αr is proportional to range and predicts the total sound attenuation. Nearest to the pile (closer than say 100 m), αr is essentially zero because r is small. As range increases (between 1 and 5 km), this attenuation term becomes increasingly important (**Figure 3-4**). However, at greater ranges (beyond 5 km), the DCS model (which incorporates αr) begins to overestimate the attenuation and deviates from the trend apparent in the COMPILE data (**Figure 3-5**). When DCS is subtracted from the PSLM based on $F = 10$, the DCS is accurate in the region where the difference is less than 20 dB (i.e., αr < 20 dB; **Figure 3-5**). Beyond 20 dB, the TL is not accurately predicted because it appears to follow a power law; therefore, the sound exposure ceases to decay exponentially with range.

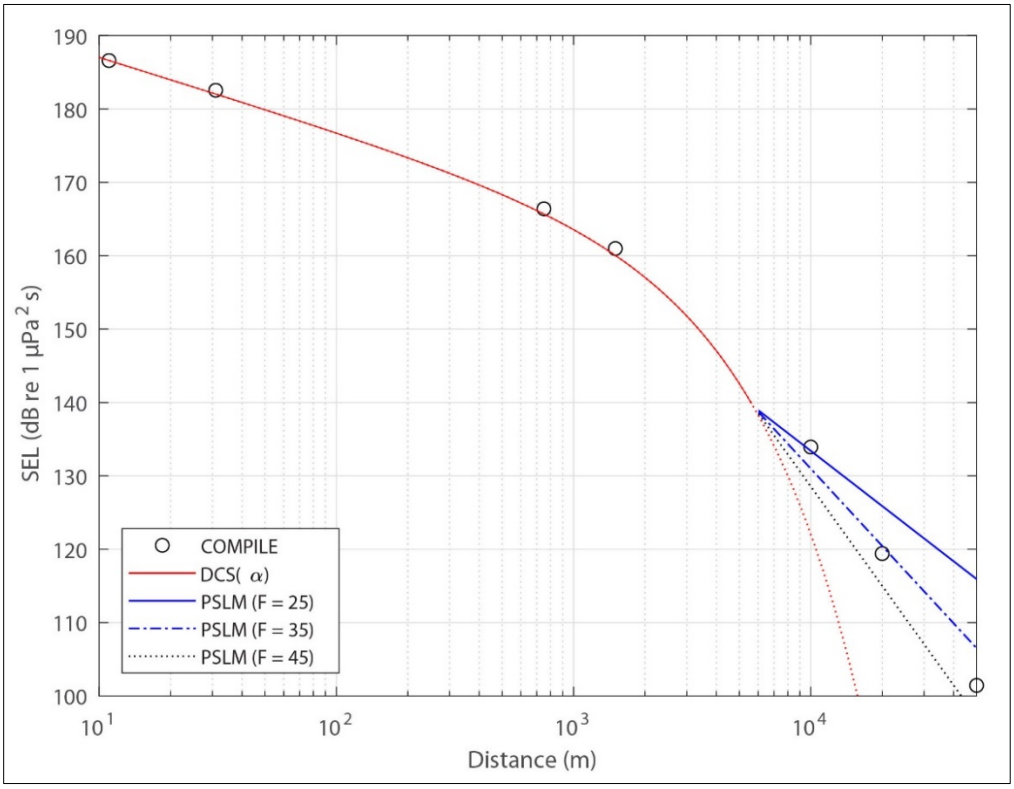

Figure 3-5. COMPILE: SEL versus range using the DCS model.
When the attenuation term (αr) exceeds 20 dB, the damped cylindrical spreading model (red line) overestimates transmission loss, which then underestimates sound exposure level, after which a power law using F = 25, 35, 45 (blue lines) provides a better match to the simulated COMPILE data. µPa = micropascal; dB = decibel; DCS = damped cylindrical spreading; re = with reference to; SEL = L_E= sound exposure level.

3.3 Empirical Regressions for $L_{p,\mathrm{pk}}$ and $L_{p,\mathrm{rms}}$

Using the DCS model, L_E can be predicted up to a few kilometers (the precise maximum range depends on water depth and decay rate; for **Figure 3-5**, it is accurate up to 5 or 6 km). L_E is a natural product of the DCS model because the derivation uses an energy conservation approach. It is also desirable to predict $L_{p,\mathrm{pk}}$ and $L_{p,\mathrm{rms}}$, but these do not follow naturally from DCS. However, $L_{p,\mathrm{pk}}$ is known to be correlated with L_E (Lippert et al., 2015), and a similar correlation is expected between $L_{p,\mathrm{rms}}$ and L_E.

3.3.1 Regressions Based on Lippert et al. (2015)

Lippert et al. (2015) demonstrated an empirical linear correlation (**Figure 3-6**) between L_E and the peak to peak sound pressure level ($L_{p,\mathrm{pk-pk}}$).

$$L_{p,\mathrm{pk-pk}} = AL_E + B_{\mathrm{pk-pk}} \qquad \textit{Equation 3.7}$$

Where:

$L_{p,\mathrm{pk-pk}}$ = peak to peak sound pressure level
A = constant gradient (regression coefficient)
L_E = sound exposure level
$B_{\mathrm{pk-pk}}$ = constant intercept (regression coefficient)

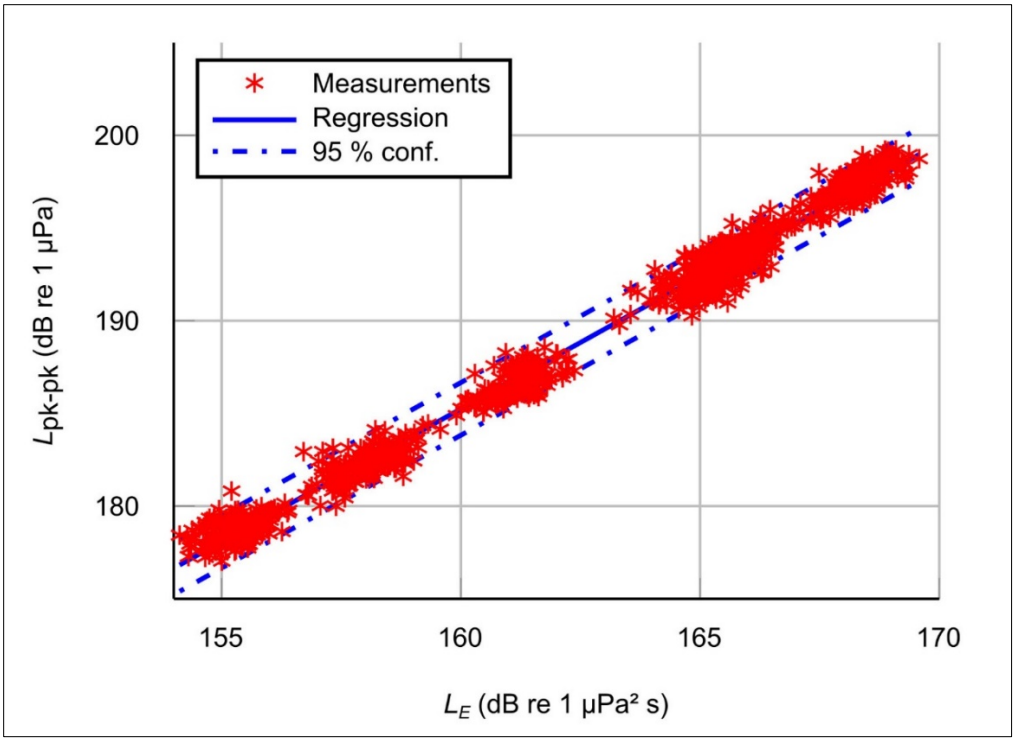

Figure 3-6. Scattergram of $L_{p,\mathrm{pk-pk}}$ versus SEL
Illustrates the correlation between these two quantities for the wind farm construction site Global Tech I (Lippert et al., 2015). µPa = micropascal; dB = decibel; $L_{p,\mathrm{pk-pk}}$ = peak to peak sound pressure level; re = with reference to; SEL = L_E = sound exposure level.

For the present application, focus was on $L_{p,\mathrm{pk}}$, which is related to $L_{p,\mathrm{pk-pk}}$, via the equation:

$$L_{p,\mathrm{pk}} = L_{p,\mathrm{pk-pk}} - \mu \qquad \textit{Equation 3.8}$$

Where:

μ = the difference between $L_{p,\mathrm{pk-pk}}$ and $L_{p,\mathrm{pk}}$ (typically between 5 and 6 dB).

It follows that:

$$L_{p,\mathrm{pk}} = AL_E + B_{\mathrm{pk}} \qquad \textit{Equation 3.9}$$

Where:

$L_{p,\mathrm{pk}}$ = peak sound pressure level
A = constant gradient (regression coefficient)
L_E = sound exposure level
B_{pk} = constant intercept (regression coefficient)

Therefore (**Table 3-2**):

$$B_{\mathrm{pk}} = B_{\mathrm{pk-pk}} - \mu \qquad \textit{Equation 3.10}$$

Table 3-2. Coefficients A, $B_{\mathrm{pk-pk}}$, and the derived values of B_{pk}.

Site[1]	A	$B_{\mathrm{pk-pk}}$	μ	$B_{\mathrm{pk}} = B_{\mathrm{pk-pk}} - \mu$
BARD Offshore I (BO1)	1.40	-43.4 dB	5.7 dB	-49.1 dB
Global Tech I (GT1)	1.39	-39.4 dB	5.3 dB	-44.7 dB
Borkum Riffgrund I (BR1)	1.43	-44.0 dB	5.7 dB	-49.7 dB

μ = difference between peak-to-peak and zero-to-peak sound pressure; A = constant gradient; B = constant intercept; dB = decibel.
[1] Lippert et al. (2015).

3.3.2 Regressions Based on Luchterduinen Measurements

The DCS model provides a reliable means of predicting L_E up to a few kilometers from an impact-driven pile. For the acoustic injury criteria, $L_{p,\mathrm{pk}}$ is also needed, which cannot be calculated directly using DCS because the output of DCS is L_E, not $L_{p,\mathrm{pk}}$. Nevertheless, a strong correlation is known to exist between $L_{E,\mathrm{ss}}$ and $L_{p,\mathrm{pk}}$ (Lippert et al., 2015), and this correlation can be exploited to estimate $L_{p,\mathrm{pk}}$ if L_E is known.

In principle, a correlation obtained for one of the three sites analyzed by Lippert et al. (2015) could be applied, unmodified, to another site. Alternatively, data could be analyzed from multiple sites to obtain a more generally applicable correlation, and that is the method used for this project. Measurements made of the installation of two monopiles (EL39 and EL42) during construction of the Luchterduinen wind farm were analyzed (**Figure 3-7**). The measurement ranges from the piles are provided in **Table 3-3**. The locations of the Luchterduinen and other wind farms are shown in **Figure 3-8**.

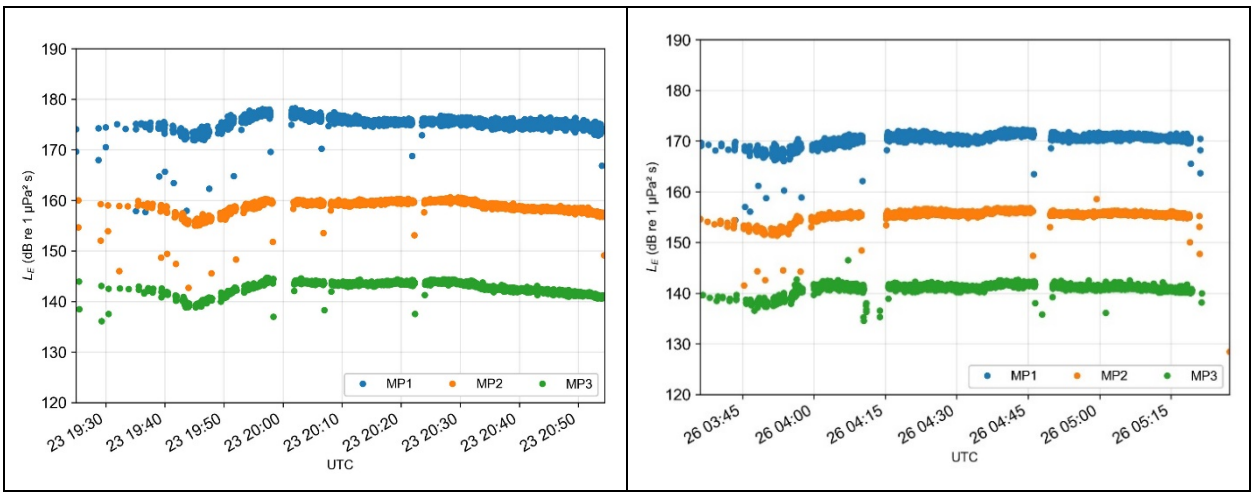

Figure 3-7. SEL at Luchterduinen wind farm.
For two monopiles (left: EL39; right: EL42), the sound exposure level per hammer blow at three measurement ranges, 2 m above the seafloor (From: ITAP, 2015a). µPa = micropascal; dB = decibel; re = with reference to; SEL = L_E = sound exposure level.

Table 3-3. Ranges of measurement positions for Luchterduinen monopiles EL39 and EL42.

Monopile ID	Position (km)	Position 2 (km)	Position 3 (km)
EL39[1]	0.75	4.72	13.23
EL42[1]	0.75	5.24	13.75

km = kilometer.
[1] ITAP (2015a).

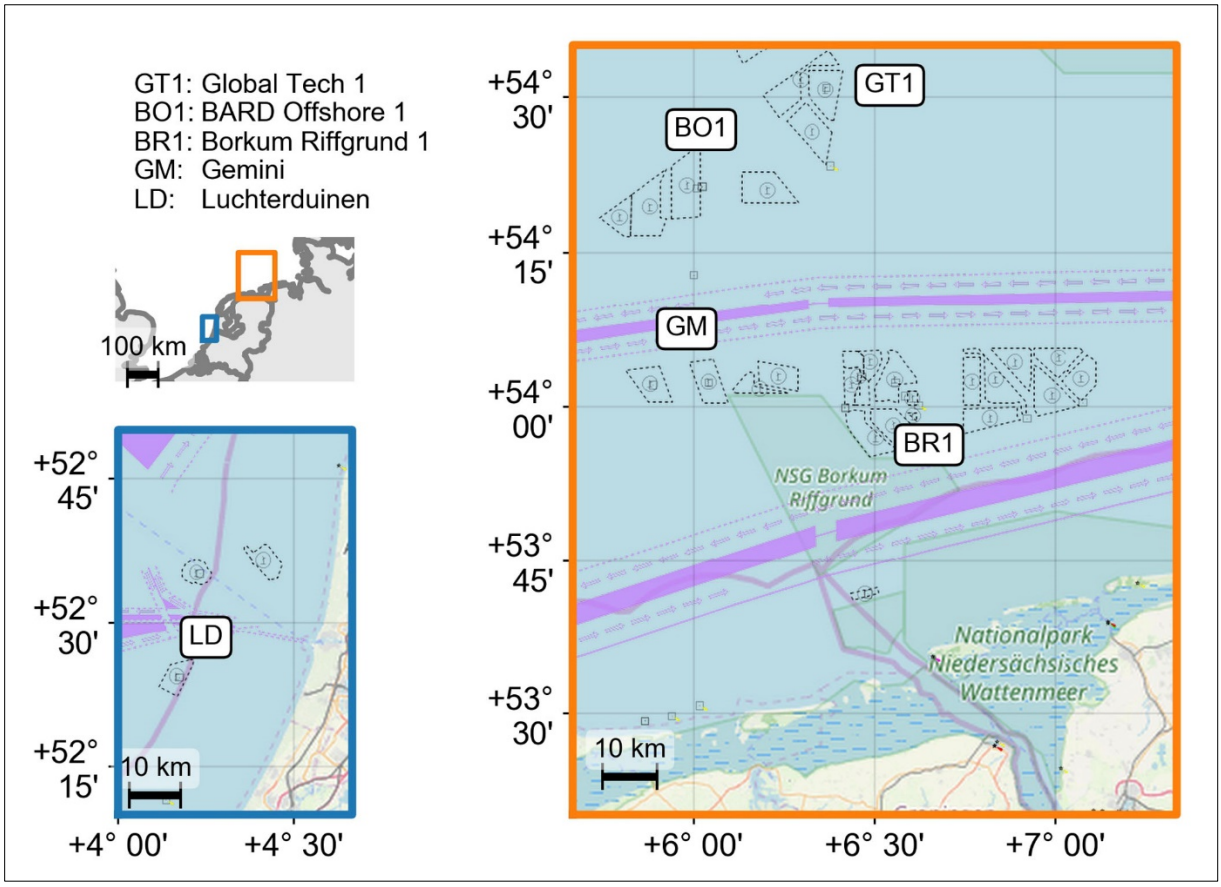

Figure 3-8. Location of the relevant wind farms.
Left: Wind farms off the western Dutch coast. Right: Wind farms off the northern Dutch-German coast (Images from: thematicmapping.org, map.openseamap.org, www.openstreetmap.org).

Correlation Between L_E and $L_{p,\mathrm{pk}}$

In the following text, only B_{pk} (not $B_{\mathrm{pk-pk}}$) will be discussed; thus, the subscript will be dropped, making no further distinction between B and B_{pk}. Lippert et al. (2015) demonstrated a strong correlation that $L_{p,\mathrm{pk}}$ is approximately equal to $AL_E + B$. For this project, a similar analysis was performed on the EL39 and EL42 data, and the results show that although such a relation can be found (**Figure 3-9**), the coefficients (**Table 3-4**) are different from those determined by Lippert et al. (2015; **Table 3-2**). The comparable data from **Table 3-2** are included at the bottom of **Table 3-4**. The last column of **Table 3-4** lists the spread of the $L_{p,\mathrm{pk}}$ to L_E distribution (uncertainty in $L_{p,\mathrm{pk}}$ for fixed L_E), which defines the vertical deviation from the correlation line where 95% of the data points are found (i.e., $B_{95\%}$). In other words, 95% of the $L_{p,\mathrm{pk}}$ values are within $B_{95\%}$ of the regression line.

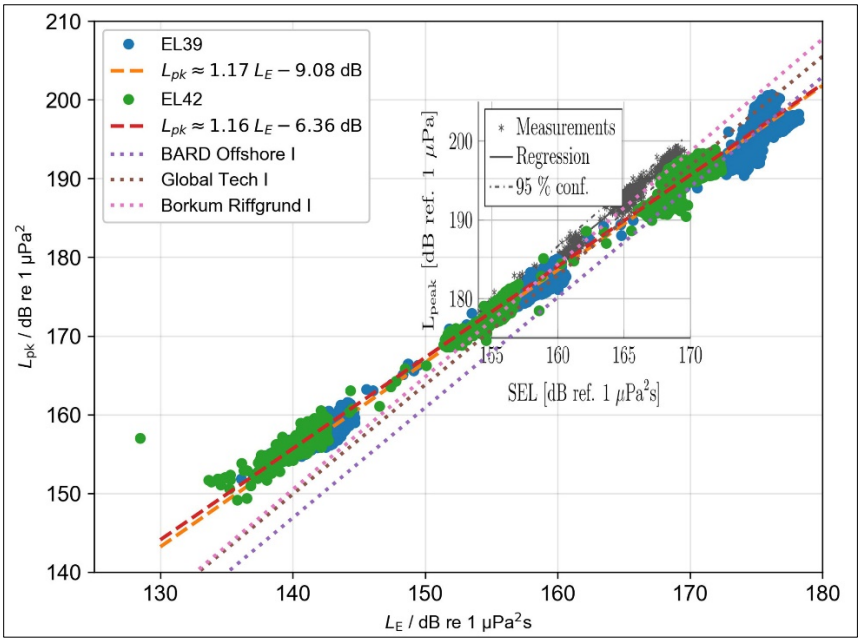

Figure 3-9. Linear regression analysis comparing SEL and $L_{p,\mathrm{pk}}$.

The inset is the original figure by Lippert et al. (2015) for Global Tech I, shown as grayscale, and scaled to match the main graph's x-axis, while the y-axis does not coincide because of the offset between $L_{p,\mathrm{pk-pk}}$ and $L_{p,\mathrm{pk}}$. Colored dots represent measured data, and each straight line is an individual correlation as specified in the legend.
µPa = micropascal; dB = decibel; $L_{p,\mathrm{pk}}$ = peak sound pressure level; $L_{p,\mathrm{pk-pk}}$ = peak to peak sound pressure level; re = with reference to; SEL = L_E = sound exposure level.

Table 3-4. Linear regression coefficients relating $L_{p,\mathrm{pk}}$, $L_{p,90\%}$, and $L_{p,\mathrm{eff}}$ to L_E at Luchterduinen EL39 and EL42

Acoustic metric	Luchterduinen monopile ID	A	B (dB)	95% confidence bound[1] $B_{95\%}$ (dB)
$L_{p,\mathrm{pk}}$	EL39	1.172	-9.1	2.1
	EL42	1.157	-6.4	1.5
	EL39 and EL42	1.162	-7.3	1.8
$L_{p,90\%}$	EL39	1.172	-18.7	1.6
	EL42	1.132	-12.0	1.5
	EL39 and EL42	1.150	-15.0	1.7
$L_{p,\mathrm{eff}}$	EL39	1.185	-17.9	1.5
	EL42	1.175	-15.3	1.1
	EL39 and EL42	1.176	-15.8	1.5
Lippert et al. (2015)				
--	Wind farm site	A	B (dB)	--
$L_{p,\mathrm{pk}}$	BARD Offshore I (BO1)	1.40	-49.1	--
	Global Tech I (GT1)	1.39	-44.7	--
	Borkum Riffgrund I (BR1)	1.43	-49.7	--

-- = not applicable; *A* = constant gradient; *B* = constant intercept; dB = decibel; L_E = sound exposure level; $L_{p,\mathrm{eff}}$ = effective sound pressure level; $L_{p,\mathrm{pk}}$ = peak sound pressure level; $L_{p,90\%}$ = 90% energy sound pressure level.
[1] The distance within which 95% of the measurements lie (difference between the 2.5% and 97.5% percentiles).

The difference between the three sets of coefficients (for EL39, EL42, and the average of EL39 combined with EL42) is small. Therefore, only the coefficients from the averaged combined data set are considered further.

Lippert et al. (2015) wrote about the piling situations in the North Sea:

> *These sites represent different environmental conditions and source types, with water depths ranging from 27 to 40 m, strongly varying pile dimensions, and different foundation types, i.e., tri-piles, tripods and mono piles. The acoustic far-field measurements for these sites were taken at ranges varying from 250 to 5,000 m from the pile, and at a depth of approximately 2 m above the seafloor. In all three cases, no sound mitigation system was employed during the measurements.*

The description of the study sites was compared to the conditions for the Luchterduinen and Gemini wind farms (**Table 3-5**). Furthermore, the sediment type between the Lippert et al. (2018) study sites and the two Dutch sites, Luchterduinen and Gemini (ITAP, 2015a,b), was medium sand.

Table 3-5. Comparison of depths and ranges between the current investigation and Lippert et al. (2015).

Study site and monopile ID	Site water depth (m)	Minimum measurement range (km)	Maximum measurement range (km)	Sediment type
Lippert et al. (2015)	Minimum: 27; Maximum: 40	0.25	5.0	Medium sand
Current study				
Luchterduinen EL39	21.5	0.75	31.0	Medium sand
Luchterduinen EL42	20.6	0.75	13.8	Medium sand
Gemini U8	34.1	0.73	66.0	Medium sand
Gemini Z2	30.0	0.73	66.0	Medium sand

km = kilometer; m = meter.

Correlation Between L_E and $L_{p,\mathrm{rms}}$

In addition to L_E and $L_{p,\mathrm{pk}}$, the $L_{p,\mathrm{rms}}$ was used for acoustic criteria. To incorporate $L_{p,\mathrm{rms}}$, two different calculations were introduced: (1) 90% energy sound pressure level ($L_{p,90\%}$) averaged over the 90% energy signal duration (90% is assumed to be used in typical calculations of this metric), and (2) effective sound pressure level ($L_{p,\mathrm{eff}}$) derived from the effective signal duration; a new approach employed during this project for addressing the $L_{p,\mathrm{rms}}$ metric and its inherent variability.

Correlation Between L_E and $L_{p,90\%}$

A correlation analysis was performed by replacing $L_{p,\mathrm{pk}}$ with $L_{p,90\%}$, defined by:

$$L_{p,90\%} = 10 \log_{10} \left(\frac{0.9\, E/\tau_{90}}{p_0^2} \right) \mathrm{dB}\,, \qquad \textit{Equation 3.11}$$

Where:

$p_0 = 1$ µPa
$L_{p,90\%}$ = 90% energy sound pressure level
τ_{90} = 90% energy signal duration
E = single strike sound exposure (100% energy)

The results of replacing $L_{p,\mathrm{pk}}$ with $L_{p,90\%}$ are shown with the results of $L_{p,\mathrm{pk}}$ in **Figures 3-10** to **3-12**. The resulting coefficients for $L_{p,90\%}$ are listed in **Table 3-4**.

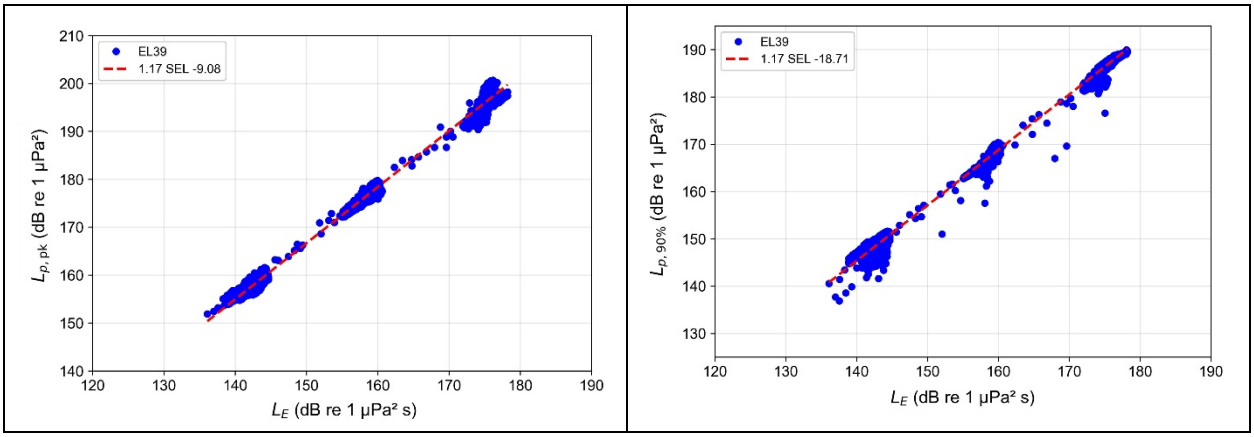

Figure 3-10. Correlations at Luchterduinen EL39.
Left: Correlations between peak sound pressure level, 'Lpk' ($L_{p,\mathrm{pk}}$), and sound exposure level (L_E). Right: Correlations between the 90% energy sound pressure level, 'L90' ($L_{p,90\%}$), and L_E. Colored dots are measured data; straight lines are correlations. µPa = micropascal; dB = decibel; $L_{p,\mathrm{pk}}$ = peak sound pressure level; re = with reference to; SEL = L_E = sound exposure level.

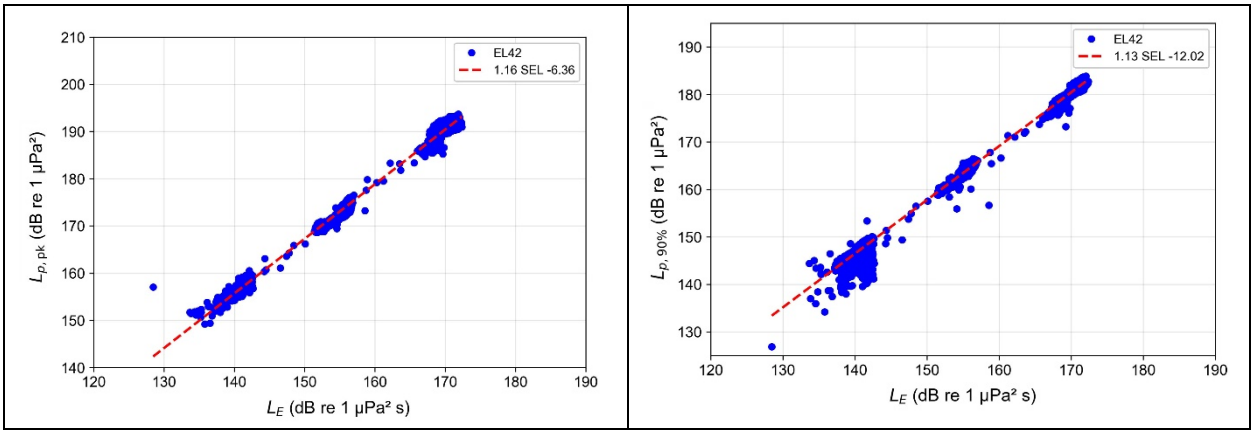

Figure 3-11. Correlations at Luchterduinen EL42.
Left: Correlations between peak sound pressure level ($L_{p,\mathrm{pk}}$) and sound exposure level (L_E). Right: Correlations between the 90% energy sound pressure level ($L_{p,90\%}$) and L_E . µPa = micropascal; dB = decibel; $L_{p,\mathrm{pk}}$= peak sound pressure level; re = with reference to; SEL = L_E = sound exposure level.

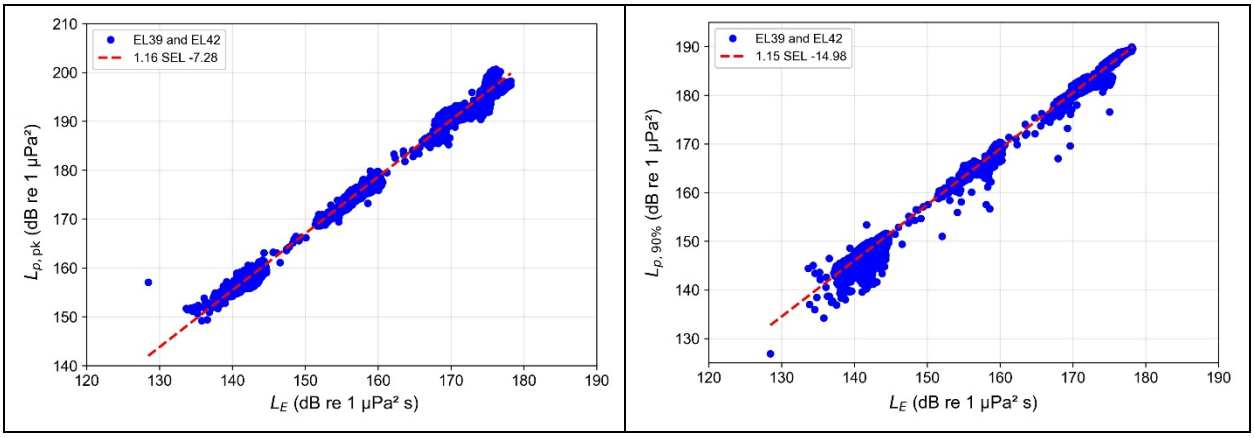

Figure 3-12. Correlations at Luchterduinen EL39 and EL42.
Left: Correlations between peak sound pressure level ($L_{p,\mathrm{pk}}$) and sound exposure level (L_E). Right: Correlations between the 90% energy sound pressure level ($L_{p,90\%}$) and L_E. µPa = micropascal; dB = decibel; $L_{p,\mathrm{pk}}$ = peak sound pressure level; re = with reference to; SEL = L_E = sound exposure level.

Correlation Between L_E and $L_{p,\mathrm{eff}}$

In **Figure 3-12**, the spread in $L_{p,90\%}$ (right graph) for a fixed L_E is noticeably larger than the corresponding spread in $L_{p,\mathrm{pk}}$ (left graph). This spread is attributed to a spread in the 90% energy signal duration, τ_{90}. A signal consisting of two bursts, caused by the bounce of a hammer, will show variation in $L_{p,90\%}$, depending on the interval between the bursts, and the proportion of the total energy contained in the weaker burst. Therefore, in this section, an alternative to $L_{p,90\%}$ was considered for the $L_{p,\mathrm{rms}}$.

The alternative is motivated by the arbitrary choice of 90% energy for the averaging window (e.g., *why should 90% be preferred over 50% or 99%?*) and suggests the effective duration of the envelope function (Burdic, 1991) for the entire pulse, thus precluding the need for an arbitrary choice for the duration. This duration is the effective signal duration, τ_{eff} (defined in **Appendix A**), which is strongly correlated with but shows less variability than τ_{90} (**Figure 3-13**, left graph).

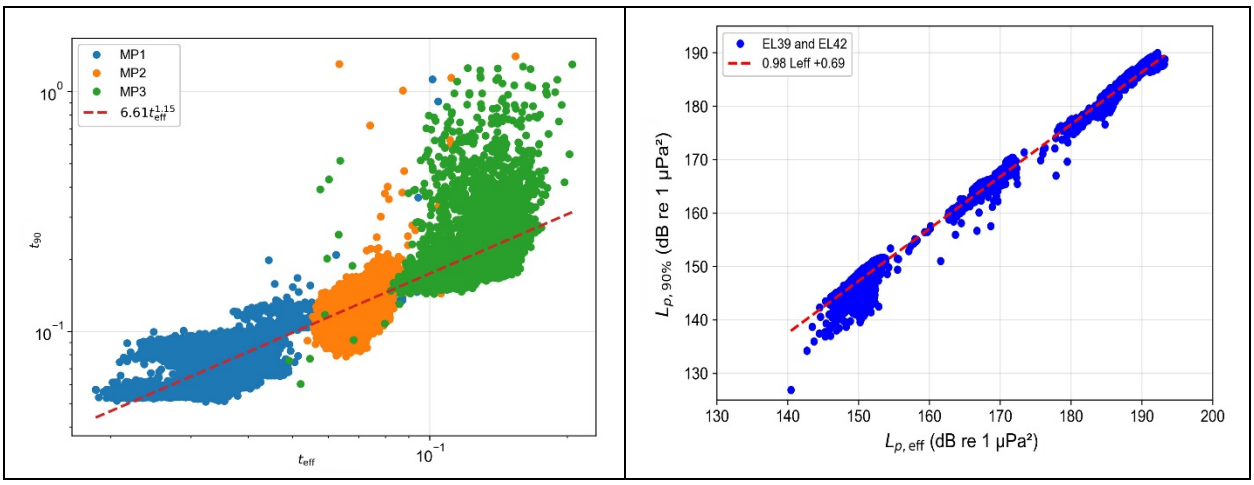

Figure 3-13. Correlations at Luchterduinen EL42.

Left: EL42, correlations between effective signal duration (τ_{eff}) and the 90% signal duration (τ_{90}), both in seconds. Right: EL42 and EL39 combined, correlations between 90% energy sound pressure level ($L_{p,90\%}$) and effective sound pressure level ($L_{p,\text{eff}}$). Colored dots are measured data; straight lines are correlations. µPa = micropascal; dB = decibel; re = with reference to; SEL = L_E = sound exposure level.

Given a value of τ_{eff} of a pulse, it seems natural to introduce an effective value of the mean-square sound pressure (MSP), defined as the value of MSP that, if held constant for a signal of duration τ_{eff}, would result in the observed sound exposure of that pulse, E. In other words, $E = \left(\overline{p^2}\right)_{\text{eff}}\tau_{\text{eff}}$, or (equivalently) $\left(\overline{p^2}\right)_{\text{eff}} = \frac{E}{\tau_{\text{eff}}}$. Thus, the effective sound pressure level ($L_{p,\text{eff}}$) is the sound pressure level corresponding to a pulse whose sound exposure, E, is compressed into a time interval of duration τ_{eff} that captures the main energy of the signal:

$$L_{p,\text{eff}} = 10\log_{10}\left(\frac{E/\tau_{\text{eff}}}{p_0^2}\right)\text{dB}\,, \qquad \textit{Equation 3.12}$$

where:

$p_0 = 1$ µPa
$L_{p,\text{eff}}$ = effective sound pressure level
τ_{eff} = effective signal duration
E = single strike sound exposure.

The right graph of **Figure 3-13** illustrates the spread in $L_{p,90\%}$ (for fixed $L_{p,\text{eff}}$), which is a result of the scatter in τ_{90} (for fixed τ_{eff}). The scatter is visible in the left graph. This reduced scatter in $L_{p,\text{eff}}$ results in better correlation between $L_{p,\text{eff}}$ and L_E (**Figures 3-14** and **3-15**). Therefore, it would be reasonable to use $L_{p,\text{eff}}$ instead of $L_{p,90\%}$ to lead to a more robust estimate of $L_{p,\text{rms}}$.

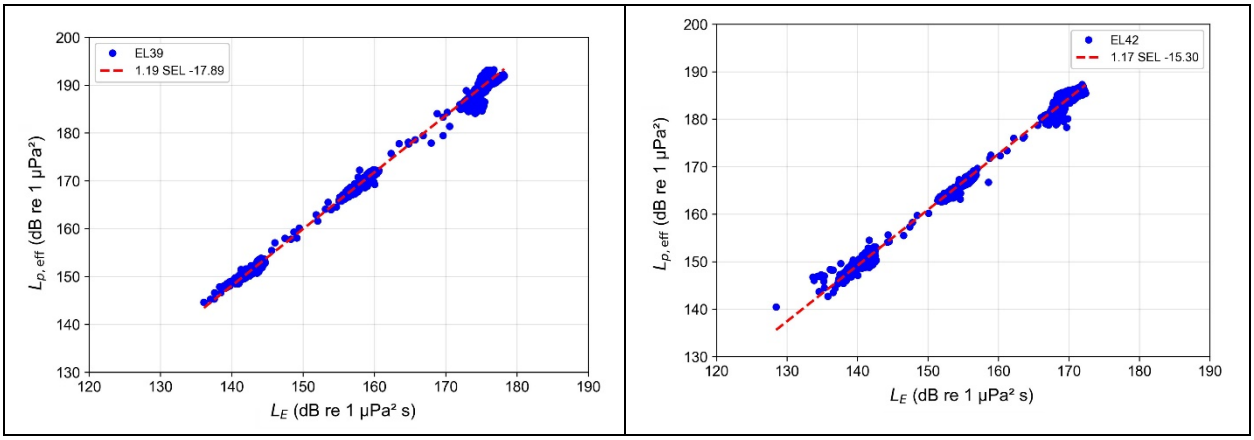

Figure 3-14. Correlations at Luchterduinen EL42 and EL39.
Left: EL39, correlations between effective sound pressure level, L_{eff} ($L_{p,\mathrm{eff}}$) and sound exposure level (L_E). Right: EL42, correlations between $L_{p,\mathrm{eff}}$ and L_E. Colored dots are measured data; straight lines are correlations. µPa = micropascal; dB = decibel; re = with reference to; SEL =L_E= sound exposure level.

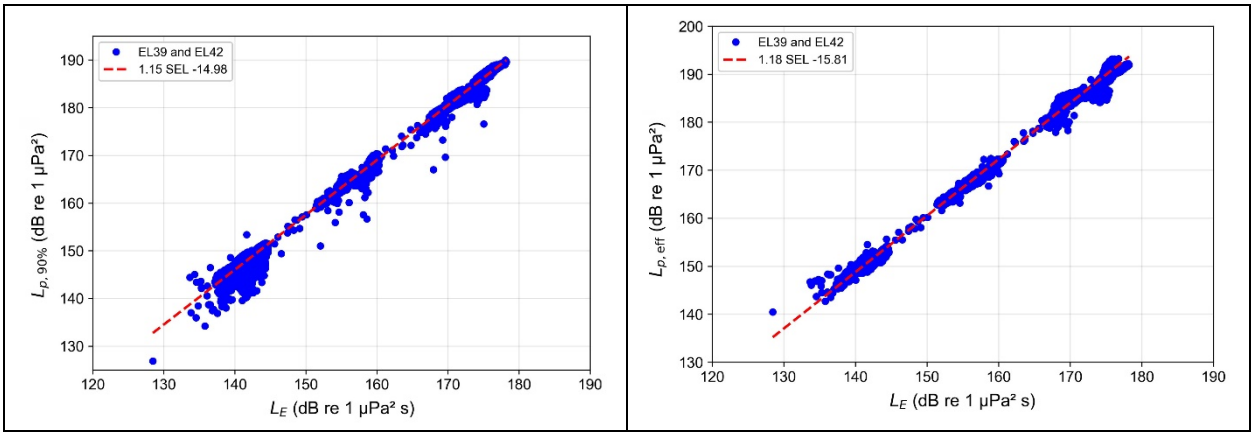

Figure 3-15. Correlations at Luchterduinen EL42 and EL39.
Left: EL39 and EL42, correlations between 90% energy sound pressure level, L90 ($L_{p,90\%}$) and sound exposure level (L_E). Right: EL39 and EL42, correlations between effective sound pressure level, L_{eff} $\left(L_{p,\mathrm{eff}}\right)$ and L_E. Colored dots are measured data; straight lines are correlations. µPa = micropascal; dB = decibel; re = with reference to; SEL = L_E= sound exposure level.

To emphasize the benefit of using $L_{p,\mathrm{eff}}$, one final comparison is provided, plotting $L_{p,\mathrm{eff}}$ alongside $L_{p,\mathrm{pk}}$ (**Figure 3-16**). The small spread on both graphs is immediately apparent, indicating strong correlations with L_E in both cases. There also is a similarity in shape that is not apparent from **Figure 3-13**, suggesting further correlation between $L_{p,\mathrm{eff}}$ and $L_{p,\mathrm{pk}}$.

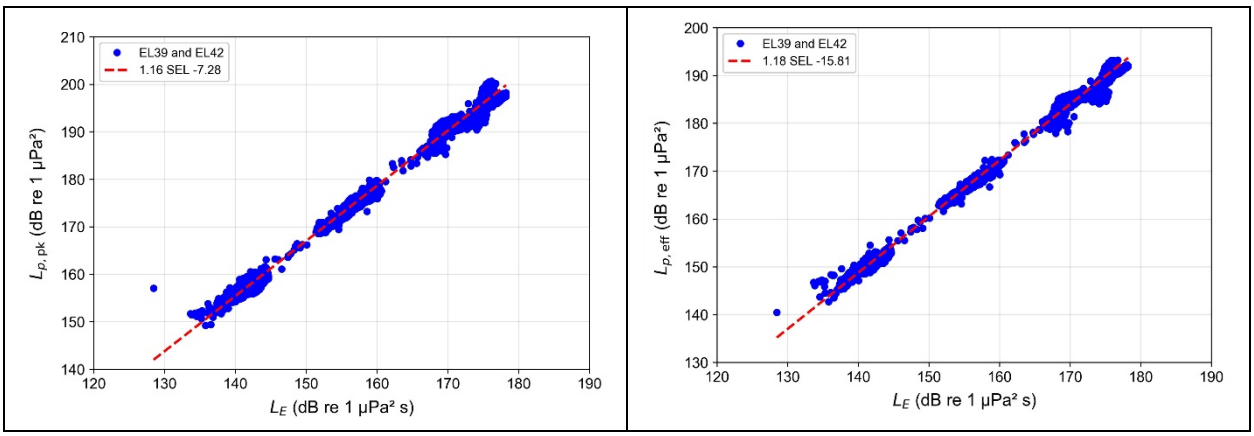

Figure 3-16. Correlations at Luchterduinen EL39 and EL42.
Left: EL39 and EL42, correlations between peak sound pressure level, L_{pk} ($L_{p,\mathrm{pk}}$) and SEL (L_E). Right: EL39 and EL42, correlations between effective sound pressure level, L_{eff} ($L_{p,\mathrm{eff}}$) and SEL (L_E). Blue dots are measured data; straight lines are correlations. µPa = micropascal dB = decibel; re = with reference to; SEL = L_E = sound exposure level.

3.3.3 Regressions Based on Combining all Four Data Sets

Thus far, the data sets considered in the regression analyses were the Dutch site (Luchterduinen) and three German sites (BO1, GT1, and BR1), separately. One final regression analysis on the measurements from all four sites combined yielded the coefficients $A = 1.201$ and $B = -12.8$ dB.

3.3.4 Extrapolating to Long Range

As seen in **Figure 3-5**, the DCS is limited to $\alpha r < 20$ dB, at least for the theoretical example from the COMPILE workshop. However, at longer ranges, the mechanism is unclear, and the acoustics follow a different propagation behavior. Based on **Figure 3-5**, preliminary indications are that a power law is followed at ranges beyond $\alpha r = 20$ dB. This power law seems to correspond to application of the PSLM with a value of F between 25 and 45. Measurements are needed to support any modeling for this region to be certain. Until such measurements are available, extrapolating DCS predictions to distances beyond $\alpha r = 20$ dB could be done using the PSLM with $F = 25$, as a precautionary interim approach.

3.4 Recommendations for Predicting L_E, $L_{p,\mathrm{pk}}$, and $L_{p,\mathrm{rms}}$

Step 1 (L_E):

Calculate L_E as a function of a measurement (from the center of the monopile) at range r_1 using **Equation 3.5** and determine α using **Equation 3.6**. For best results, range r_1 should be chosen in the region where the cumulative reflection loss is small, such that $\alpha r_1 < N_1$ dB, where N_1 is a constant to be decided. For example, choosing $N_1 = 3$ gives:

$$r_1 < \frac{3 \text{ dB}}{\alpha} \qquad \textit{Equation 3.13}$$

where:

α = attenuation coefficient

r_1= range for L_E measurement.

The DCS formula is assumed valid up to a maximum range determined by $\alpha r_2 = N_2$ dB. Assuming $N_2 = 20$ (**Figure 3-5**), the condition becomes:

$$r < r_2 \qquad \textit{Equation 3.14}$$

where:

r_2 = range limit of maximum range validity (= (20 dB)/ α).

Continuing with the example, if $\alpha = 2$ dB/km (corresponding to a cycle distance of 200 m and a reflection loss of 0.4 dB per cycle; **Equation 3.6**), then **Equations 3.13** and **3.15** yield the constraints $r_1 < 1.5$ km for the measurement position and $r < 10$ km for the limit of maximum range validity. While these values seem plausible, they have not been tested.

At ranges exceeding r_2, where $r_2 = (20 \text{ dB})/\alpha$, the suggested (and untested) PSLM extrapolation with $F = 25$ results in:

$$L_E(r) = L_E(r_2) - 25 \log_{10} \frac{r}{r_2} \text{ dB} \qquad \textit{Equation 3.15}$$

Step 2 ($L_{p,\text{pk}}$):

From Step 1, given a value of L_E at a range of interest, the $L_{p,\text{pk}}$ can be estimated at the same range using the coefficients (A = 1.201 and B = 12.8) derived by combining the Luchterduinen data set with the three German sites:

$$L_{p,\text{pk}} = 1.201 L_E - 12.8 \text{ dB} \qquad \textit{Equation 3.16}$$

Step 3 ($L_{p,\text{rms}}$):

$L_{p,90\%}$ or $L_{p,\text{eff}}$ can be estimated from L_E in the same way as $L_{p,\text{pk}}$, using the linear regression coefficients in **Table 3-4**:

$$L_{p,90\%} = 1.150 L_E - 15.0 \text{ dB} \qquad \textit{Equation 3.17}$$

and

$$L_{p,\text{eff}} = 1.176 L_E - 15.8 \text{ dB}. \qquad \textit{Equation 3.18}$$

Worked Example

Step 1: Consider a measurement of $L_E = 160$ dB made at $r_1 = 0.2$ km, with a decay rate (calculated using **Equation 3.6**) of $\alpha = 2.3$ dB/km (corresponding to a water depth of 20 m, Mach cone angle of 17°, and reflection loss of 0.3 dB per cycle). Substituting these values into **Equation 3.5** gives (for $R < R_2 = 8.7$):

$$\frac{L_E(R)}{\text{dB}} = 160.0 - 10\log_{10}\frac{R}{0.2} - 2.3(R - 0.2)$$

where L/dB is the level in decibels and R is the range in kilometers. It follows that:

$$\frac{L_E}{\text{dB}} = 153.5 - 10.0\log_{10} R - 2.30R \quad R < 8.70.$$

At ranges exceeding $R_2 = 8.7$, the PSLM with $F = 25$ gives:

$$\frac{L_E}{\text{dB}} = 133.5 - 25\log_{10}\frac{R}{R_2} \quad R > 8.70,$$

i.e.,

$$\frac{L_E}{\text{dB}} = 147.6 - 25\log_{10} R \quad R > 8.70.$$

Step 2: Substituting the result from Step 1 into **Equation 3.16** gives (for $R < 8.7$):

$$\frac{L_{p,\text{pk}}}{\text{dB}} = 1.201(153.5 - 10\log_{10}R - 2.3R\ ) - 12.8,$$

therefore:

$$\frac{L_{p,\text{pk}}}{\text{dB}} = 171.5 - 12.0\log_{10}R - 2.76R.$$

Application of **Equation 3.16** to the L_E formula for ranges exceeding 8.7 km gives:

$$\frac{L_{p,\text{pk}}}{\text{dB}} = 1.201(147.6 - 25\log_{10}R\ ) - 12.8$$

$$\frac{L_{p,\text{pk}}}{\text{dB}} = 164.5 - 30.0\log_{10}R.$$

Step 3: Substituting the result from Step 1 into **Equations 3.17** and **3.18** results in the following equations for $L_{p,90\%}$ and $L_{p,\text{eff}}$, respectively (for $R < 8.7$):

$$\frac{L_{p,90\%}}{\text{dB}} = 1.150(153.5 - 10\log_{10}R - 2.3R) - 15.0$$

$$\frac{L_{p,90\%}}{\text{dB}} = 161.5 - 11.5\log_{10}R - 2.64R$$

and

$$\frac{L_{p,\text{eff}}}{\text{dB}} = 1.176(153.5 - 10\log_{10}R - 2.3R) - 15.8$$

$$\frac{L_{p,\text{eff}}}{\text{dB}} = 164.7 - 11.8\log_{10}R - 2.70R.$$

Application of **Equations 3.17** and **3.18** to the L_E formula for ranges exceeding 8.7 km gives:

$$\frac{L_{p,90\%}}{\text{dB}} = 1.150(147.6 - 25\log_{10}R\ ) - 15.0$$

$$\frac{L_{p,90\%}}{\text{dB}} = 154.7 - 28.8\log_{10}R$$

and

$$\frac{L_{p,\text{eff}}}{\text{dB}} = 1.176(147.6 - 25\log_{10}R\ ) - 15.8$$

$$\frac{L_{p,\text{eff}}}{\text{dB}} = 158.6 - 29.4\log_{10}R.$$

The resulting levels, extrapolated from a single measurement of L_E at 200 m, are plotted versus range in **Figure 3-17**.

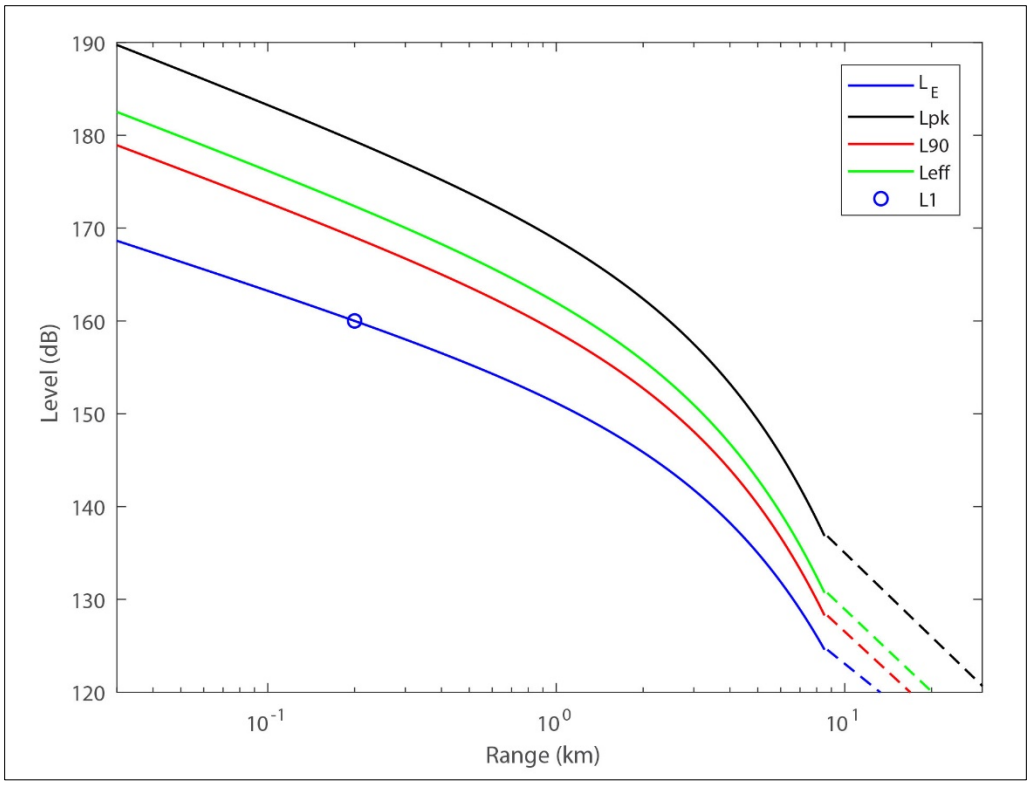

Figure 3-17. Worked example of extrapolation from L_E.
Shows the measurement of sound exposure level at range $[L_E(R_1)] = 160$ dB re 1 µPa² s at $r_1 = 200$ m (blue circle), extrapolation using damped cylindrical spreading (L_E) (solid blue curve), regression for peak sound pressure level $L_{p,\mathrm{pk}}$ (dB re 1 µPa) using **Equation 3.15** (solid black curve), and regressions for 90% energy sound pressure level ($L_{p,90\%}$, dB re 1 µPa) and effective sound pressure level ($L_{p,\mathrm{eff}}$, dB re 1 µPa) using **Equations 3.17** and **3.18** (solid red and green curves). The dashed curves show the suggested practical spreading loss model extrapolation. µPa = micropascal; dB = decibel; km = kilometer; re = with reference to; SEL = L_E = sound exposure level.

3.5 Validation

3.5.1 Borkum Riffgrund 1

BR1 measurements from ITAP (2015c) (**Appendix C**), were power averaged over the two measurement depths and are shown as circles (blue: median L_E; black: $L_{p,\mathrm{pk}}$) in the upper graph of **Figure 3-18**. Asterisks indicate the result of applying the Luchterduinen correlations for $L_{p,\mathrm{pk}}$, $L_{p,90\%}$, and $L_{p,\mathrm{eff}}$ to the median L_E values. The upper graph of **Figure 3-18** includes additional measurement positions from ITAP (2015c) and is for the same case as that shown in the lower graph of **Figure 3-4**, where the DCS prediction is compared with three different power laws (F = 5, 10, 15). Similar results were reported for BO1 in ITAP (2014) and GT1 in ITAP (2015d).

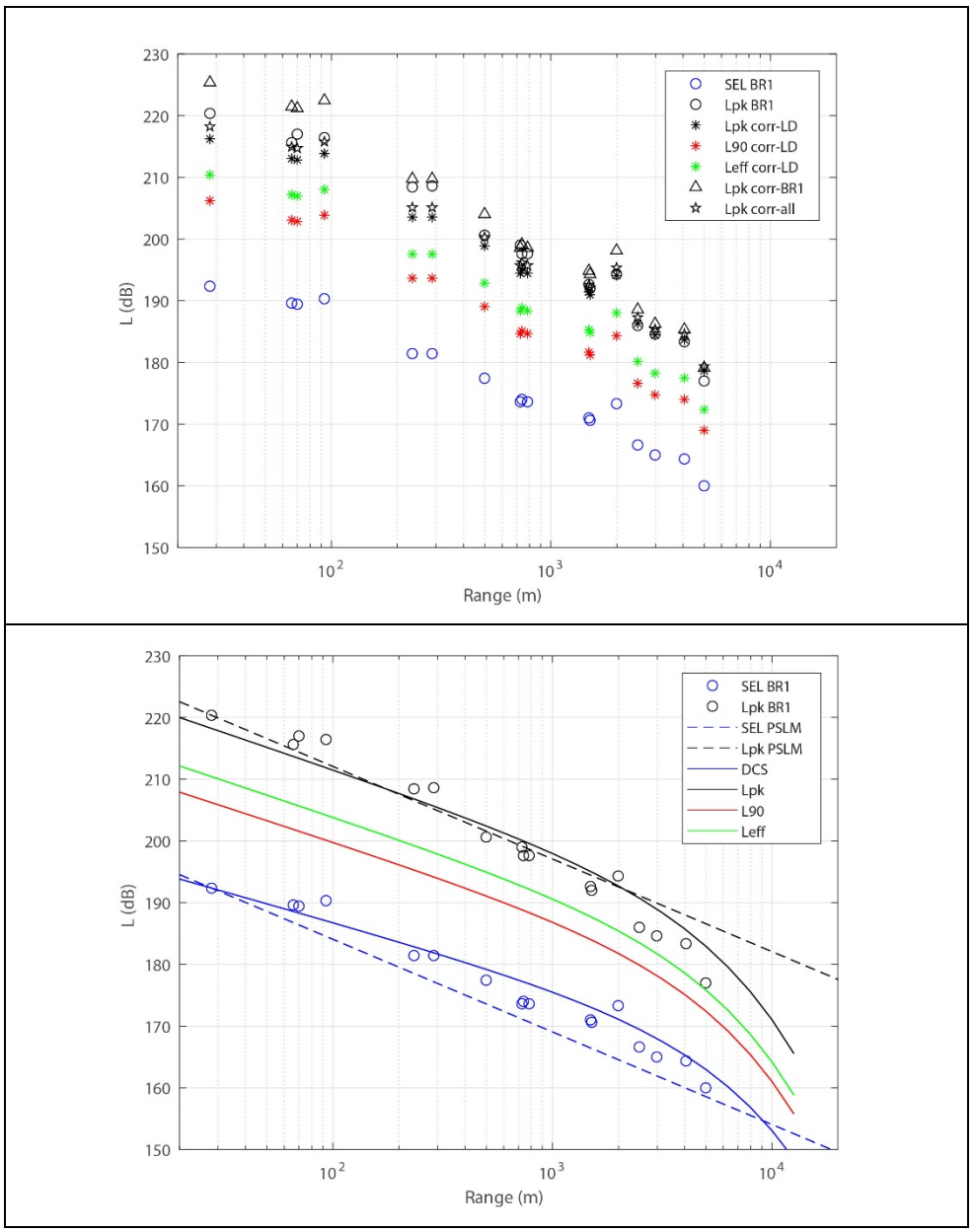

Figure 3-18. Single strike L_E and $L_{p,\mathrm{pk}}$ versus range at Borkum Riffgrund 1.

Top: Extrapolation results of peak sound pressure level ($L_{p,\mathrm{pk}}$, in dB re 1 µPa) and root-mean-square sound pressure level ($L_{p,\mathrm{rms}}$, in dB re 1 µPa^2 s) based on sound exposure level (L_E, in dB re 1 µPa^2 s) measurements, using DCS correlations identified in the legend. Bottom: Results of modeling L_E, $L_{p,\mathrm{pk}}$, $L_{p,\mathrm{rms}}$ using each spreading model method. Blue circles = single strike L_E; black circles = $L_{p,\mathrm{pk}}$. µPa = micropascal; dB = decibel; DCS = damped cylindrical spreading; m = meter; PSLM = practical spreading loss model; re = with reference to; s = second; SEL = L_E = sound exposure level.

The results from a test of the recommended algorithm are shown in the lower graph of **Figure 3-18**. Specifically:

- L_E curve is based on **Equation 3.5**, derived from the measurement at $r_1 = 28\ m$ (blue);
- $L_{p,\mathrm{pk}}$ curve is based on **Equation 3.15** (black);
- $L_{p,90\%}$ curve is based on **Equation 3.16** (red);
- $L_{p,\mathrm{eff}}$ curve is based on **Equation 3.17** (green).

DCS enabled accurate estimations of L_E at all ranges considered. While a systematic validation of the empirical correlations for $L_{p,\mathrm{pk}}$ and $L_{p,\mathrm{rms}}$ is needed, their use permits extrapolation from L_E to obtain estimates of $L_{p,\mathrm{pk}}$ and $L_{p,\mathrm{rms}}$.

For comparison, the equivalent PSLM results with $F = 15$ were plotted (dashed lines) in the lower graph of **Figure 3-18**. Using $F = 15$, the PSLM overestimates the initial slope of the TL curve, resulting in the following consequences:

- PSLM overestimates L_E for $r < r_1$
- PSLM underestimates L_E for $r > r_1$ (up to 8 km)

Furthermore, using $F = 10$ leads to the correct TL slope; however, L_E is overestimated for $r > 1$ km in the absence of an attenuation (αr) term.

3.5.2 Gemini

The original DCS enabled calculation of L_E as a function of range from the pile (Lippert et al., 2018). The correlation observed is between L_E and $L_{p,\mathrm{pk}}$ (Lippert et al., 2015) and was extended in **Section 3.3.2** by analyzing the correlation between L_E and $L_{p,\mathrm{rms}}$, which permitted estimation of $L_{p,\mathrm{rms}}$ and $L_{p,\mathrm{pk}}$, and extended the correlation to a wider range of L_E values (roughly 138 to 178 dB).

The purpose of this section is to investigate the regression formula for $L_{p,\mathrm{pk}}$ (**Equation 3.15**) by applying it to an additional data set. The additional data set was from the Gemini wind farm, which was not used in the development of the regression formula. The results were a comparison of the predicted values of $L_{p,\mathrm{pk}}$ using **Equation 3.15** with the measured values of that quantity.

Three different regression lines are shown in **Figure 3-19**. The first is based on measurements at the Luchterduinen (orange line; $1.162L_E$), the second is based on site GT1 (green line; $1.4L_E$), and the third is based on the four-site regression (red; $1.201L_E$) (**Equation 3.15**). The three regression lines were compared with measurements made during construction of the Gemini wind farm (dots). The four-site regression (red) and the Luchterduinen regression (orange) are similar, and both have reasonable agreement with the Gemini measurements (dots) over a range of 50 dB for L_E values (130 to 180 dB). The four-site regression is referred to henceforth as the DCSiE regression because it is used in the spreadsheet tool of that name, described in **Section 3.5.3**.

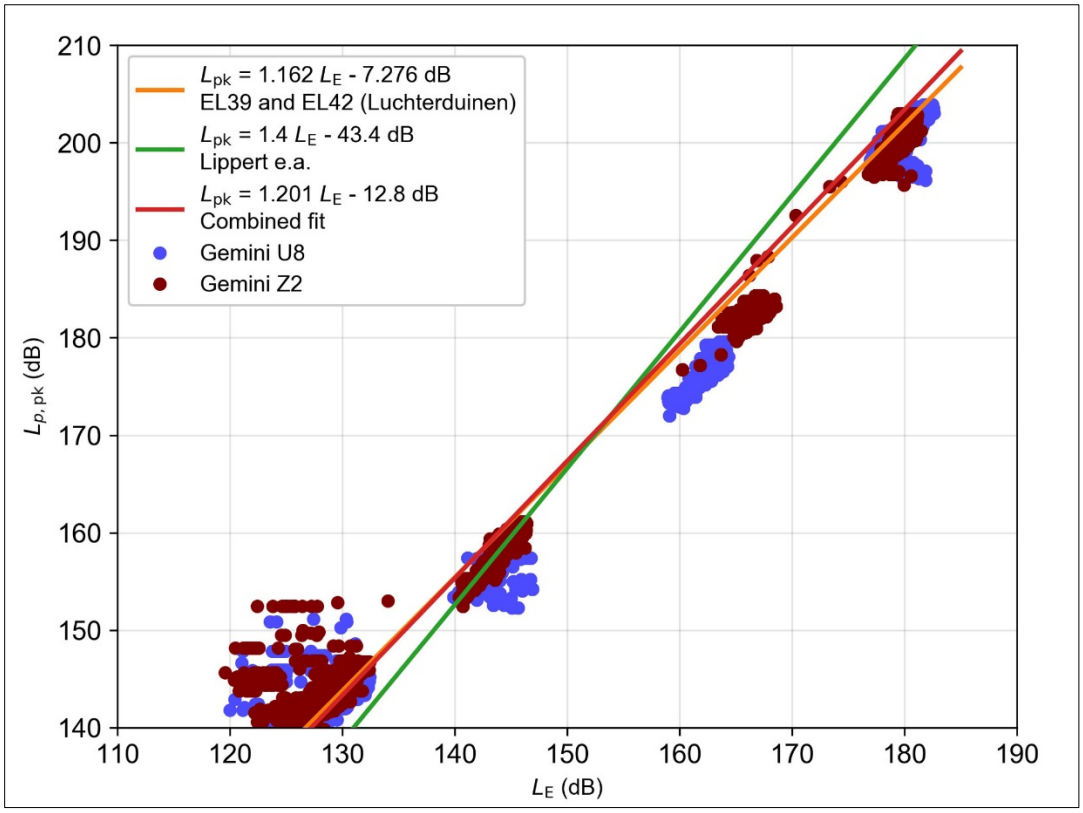

Figure 3-19. Measured $L_{p,pk}$ versus L_E at Gemini wind farm.

Dots = measurements from Gemini wind farm. L_{pk} ($L_{p,pk}$) = peak sound pressure level, which is compared with three trend lines: (1) green = applied correlations from Lippert et al. (2015); (2) orange = applied Luchterduinen regression; (3) red = applied DCSiE regression representing a combination of the four sites. dB = decibel; DCSiE = damped cylindrical spreading in Excel; re = with reference to; SEL = L_E = sound exposure level.

3.5.3 DCS-based Spreadsheet (DCSiE)

The DCS model was implemented in an Excel spreadsheet (DCSiE). The user can enter values for the parameters H (water depth, H), $L_{E,ss}$ (measured value of single strike, SEL_{ss}_1), r_1 (range from pile axis of symmetry at which $L_{E,ss}$ is measured, R_1), N (number of hammer strikes # Pile Strikes), and D (pile diameter, D). Optionally, the user may also enter values for c_w (water sound speed, cw), ρ_w (water density, rhow), Φ (sediment grain size, Mz), $\beta_{sed}(\alpha/f$, betased), and θ (Mach cone angle, thetaMach). For values not entered by the user, the calculator will apply the default values shown in **Figure 3-20**, which are based on BR1 (Lippert et al., 2018).

USER INPUT PARAMETERS			Descriptions
Name	**Value**	**units**	**notes**
Project variables to input (required)			
H	29	m	water depth
SEL_{ss}_1	179	dB	measured SEL re 1 μPa^2 s
R_1	234	m	distance of measured SELss (B8); R_1 > D/2
# Pile Strikes	50	--	over 24 h period
Pile Diameter (D)	6	m	
Advanced project variables (not required)			
cw	1500	m/s	sound speed in water
rhow	1029	kg/m^3	density of water (could be frozen at this value)
Mz	1.5	phi	grain size (medium sand)
betased	0.2783	dB/(m kHz)	corresponds to 0.5 dB per wavelength (Lippert et al 2018)
thetaMach	17	deg	Mach cone angle, based on steel sound speed

Figure 3-20. Input parameters for the DCSiE model.
Default values of the DCSiE inputs based on Borkum Riffgrund 1: H = water depth; SEL_{ss}_1 = single strike sound exposure level at distance R_1; R_1 = distance at which measured single strike sound exposure level (SEL_{ss}_1); # Pile Strikes = number of pile strikes; cw = sound speed in water; rhow = density of water; Mz = grain size; betased = α/f; and thetaMach = Mach cone angle. µPa = micropascal; dB = decibel; DCSiE = damped cylindrical spreading in Excel; kg = kilogram; kHz = kilohertz; m = meter; re = with reference to; s = second; SEL = L_E = sound exposure level.

The parameter betased (β_{sed}) is related to the sediment attenuation coefficient α according to:

$$\beta_{\text{sed}} = \frac{\alpha}{f} \qquad \textit{Equation 3.19}$$

Often the value of α is specified in decibels per wavelength (abbreviated dB/λ or $\text{dB}\ \lambda^{-1}$), in which case it can be converted to β_{sed} (in dB (m kHz)$^{-1}$) by dividing by the sediment sound speed (in km s^{-1}). Thus:

$$\frac{\beta_{\text{sed}}}{\text{dB (m kHz)}^{-1}} = \frac{\alpha/(\text{dB}\ \lambda^{-1})}{c/(\text{km s}^{-1})}. \qquad \textit{Equation 3.20}$$

In this example, $\alpha = 0.5\ \text{dB}/\lambda$ and c = 1.7967 km s^{-1}. Therefore (to four significant figures):

$$\beta_{\text{sed}} = \frac{\alpha}{f} = 0.2783\ \text{dB (m kHz)}^{-1} \qquad \textit{Equation 3.21}$$

The main DCSiE outputs predict effect ranges to PTS, TTS, injury, and behavior using the criteria from **Section 1.5**. The tool is applicable to marine mammals (LF cetaceans, MF cetaceans, HF cetaceans, and phocid pinnipeds), fishes and sea turtles. For fishes, both Stadler and Woodbury (2009) and Popper et al. (2014) criteria were considered, enabling their implications to be compared for identical conditions. An example is shown for marine mammals in **Figure 3-21**.

Figure 3-21 shows the ranges to TTS for MF cetaceans based on the BR1 example given in **Figure 3-18**. Predicted effect ranges are plotted from the pile axis of symmetry (between half the pile diameter [or 1 m if larger]) to 5,000 m. Results are not given at ranges greater than 5,000 m because the measurements used for validation (**Figure 3-18**) only extend to 5,000 m.

However, **Figure 3-5** suggests the DCS validity holds for ranges where r < 8.7 km; based on ranges that satisfy $\alpha r < 20$ dB and based on the example of α = 2.3 dB km^{-1}. Until new measurements become available, the interim suggestion is to use DCS up to this distance (20 dB/α); beyond that distance, switch to applying a power law using $F = 25$. ($F = 25$ corresponds to dipole propagation and is in reasonable agreement with measurements for the Gemini wind farm.).

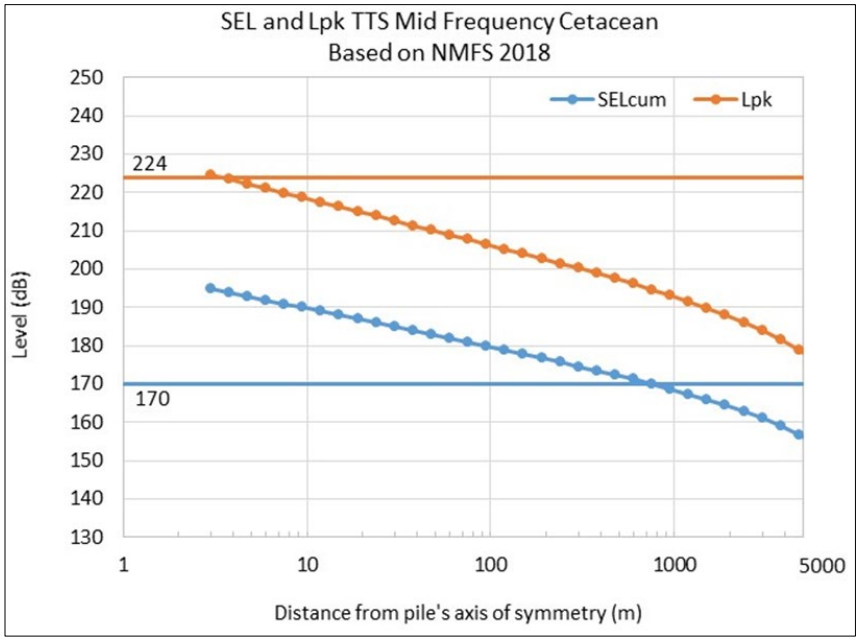

Hearing Group	Impulsive Signals (NMFS 2018)				
	PTS Onset		TTS Onset		Behavior
	$SEL_{w,24h}$	L_{pk}	$SEL_{w,24h}$	L_{pk}	L_{rms}
	dB re 1 µPa^2·s	dB re 1 µPa (unweighted)	dB re 1µPa^2·s	dB re 1 µPa (unweighted)	dB re 1 µPa (unweighted)
Mid-frequency cetaceans	185	230	170	224	160
RESULTS (m)					
Mid-frequency cetaceans	30	0	753	3	> 5000

Figure 3-21. DCSiE model example outputs for MF cetacean criteria.
Upper panel: graph of SEL_{cum} (dB re 1 µPa^2 s) and L_{pk}, $L_{p,\mathrm{pk}}$ (dB re 1 µPa) versus range (m), calculated using the input parameters shown in **Figure 3-20**. Lower panel: table of effect ranges in meters (green cells), and the criteria (white cells). µPa = micropascal; dB = decibel; DCSiE = damped cylindrical spreading in Excel; L_{pk} = $L_{p,\mathrm{pk}}$ = peak sound pressure level; m = meter; MF = mid-frequency; NMFS = National Marine Fisheries Service (2018a); PTS = permanent threshold shift; re = with reference to; s = second; SEL_{cum} = $L_{E,\mathrm{cum}}$ = cumulative sound exposure level; $SEL_{w,24h}$ = $L_{E,\mathrm{w24h}}$ = cumulative sound exposure level; TTS = temporary threshold shift.

3.6 Conclusions

A recently developed DCS model permits extrapolation of acoustic metrics from L_E based on physical principles, leading to an improved understanding and prediction of the propagation mechanism in the first few kilometers from the pile. The form of TL in DCS is $10\log_{10}\frac{r}{r_1}$ dB + $\alpha(r - r_1)$. A comparison between the DCS and PSLM revealed the DCS model performs better out to 5 or 6 km, after which it reaches its limitations and underestimates L_E beyond this range for the COMPILE test case. For the

German wind farm site BR1, there are measurements showing good agreement with DCS predictions up to 5 km, and no measurements beyond that range.

DCS enables estimation of L_E at ranges that satisfy $\alpha r < 20$ dB. For ranges that do not satisfy this inequality, the DCS model is expected to overestimate TL and underestimate L_E. Therefore, it remains necessary to supplement the DCS model with an alternative method at long ranges, where the field appears to follow a power law instead of an exponential decay. **Figure 3-5** suggests the possibility of extrapolating for $\alpha r < 20$ dB using the PSLM with $F \sim 35$ (based empirically), although caution is warranted and validation is needed for this untested approach. In **Section 3.5.3**, extrapolating using $F = 25$ was recommended as a precautionary approach.

While systematic validation of the empirical correlations for $L_{p,\mathrm{pk}}$ and $L_{p,\mathrm{rms}}$ to L_E is needed, extrapolation of L_E to estimates of $L_{p,\mathrm{pk}}$ and $L_{p,\mathrm{rms}}$ may be permitted. In this way, impact assessments involving the metrics L_E, $L_{p,\mathrm{pk}}$, and $L_{p,rms}$ can be carried out based on a single measurement of L_E near the pile, without requiring measurements of $L_{p,\mathrm{pk}}$ or $L_{p,\mathrm{rms}}$.

Conversion from L_E to $L_{p,\mathrm{pk}}$ (and $L_{p,\mathrm{rms}}$) remains an empirical correlation, and thus is limited to the range of parameters (water depth, sediment type, hammer energy, and pile diameter) considered during the regression analysis. Therefore, the approach described in this chapter is applicable, but the values are site specific. A validation of the recommended method at a suitable U.S. site, though outside this project's scope, is needed to test the accuracy of the predictions of L_E, $L_{p,\mathrm{pk}}$, and $L_{p,\mathrm{rms}}$. A validation study likely would lead to improved understanding of the observed correlations and the possibility of improving these further.

Finally, the concept of $L_{p,\mathrm{eff}}$ was introduced alongside $L_{p,90\%}$ as an alternative metric to represent $L_{p,\mathrm{rms}}$. Both $L_{p,\mathrm{eff}}$ and $L_{p,90\%}$ are measures of the $L_{p,\mathrm{rms}}$, but they are calculated in different ways. Using $L_{p,\mathrm{eff}}$ leads to stronger (more robust) correlations with L_E than $L_{p,90\%}$. Therefore, the $L_{p,\mathrm{eff}}$ metric is suggested as a supplement to $L_{p,90\%}$.

4 Model Verification and Validation Methods

This section describes the verification and validation of the acoustic modeling approach composed of an FE model of the pile (driven by a hammer forcing function) and a PE of sound propagation from the pile to a distant receiver. The FE output generated the sound field around the pile, which was then used as the PE starter field. The acoustic model (comprising the FE model and PE propagation model) was validated by comparison to available field measurements. The primary data set was the field observations that included received acoustic pressure versus range in shallow water from the Gemini wind farm in the North Sea (http://geminiwindpark.nl/e_home.html; Binnerts et al., 2016). For each site, a full numerical acoustic computation was performed and compared with the measured data, then a parametric fit to the data was generated. In general, a comparison of measurements with an acoustic model is only a validation of the model to the extent that the environment is well measured (e.g., sediment, bathymetry, water properties) and the source forcing function (COMPILE, 2014) is understood. A comparable location of a pile driven by an impact hammer was selected, appropriate databases were used for environmental variables, and the full acoustic-field computation was performed to calculate the acoustic metrics. The site-specific parameters from Gemini permitted the definition of a subgroup of parameters used for

selecting the acoustic geometric fits. A statistical analysis (goodness of fit, root-mean-square-error) was performed to test the ability of the modeled data and the parametric fit to match the measured acoustic metrics.

Data from the 2014 COMPILE workshop (Lippert et al., 2016) were used for model verification, data from Gemini for model validation, and data from Gemini or Luchterduinen for the DCSiE spreadsheet calculator (**Section 3**).

Model verification was intended to check that model outputs were consistent with expectation (i.e., *did the models solve the specified equations correctly?*). By comparison, the purpose of model validation was to investigate the extent to which these models predicted the measured sound field in the vicinity of a pile-driving operation (i.e., *how well did the specified equations represent reality?*).

For model verification, the results of the 2014 COMPILE workshop (henceforth referred to as COMPILE I; Lippert et al., 2016, to distinguish it from the second COMPILE workshop [COMPILE II]) were used. The COMPILE I workshop aimed to gain insight into the advantages and disadvantages of different methods for modeling the sound field radiated by underwater pile driving. To achieve this goal, workshop participants were supplied with a fully specified test scenario and requested to make predictions based on the specifications. The workshop itself provided a forum for model-to-model comparisons (Lippert et al., 2016). The test scenario involved a pile that was 25 m long and 2 m in diameter driven by a particular hammer forcing function. The propagation medium was a Pekeris waveguide with a water depth of 10 m and a sandy sediment.

The model validation used measurements made during construction of the Gemini wind farm in the North Sea on the Dutch continental shelf at a water depth of approximately 30 m (**Figure 4-1**; ITAP, 2015b). These measurements had been used for the validation of the TNO's Aquarius model (Binnerts et al., 2016).

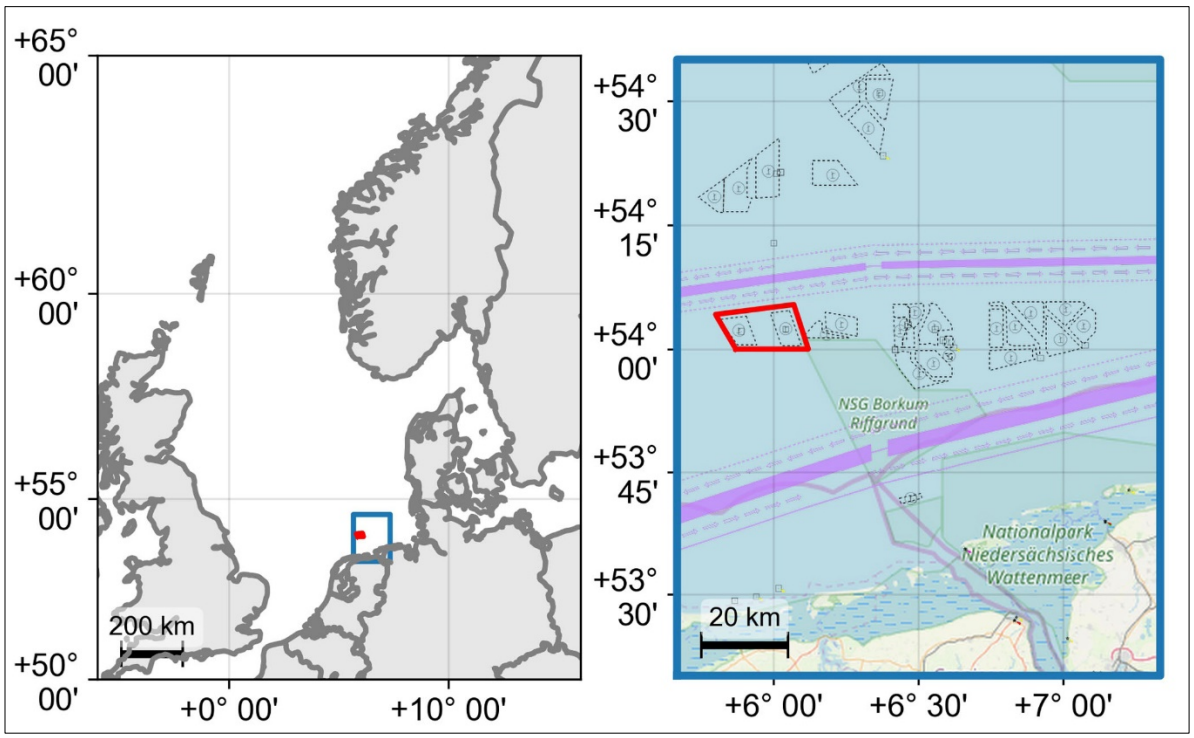

Figure 4-1. Location of the Gemini wind farm.
In the North Sea (54.036 N, 5.963 E), about 60 km north of the Netherlands' coast. Source of background map: Thematicmapping.org, OpenStreetMaps, and OpenSeaMap.

Three different versions of Aquarius were considered in Binnerts et al. (2016). The Aquarius version of interest for this project used an FE source model coupled with an NM acoustic propagation model. For model verification and validation, the same FE source model was used and coupled with Peregrine, a PE propagation model. The FE model predicts the sound field at a specified range, which was used as a starting field for Peregrine.

4.1 Finite Element Method to Estimate the Sound Field Around the Source

The source model consisted of a linear, axially symmetric frequency domain FE model in COMSOL, a Multiphysics® simulation software. A schematic overview of the FE setup is provided in **Figure 4-2**. The depth and range dimensions of the sediment and water waveguide had infinite extent and were modeled by lining the bottom and outer range of the domain with perfectly matched layers (PMLs), which quickly attenuate all outgoing waves (Berenger, 1994; Zampolli et al., 2008). This heavy attenuation prevented substantial reflections at the FE domain boundaries. The FE model was excited by applying a unit force to the area of the hammer impact (**Figure 4-2**). When a pile is in sediment and receives a hammer impact, acoustic waves enter the sediment and generate seismic body waves called P- and S-waves that move through the sediment. Damping due to friction between the pile and sediment was represented by applying an equivalent damping to the P- and S-waves along the section of the pile embedded in the sediment. The equivalent damping was empirically determined using the FE source model for a pile-driving scenario in combination with acoustic measurements at close range (a few meters) to the pile.

Boundary conditions occur between materials with different states (i.e., air, solid, and fluid). In pile driving, three interfaces were addressed: solid/air, air/water, and solid/fluid-sediment. For the interface between the solid (hammer) and air, stress release boundary conditions were applied. For the interface between air and water, pressure release boundary conditions were applied. The boundary conditions between solid (pile surface) and fluid (water) consisted of enforced continuity of normal force and normal velocity. A slip condition was applied in the direction tangential to this interface.

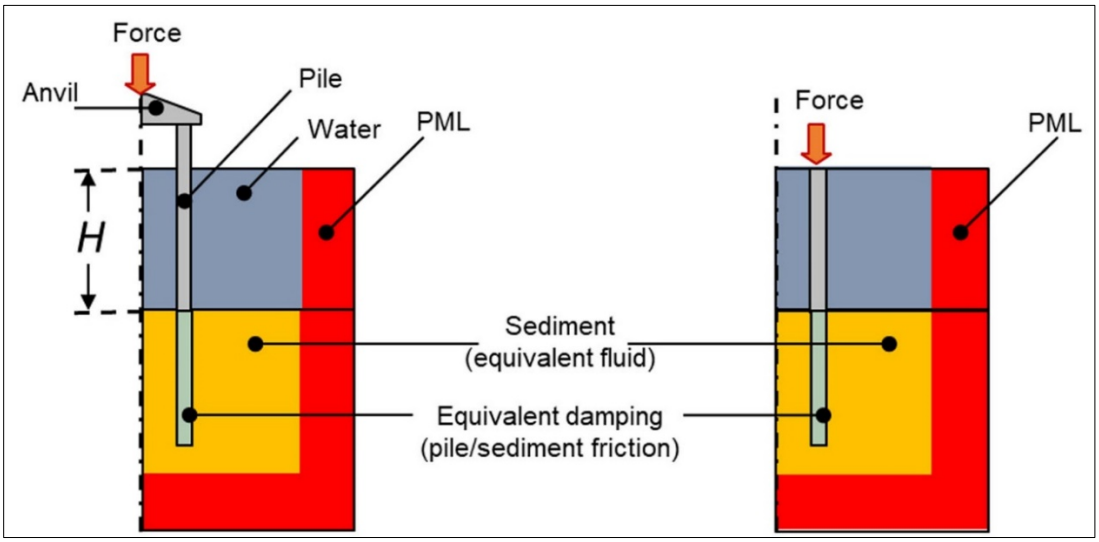

Figure 4-2. Schematic overview of a Finite Element model.
A generic pile driving case (left) and the COMPILE I benchmark case (right). H = water depth; PML = perfectly matched layers.

The sediment can be modeled as either (1) an elastic solid (i.e., a solid that is deformed by application of a force that returns to its original shape once the force is removed, thus supporting shear waves), or (2) an equivalent fluid (i.e., a medium that supports compressional waves but not shear waves). The FE model allows the sediment material properties to vary with depth for an accurate representation of the effects of sub-bottom layering. In addition, the FE model allows the sediment material properties to be defined as a function of frequency for an accurate representation of the effects of material dispersion caused by the pile and sound waves.

In the absence of relevant information about the dependence of sediment properties on depth and frequency, constant values (i.e., no sub-bottom layering) were assumed for the validation cases. This means the sound speed and density were constants, while a constant damping term means the absorption coefficient increased linearly with frequency. The absence of sub-bottom layering implies downward-traveling waves in the sediment will not re-enter the water column, as they would if there were reflective sediment layers. The downward-only waves condition allows for the use of an equivalent fluid. The effects of shear waves in the sediment, on the reflection coefficient of the water-sediment interface, were represented by changing the density and damping of the fluid. For the validation case, the sediment was modeled as an equivalent fluid. Therefore, the source model involved a range-independent bathymetry with a fluid sediment (i.e., the water waveguide in the source model was a Pekeris waveguide) (Jensen et al., 1994). Use of a Pekeris waveguide implies a perfectly reflecting sea surface, an isovelocity water column (i.e., uniform sound speed throughout the water column), and an infinite uniform fluid sediment.

4.2 Parabolic Equation Method

The PE model interfaced with the FE model and was used to propagate the sound field.

4.2.1 Propagation

The PE model was the method used for solving the wave equation by marching the outgoing field (and ignoring the incoming field) one range step at a time using a one-way propagator. This method was efficient and handled high-angle energy (up to 88° from the horizontal) as well as range dependence in the environment. Range dependence was not an issue for the model verification and validation because the validation environments had uniform bathymetries, SSPs, and waveguides. This is not always the case, however, and use of a RAM is appropriate for impact studies in shallow water where bathymetric changes are substantial. The types of bathymetric changes that require special modeling were addressed in the sensitivity analysis (**Section 6**).

4.2.2 Integration with Finite Element Starter Field

The PE model used in this study was a fluid-fluid model, meaning it did not handle shear waves in the sediment or in the pile. Also, the water column did not support shear wave propagation; it is expected that this is a reliable approximation for modeling the propagation from a few meters beyond the pile out to substantial ranges. The model used an FD approach, meaning differential operators were approximated by taking small finite steps, with the size of the range and depth steps being inversely proportional to frequency. Therefore, the size of the two-dimensional (2D) computational grid (and hence the computational cost) increased with the frequency squared. The PE typically is run using a point-source starter function generated by allowing the sound waves to spread spherically from the source location, and the PE algorithm marches the complex pressure field forward one range step at a time. However, the FE model provided the field generated by the whole pile, which did not approximate to a point source; thus, the sound field did not propagate spherically. In order to accommodate the FE starter field at a specified range, the PE algorithm was modified and then allowed to march the complex pressure field forward one range step at a time.

The complex pressure field generated by the FE model at 3 m was used as the starter field for the PE model. Both the PE and FE models are frequency-domain models, meaning each frequency is run independently. The band from 0 to 2,000 Hz was computed with 0.5 Hz steps. When the output pressure field was mapped to the time domain by taking the inverse fast Fourier transform (IFFT), the 0.5 Hz frequency spacing produced a time window of 2 seconds. The pressure field predicted by the FE model was sampled 3 m from the pile center, from the water surface down to a depth well below the pile toe (95 m and 65 m for Gemini and COMPILE I, respectively) with a resolution of 0.05 m. This sampled field was used as the starter field for the PE. Thus, the acoustic field was computed out to long ranges efficiently with high-angle support and range dependence (when necessary).

4.3 Model Verification – COMPILE I

The COMPILE I scenario (2014) is fully defined in Lippert et al. (2016). The scenario involves a straight homogenous steel pile without an anvil; the hammer force was applied directly to the top surface of the pile. The pile length, outer diameter, and thickness were 25, 2, and 0.05 m, respectively. The height of the

water column was 10 m, and the pile penetrated 15 m into the sediment, implying the pile top aligned with the water surface.

4.3.1 Pile Characterization and Forcing Function

The parameters defining the steel pile are listed in **Table 4-1** and were converted to density, wave speed, and absorption coefficients in **Table 4-2**. For more information, see Lippert et al. (2016).

Table 4-1. COMPILE I steel pile parameters (From: Lippert et al., 2016).

Material property	Unit	Value
Young's modulus	GPa	210
Poisson ratio	1	0.30
Density	kg m^{-3}	7,850
Absorption P-wave α/f (section in the sediment)	Np m^{-1} Hz^{-1}	$3 \cdot 10^{-5}$
Absorption S-wave α/f (section in the sediment)	Np m^{-1} Hz^{-1}	$11 \cdot 10^{-5}$

α = absorption coefficient; f = frequency; GPa = gigapascal; Hz = hertz; m = meter; Np = neper.

Table 4-2. COMPILE I steel pile parameters, derived from Table 4-1.

	density (kg m^{-3})	P-wave speed c_p (m s^{-1})	P-wave absorption α (dB λ^{-1})	S-wave speed c_s (m s^{-1})	S-wave absorption α (dB λ^{-1})
Pile in water	7,850	6,001	0	3,208	0
Pile in sediment	7,850	6,001	1.564	3,208	3.065

α = absorption coefficient; λ = wavelength; dB = decibel; kg = kilogram; m = meter; s = second. P-wave speed c_p = speed of sound (compressional wave) in steel; S-wave speed c_s = speed of shear wave in steel.

For COMPILE I, the forcing function was specified by the organizers (Lippert et al., 2016). The specified forcing function is plotted in **Figure 4-3** and given by the following formula:

$$F(t) = F_p \begin{cases} t/t_r & t < t_r \\ \exp \dfrac{t_r - t}{t_d} & t > t_r \end{cases} \qquad \textit{Equation 4.1}$$

where:

F = force
t = time
F_p = peak force (equal to 20 meganewtons [MN])
t_r = time of maximum force (equal to 0.2 milliseconds [ms])
t_d = pulse duration (equal to 1.6 ms)

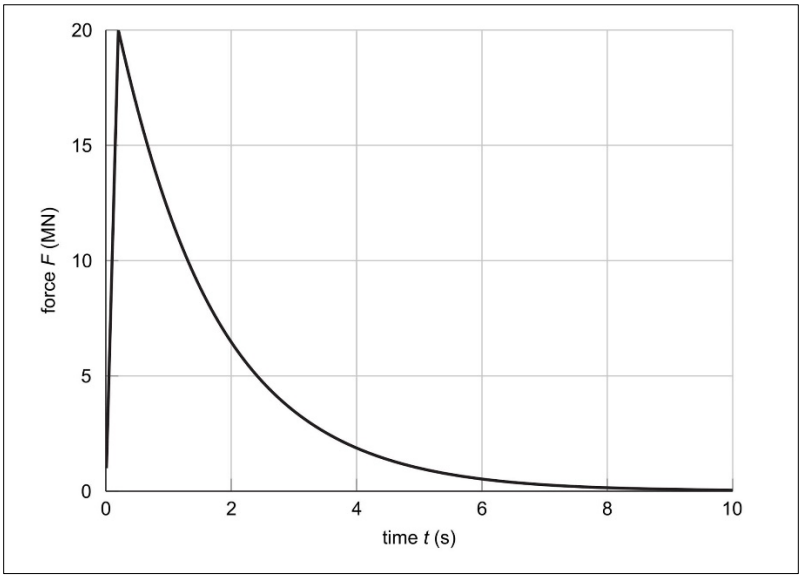

Figure 4-3. COMPILE I forcing function
(from Lippert et al., 2016). MN = meganewton; s = second.

The resulting impulse is:

$$I = F_{\mathrm{p}}\left(\frac{t_{\mathrm{r}}}{2} + t_{\mathrm{d}}\right) = 34 \text{ kN s}, \qquad \textit{Equation 4.2}$$

where:

I = impulse
F_{p} = peak force (20 MN)
t_{r} = time of maximum force
t_{d} = pulse duration
kN s = kilonewton second

The acoustic energy flux density in the water column is calculated as the integral over depth (through the height of the water column) and time of the horizontal component of sound intensity. The total (horizontal) energy flux, in joules (J), at any distance (r) is obtained by multiplying this quantity with the circumference of a circle of radius r. The energy flux values are shown in **Table 4-3** at the eight ranges defined in COMPILE I.

Table 4-3. Calculated (horizontal) energy flux density and total (horizontal) energy flux at eight ranges.

Parameter Range	Unit	Range (m)							
		1	11	31	750	1,500	$10 \cdot 10^3$	$20 \cdot 10^3$	$50 \cdot 10^3$
Energy flux density	J m^{-1}	930	80.6	26.5	0.503	0.152	0.00109	$6.74 \cdot 10^{-5}$	$2.21 \cdot 10^{-6}$
Total energy flux	kJ	5.84	5.57	5.16	2.37	1.43	0.0685	0.0085	0.0007

J = joule; kJ = kilojoule; m = meter.

4.3.2 Propagation Medium

Density, Sound Speed, and Attenuation

Density, sound speed, and attenuation profiles in the water and sediment layers are specified in **Table 4-4**.

Table 4-4. COMPILE I water and sediment parameters.

	Density ρ (kg m^{-3})	P-wave speed c (m s^{-1})	P-wave absorption α (dB λ^{-1})
water	1,025	1,500	See explanation below and Lippert et al. (2016)
sediment	2,000	1,800	0.4690

α = absorption coefficient; c = water or sediment sound speed; λ = wavelength; ρ = water or sediment density; dB = decibel; kg = kilogram; m = meter; s = second.

Absorption Coefficient in Water and Sediment

In the water, the absorption coefficient (α) in nepers per meter (Np m^{-1}) is (Lippert et al., 2016):

$$\frac{\alpha}{\mathrm{Np/m}} = 1.4 \cdot 10^{-5} \frac{f^2}{f^2 + f_{\mathrm{B}}^2} + 5.58 \cdot 10^{-3} \frac{f^2}{f^2 + f_{\mathrm{Mg}}^2}. \qquad \textit{Equation 4.3}$$

Converting to decibels per kilometer gives:

$$\frac{\alpha}{\mathrm{dB/km}} = \frac{20}{\log_{\mathrm{e}} 10} \left(0.014 \frac{f^2}{f^2 + f_{\mathrm{B}}^2} + 5.58 \frac{f^2}{f^2 + f_{\mathrm{Mg}}^2} \right) \qquad \textit{Equation 4.4}$$

The absorption coefficient in the sediment is (Lippert et al., 2016):

$$\alpha / f = 3 \cdot 10^{-5} \mathrm{Np/(m\ Hz)}$$

or (to 5 significant figures):

$$\alpha / f = 0.26058\ \mathrm{dB/(m\ kHz)}.$$

The attenuation per cycle is obtained by multiplying left and right sides by the speed of sound in the propagation medium (in this case the sediment):

$$c = 1{,}800\ \mathrm{m\ s^{-1}}$$

$$\alpha\, \lambda = 0.4690\ \mathrm{dB}.$$

Dividing through by λ gives the value shown in **Table 4-4**:

$$\alpha = 0.4690 \text{ dB}/\lambda,$$

where:

dB = decibel
Hz = hertz
Np = neper
α = absorption coefficient
f = acoustic frequency
λ = acoustic wavelength in the sediment

5 Verification and Validation Results

5.1 Model Verification Results for COMPILE I

In order to validate the hybrid approach combining FE/PE models, the same output fields as the COMPILE I workshop were computed. For COMPILE I, the FE model was combined with an NM propagation model (FE/NM). The same FE model was used in the present study. Given there is no "true" solution for this scenario, in order to be considered verified, the hybrid FE/PE model approach's results would need to agree with the hybrid $p(t)$ predictions at depths of 3, 11, and 31 m, and with the FE/NM L_E predictions at ranges 1 and 3 km. These distances are from the pile axis of symmetry. (The same distance convention is adopted throughout this report). At greater distances, there are larger spreads between model predictions caused by different assumptions made by the various propagation models. FE model outputs were requested at depths of 1, 5, and 9 m at nearby receivers at 1, 11, and 31 m range. The distant receiver positions are illustrated in **Figure 5-1**. The FE field was matched with the PE at a range of 3 m, meaning there would be no meaningful PE results less than 3 m (from the pile axis of symmetry). Therefore, the only relevant nearby results were at ranges of 11 and 31 m. Other acoustic metrics such as $L_{p,\text{pk}}$ and $L_{p,\text{rms}}$ were derived from $p(t)$.

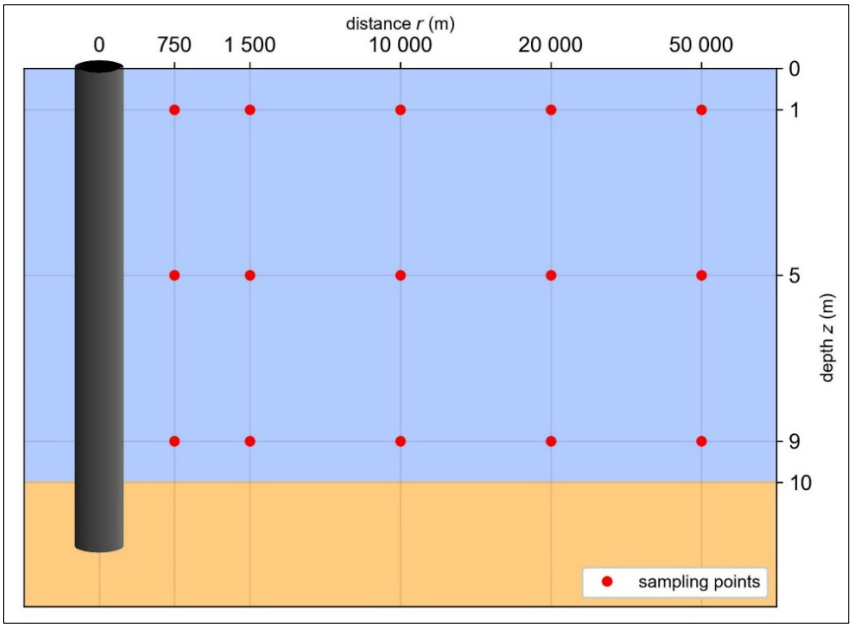

Figure 5-1. COMPILE I output grid for distant receivers.
From: Lippert et al., 2016. m = meter.

5.1.1 Comparisons

The first comparison of $p(t)$ was between the PE field and the FE/NM field. **Figure 5-2** shows $p(t)$ for a 5 m deep receiver at range of 31 m. The results provided verification of the FE/PE model predictions for $p(t)$.

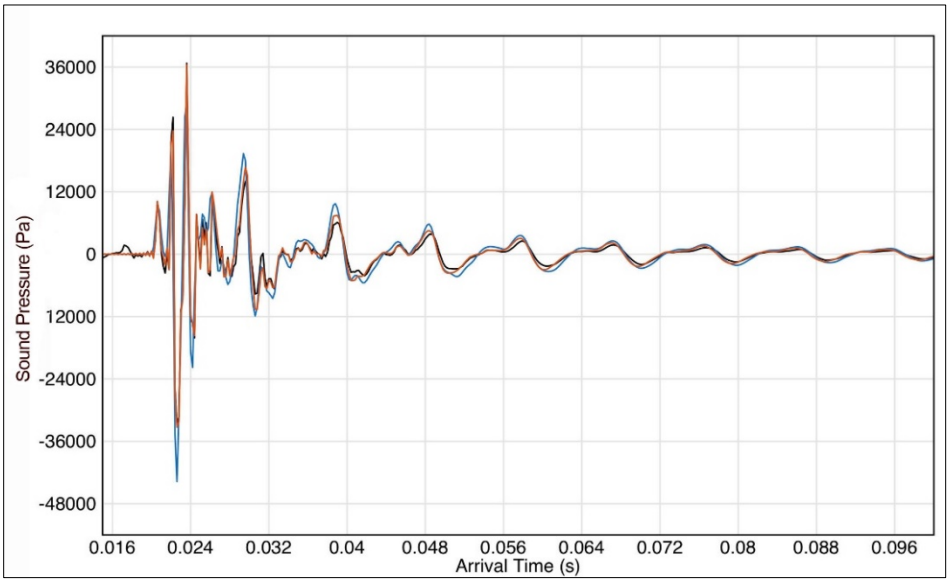

Figure 5-2. Verification of FE/PE with the FE/NM models based on the COMPILE I workshop.
Sound pressure versus time at 5 m depth and 31 m range. The TNO FE/NM model (blue), FE/PE model (black); UoS/NPL FE model (orange). FE = finite element; NM = normal mode; Pa = pascal; PE = parabolic equation; s = second; TNO = Netherlands Organisation for Applied Scientific Research; UoS/NPL = University of Southampton/National Physical Laboratory.

The following research institutions participated in and contributed results to the COMPILE I workshop (**Figure 5-3**): Curtin University, Centre for Marine Science and Technology (Australia, CMST), Hamburg University of Technology (Germany, TUHH), Bundeswehr Technical Centre for Ships and Naval Weapons (Germany, WTD 71), JASCO Applied Sciences (Canada, JASCO), Seoul National University (South Korea, SNU), Netherlands Organisation for Applied Scientific Research (Netherlands, TNO), and University of Southampton (UK, UoS) in collaboration with National Physical Laboratory (UK, NPL).

Group	Close range model	Far range model
CMST	FEM (PAFEC C-FE, FRD)	Normal mode expansion of close range prediction (ORCA)
TUHH	FEM (ABAQUS, TD)	Wave number integration method coupled by vertical array of point sources (in-house)
WTD 71	FEM (COMSOL Multiphysics, FRD)	Parabolic equation approximation directly coupled to close range prediction (in-house)
JASCO	FDM (in-house, TD)	Normal mode expansion coupled by vertical array of monopole sources (ORCA)
SNU	FEM (COMSOL Multiphysics, FRD)	Parabolic equation approximation directly coupled to close range prediction (in-house)
TNO	FEM (COMSOL Multiphysics, FRD)	Normal mode decomposition of close range prediction (in-house)
UoS/NPL	FEM (COMSOL Multiphysics, TD)	*not modeled*

Figure 5-3. COMPILE I participants and models.
(From: Lippert et al., 2016)

Acoustic metrics were computed for the ranges and depths of the COMPILE I workshop. L_E and $L_{p,\mathrm{pk}}$ were compared. For L_E, the time-integrated squared sound pressure was plotted as a function of range (**Figure 5-4**). This figure is an overlay of six results from the COMPILE I workshop participants, including the FE/NM and FE/PE model results. The top panel of **Figure 5-4** is L_E at a depth of 9 m for receivers at ranges of 1, 11, and 31 m. The PE result was valid from a distance of 3 m because that is the range at which the field was mapped from the FE code to the PE code. The FE/PE results for L_E at 11 and 31 m aligned with the other five predictions. The bottom panel is the received L_E at 1 m depth at ranges of 0.75, 1.5, 10, 20, and 50 km. The FE/PE model results aligned with the other COMPILE I results. These results provided verification of the FE/PE model predictions for L_E.

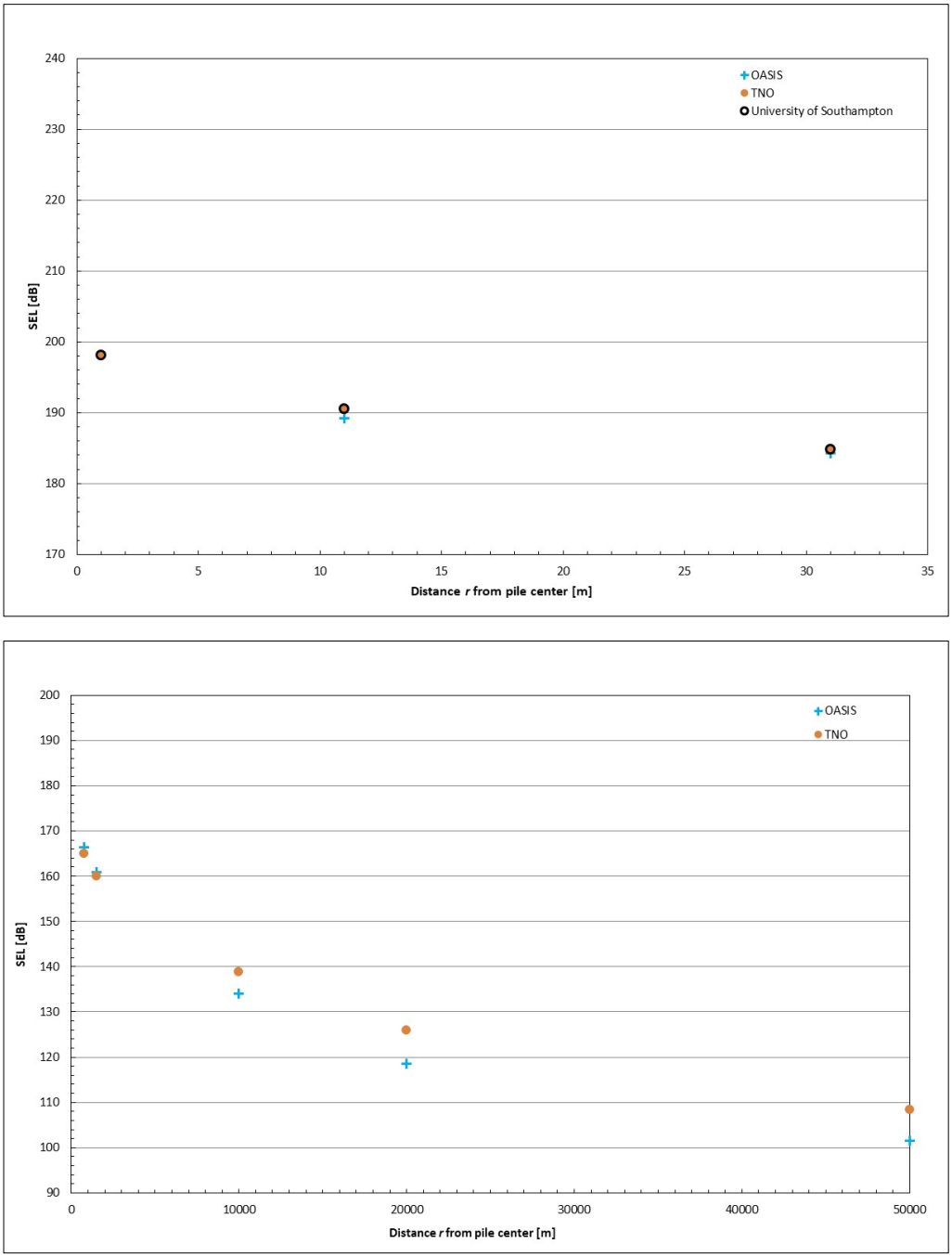

Figure 5-4. Verification of FE/PE with the COMPILE I workshop results for SEL versus range.
Top: SEL in the nearby receivers at 9 m depth; Bottom: SEL in the distant receivers at 1 m depth. The FE/PE (cyan +) are overlaid on the COMPILE I data (From: Lippert et al., 2016). µPa = micropascal; dB = decibel; FE = finite element; m = meter; PE = parabolic equation; re = with reference to; s = second; SEL = L_E = sound exposure level. SEL units = dB re 1 µPa^2 s.

$L_{p,\mathrm{pk}}$ was plotted, and **Figure 5-5** is an overlay of six results from the COMPILE I workshop and the FE/PE results (plotted as the cyan +). The top panel of **Figure 5-5** is $L_{p,\mathrm{pk}}$ at a depth of 1 m for the nearby

receivers at 1, 11, and 31 m ranges. The FE field is matched to the PE at a range of 3 m; thus, the PE results were not plotted for 1 m. The FE/PE model results for L_E at 11 and 31 m ranges aligned with the other six predictions. The lower panel of **Figure 5-5** is $L_{p,\mathrm{pk}}$ at a depth of 5 m at the distant receivers at ranges of 0.750, 1.5, 10, 20, and 50 km. The FE/PE result aligned with the other COMPILE I results. These results provided verification of the FE/PE model predictions for $L_{p,\mathrm{pk}}$.

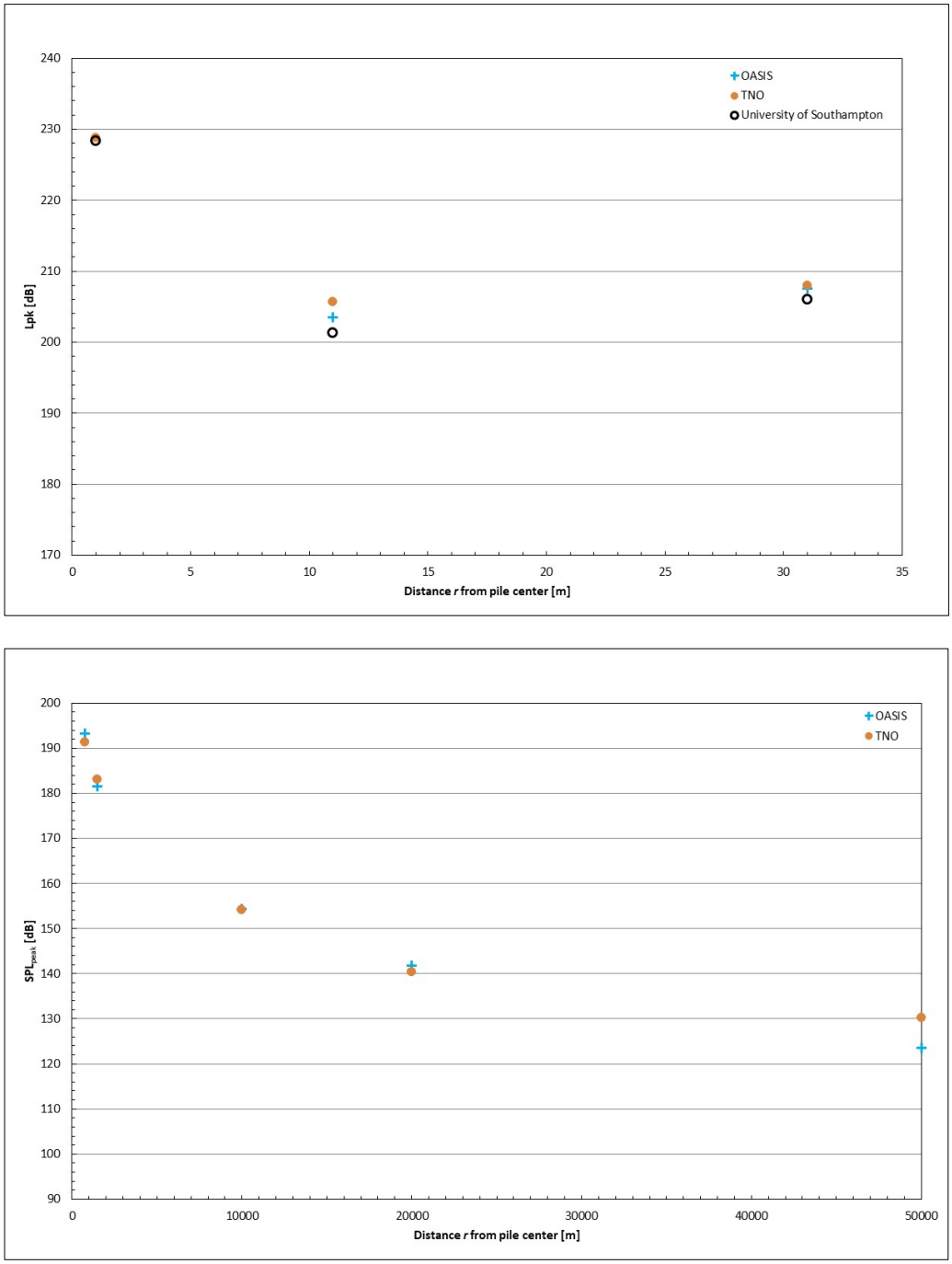

Figure 5-5. Verification of FE/PE with the COMPILE I workshop results for $L_{p,\mathrm{pk}}$.
Top: nearby receivers at 1 m depth (From: Lippert et al., 2016). Bottom: the distant receivers at 5 m depth (From: Lippert et al., 2014). The FE/PE model solutions (cyan +) are within the spread of the other models. µPa = micropascal; dB = decibel; FE = finite element; m = meter; PE = parabolic equation; re = with reference to; SEL = L_E = sound exposure level; $\mathrm{SPL}_{\mathrm{peak}}$ = $L_{p,\mathrm{pk}}$ = peak sound pressure level. $L_{p,\mathrm{pk}}$ units = dB re 1 µPa.

5.1.2 Weighted SEL Comparisons

The TNO and Curtin University $p(t)$ submissions to the COMPILE I workshop and the FE/PE modeled fields were made available. Each COMPILE I workshop participant's $p(t)$ was only available at 31 m; therefore, that was the range where $L_{E,w}$ was computed. A comparison was made of the $L_{E,w}$ computations for these three modeled results. **Figures 5-6**, **5-7**, and **5-8** show the comparison for the LF, MF, and HF cetacean frequency weightings, respectively. There is consistent agreement across all models for the three groups of weightings and most decidecade bands. The decidecade bands with the largest discrepancies between the models were the frequencies below 32 Hz, which were low level and difficult to model accurately in shallow water.

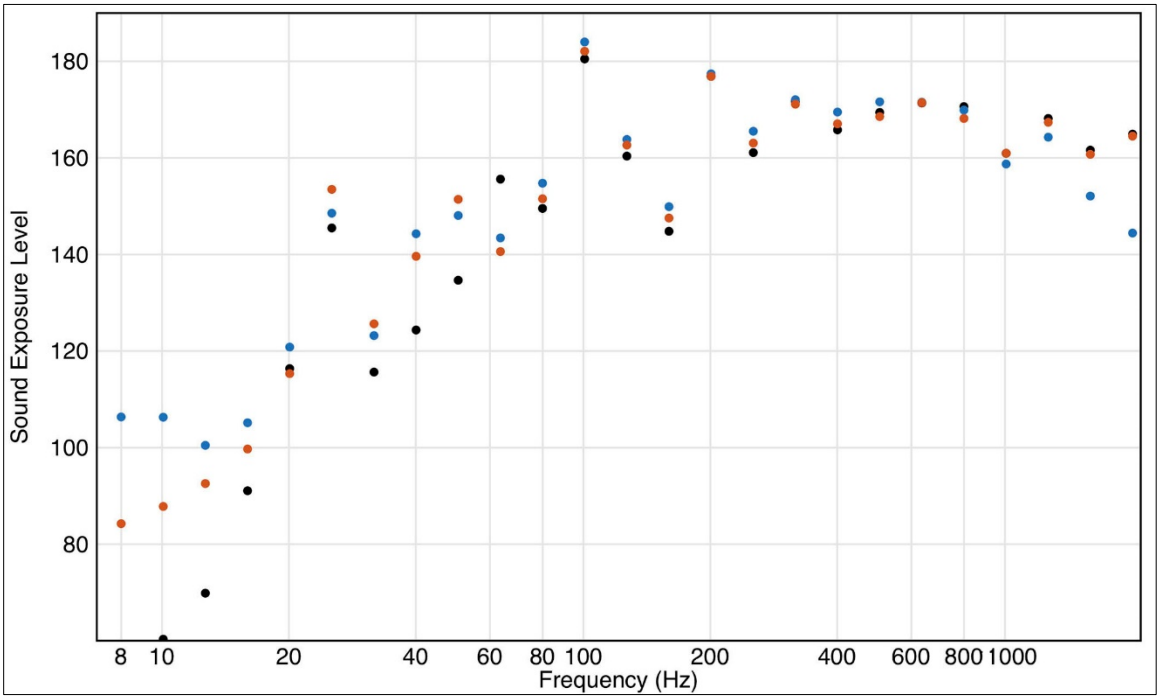

Figure 5-6. Comparison of the decidecade band SEL computation for LF cetaceans. Decidecade band nominal center frequencies are 8 Hz to 2 kHz.

The total frequency range covered by these bands is 7.1 Hz to 2.2 kHz. TNO (black), Curtin University (red), FE/PE (blue). µPa = micropascal; dB = decibel; FE = finite element; Hz = hertz; LF = low-frequency; PE = parabolic equation; re = with reference to; s = second; SEL = L_E = sound exposure level; TNO = Netherlands Organisation for Applied Scientific Research. SEL units = dB re 1 µPa^2 s.

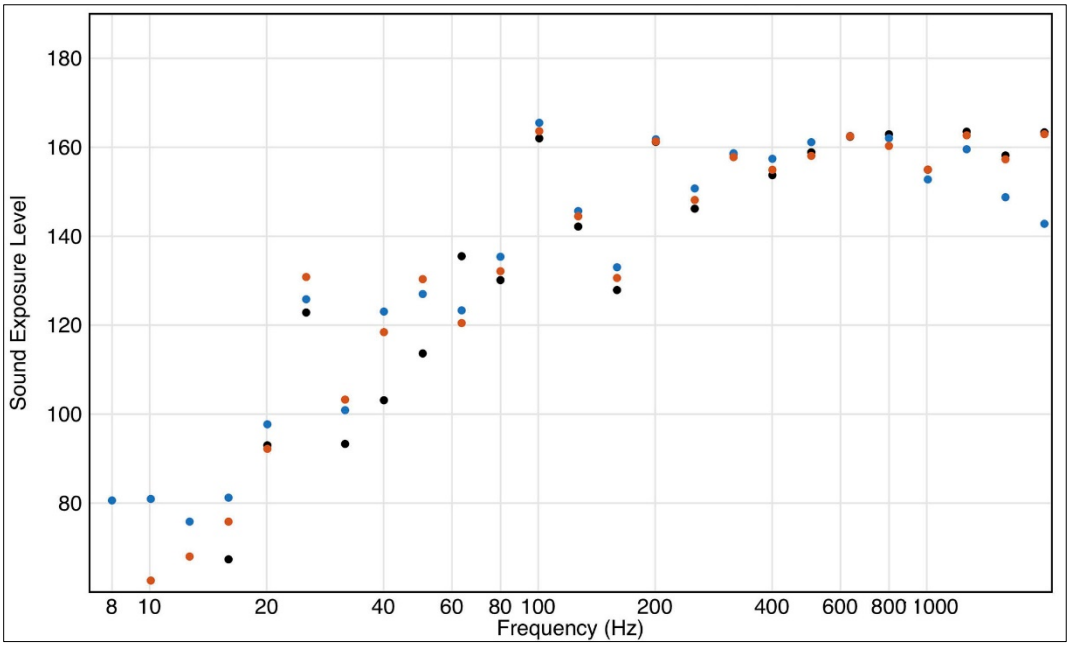

Figure 5-7. Comparison of the decidecade band SEL computation for MF cetaceans.
TNO (black), Curtin University (red), FE/PE (blue). µPa = micropascal; dB = decibel; FE = finite element; Hz = hertz; MF = mid-frequency; PE = parabolic equation; re = with reference to; s = second; SEL =L_E= sound exposure level; TNO = Netherlands Organisation for Applied Scientific Research. SEL units = dB re 1 µPa^2 s.

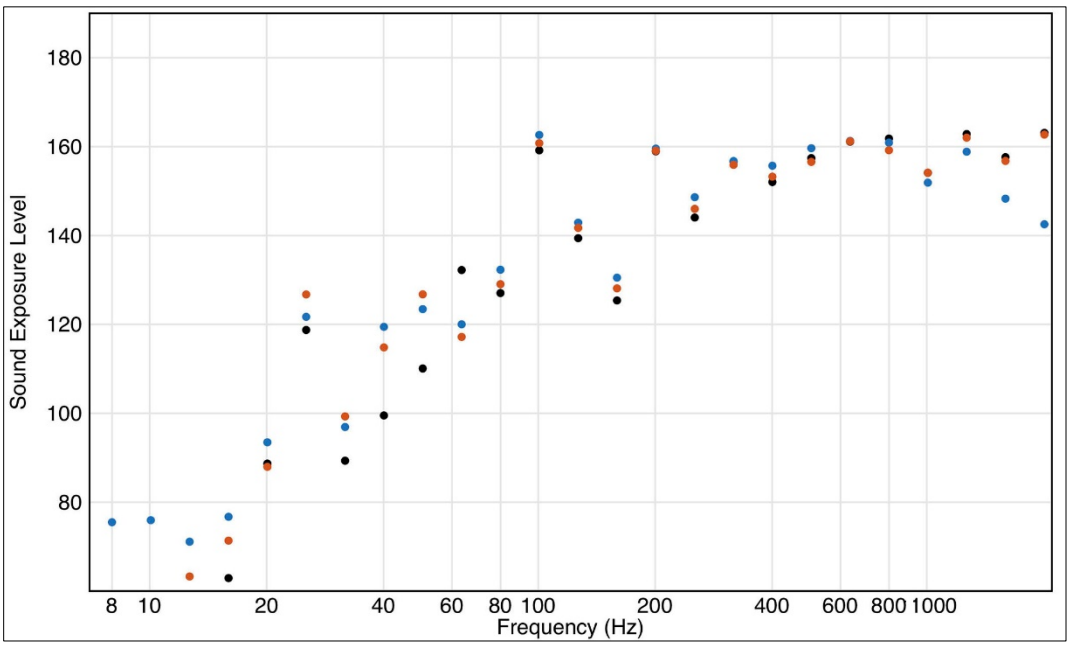

Figure 5-8. Comparison of the decidecade band SEL computation for HF cetaceans.
TNO (black), Curtin University (red), FE/PE (blue). µPa = micropascal; dB = decibel; FE = finite element; HF = high-frequency; Hz = hertz; PE = parabolic equation; re = with reference to; s = second; SEL = L_E = sound exposure level; TNO = Netherlands Organisation for Applied Scientific Research. SEL units = dB re 1 µPa^2 s.

5.1.3 Frequency Accumulation of Weighted Sound Exposure Level

The impact of the frequency weighting (**Figure 1-6**; NMFS, 2018) on the decidecade band L_E received by selected marine mammal hearing groups was examined. Of particular interest was whether the assumption of truncating the propagation modeling at an upper frequency band of 1 kHz was justifiable (to address the concern: *is there energy above 1 kHz that affects the broadband L_E?*). To determine this, the $L_{E,\mathrm{w}}$ was added across all decidecade bands from the lowest frequency to an upper frequency limit, and the result was calculated as a function of the upper frequency. This resulting quantity is referred to as the frequency-accumulated SEL (faSEL). The faSEL result for LF cetaceans is plotted in **Figure 5-9**.

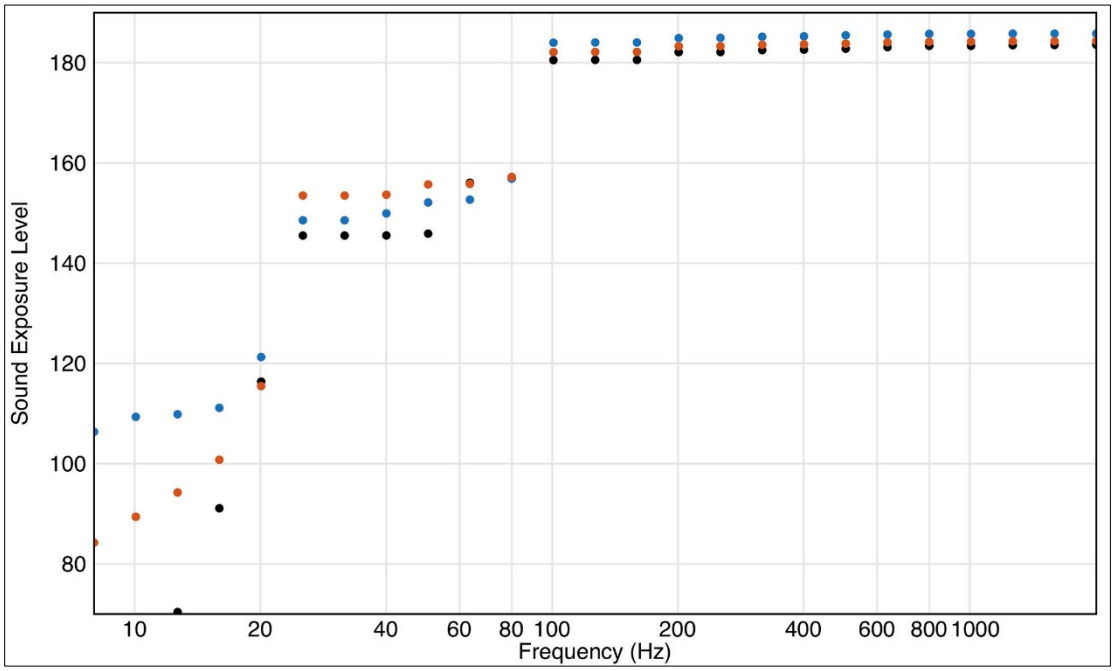

Figure 5-9. Comparison of the frequency-accumulated SEL (faSEL) computation for LF cetaceans.

TNO (black), Curtin University (red), FE/PE (blue). µPa = micropascal; dB = decibel; FE = finite element; LF = low-frequency; PE = parabolic equation; re = with reference to; s = second; SEL = L_E = sound exposure level; TNO = Netherlands Organisation for Applied Scientific Research. SEL units = dB re 1 µPa^2 s.

The majority of energy contributing to the faSEL was from frequencies below 400 Hz. There was approximately a 1 dB loss of the broadband L_E (accumulated over all frequencies from 7.1 Hz to 2.2 kHz) for LF cetaceans, and this assumed there was no net contribution of energy from above 2.2 kHz. The MF cetacean faSEL is plotted in **Figure 5-10**. Frequencies above 1 kHz will impact the weighted $L_{E,\mathrm{cum}}$ for MF and HF cetaceans.

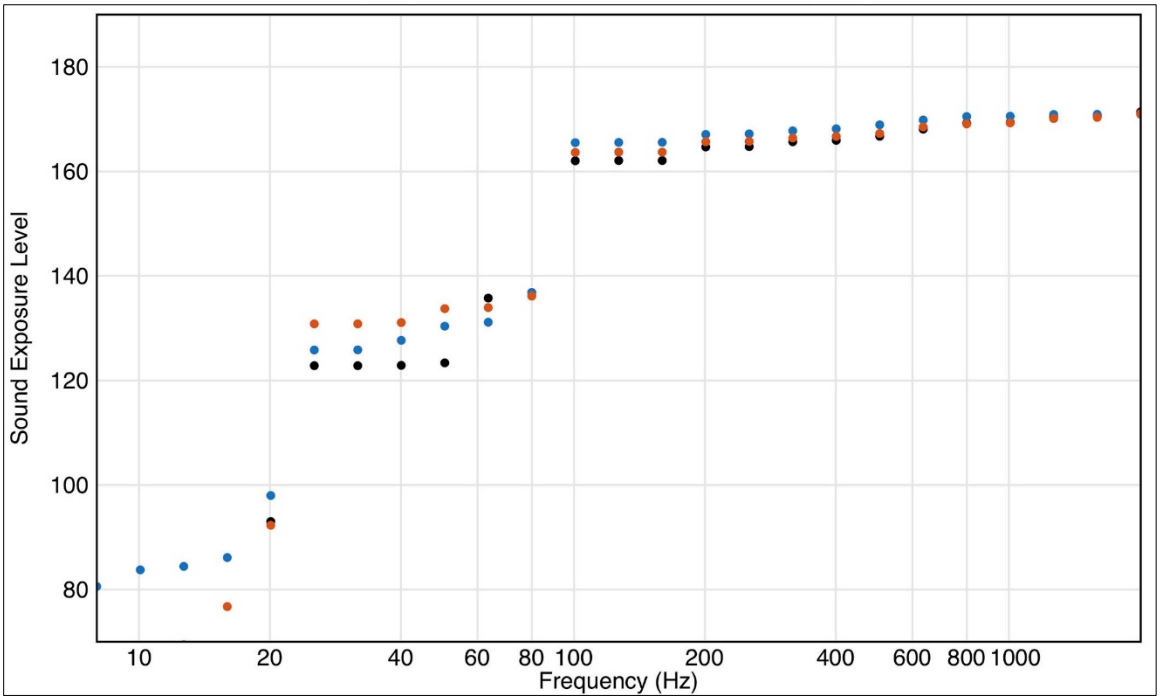

Figure 5-10. Comparison of the frequency-accumulated SEL (faSEL) computation for MF cetaceans.

TNO (black), Curtin University (red), FE/PE (blue). µPa = micropascal; dB = decibel; FE = finite element; Hz = hertz; MF = mid-frequency; PE = parabolic equation; re = with reference to; s = second; SEL = L_E = sound exposure level; TNO = Netherlands Organisation for Applied Scientific Research; SEL units = dB re 1 µPa^2 s.

To determine the contribution to the $L_{E,\mathrm{w}}$ from frequencies above 2.2 kHz on the broadband L_E, the full spectrum was needed up to 20 kHz. This was not possible with the COMPILE I data set because the upper frequency bound was 2.2 kHz. Therefore, to address energy at frequencies above 2.2 kHz, measured data from the Gemini wind farm were used.

5.2 Model Validation for Gemini Measurements: Piles U8 and Z2

5.2.1 Inputs – Gemini

5.2.1.1 Pile Geometry and Forcing Function

The forcing function [g(t)] was determined by matching the measured and modeled sound fields at 732 m from the U8 pile. This forcing function was used to predict the sound field for U8 at other distances and for Z2 (**Figure 5-11**). (U8 and Z2 are the names of two piles from the Gemini wind farm.) The length, thickness, and diameter (at the top and bottom of each pile section) are provided in **Table 5-1**. The water depth, pile penetration, sample interval, and range for the U8 and Z2 piles are provided in **Table 5-2**. The material properties used for the U8 and Z2 pile scenarios are provided in **Table 5-3.**

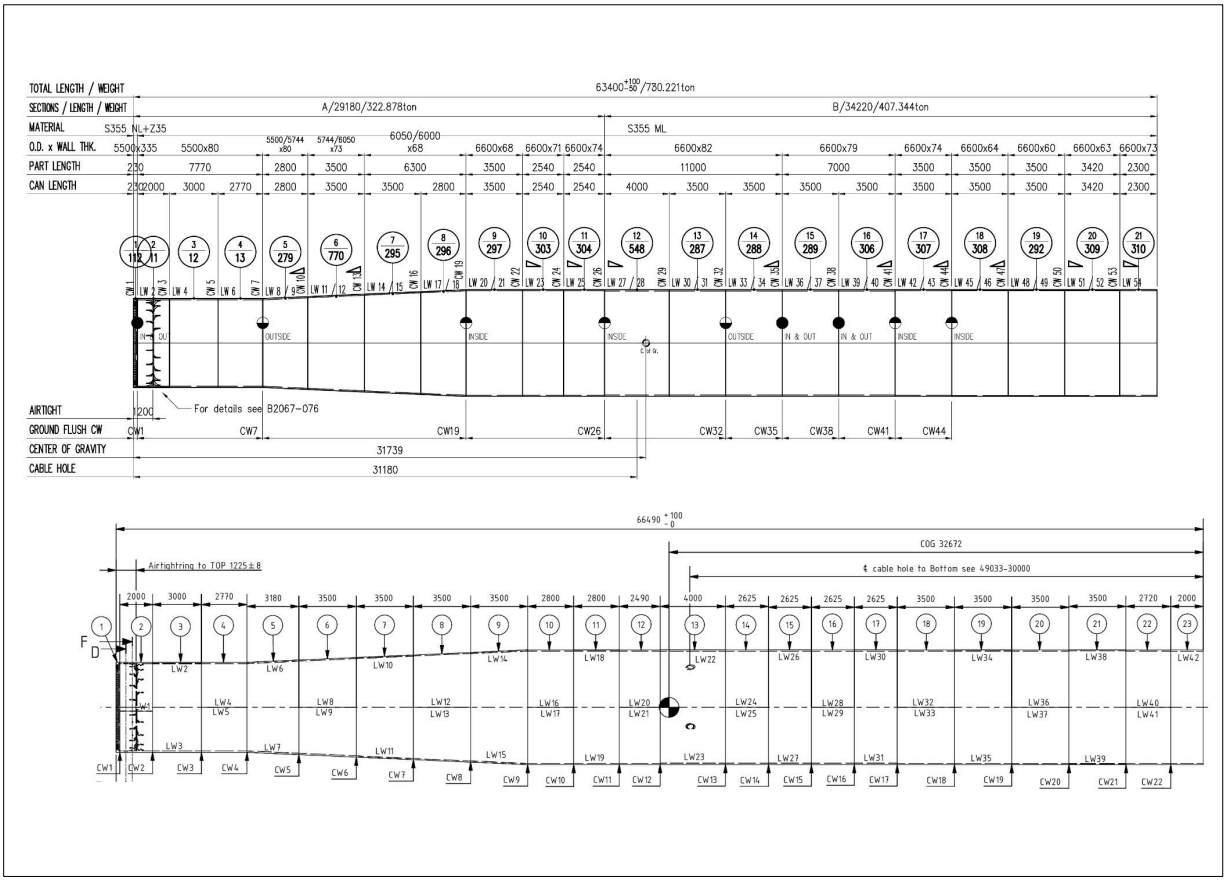

Figure 5-11. Definition of the pile geometries.
Top: U8; Bottom: Z2. The length, thickness, and diameter (at top and bottom of each section) are provided in **Table 5-6**.

Table 5-1. Dimensions of the U8 and Z2 pile geometries.

Section	U8				Z2			
	Length (m)	Diameter (m)		Thickness (mm)	Length (m)	Diameter (m)		Thickness (mm)
		Upper	Lower			Upper	Lower	
1	0.230	5.500	5.500	80	0.230	5.500	5.500	80
2	2.000	5.500	5.500	80	2.000	5.500	5.500	80
3	3.000	5.500	5.500	80	3.000	5.500	5.500	80
4	2.770	5.500	5.500	80	2.770	5.500	5.500	80
5	3.180	5.500	5.778	80	2.800	5.500	5.744	80
6	3.500	5.778	6.083	73	3.500	5.744	6.050	73
7	3.500	6.083	6.388	68	3.500	6.050	6.600	68
8	3.500	6.388	6.694	68	2.800	6.600	6.600	68
9	3.500	6.694	7.000	70	3.500	6.600	6.600	68
10	2.800	7.000	7.000	70	2.540	6.600	6.600	71
11	2.800	7.000	7.000	73	2.540	6.600	6.600	74
12	2.490	7.000	7.000	73	4.000	6.600	6.600	82
13	4.000	7.000	7.000	83	3.500	6.600	6.600	82
14	2.625	7.000	7.000	80	3.500	6.600	6.600	82
15	2.625	7.000	7.000	80	3.500	6.600	6.600	79
16	2.625	7.000	7.000	80	3.500	6.600	6.600	79
17	2.625	7.000	7.000	80	3.500	6.600	6.600	74
18	3.500	7.000	7.000	76	3.500	6.600	6.600	64
19	3.500	7.000	7.000	70	3.500	6.600	6.600	60
20	3.500	7.000	7.000	65	3.420	6.600	6.600	63
21	3.500	7.000	7.000	60	2.300	6.600	6.600	73
22	2.720	7.000	7.000	67	--	--	--	--
23	2.000	7.000	7.000	77	--	--	--	--

m = meter; mm = millimeter.

Table 5-2. Water depth, pile penetration, and sample interval for the U8 and Z2 piles.

Parameter	U8		Z2	
	Value	Unit	Value	Unit
Water depth, at pile	34	m	30	m
Sediment penetration, final	27.41	m	28.4	m
Sediment penetration, model	20.8	m	20.8	m
Sample interval	0 – 95	m	0 – 95	m
Sample range	5	m	5	m

m = meter.

Table 5-3. Material properties used for the U8 and Z2 cases.

Parameter	Value	Unit
Sound speed water	1,510	m s^{-1}
Density water	1,026	kg m^{-3}
Sound speed sediment	1,810	m s^{-1}
Density sediment	2,140	kg m^{-3}
Young's modulus steel	210	GPa
Poisson's ratio steel	0.3	--
Density steel	7,850	kg m^{-3}
Sediment damping*	0.88	dB λ^{-1}
P-wave steel (in sediment**), α	1.5	dB λ^{-1}
S-wave steel (in sediment**), α	3.0	dB λ^{-1}

α = absorption coefficient; λ = wavelength in the sediment or steel, as appropriate; dB = decibel; GPa = gigapascal; kg = kilogram; m = meter; s = second.
* The sediment damping was not used in the source model.
** This equivalent damping value accounts for losses due to pile/sediment interaction and was only applied to the pile section that penetrated the sediment.

The hammer used to drive the pile was an IHC Hydrohammer S-2000. It was assumed the hammer was mounted on the pile via an anvil, as sketched in the IHC Merwede (2015), "Large pile diameters" brochure (**Figure 5-12**). The mass of the anvil is listed as 120 metric tons. A detailed view of the anvil geometry in the FE model is shown in the right panel of **Figure 5-12**. The excitation force is distributed over the flat top surface. Based on this geometry and the density of steel in the model, the mass of the anvil in the model is approximately 135 metric tons. The axisymmetric representation of the meshed pile, anvil, and environments as seen in COMSOL-software is shown in **Figure 5-13**. A close-up comparison of the mesh at the water surface and between the grids is shown as well.

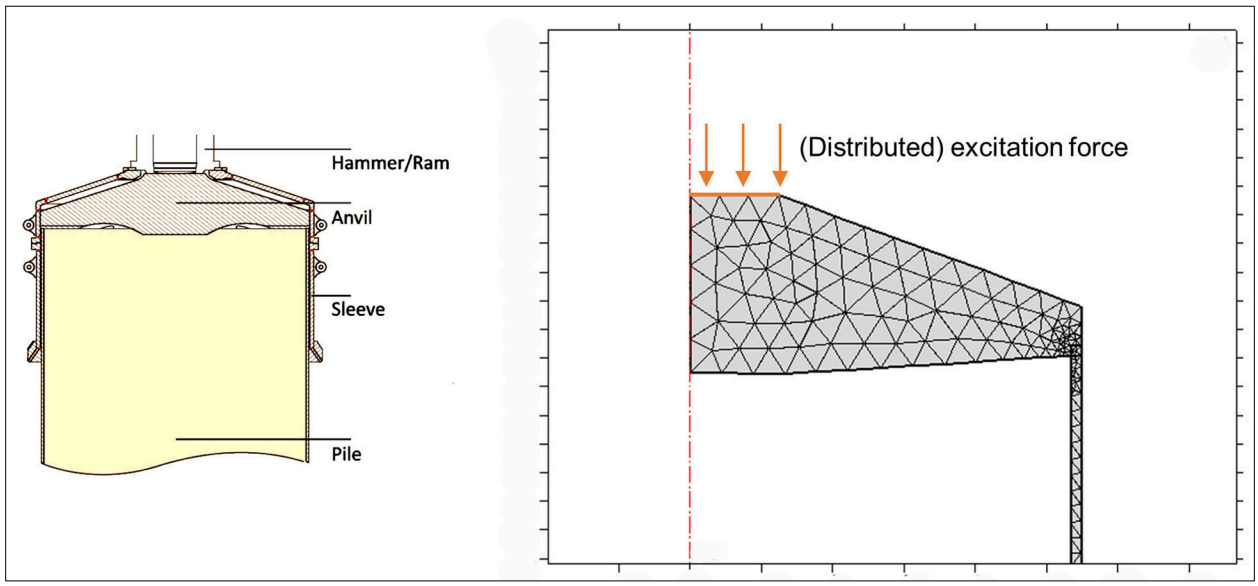

Figure 5-12. Sketch and detail of the anvil.
Sketch of the anvil used for piles U8 and Z2 from brochure IHC Hydrohammer (left; IHC Merwede [2015]). Detailed view of the anvil geometry in the finite element model (right). The excitation force is distributed over the flat top surface.

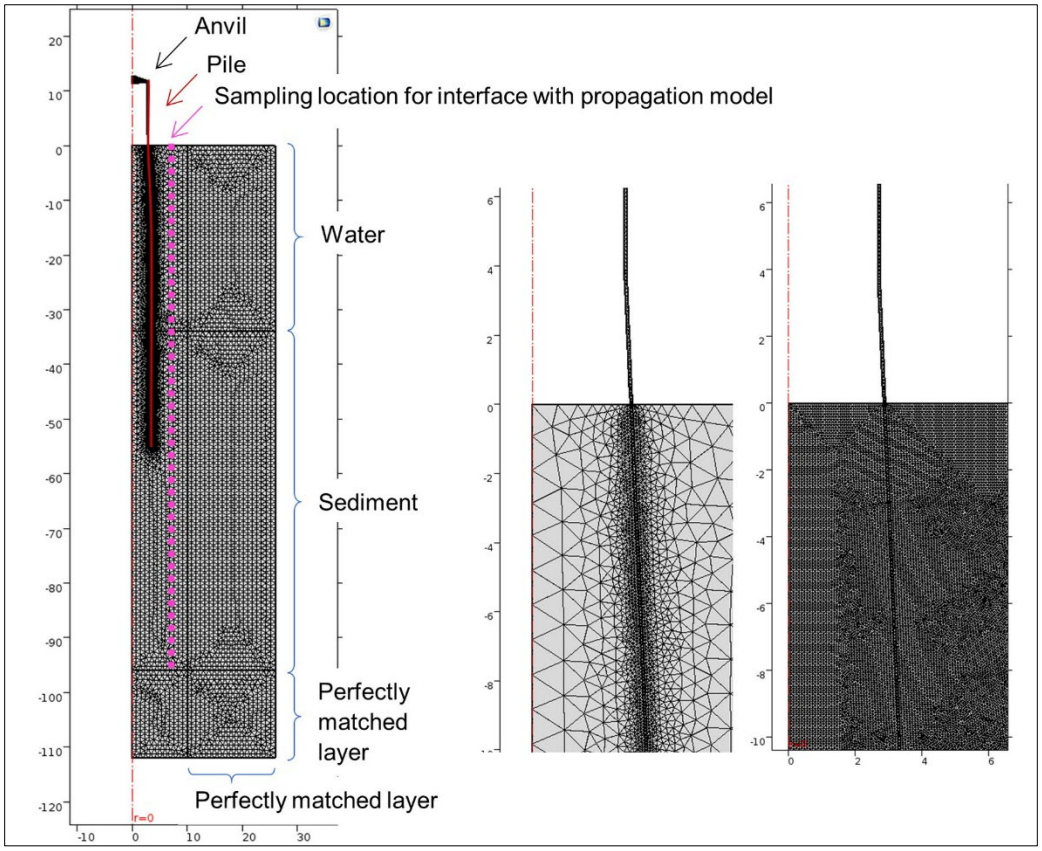

Figure 5-13. Axisymmetric representation of the meshed pile, anvil, and environments.
Representation in COMSOL (left). Comparison of a close-up of the mesh at the water surface, between the grid for lowest frequencies (middle) and highest frequencies (right).

5.2.1.2 Gemini Wind Farm Model Validation

The combined FE/PE methodology was validated by comparing modeled results to measurements obtained during construction of the Gemini wind farm.

5.2.2 Data Analysis

In order to compare acoustic model predictions with observations, it was necessary to compute quantitative acoustic metrics from the measured and simulated time series. The three acoustic metrics chosen were $L_{p,\mathrm{pk}}$, L_E, and $L_{p,90\%}$. $L_{p,\mathrm{pk}}$ is the maximum received pressure across the signal reception. L_E is the level of the time-integrated sound pressure squared. $L_{p,90\%}$ is the root-mean-square pressure evaluated in the time window between the 5$^{\mathrm{th}}$ and 95$^{\mathrm{th}}$ signal energy percentiles.

After processing, the measurements generated a set of files with time series from single hydrophone sites at ranges of 0.732, 7.017, 31.816, and 65.764 km. Each site had two receivers, positioned 2 and 10 m above the seafloor. The water depth varied by less than 2 m for the entire region. Data were sampled at a rate of 48 kHz and were time-aligned for each location. A 3-minute piling sequence was selected with a hammer energy of 750 kilojoules (kJ), approximately constant across the sequence. The start time of this sequence was 12:34 UTC on July 21, 2015. The pile strike rate was 0.76 Hz (one strike every

1.32 seconds). The data were further processed to isolate the received signal for each strike. This was done by reshaping the single time-series vector into a slow-time/fast-time matrix corresponding to 1.3 seconds of fast-time data. A matrix was generated for each pile strike. This approach worked well, but occasionally a strike arrival was on the boundary between two windows and resulted in a mislabel or mis-association of strike arrivals between two instruments. This is problematic because, if an arrival spans the boundary, then the L_E computation only includes a portion of the signal. This issue was addressed by manually discarding outliers. An example of a single received pile signal for U8 for measurement position 1 (MP1) at 732 m range, recorded from a 2-m depth hydrophone, is shown in **Figure 5-14**.

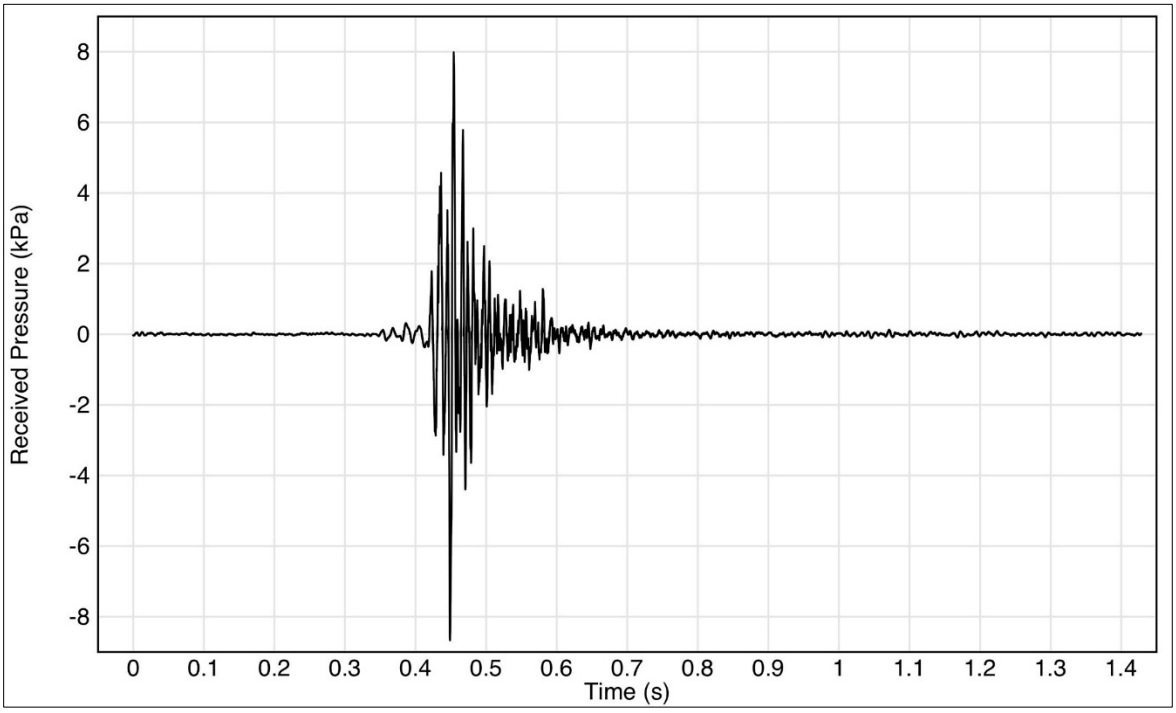

Figure 5-14. Sound pressure time series, *p*(*t*), recorded at 732 m range, for the U8 pile.
kPa = kilopascal; s = second.

Acoustic metrics were computed for each pile strike (i.e., across each row of fast-time in the fast-time/slow-time matrix); those computed for the MP1 location of the U8 pile are shown in **Figure 5-15**. The acoustic metrics shown in **Figure 5-15** for the 10- and 2-m height hydrophones were grouped by series, meaning pile strikes 1 to 287 are from the 10-m hydrophone. The two notable drops in level correspond to the 1-minute periods when there were no pile strikes. There are a few pile strikes for each metric that fall as much as 10 dB. These represent pile strikes where the received signal spanned two different slow-time rows, so the L_E computation only included a portion of the signals. Values more than 5 dB below the median were dropped manually from the statistics so they would not be used in the computation of the received level distributions in subsequent analyses. A notable observation from the MP1 location is the uniform 2 to 3 dB difference between the 2- and 10-m hydrophones.

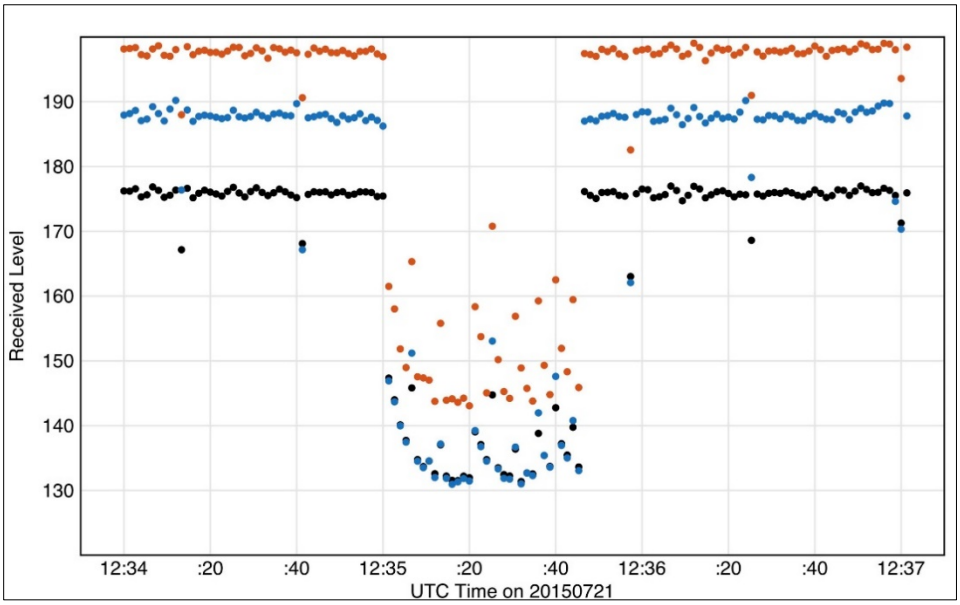

Figure 5-15. Measured acoustic metrics for the U8 pile at 732 m range.
Peak sound pressure level ($L_{p,\mathrm{pk}}$) (Red); SEL (Black); Root-mean-square sound pressure level ($L_{p,\mathrm{rms}}$) (Blue). Measurements are from the 2-m and 10-m hydrophones. µPa = micropascal; dB = decibel; re = with reference to; s = second; SEL = L_E = sound exposure level. $L_{p,\mathrm{pk}}$ and $L_{p,\mathrm{rms}}$ units = dB re 1 µPa; SEL units = dB re 1 µPa^2 s.

In order to compare the model results and measured observations, a distribution of each data set was computed. After manual thresholding (low values being discarded due to the signal straddling a boundary), the probability density function (PDF) and cumulative density function (CDF) were computed. The PDF and CDF for the U8 pile at 732 m range are shown in **Figure 5-16**.

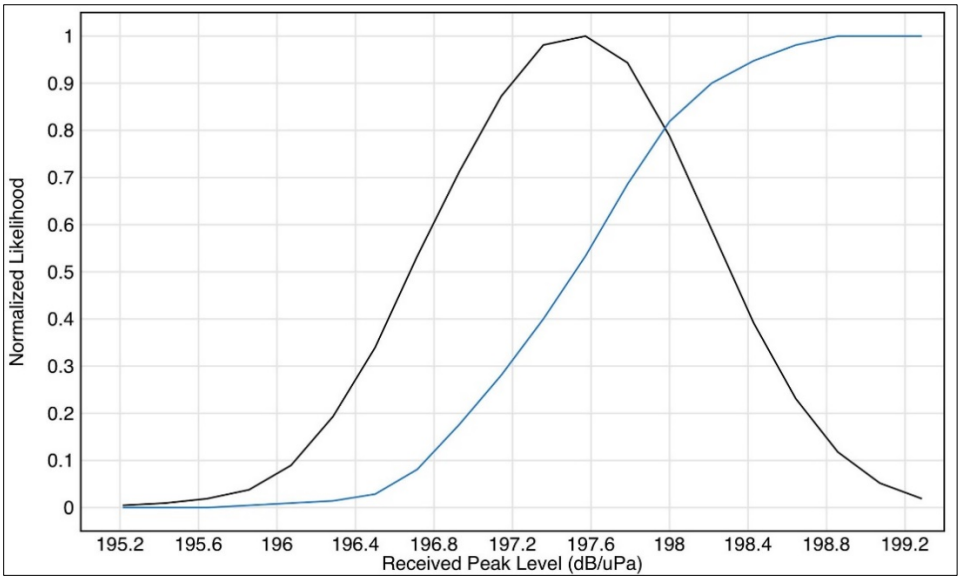

Figure 5-16. Normalized likelihood for $L_{p,\mathrm{pk}}$, for the U8 pile at 732 m range.
Probability density function (PDF) (Black) and cumulative density function (CDF) (Blue). µPa = micropascal; dB = decibel; m = meter; re = with reference to; $\mathrm{SPL_{peak}}$ = $L_{p,\mathrm{pk}}$ = peak sound pressure level.
$L_{p,\mathrm{pk}}$ units = dB re 1 µPa.

The statistics at the MP2 location (7 km) show a higher right-hand tail, which is driven by the rise in received values at the end of the sequence of strikes (**Figure 5-17**). The PDF and CDF for the U8 pile at 7 km range are shown in **Figure 5-18**.

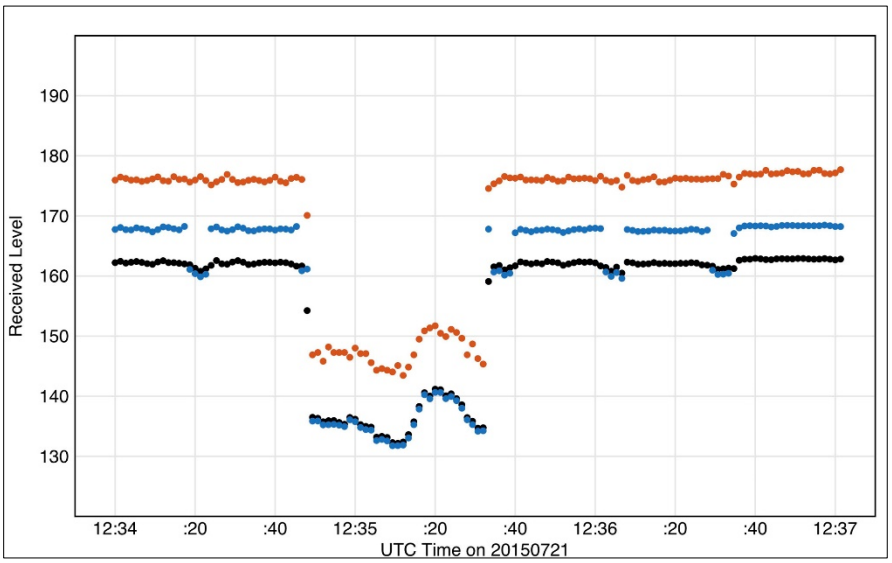

Figure 5-17. Acoustic metrics for the U8 pile at 7 km range.
Red: peak sound pressure level ($L_{p,\mathrm{pk}}$); Black: SEL; Blue: root-mean-square sound pressure level ($L_{p,\mathrm{rms}}$). Measurements are from 2-m and 10-m hydrophones. µPa = micropascal; dB = decibel; km = kilometer; $L_{p,\mathrm{pk}}$ = peak sound pressure level; m = meter; re = with reference to; s = second; SEL = L_E = sound exposure level. $L_{p,\mathrm{pk}}$ and $L_{p,\mathrm{rms}}$ units = dB re 1 µPa; SEL units = dB re 1 µPa^2 s.

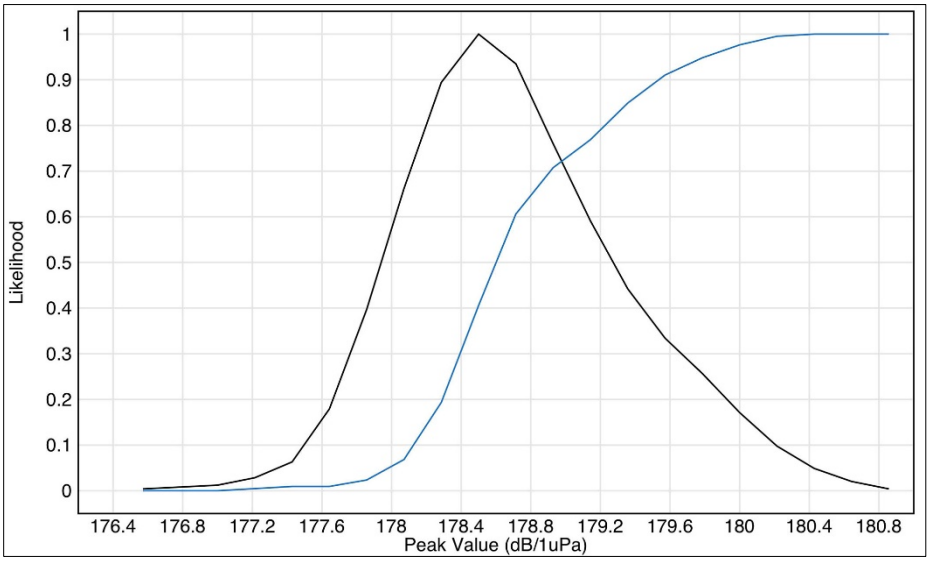

Figure 5-18. Normalized likelihood statistics for $L_{p,\mathrm{pk}}$, for the U8 pile at 7 km range.
Probability density function (PDF) (Black) and cumulative density function (CDF) (Blue). µPa = micropascal; dB = decibel; km = kilometer; $L_{p,pk}$ = peak sound pressure level; re = with reference to. $L_{p,\mathrm{pk}}$ and $L_{p,\mathrm{rms}}$ units = dB re 1 µPa.

The MP3 location's (32 km) acoustic metric values are shown in **Figure 5-19**. At this range, the signal-to-noise ratio dropped, which complicated the computation of $L_{p,\mathrm{rms}}$ because the noise was included in the computation of the root-mean-square sound pressure. The effect of this noise is observed in the blue dots, showing a repetitive structure of high values and then lower values. The effect by the noise was even more pronounced at the farthest range in the MP4 (66 km range) reception. $L_{p,\mathrm{pk}}$ was not affected by this signal-to-noise issue.

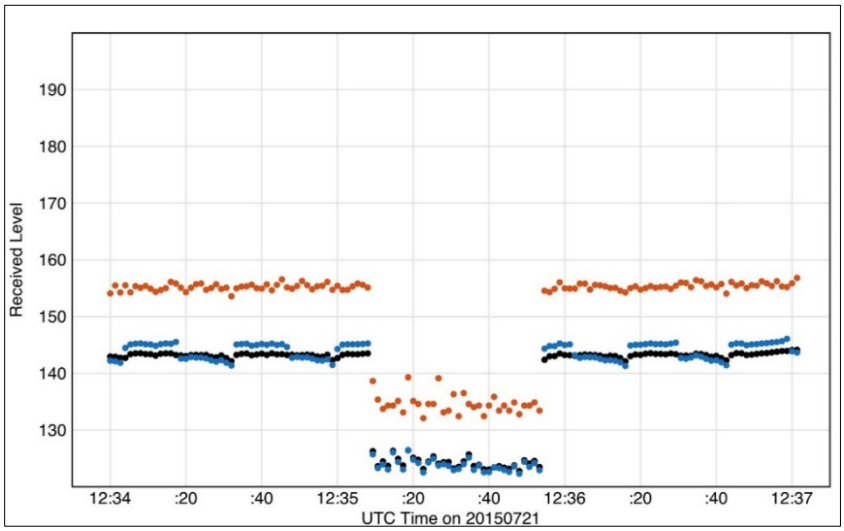

Figure 5-19. Acoustic metrics for the U8 pile at 32 km range.
Red: peak sound pressure level ($L_{p,\mathrm{pk}}$); Black: SEL; Blue: root-mean-square sound pressure level ($L_{p,\mathrm{rms}}$). Measurements are from 2-m and 10-m hydrophones. µPa = micropascal; dB = decibel; km = kilometer; m = meter; re = with reference to; s = second; SEL = L_E = sound exposure level. $L_{p,\mathrm{pk}}$ and $L_{p,\mathrm{rms}}$ units = dB re 1 µPa; SEL units = dB re 1 µPa^2 s.

At MP4 (66 km range, **Figure 5-20**), there was a 4-dB difference between the 10- and 2-meter receivers. The $L_{p,\mathrm{rms}}$ value was affected by the position of the signal within the window, making it difficult to determine the best values. It was also likely that the L_E value had acoustic noise increasing its value.

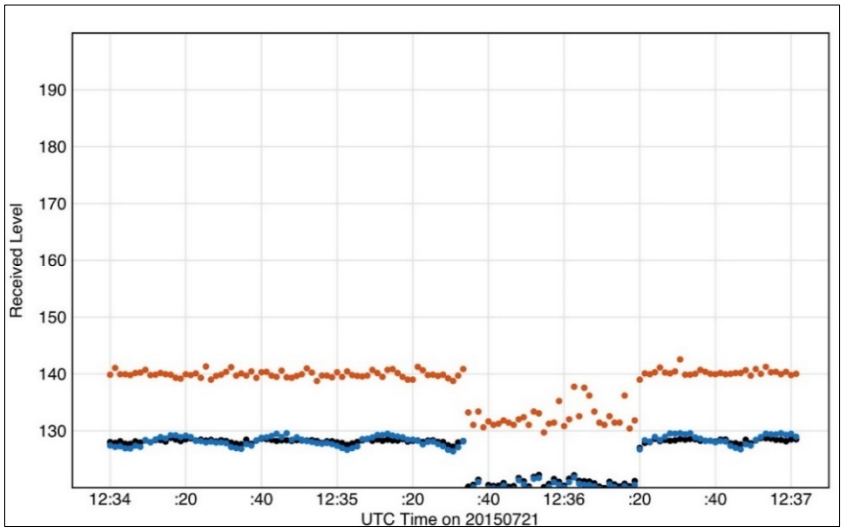

Figure 5-20. Acoustic metrics for the U8 pile at 66 km range.
Red: peak sound pressure level ($L_{p,pk}$); Black: SEL; Blue: root-mean-square sound pressure level ($L_{p,\mathrm{rms}}$). Measurements are from 2-m and 10-m hydrophones. µPa = micropascal; dB = decibel; km = kilometer; m = meter; re = with reference to; s = second; SEL = L_E = sound exposure level. $L_{p,\mathrm{pk}}$ and $L_{p,\mathrm{rms}}$ units = dB re 1 µPa; SEL units = dB re 1 µPa^2 s.

5.2.2.1 Sediment Modeling

One of the purposes of this project is to evaluate the influence of critical environmental parameters on the propagation of acoustic energy radiating from pile-driving activity. Sediment characteristics are a key environmental parameter. Particularly, sediment structure versus depth, which can be a driver in the frequency dependence of the propagation. For the analysis performed by TNO on Gemini wind farm data, a single half-space seafloor (meaning a seafloor of infinite thickness and uniform properties throughout) was used to approximate hard sand, which was the expected sediment type in the North Sea. The seafloor was modeled as a semi-infinite uniform sediment of sound speed 1,810 m s^{-1}, density 2,140 kilograms per cubic meter (kg m^{-3}), and HF attenuation 0.88 dB λ^{-1}, implying an attenuation coefficient proportional to frequency *f*. At LFs, it was recognized that the sediment attenuation decreased with decreasing frequency more quickly due to dispersion, an effect that was modeled by a frequency-dependent attenuation with alpha proportional to $f^{1.8}$ at LF (Binnerts et al., 2016).

In addition to the rapid decrease of alpha with decreasing frequency modeled in the TNO report, dispersion is known to result in a sound speed that also decreases with decreasing frequency (Zhou et al., 2009). For this project, rather than model dispersion, the effect of a sediment sound speed gradient was applied. In order to model the received energy across the frequency band of 10 to 2,500 Hz, a sediment model that had some depth dependence to it was necessary. A deep (infinite), unconsolidated single layer sediment model with a uniform sediment grain size was chosen, implying that sound speed increases with depth due to increasing pressure. This model was completely defined by the sediment grain size (which, in "phi" **ϕ** units, is the negative $\log_2$ of the mean sediment grain diameter in millimeters). A valuable way

of seeing how grain size relates to sediment type is through the Wentworth grain size chart, originally created in 1922, and presented in **Figure 5-21** from the U.S. Geological Survey (USGS) Open File Report 2006-1195 (Williams et al., 2007).

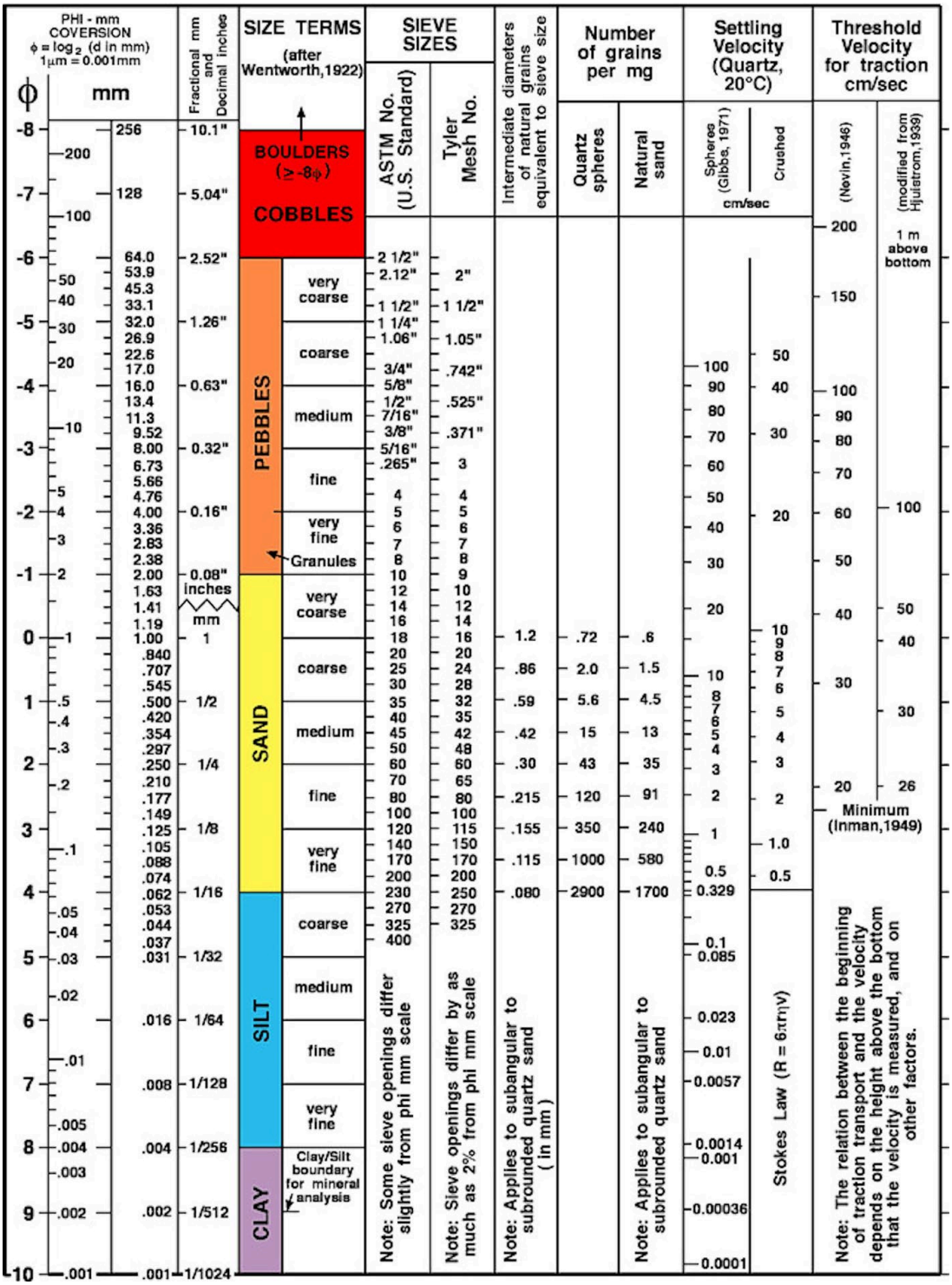

Figure 5-21. Wentworth grain size (ϕ) distribution table.
(From: Williams et al., 2007).

The mapping from sediment grain size to compressional speed, density, and attenuation was performed based on the work of Bachman et al. (1996).

For a sediment grain size 0 **ϕ**, which corresponds to the boundary between coarse sand and very coarse sand (referred to henceforth as "hard sand"), the compressional speed and attenuation as a function of depth is shown in **Figure 5-22**.

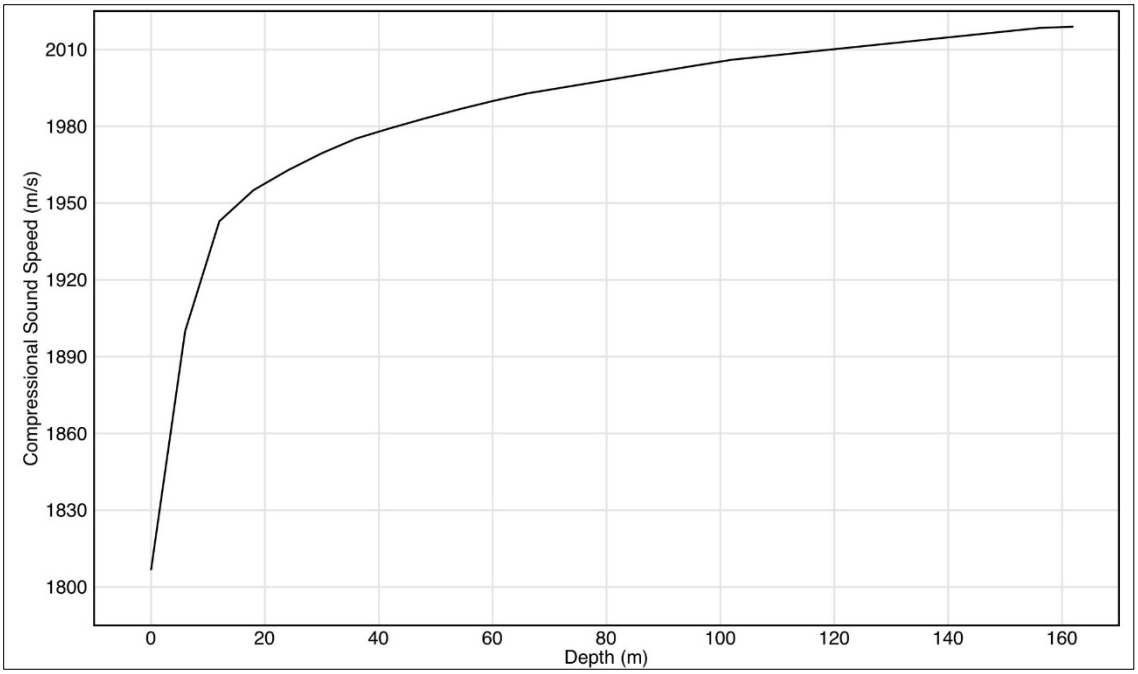

Figure 5-22. Hamilton-Bachman sediment profile of compressional speed for hard sand (0 ϕ).
ϕ = grain size.

The broadband acoustic pressure field was computed as a function of range (at a receiver depth of 2 m above the sediment) for each integer grain size between -3 **ϕ** (pebbles) and +3 **ϕ** (soft sand). The broadband L_E as a function of range for these seven sediment types is shown in **Figure 5-23**. A flat spectral source provided a received L_E at 731 m of 196 dB re 1 µPa² s (for 0 **ϕ**). At close ranges (<1 km), the sediment influence on received L_E was negligible. At farther ranges (1 to 10 km), the sediment influence on received L_E increased and became even more substantial at far ranges (10 to 70 km). The received L_E at 65 km varied by 30 dB between pebbles (-3 **ϕ**) and soft sand (+3 **ϕ**) sediments.

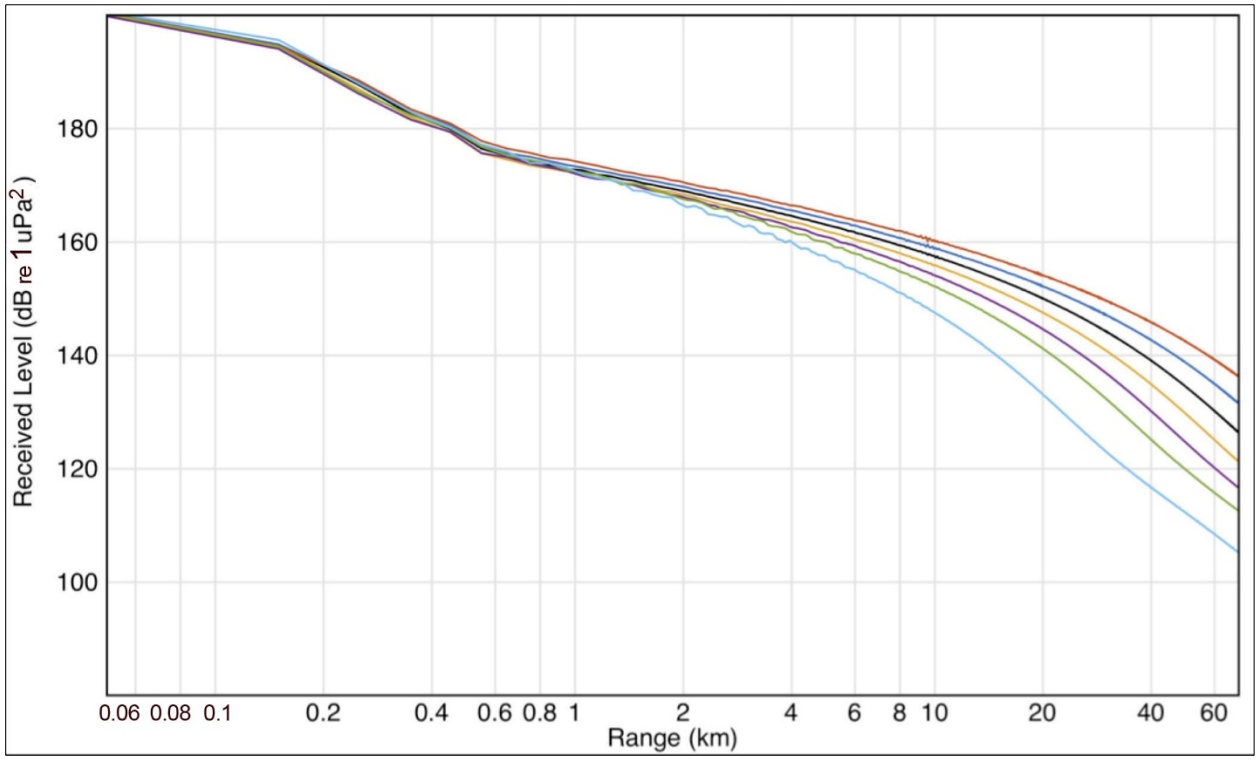

Figure 5-23. Modeled broadband SELs versus range.
For sediment grain size from -3 **ϕ** (pebbles) to +3 **ϕ** (soft sand). Orange = -3 **ϕ**, dark blue = -2 **ϕ**, black = -1 **ϕ**, yellow = 0 **ϕ**, purple = 1 **ϕ**, green = 2 **ϕ**, light blue = 3 **ϕ**. µPa = micropascal; **ϕ** = grain size; dB = decibel; re = with reference to; SEL = L_E = sound exposure level. SEL units = dB re 1 µPa^2 s.

5.2.2.2 Model-Data Comparison

The measured L_E at each range from MP1 through MP4 (732 m to 65 km) for the broadband L_E were compared, as were the decidecade bands centered at 125, 250, and 1,000 Hz. For each comparison, the measured L_E at 732 m range was used as the calibration point. **Figure 5-24** shows the model-measurement comparison as a function of range for each band of hard sand (0 **ϕ**). The full band comparison is excellent at all ranges. The model under-predicts the 125 Hz band at 7 km range and the 250 Hz band at 32 and 65 km, each by approximately 5 dB.

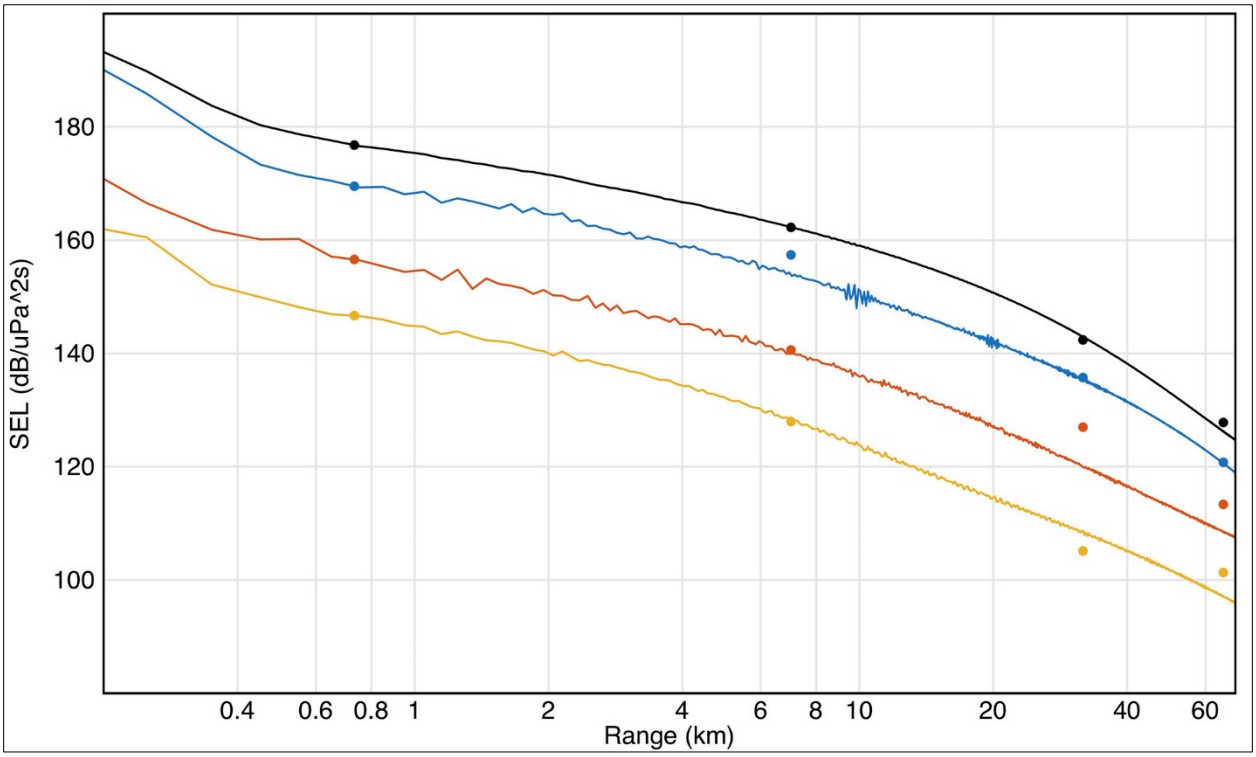

Figure 5-24. Comparison of measured (dots) and modeled (lines) SEL for hard sand (0 ϕ).
For full band (black) and decidecade bands at 125 Hz (blue), 250 Hz (red), and 1,000 Hz (yellow). Modeled data were normalized to be correct at 732 m range. µPa = micropascal; ϕ = grain size; dB = decibel; Hz = hertz; km = kilometer; m = meter; re = with reference to; s = second; SEL = L_E = sound exposure level. SEL units = dB re 1 µPa^2 s.

To demonstrate that the 0 ϕ sediment was the best match, the modeled and measured L_E were compared using the same frequency bands for softer sediment (+2 ϕ) (**Figure 5-25**) and for harder sediment (-2 ϕ) (**Figure 5-26**). In both figures, the values at -2 ϕ and +2 ϕ were plotted instead of -1 ϕ and +1 ϕ simply to highlight the differences of the L_E sensitivity to this environmental parameter more clearly. Modeled L_E were normalized to be correct at 732 m range.

For the softer sediment (+2 ϕ; **Figure 5-25**), all frequency band modeled L_E were approximately 5 dB lower than measured L_E when considering the 7 km range. At large ranges, the modeled L_E were lower by approximately 20 dB (particularly for the 125 Hz decidecade band and the broadband) near the 65 km range. Modeled L_E being consistently lower than measured L_E across all ranges indicated the modeled sediment was, as expected, softer than the true sediment. This is because the model lost more sound energy (attenuated it) than was attenuated by the actual water column sediments.

For the harder "fine pebble" sediment (-2 ϕ; **Figure 5-26**), all frequency band modeled L_E were 2 to 3 dB too high at 732 m range and 5 to 10 dB too high for the 125 Hz and full band at 65 km range. The modeled higher-frequency band results (particularly at 1,000 Hz) were better matches to the measurements. But, the mismatches between modeled and actual L_E at lower frequencies, particularly at larger ranges, indicated the modeled sediment was harder than the true sediment. Given that HF sound does not penetrate the seafloor to a great extent (due to the shorter wavelength), this "better match" at 125 Hz could be explained by a harder sediment near the seafloor interface with a soft sediment below.

However, a full geoacoustic inversion was beyond the scope of this work and this proof of concept to illustrate that 0 **ϕ** was the most appropriate grain size to use held true.

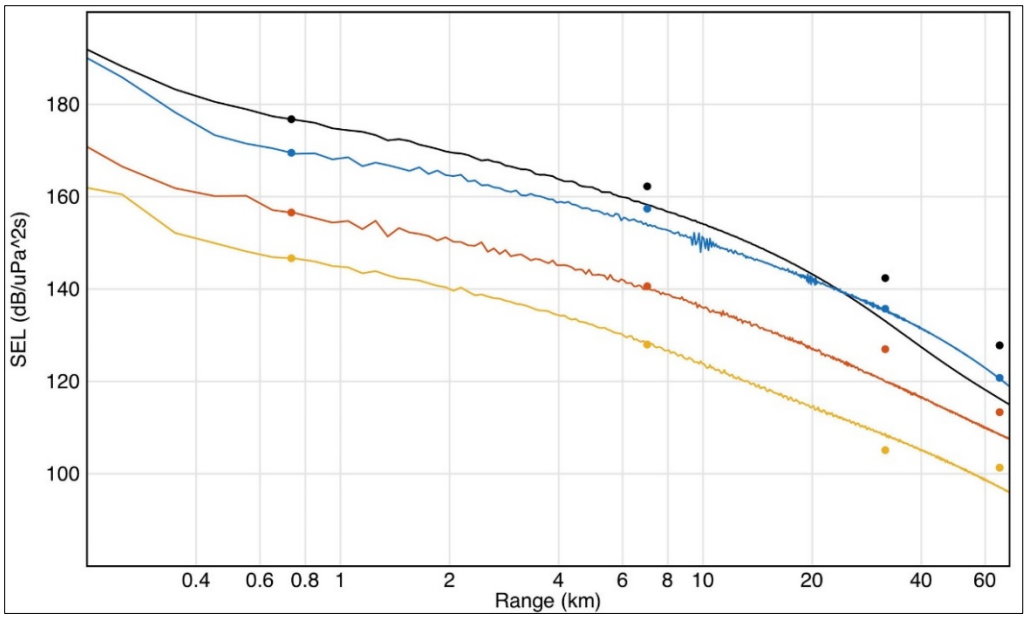

Figure 5-25. Comparison of measured (dots) and modeled (lines) SELs for soft sand (2 ϕ).
For full band (black) and decidecade bands centered at 125 Hz (blue), 250 Hz (red), and 1,000 Hz (yellow). µPa = micropascal; **ϕ** = grain size; dB = decibel; re = with reference to; s = second; SEL = L_E = sound exposure level. SEL units = dB re 1 µPa^2 s.

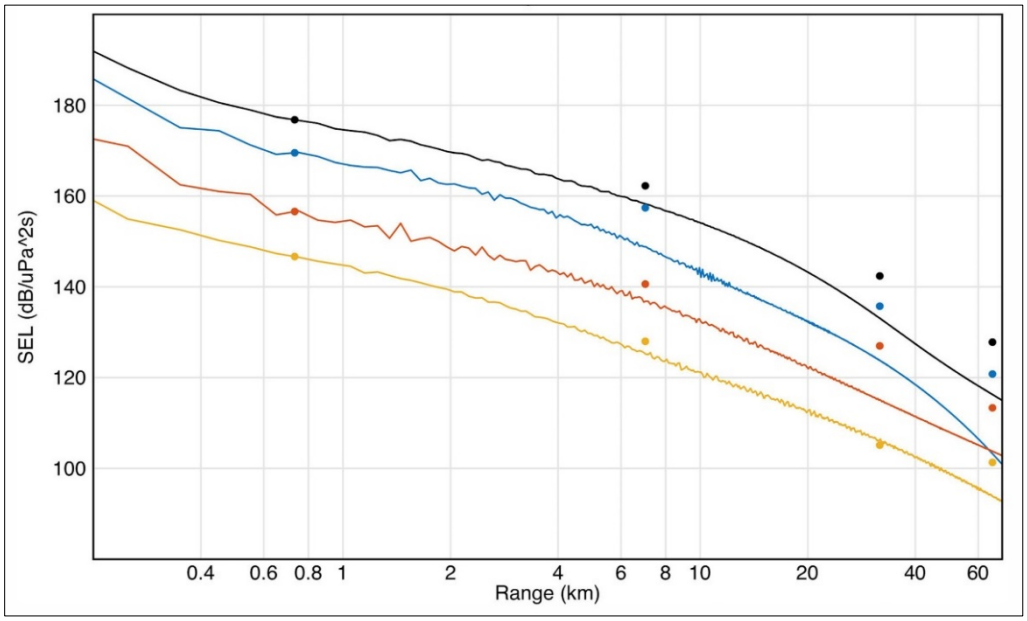

Figure 5-26. Comparison of measured (dots) and modeled (lines) SELs for pebble sediment (-2 ϕ).
For full band (black) and decidecade bands centered at 125 Hz (blue), 250 Hz (red), and 1,000 Hz (yellow). Modeled data were normalized to be correct at 732 m range. µPa = micropascal; **ϕ** = grain size; dB = decibel; m = meter; re = with reference to; s = second; SEL = L_E = sound exposure level. SEL units = dB re 1 µPa^2 s.

The measured and modeled $L_{p,\mathrm{pk}}$ were compared and plotted (**Figure 5-27**). The band source integer source strength was set so the measured and modeled L_E matched at the 732 m range. The source spectrum was assumed to be flat across frequency for the calculation of the peak sound pressure. This had the advantage that the frequency dependence (and thus pulse shape and dispersion) of the propagation was consistently handled by the numerical models. However, this was likely inaccurate because the flat spectral hammer model is equivalent to a delta function in time (an impulse of infinitesimal duration), which is not the case in practice. The agreement of the modeled peak and the measured peak is very good, particularly at distances beyond 10 km.

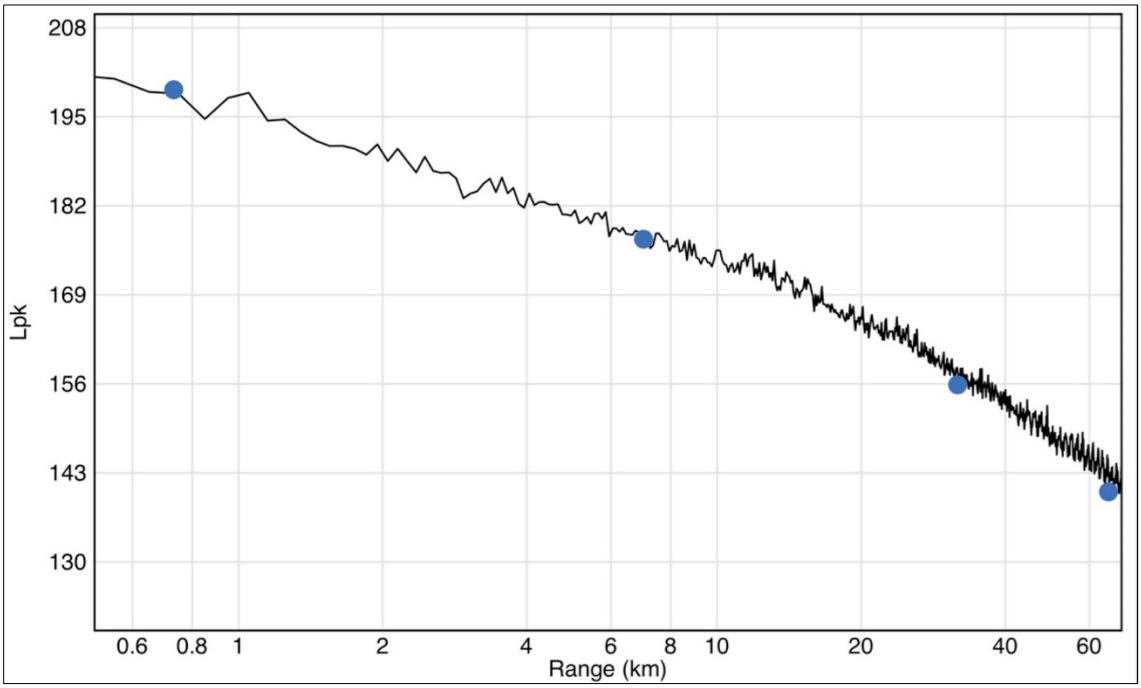

Figure 5-27. Comparison of the modeled broadband $L_{p,\mathrm{pk}}$ (line) for hard sand (0 ϕ) with Gemini U8 measurements (dots).

The model used a source hammer function with a flat spectrum with a power spectral density of 188 dB re 1 µPa^2 Hz^{-1}. µPa = micropascal; ϕ = grain size; dB = decibel; Hz = hertz; km = kilometer; $L_{p,\mathrm{pk}}$ = peak sound pressure level; re = with reference to. $L_{p,\mathrm{pk}}$ units = dB re 1 µPa.

The measured and modeled $L_{p,\mathrm{rms}}$ metrics were compared (**Figure 5-28**). The comparisons were not as good as for $L_{p,\mathrm{pk}}$ or L_E. The model appeared to under-predict these levels beyond 732 m range. This could be due to the flat spectral approximation or the addition of background noise in the measured rms computation. The model had no noise in it. The match between the measurements and model for $L_{p,\mathrm{rms}}$ was not as good as for $L_{p,\mathrm{pk}}$, likely because of the approximation of the impulse spectra being flat as a function of frequency, which leads to higher-frequency oscillations than are present in the true impact pile-forcing function.

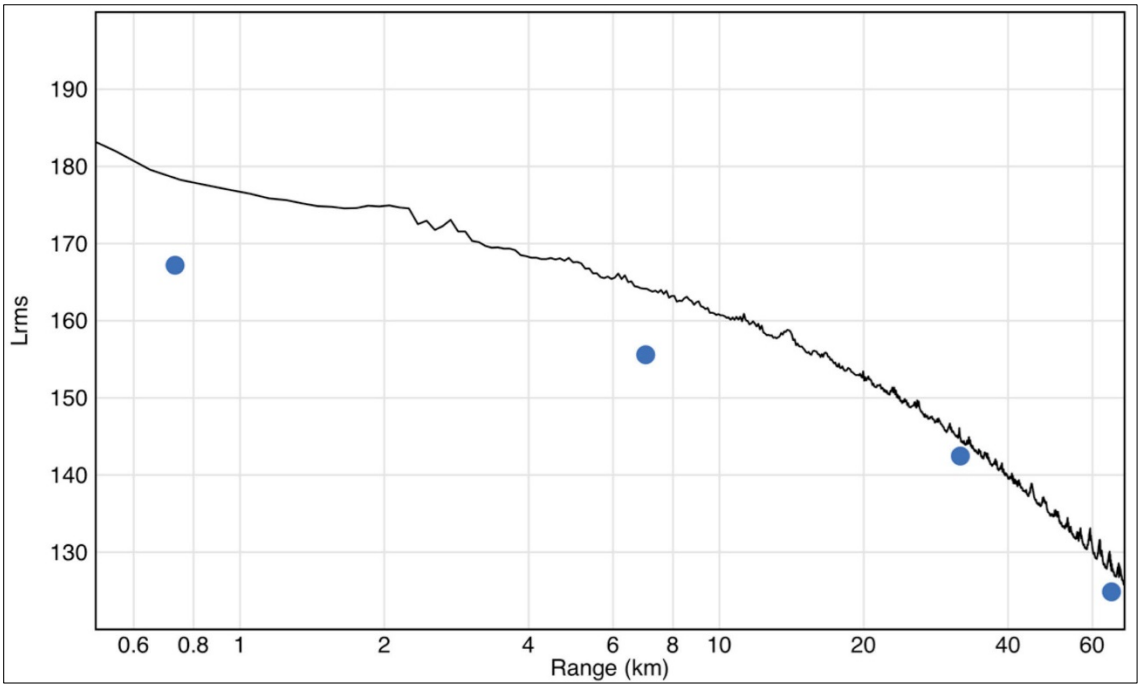

Figure 5-28. Comparison of the broadband $L_{p,\mathrm{rms}}$ (line) for hard sand (0 ϕ) with Gemini U8 measurements (dots).

The model used a source hammer function that has a flat spectrum with a power spectral density of 188 dB re 1 μPa^2 Hz^{-1}. μPa = micropascal; ϕ = grain size; dB = decibel; Hz = hertz; km = kilometer; re = with reference to; $L_{p,\mathrm{rms}}$ = root-mean-square sound pressure level. $L_{p,\mathrm{rms}}$ units = dB re 1 μPa.

L_E as a function of frequency, and range for all decidecade bands below 2.5 kHz were compared. The decidecade band source strength was estimated to match the measured L_E at 732 m range. The frequency and range-dependent comparison is shown in **Figure 5-29**. The agreement in both range and frequency was excellent. The model over-predicted the loss for frequencies 7 to 18 Hz (decidecade bands centered on 8 through 16 Hz). The very LF sound was sensitive to the seafloor at great depths (the wavelength is 100 m) and therefore was possibly being affected by a basement layer that is not in the model. An alternative explanation for the discrepancy is the effect of dispersion below 1 kHz (Zhou et al., 2009). This was not of considerable importance, however, because the measured energy levels of the pile hammer were small (below 18 Hz).

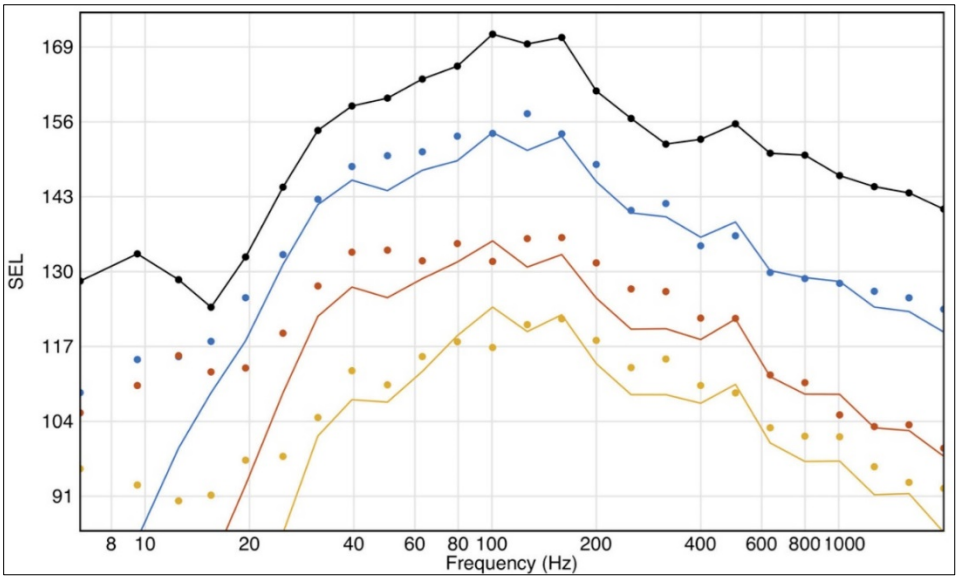

Figure 5-29. Comparison of measured (dots) and modeled (lines) decidecade SELs for hard sand (0 ϕ).

As a function of decidecade band center frequencies (8 Hz to 2 kHz) at receivers 732 m (black), 7,017 m (blue), 32 km (red), and 65 km (yellow). The source strengths per decidecade band were set to provide consistent results at 732 m range. µPa = micropascal; ϕ = grain size; dB = decibel; Hz = hertz; m = meter; re = with reference to; s = second; SEL = L_E = sound exposure level. SEL units = dB re 1 µPa^2 s.

The modeled and measured $p(t)$ at 732 m range from the U8 pile were compared. The phase coherence of the FE and PE solutions needed to be maintained, thus there was hesitation in estimating the complex source function for each frequency by matching the L_E at the 732 m range. Therefore, the single source strength (flat across the band) estimated in the comparison of **Figure 5-24** was used. This meant the calibration was not across frequency, but rather considered the source to be a flat spectrum one equivalent to a delta function in time. The comparison of the two $p(t)$ is shown in **Figure 5-30**. The peak correction was well matched (by design), and the time spread of the pulse, which was on the order of 0.2 seconds, also was well matched. The modeled signal had a substantial amount of energy at very low frequencies, which did not appear in the measured data.

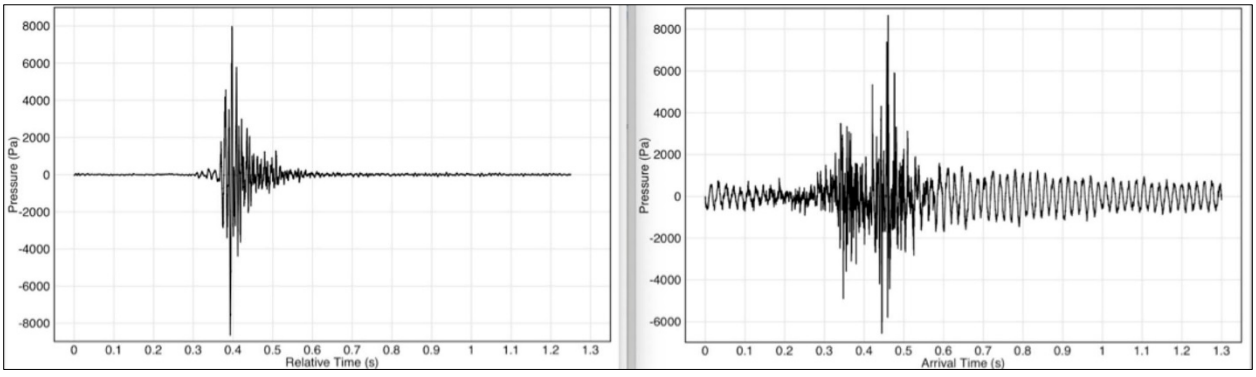

Figure 5-30. Comparison of measured (left) and modeled (right) time series *p*(*t*) of the U8 pile at 732 m range.

Using the peak sound pressure matching as the broadband calibration level. There is no phase correction. M = meter; Pa = pascal; s = second.

5.2.3 Z2 Pile Comparison

In addition to the recordings of the U8 pile hammer strikes, recordings were made available from the Z2 pile hammer strikes in the same environment for three sequences. The environment was similar, though the ranges and azimuthal propagation angles were slightly different. A sample of the results are presented, comparing the modeled and measured L_E. **Figure 5-31** presents the broadband and 125, 250, and 1,000 Hz decidecade bands as a function of range (similar to the U8 result in **Figure 5-24**). These results validated the model, demonstrating the calibration from one pile could be applied to a similar pile and the propagation versus range and frequency band was reproduced well.

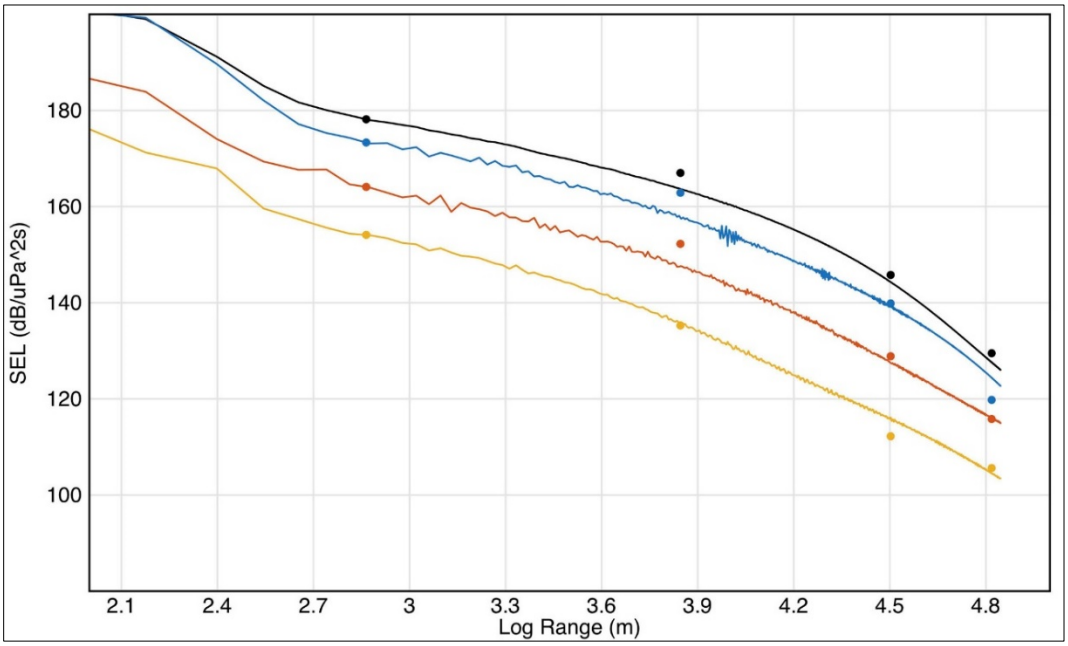

Figure 5-31. Comparison of measured (dots) and modeled (lines) received SELs for the Z2 pile for hard sand (0 ϕ).

Full band (black) and decidecade bands centered at 125 Hz (blue), 250 Hz (red), and 1,000 Hz (yellow). µPa = micropascal; ϕ = grain size; dB = decibel; Hz = hertz; m = meter; re = with reference to; s = second; SEL = L_E = sound exposure level. SEL units = dB re 1 µPa^2 s.

The decidecade band L_E was compared for the Z2 pile at each range (0.732, 7.017, 31.816, and 65.764 km) where the levels at 732 m were used for the calibrated decidecade band level. The results in **Figure 5-32** are similar to those in **Figure 5-29**. In both cases, there was a tendency to underestimate the L_E at low frequencies, but these values contributed little to the broadband calculations. In the case of the Z2 pile, there was a tendency to underestimate L_E at frequencies around 300 Hz and above 600 Hz; this discrepancy was more important because these frequencies contribute substantially to the broadband $L_{E,\mathrm{w}}$.

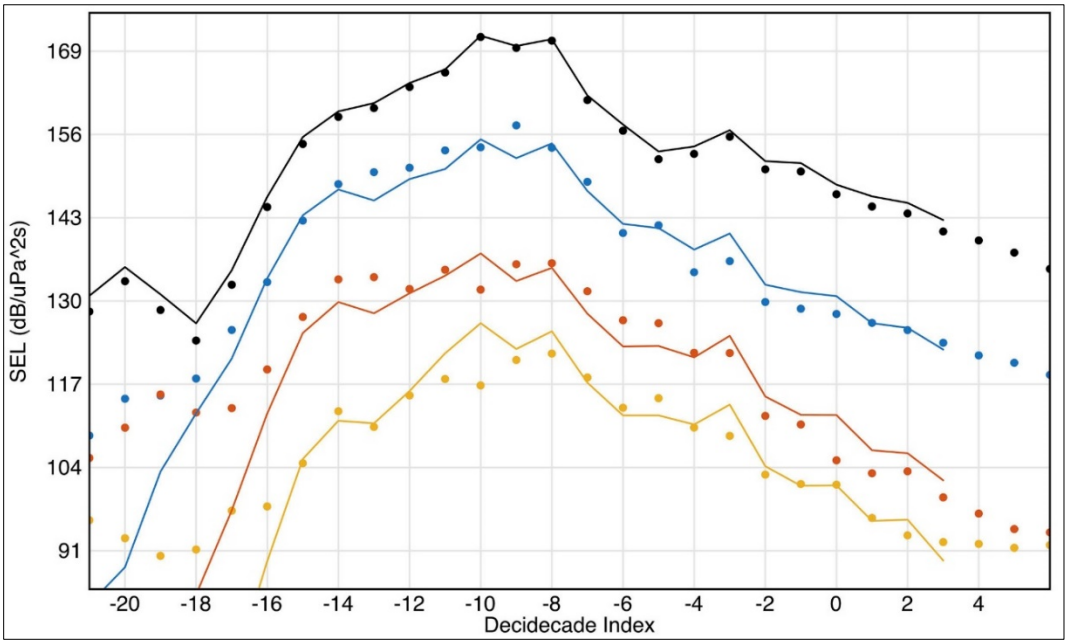

Figure 5-32. Comparison of measured (dots) and modeled (lines) SELs for the Z2 pile for hard sand (0 ϕ).

As a function of decidecade band center frequency (from 8 Hz to 2 kHz) at receivers 732 m (black), 7,017 m (blue), 32 km (red), and 65 km (yellow). The levels per decidecade band were set to match the U8 pile data at 732 m range. µPa = micropascal; ϕ = grain size; dB = decibel; km = kilometer; m = meter; re = with reference to; s = second; SEL = L_E = sound exposure level. SEL units = dB re 1 µPa^2 s.

5.2.3.1 Weighted Spectra for Gemini U8

The piles used in the COMPILE I study and those measured at the Gemini wind farm had peak energy in the 100 to 200 Hz frequency range. To evaluate whether the higher frequencies have an impact on the species-specific $L_{E,\mathrm{w}}$, it is important to have signals of interest beyond 2.5 kHz (the upper band for COMPILE I and the Gemini modeling). The Gemini data were reprocessed with an upper frequency bound of 20 kHz. The unweighted (uniform weighting) decidecade L_E is plotted as a function of frequency and range in **Figure 5-33**. The peak is between 100 to 200 Hz for 0.732 and 7 km ranges. Higher frequencies attenuate more quickly with range than lower frequencies, and the noise floor is evident above 1, 2, and 8 kHz at 65, 32, and 7 km ranges, respectively.

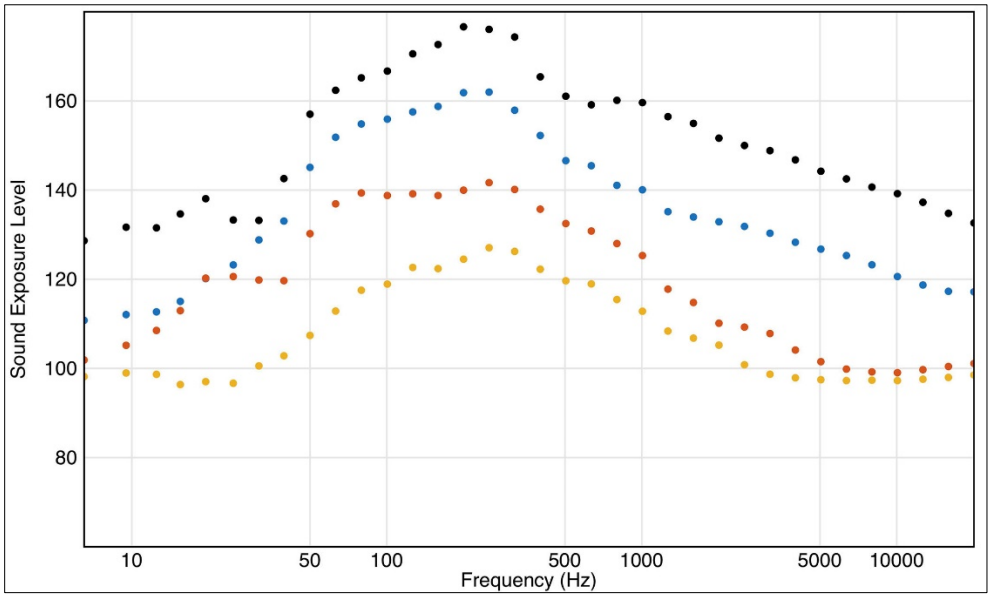

Figure 5-33. U8 measured unweighted decidecade band single strike SEL.
Using a uniform weighting (unweighted) with nominal center frequencies 8 Hz to 20 kHz, at receivers 732 m (black), 7,017 m (blue), 32 km (red), and 65 km (yellow). µPa = micropascal; dB = decibel; Hz = hertz; km = kilometer; m = meter; re = with reference to; s = second; SEL = L_E = sound exposure level. SEL units = dB re 1 µPa^2 s.

The LF cetacean weighting was applied, and the decidecade L_E is plotted for the four receiver ranges in **Figure 5-34**. The fall-off with frequency was severe for this species group, as seen by the approximately 30 dB drop from 3.2 to 20 kHz at 732 m range. These results validated the decision to limit modeling to 2.5 kHz for LF cetaceans.

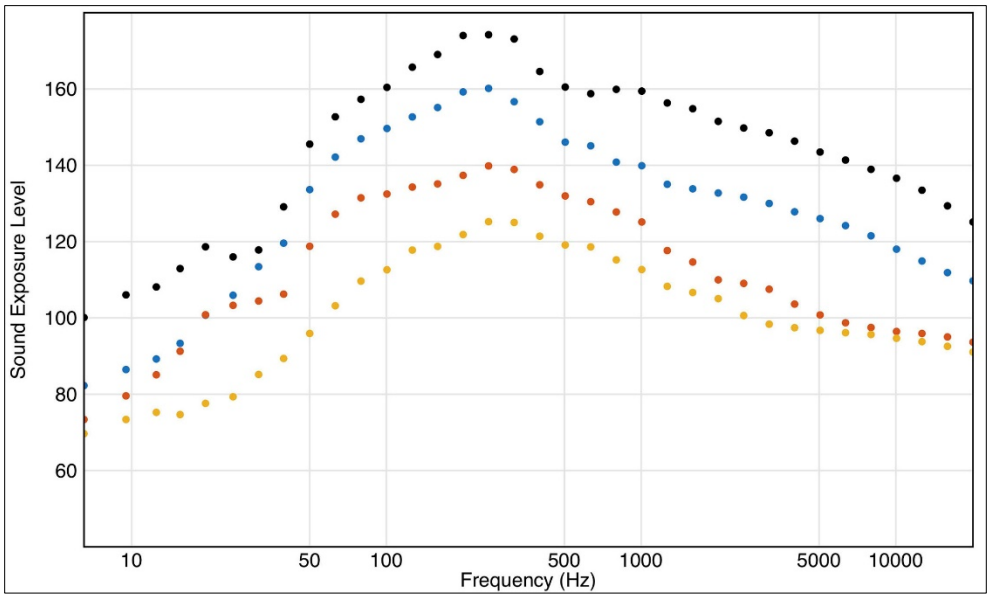

Figure 5-34. U8 measured low-frequency weighted decidecade band single strike SEL.
Using the low-frequency cetacean weighting with nominal center frequencies 8 Hz to 20 kHz, at receivers 732 m (black), d(blue), 32 km (red), and 65 km (yellow). µPa = micropascal; dB = decibel; Hz = hertz; km = kilometer; m = meter; re = with reference to; s = second; SEL = L_E = sound exposure level. SEL units = dB re 1 µPa^2 s.

The results were different for MF cetacean weighting, shown in **Figure 5-35**. For this weighting, although the levels are relatively low, the peak frequency is on the order of 4 kHz. At ranges of 7 km and greater (up to 65 km), the noise floor is likely impacting the measurement. However, there is energy above 2.5 kHz that must be accounted for when modeling $L_{E,\mathrm{w}}$ for MF species. Therefore, $L_{E,\mathrm{w}}$ predictions for the MF hearing group included frequencies between up to 20 kHz.

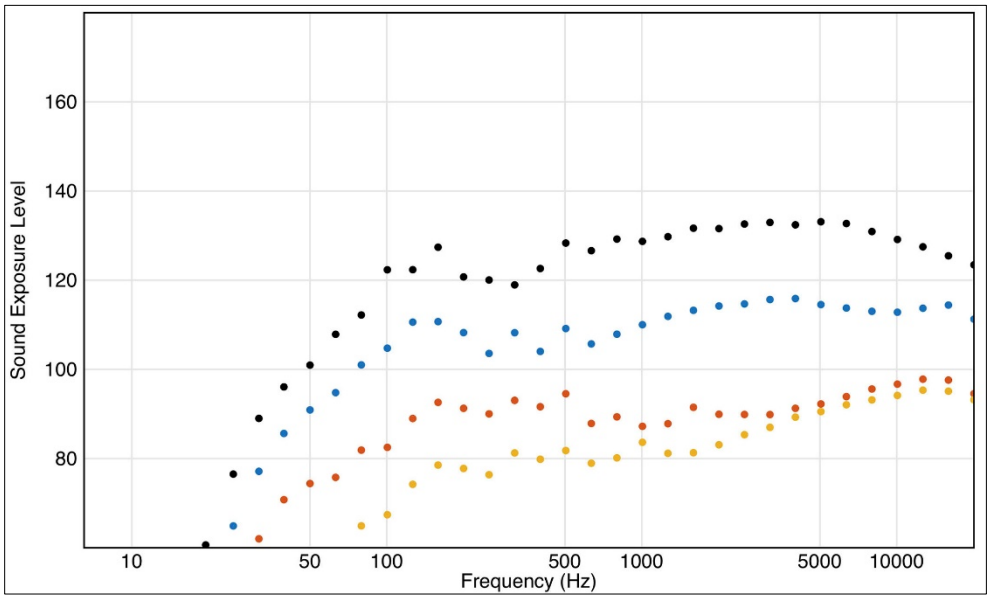

Figure 5-35. U8 measured mid-frequency weighted decidecade band single strike SEL.
Using the mid frequency cetacean weighting with nominal center frequencies 8 Hz to 20 kHz, at receivers 732 m (black), d(blue), 32 km (red), and 65 km (yellow). µPa = micropascal; dB = decibel; Hz = hertz; km = kilometer; m = meter; re = with reference to; s = second; SEL = L_E = sound exposure level. SEL units = dB re 1 µPa^2 s.

The HF cetacean $L_{E,\mathrm{w}}$ is plotted in **Figure 5-36**. The peak at 732 m range is 6 kHz. At ranges of 32 and 65 km, the noise floor likely affected measurements at 3 kHz and above. Therefore, $L_{E,\mathrm{w}}$ predictions for HF hearing groups included frequencies up to 20 kHz.

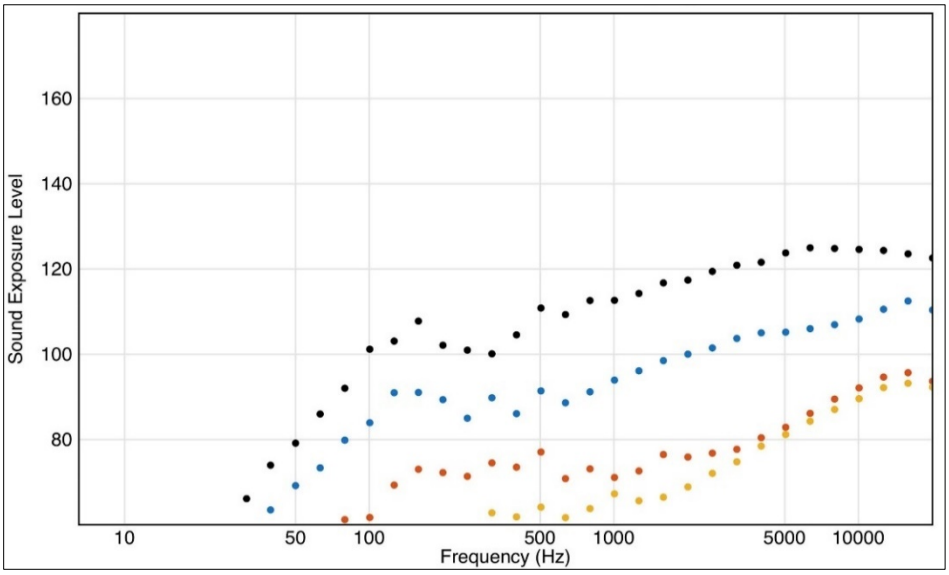

Figure 5-36. U8 measured high-frequency weighted decidecade band single strike SEL.
Using the high frequency cetacean weighting with nominal center frequencies 8 Hz to 20 kHz, at receivers 732 m (black), 7,017 m (blue), 32 km (red), and 65 km (yellow). µPa = micropascal; dB = decibel; Hz = hertz; km = kilometer; m = meter; re = with reference to; s = second; SEL = L_E = sound exposure level. SEL units = dB re 1 µPa^2 s.

The final hearing group-specific $L_{E,\mathrm{w}}$ was for phocid pinnipeds (**Figure 5-37**). The peak energy is between 100 and 200 Hz at closer ranges and migrates up to 200 to 400 Hz at ranges beyond 32 km. The noise floor was encountered above 3 kHz at 32 and 65 km ranges so to accommodate for this, modeled $L_{E,\mathrm{w}}$ predictions for phocid pinnipeds included frequencies up to 20 kHz.

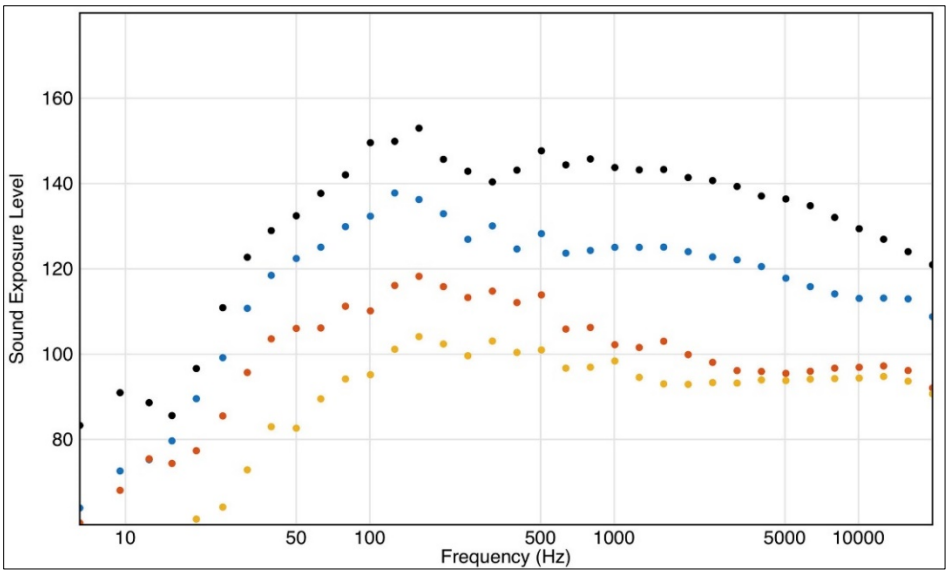

Figure 5-37. U8 measured phocid-underwater weighted decidecade band single strike SEL.
Using the phocid pinniped weighting with nominal center frequencies 8 Hz to 20 kHz, at receivers 732 m (black), 7,017 m (blue), 32 km (red), and 65 km (yellow). µPa = micropascal; dB = decibel; Hz = hertz; km = kilometer; m = meter; re = with reference to; s = second; SEL = L_E = sound exposure level. SEL units = dB re 1 µPa^2 s.

5.3 Summary of Model Verification and Validation

5.3.1 Verification

To address the issue of sound radiation from pile driving, an FE model was used to generate the sound field close to the pile. This sound field then was matched to a PE propagation model, and the pile signals were propagated out to distances of interest. Using this combination of models (FE/PE), the results from the COMPILE I workshop were successfully reproduced, which verified the approach used for this project.

5.3.2 Validation

Validation of the combined FE/PE model prediction showed differences when compared to the measurements from the construction of the Gemini wind farm (ITAP, 2015b). To address these differences, it was necessary to introduce a layered sediment. Validation was carried out against two Gemini piles, U8 and Z2.

For U8, good agreement was obtained with measurements at all frequencies above approximately 30 Hz. Frequencies lower than 30 Hz did not contribute substantially to the broadband L_E, even before frequency weighting. After weighting, they were negligible.

For Z2, at 3 m range from the pile axis of symmetry, the L_E spectrum was assumed to be the same as for U8. Under this assumption, the same LF discrepancies were seen as for U8, but these were unimportant for the reasons already stated. For Z2, there were additional discrepancies at frequencies around 300 Hz and above 600 Hz, where the L_E spectrum was underestimated.

6 Sensitivity Study

Modeling pile-driving sound as it radiates through an environment is not a one-size-fits-all scenario. The variables of bathymetries, seasonal temperature cycles, water column depths, and sediment types affect how sound travels through the water column, and the extent to which each variable influences acoustic modeling predictions is unknown. The influence of these variables is particularly unknown for the U.S. Atlantic Coast that crosses many latitudinal lines, making it difficult to assume seasonal temperature or sediment type homogeneity. The sensitivity of acoustic models to each environmental parameter in a unique sound propagation location is best modeled site by site to rank the degree to which parameters influence the model results.

The primary goals of the sensitivity study were to (1) improve predictive acoustic modeling by understanding how select environmental parameters influence propagation within a single site and between sites, and (2) identify the most influential environmental parameters on acoustic propagation.

6.1 Sensitivity Study Methods

To determine the sensitivity of the acoustic modeling predictions to environmental parameters, the propagation of pile-driving sounds up to 2,238.5 Hz was modeled (see **Section 2.2** for the reasoning behind this delineation). Propagation modeling incorporated environmental parameters at different sites

(a water depth proxy), across different seasons (an SSP proxy), for three sediment types, and along four bearings (a bathymetric shoaling proxy). Using the same FE starter field (a non-point source) at each site, the received level (via the computed metrics L_E, $L_{p,\mathrm{pk}}$, and $L_{p,\mathrm{rms}}$) at each range and depth were plotted to show the relative sensitivity to each parameter: bathymetry, SSP, sediment type, and water depth.

The influence on propagation of the selected environmental parameters were ranked in each environment. This was achieved by listing the acoustic metric means for each variable and ranking the differences between them from largest to smallest. Disturbances to animals were quantified in L_E, $L_{p,\mathrm{pk}}$, and $L_{p,\mathrm{rms}}$; thus, the means, medians, and interquartile ranges for these metrics were used to investigate the influence of the environmental parameters on the sensitivity in each acoustic metric.

The sensitivity of the impact volumes (based on acoustic thresholds) from the influence of environmental parameters were determined. Ranges over which sound travels from a driven pile (as a non-point source), using the three metrics, were determined at two sites during two seasons (winter and summer) for three grain sizes (0.5, 1.5, and 2.5 $\boldsymbol{\phi}$, corresponding to coarse, medium, and fine sand, respectively). Numerical values representative of impact volumes for each animal group's thresholds were calculated, and the results are presented in **Section 5**.

Impact volumes were calculated at high frequencies, specifically between 2,238.5 and 20,000 Hz. This HF band is important for delphinid and pinniped hearing groups as the $L_{E,\mathrm{w}}$ thresholds contain acoustic contributions well above 2,238.5 Hz.

The immediate environment's impact on acoustic propagation also was investigated to explain how differences between environments may affect propagation, and ultimately underscored the importance of site specificity. Traditionally, simple models such as the PSLM (often with 15logR) have been used. This sensitivity study illustrates the degree of validity of the PSLM when several environmental variables are considered.

6.1.1 Influence and Rationale of Selected Environmental Parameters

When a pile is struck by a hammer, the sound wave travels through the pile at the speed of sound in metal (approximately 6,000 m s^{-1}). This sound pressure wave is coupled to the water column, which causes an acoustic wave to propagate from the pile out to different distances underwater in all directions. The ratio of the compressional speed in the pile and that in the water (approximately 1,500 m s^{-1}) leads to a focused beam at the Mach cone angle. This focused beam interacts with the seafloor and sea surface and is attenuated at substantial distance. The energy radiated at low angles is what dominates the field at long ranges. Source vertical directionality is handled by the FE modeling in this project. Acoustic energy propagation is driven by changing SSPs, refracting sound waves, and boundary conditions, which scatter sound waves off the sea surface and seafloor. Ocean sound speed primarily is a function of temperature, with warmer water having a higher sound speed than colder water. Sound waves refract downward, away from the higher surface sound speed (especially during the summer months), and toward the seafloor. The seafloor absorbs some of the sound at each reflection cycle, and after many cycles, the sound is heavily damped. The opposite happens during winter months when sound waves are refracted upwards, toward the colder sea surface. The sea surface is an almost perfect reflector of sound, so it continues to propagate (not absorb) sound waves even after multiple surface interactions; thus, a winter SSP makes the sea

appear more conducive to long distance sound propagation. For this modeling study, summer and winter profiles taken from the World Ocean Atlas were used.

The acoustic properties (e.g., sound speed, density, attenuation) of the seafloor layers strongly influence the amount of sound reflection and thus the amount of sound that remains in the water column. Hard (coarse) sand is relatively reflective, which preserves the amount of acoustic energy in the water column. Mud and soft (fine) sand are absorptive, attenuating the acoustic energy out of the water column. Sediment grain size is categorized using the grain size variable (in ϕ units) on the Wentworth chart. Site-appropriate grain size values were used in this modeling study.

The final environmental driver addressed is bathymetric range dependence, which can lead to more (shallower) or fewer (deeper) seafloor interactions as sound moves away from the source. The ETOPO1 bathymetric database was used to provide accessible global coverage for modeling. The primary reason for placing the modeled source at a specified longitude and latitude position was to generate a realistic bathymetry versus range profile. The details are site specific, but the examples illustrate the impact that shallowing or deepening bathymetry has on acoustic propagation.

Two Test Sites

Two sites were chosen to evaluate the extent that environmental variability plays on the sensitivity of sound propagation from water depth in combination with bathymetry, sediment type, and ocean temperature structure. The two chosen sites were offshore Virginia Beach (VAbeach) and Rhode Island (RIsland) where considerable planning is under way for future wind farms. Each site was modeled for three uniform (range-independent) sediment types: coarse, medium, and fine sand (0.5, 1.5, and 2.5 ϕ, respectively). These sediment types, while not evenly distributed, are ubiquitous on the shallow continental shelf and represent most regions where pile driving is likely to be conducted. The inclusion of range dependence in the seafloor, although a real phenomenon, is strongly site specific and beyond the scope of this project. For each selected grain size, a parametrized single unconsolidated sediment was used, providing a depth-dependent compressional speed, density, and attenuation profile.

Wind speed was not included in the environmental sensitivity computations for two reasons: (1) the emphasis on LF sounds makes surface waves less important, and (2) pile-driving operations usually are limited to sea states below 3 (i.e., significant wave height less than 0.5 m) and when the wind speed is less than 7.5 m s^{-1} (15 knots). The inclusion of wind-driven waves and surface roughness can be done with the PE, as modeled earlier for this project, but was not included in the sensitivity analysis. On severe weather days, when acoustic propagation is dominated by a wind-induced rough surface, pile-driving activities are not expected to occur.

6.2 Acoustic Propagation Modeling Methods

6.2.1 Environment and Variables Selection

The influence of two environments in the western Atlantic Ocean was modeled with a starter field simulated from an actual pile installed in the North Sea off the coast of the Netherlands. RIsland was located 37.29 km offshore Rhode Island (41.08776° N, 71.22270° W) in 35 m water depth (**Figure 6-1**). VAbeach was located 43.16 km offshore Virginia (36.89629° N, 75.49163° W) in 24 m water depth

(**Figure 6-1**). For both sites, sediment grain sizes of 0.5, 1.5, and 2.5 **ϕ** were used in the propagation models to capture a pile installation in hard through soft sands.

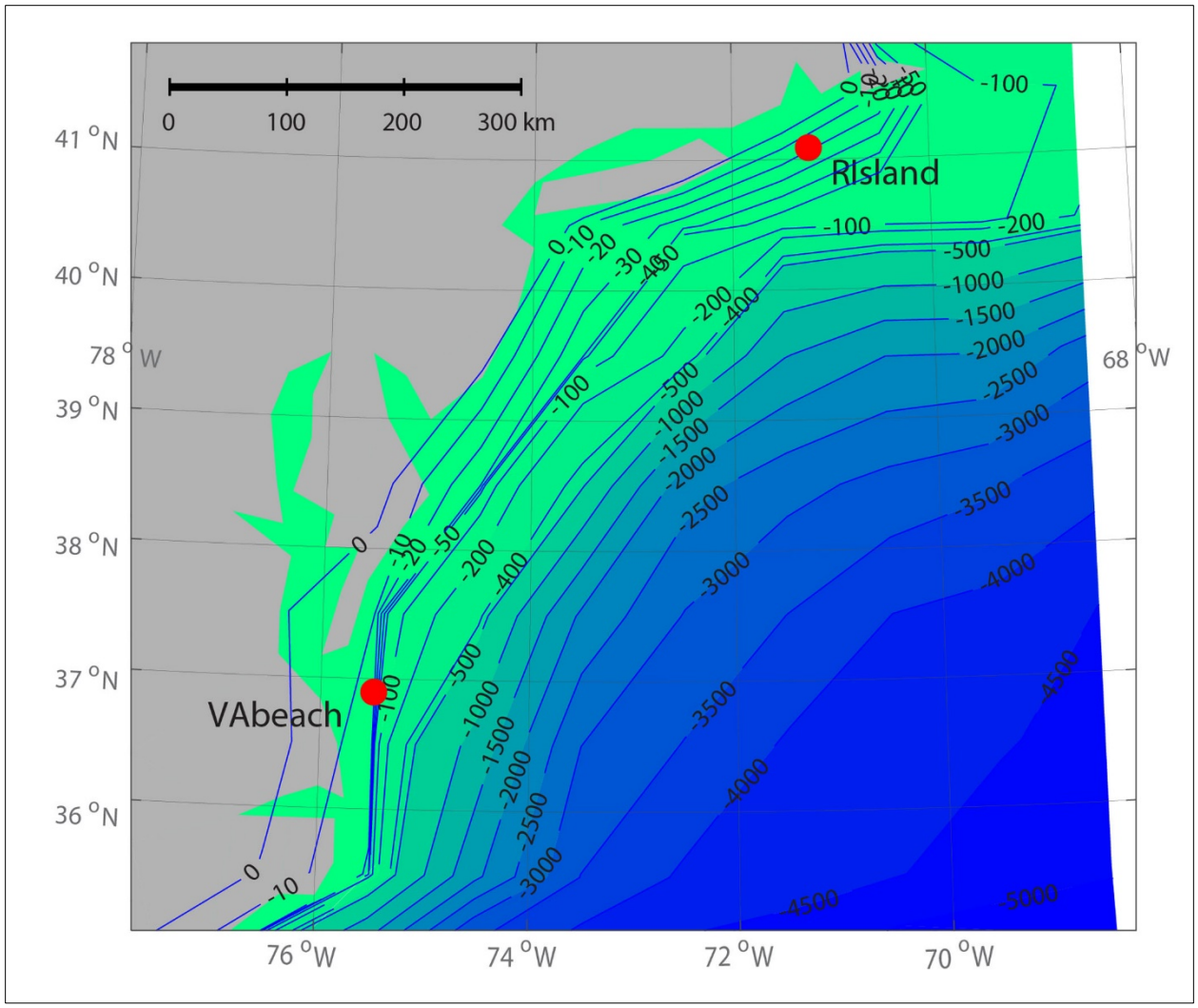

Figure 6-1. Map of RIsland and VAbeach sites.
Sites (red dots) were mapped to illustrate and compare isobaths, latitudes, distances, and orientations to shore and the edge of the continental shelf. RIsland = Rhode Island site; VAbeach = Virginia Beach site.

Two seasons (summer and winter) were used to capture the extremes of temperature and salinity, and three sediment types (coarse, medium, and fine sand) were used to represent general interactions between sound waves and the seafloor. The relative influences of these variables were explored to better understand which environmental factors most influence the size of calculated impact volumes to the various acoustic thresholds for different species groups.

Propagation modeling was performed using two databases: (1) World Ocean Atlas temperature/salinity fields for summer (August 1) and winter (February 1), and (2) ETOPO1 bathymetry for the four cardinal directions. The bathymetry for the 60-km tracks is plotted in **Figures 6-2** and **6-3** for RIsland and VAbeach, respectively.

The specific bathymetry for RIsland is shown in **Figure 6-2**. The water shoals to less than 10 m in the north and west radials. The east radial water depth increases to 60 m, and the southern radial is mostly flat around 40 m.

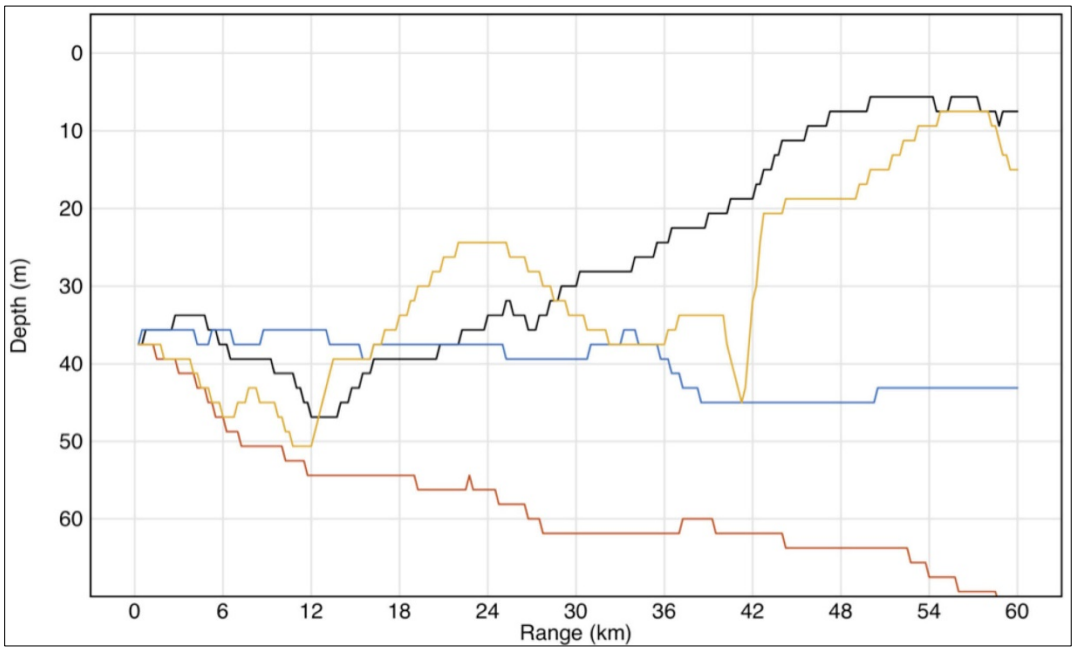

Figure 6-2. Bathymetry at RIsland.
The plotted cardinal directions are north (black), east (blue), south (red), and west (yellow). Water depth data from ETOPO1 were used in the simulation and are plotted out to 60 km. Water depth at the pile site is 35 m.
RIsland = Rhode Island site.

The specific bathymetry for VAbeach is shown in **Figure 6-3**. The water shoals to 0 m depth in the west radial, and the east radial deepens to 60 m beyond the 40-km range. The north and south radials are mostly flat around 24 m.

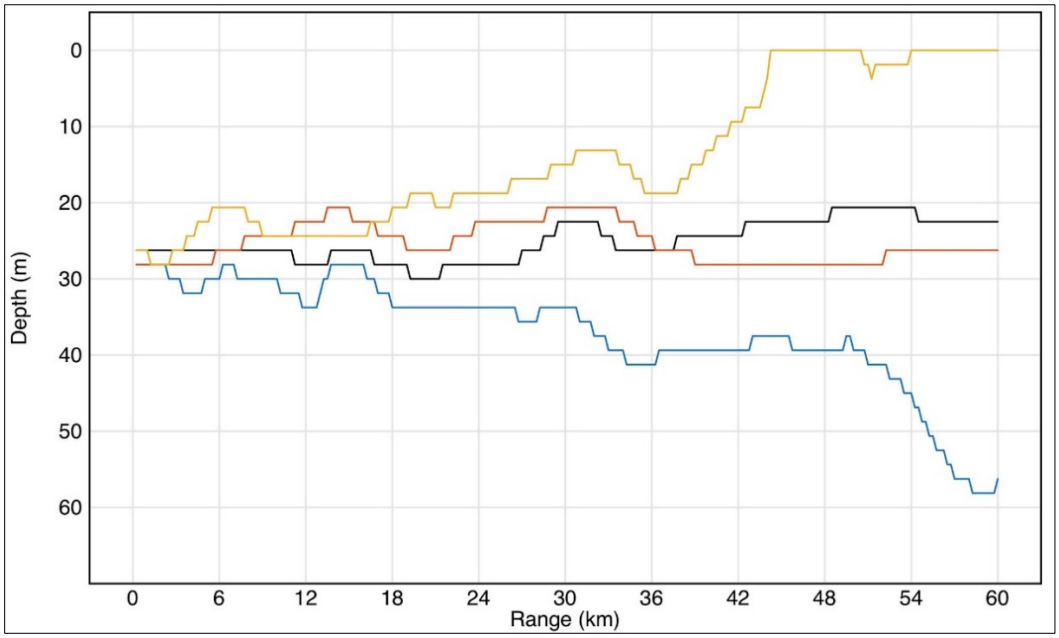

Figure 6-3. Bathymetry at VAbeach.
The plotted cardinal directions are north (black), east (blue), south (red), and west (yellow). Water depth data from ETOPO1 were used in the simulation and are plotted out to 60 km. Water depth at the pie site is 24 m. VAbeach = Virginia Beach site.

The U.S. Atlantic Coast experiences seasonal temperature changes in the Gulf Stream from seasonal solar input and because the ocean current meanders closer to and farther from shore in the fall and spring (Frankignoul et al., 2000). Preliminary analysis demonstrated that propagation measurements on May 1 (spring) and November 1 (fall) were very similar to February 1 (winter), while August 1 (summer) was the most different. Therefore, environmental data from February 1 and August 1 were chosen to represent extremes in temperature and salinity profiles. These temperature and salinity differences affect the SSP whereby the marine environment would be more or less acoustically transparent. Sound is refracted away from the warm surface in the summer and therefore hits the seafloor more times, leading to higher attenuation of acoustic energy, particularly if the seafloor is soft.

A water depth difference of only 11 m was not expected to differentially influence propagation. However, a remarkable difference between RIsland (35 m water depth) and VAbeach (24 m water depth) was observed. A downward refracting SSP resulted in greater loss because of the increased interaction with the seafloor. As shown in **Figure 6-4**, RIsland's ability to extend an extra 11 m (133% the depth of VAbeach) into colder, deeper water impacted the propagation substantially. The very cold water at the seafloor increased the grazing angle at which sound hits the seafloor (Snell's law and refraction) and led to more attenuation from seafloor interactions.

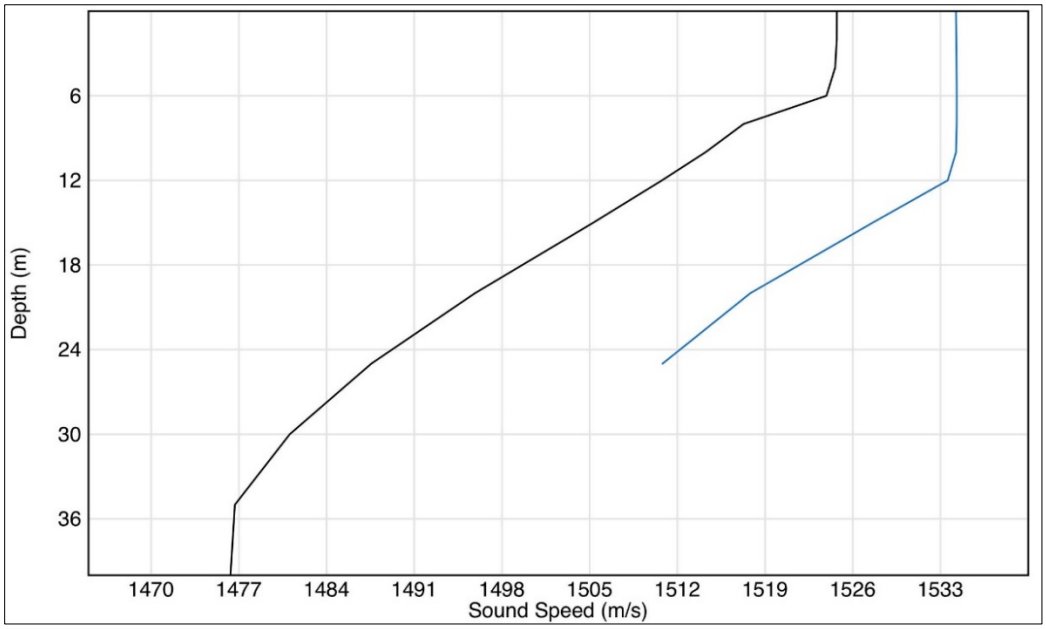

Figure 6-4. Summer SSPs.
The summer SSPs for the deeper RIsland (black) and the shallower VAbeach (blue). RIsland had a stronger gradient as well as a larger (2x) difference between the surface sound speed (1,525 m s^{-1}) and the seafloor sound speed (1,475 m s^{-1}). RIsland = Rhode Island site; SSP = sound speed profile; VAbeach = Virginia Beach site.

When the surface is not heated, the SSP tends to be an isovelocity, as shown for the winter profile in **Figure 6-5**.

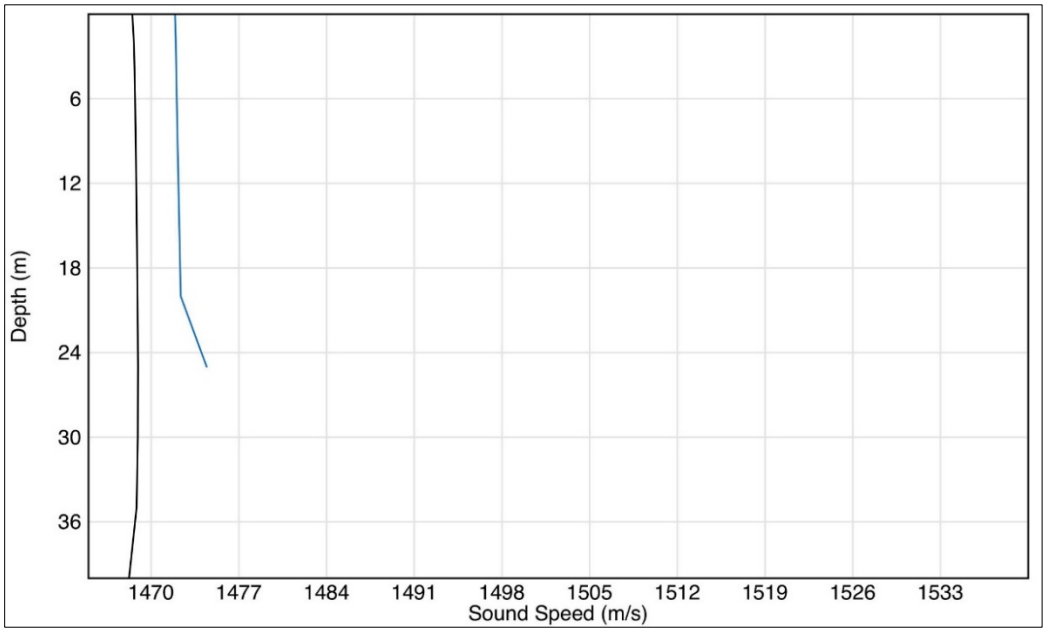

Figure 6-5. Winter SSPs.
The winter SSPs for the deeper RIsland (black) and shallower VAbeach (blue). VAbeach had a slightly higher sound speed across all depths than RIsland, but both were approximately an isovelocity compared to their respective summer SSPs. RIsland = Rhode Island site; SSP = sound speed profile; VAbeach = Virginia Beach site.

6.2.2 Methodology for 17.5 to 2,238.5 Hz

Seawater volume attenuation increases rapidly with increasing frequency and it is well known that only LF sound can travel great distances. For this reason, much of the project's effort was focused on modeling the sound in the 17.5 to 2,238.5 Hz band. Furthermore, the FE source model and the PE are well suited for this frequency band.

The FE starter field (**Section 3.1**), was generated from the sound radiated by a hammer strike on a 7-m diameter pile. The FE starter field assumed a uniform SSP and constant water depth and was computed for six different combinations of water depth and sediment grain size (two water depths for each of the three sediment **ϕ** values used). In order to model realistic pile energy, the pile's L_E was adjusted to match the acoustic measurement results from the Gemini installation. In particular, at 732 m, the measured unweighted $L_{E,\mathrm{ss}}$ was 179 dB re 1 μPa^2 s, which, for the sensitivity analysis, translated to an $L_{E,\mathrm{ss}}$ near the pile of approximately 200 dB re 1 μPa^2 s.

The PE is the industry standard modeling solution for handling LF acoustic propagation in range-dependent environments. The PE used here, Peregrine, was developed by Richard Campbell and is a modification of the RAM (Collins, 1993). The PE model was integrated with the FE starter field to model the sound pressure field every 20 m in range (2 m in depth) out to a distance of 60 km from the pile. For both sites, four radials at cardinal directions were used to sample various bathymetries, specifically, shoaling towards land to the west/northwest and sloping to deep water towards the east/southeast. The PE was run on a fixed grid for a set of decidecade bands, from 17.5 to 2,238.5 Hz. The frequency domain fields from each band were Fourier transformed, producing a pressure time series on a 2-second window that captures the entire pulse. The time series of all the decidecade bands were summed, and the acoustic metrics (L_E, $L_{p,\mathrm{pk}}$, and $L_{p,\mathrm{rms}}$) were computed in the time domain.

6.2.3 Methodology for 2,238.5 Hz to 20,000 Hz

Although sound intensity falls off exponentially with range at higher frequencies, the hearing sensitivity (and auditory frequency) of some animal groups, such as the MF and HF cetaceans, increases rapidly with frequency, making it necessary to extend the computation to higher frequencies. The methodology is described here.

The highest band computed during the LF modeling in **Section 6.2.2** for the combined FE/PE was between 1,778.5 and 2,238.5 Hz. The frequency domain fields of this band (for each of the sites, seasons, bearings, and sediment grain sizes) were mapped to higher frequency bands by accruing the additional volume attenuation as a function of range.

As an example, the volume attenuation for water at 2 kHz is 0.139 dB km^{-1}, leading to a total volume attenuation of 1.39 dB at 10 km. For 10 kHz sound, the volume attenuation is 1.189 dB km^{-1}, which is 11.8 dB at 10 km. To map the acoustic field to 10 kHz, an additional 1.05 dB loss per kilometer was applied. For the L_E and $L_{p,\mathrm{pk}}$ metrics, these factors were applied to the computed decidecade band metrics. In order to compute the $L_{p,\mathrm{rms}}$, however, the full band field was reduced and the $L_{p,\mathrm{rms}}$ was recomputed.

The time domain pressure signals (via the Fourier transform) and the acoustic metrics ($L_{E,\mathrm{w}}$, $L_{p,\mathrm{pk}}$ and $L_{p,\mathrm{rms}}$) were computed. This allowed for evaluation of the metric received level for each weighting, out to 60 km, for an effective frequency band of 17.5 Hz to 20 kHz. This approach made three approximations. The first is that the acoustic time series at 20 kHz and at 2 kHz is the same, which follows the HF approximation used in ray-tracing methods. The second is that the attenuation added as a function of linear range is equivalent to the volume attenuation that should be added along the acoustic ray path (path length). For long-range propagation, where propagation angles are less than 15°, this amounts to a very small factor (approximately 4%) in volume attenuation. The third approximation is the assumption of a perfectly reflecting sea surface. Modeling the effects of rough surface scattering was outside the project scope but would have decreased contributions from frequencies above 1 kHz, especially during winter.

To evaluate the impact of adding the 2,238.5 Hz to 20 kHz acoustic energy to the modeled pile-driving signals, the L_E of four weighting categories as a function of range was plotted. The example case was RIsland during summer at 90° (east) with a sediment grain size of 0.5 $\boldsymbol{\phi}$. The 17.5 to 2,238.5 Hz sum (black line) and the full 17.5 Hz to 20 kHz sum (blue line) are shown in **Figure 6-6** for each weighting. The results indicate there is no visible difference between the received LF weighted or the full band (including up to 20 kHz) L_E values at any range for LF cetaceans (**Figure 6-6**, upper left panel) or for the unweighted fish/sea turtle groups (not plotted). Other marine mammal groups had higher levels of broadband L_E, particularly for ranges shorter than 18 km. Specifically, the L_E close to the pile for MF and HF cetaceans differed between the LF (17.5 to 2,238.5 Hz) and the full band (17.5 Hz to 20 kHz) by as much as 5 and 10 dB, respectively (**Figure 6-6**, right panels). The maximum received levels were at lower frequencies (100 to 500 Hz), but the weighting functions focus on higher frequencies for the MF and HF cetaceans; therefore, those groups have notably lower $L_{E,\mathrm{w}}$ values than the LF cetaceans. For the phocid pinnipeds, the difference between the LF and full band computation varied by 1 to 2 dB within the first 5 km from the pile (**Figure 6-6**, bottom left panel).

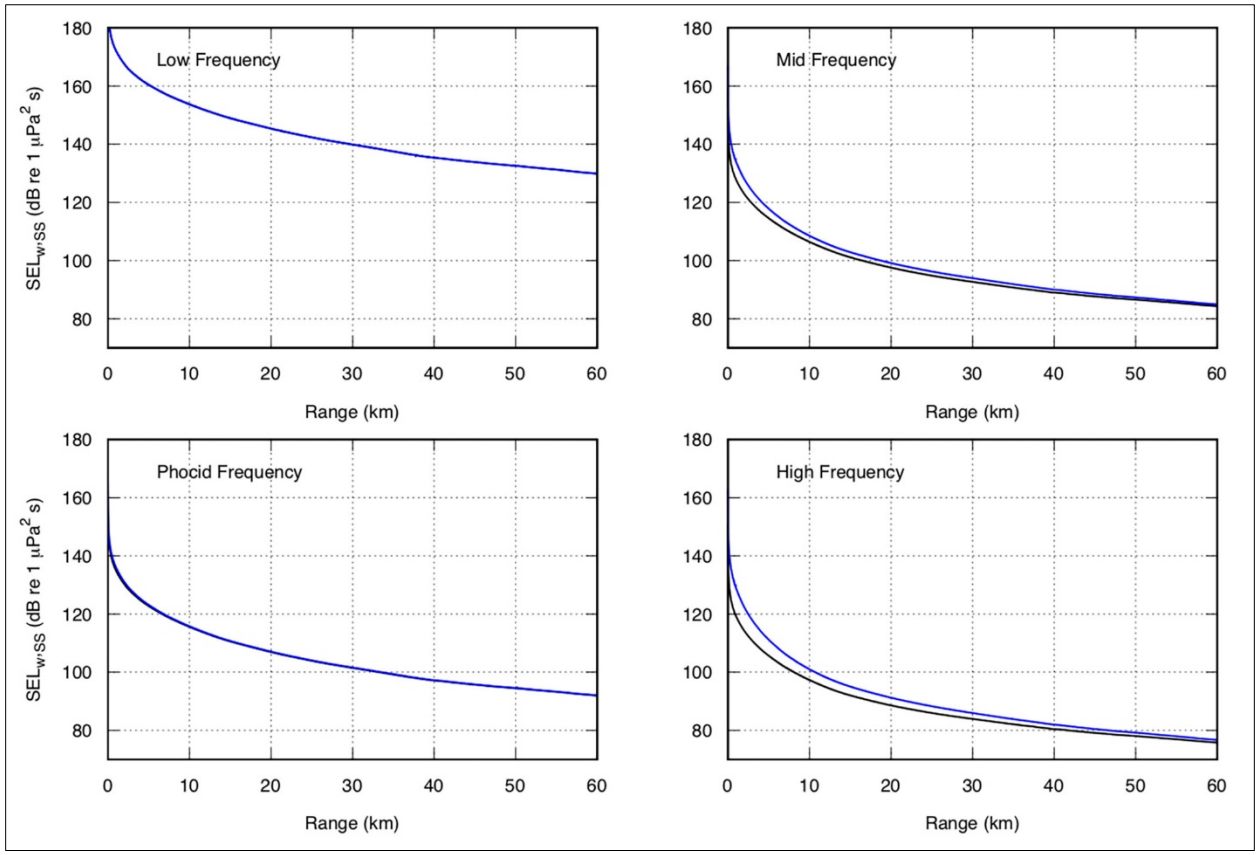

Figure 6-6. Low frequency (17.5 to 2,238.5 Hz) versus full band (17.5 to 20,000 Hz) weighted single strike SEL for marine mammal groups.

Results for RIsland to the east (90°). The $L_{E,w,SS}$ for low band (black) and full band (blue) propagation for low-frequency cetaceans (top left), mid-frequency cetaceans (top right), phocid pinnipeds (bottom left), and high-frequency cetaceans (bottom right). µPa = micropascal; dB = decibel; km = kilometer; $L_{E,w,SS}$ = weighted single strike sound exposure level; re = with reference to; RIsland = Rhode Island site; s = second; SEL = L_E = sound exposure level.

The decidecade band with the largest contribution to the unweighted broadband levels at all ranges was the 100 Hz band (**Figure 6-7**, eighth vertical column of dots from the left), followed by the 160 Hz band (tenth vertical column from left) at short range and the 125 Hz band (ninth vertical column from left) at long range. The 100, 125, and 160 Hz decidecade bands dominate the broadband value at all ranges.

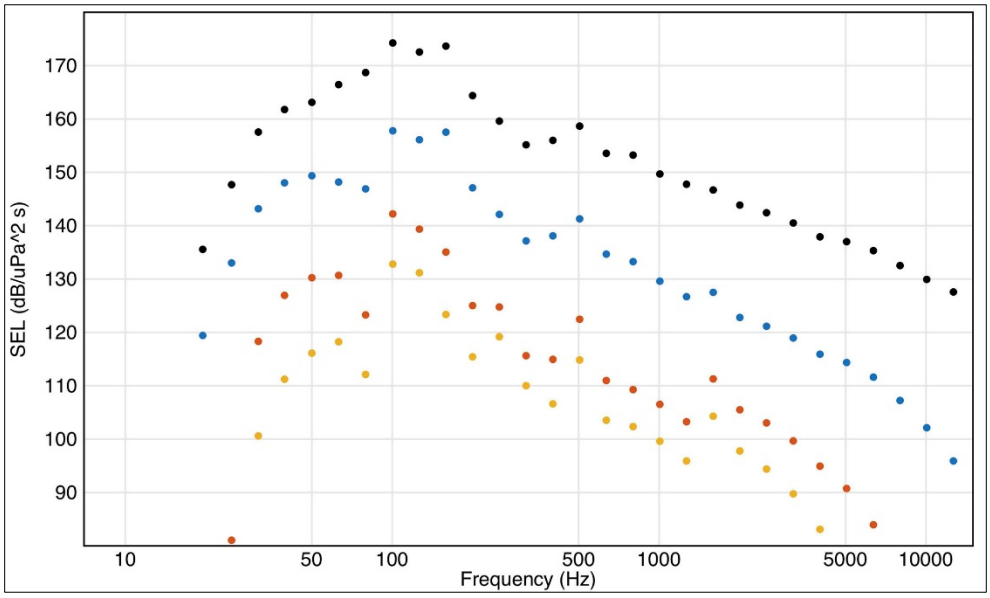

Figure 6-7. Unweighted single strike decidecade band SEL versus frequency and range.
The decidecade band $L_{E,\mathrm{ss}}$ as a function of band center frequency at the Gemini recording ranges of 0.7 km (black), 7 km (blue), 32 km (orange), and 62 km (yellow). µPa = micropascal; dB = decibel; $L_{E,\mathrm{ss}}$ = single strike sound exposure level; re = with reference to; s = second; SEL = L_E = sound exposure level.

The LF-weighted SEL was dominated by the 160 Hz band at short range (<10 km) and by the 100 and 125 Hz bands combined at long range (>30 km) (**Figure 6-8**). At all ranges, the fourth strongest band is the one centered at 200 Hz, competing with the 80 Hz band at short range (<1 km).

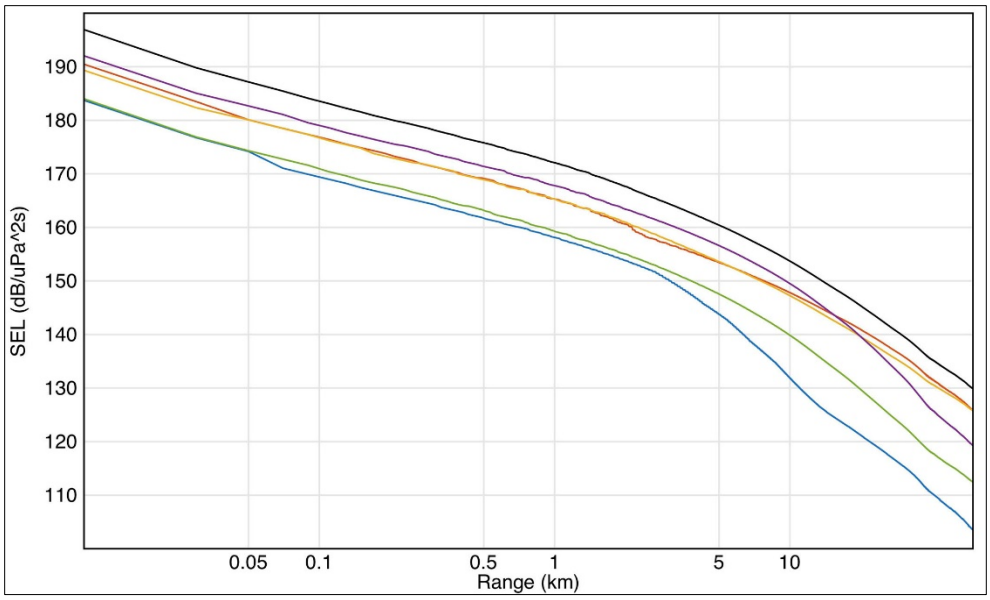

Figure 6-8. Low-frequency weighted single strike SEL decidecade band versus full band.
$L_{E,\mathrm{w,ss}}$ for full band (black) and decidecade bands from 80 to 200 Hz (colors) for low-frequency cetaceans; 80 Hz (blue), 100 Hz (red), 125 Hz (yellow), 160 Hz (purple), and 200 Hz (green); µPa = micropascal; dB = decibel; $L_{E,\mathrm{w,ss}}$ = weighted single strike sound exposure level; re = with reference to; s = second; SEL = L_E = sound exposure level.

The combined effect of a spectrum that decreases with increasing frequency and a weighting function that increases with increasing frequency is that their product is an almost flat weighted frequency spectrum. This nearly flat spectrum leads to multiple frequency bands contributing almost equally to the total short-range (<10 km) energy above 4 kHz (**Figure 6-9**). The frequencies contributing to HF-weighted levels are therefore mostly above 2 kHz, demonstrating the importance of including high frequency energy (above 2 kHz) in the calculations of $L_{E,\mathrm{w}}$.

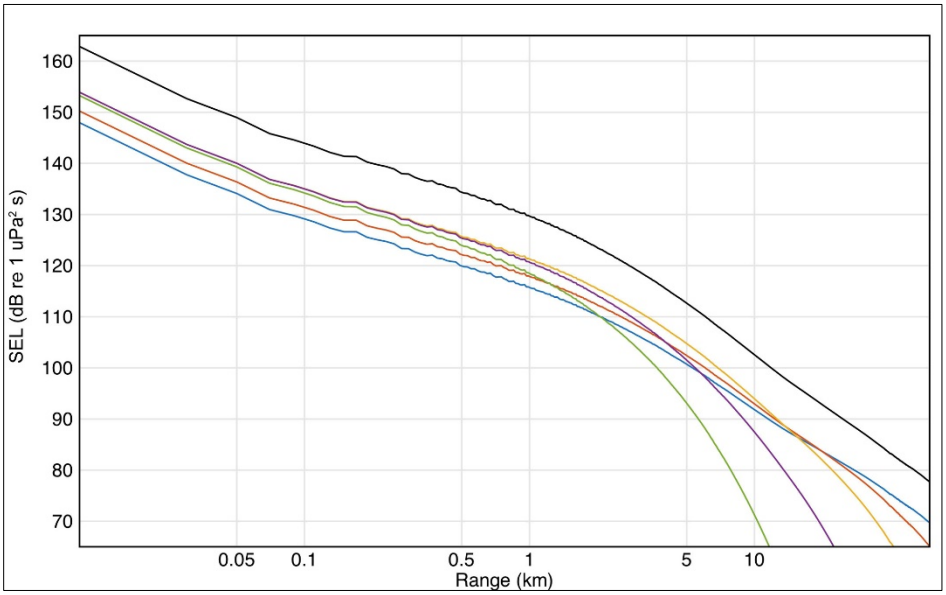

Figure 6-9. High-frequency weighted SEL decidecade band versus full band.
The $L_{E,\mathrm{w,ss}}$ for full band (black) and selected decidecade bands from 2.5 to 16 kHz for high-frequency cetaceans. Colors represent the bands centered at 2.5 kHz (blue), 4 kHz (red), 6.4 kHz (yellow), 10 kHz (purple), and 16 kHz (green). µPa = micropascal; dB = decibel; km = kilometer; $L_{E,\mathrm{w,ss}}$ = weighted single strike sound exposure level; re = with reference to; RIsland = Rhode Island site; s = second; SEL = L_E = sound exposure level.

6.2.4 Modeling Results for Acoustic Propagation from 17.5 to 2,238.5 Hz

Propagation modeling of broadband sounds up to 2,238.5 Hz (in 0.5 Hz increments) showed the environment is more conducive to acoustic propagation with increasing water depth, during colder (upward refracting) seasons, and over moderately hard sand sediments. At both modeled sites, the results were influenced by seasonality and grain size. **Figures 6-10** to **6-15** compare L_E, $L_{p,\mathrm{pk}}$, and $L_{p,\mathrm{rms}}$ versus range for both sites in the four cardinal directions during summer and winter for three sediment grain sizes. The differences in propagation as a result of these variables are noticeable approximately 20 m from the pile-driving location for all bearings at both sites and becomes more pronounced with range.

The L_E values for RIsland as a function of range, season, and sediment grain size are plotted for each cardinal direction in **Figure 6-10**. Within 10 km of the pile, there were small differences of less than 5 dB between the grain sizes across seasons. The sensitivity to bathymetry is demonstrated by comparing the four cardinal directions, one in each panel. As water depth decreases, there is more acoustic energy loss. At longer ranges, the consistent trends are that the summer levels are as much as 10 dB lower due to the warm surface waters refracting sound towards the seafloor, leading to more seafloor reflections with range and thereby a higher loss. Differences due to seafloor type (sediment grain size) sometimes are

negligible in winter but always are more noticeable in summer, which is due to more seafloor interactions caused by the warm, refractive surface waters. Beyond 10 km, soft sediment (2.5 **ϕ**, fine sand) sound levels are 10 to 20 dB lower than over hard sediment (0.5 **ϕ**, coarse sand). The west (270°) direction at RIsland becomes very shallow (approximately 3 m) at 40 km, causing the numerical model to become unstable. The north (0°) and west (270°) plots show a sudden drop in sound levels beyond 40 km because of the extremely shallow water. (See **Figure 6-2** for bathymetrical evidence of sudden shallowing.)

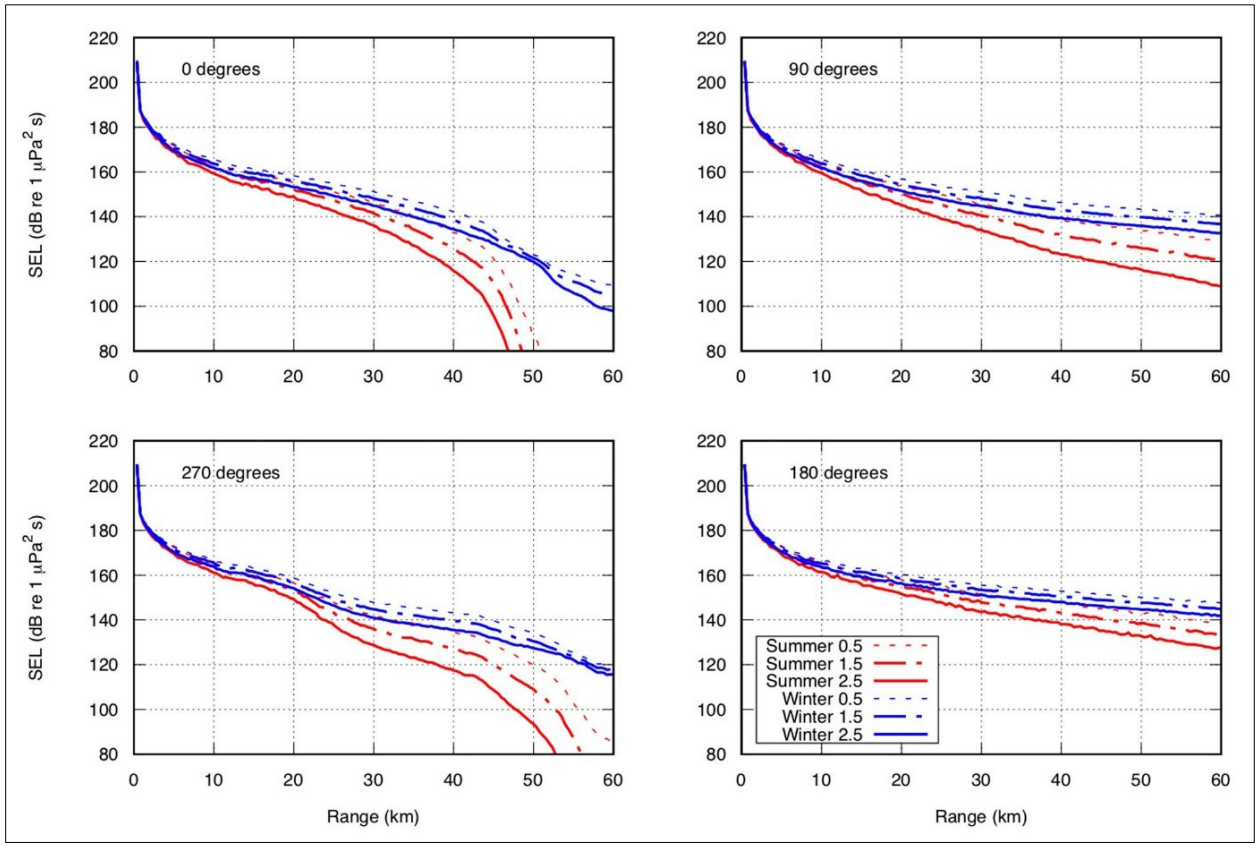

Figure 6-10. Single strike SEL as influenced by RIsland environmental variables.
Top left: north (0°), top right: east (90°), bottom right: south (180°), bottom left: west (270°). Summer (red) and winter (blue) depth-averaged propagation distances over sediments of coarse (0.5 **ϕ**, dotted lines), medium (1.5 **ϕ**, dashed lines), and fine (2.5 **ϕ**, solid lines) sand. Water depth at the source position was approximately 35 m.
µPa = micropascal; **ϕ** = grain size; dB = decibel; km = kilometer; re = with reference to; RIsland = Rhode Island site; SEL = L_E = sound exposure level.

The $L_{p,\mathrm{pk}}$ values for RIsland as a function of range, season, and sediment grain size were plotted for each cardinal direction (**Figure 6-11**). The sensitivity of $L_{p,\mathrm{pk}}$ to environmental parameters is consistent with the L_E results, with the order of importance (from high to low) being bathymetry, season, and grain size.

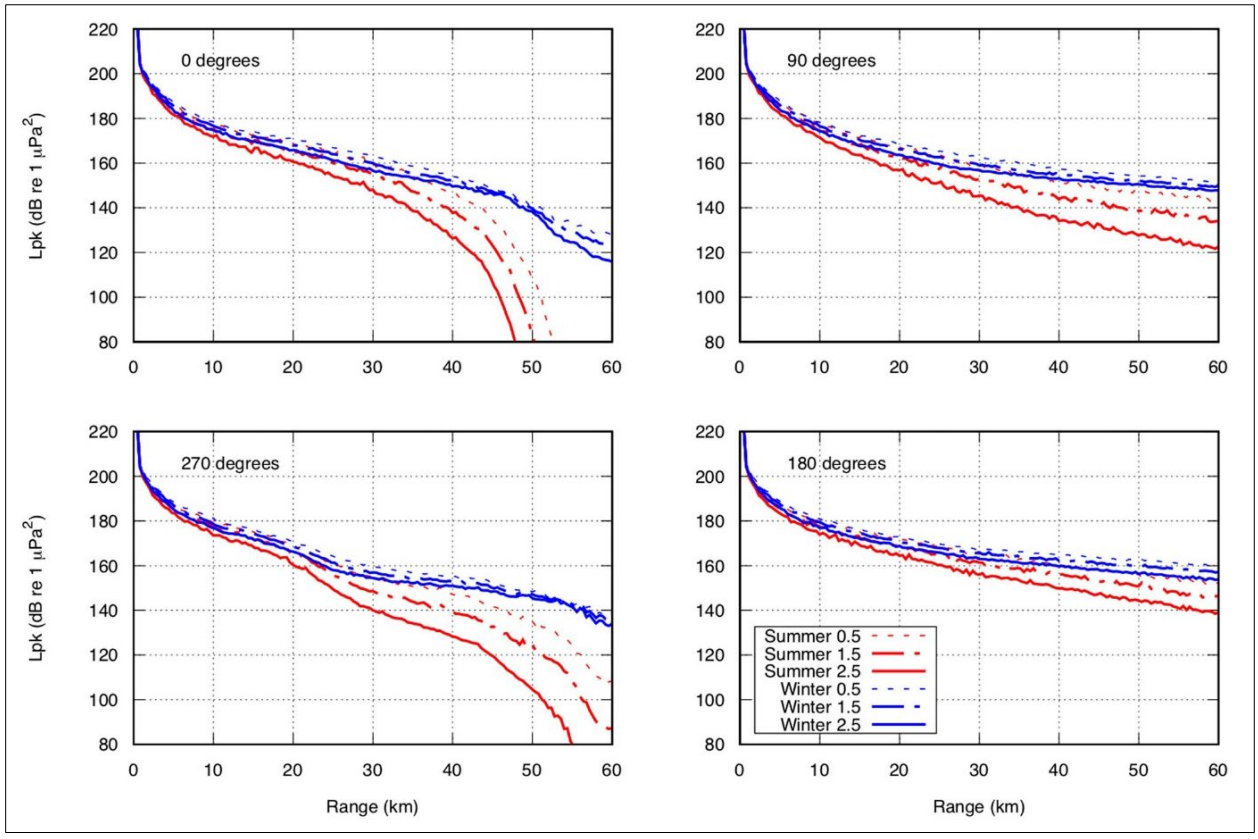

Figure 6-11. $L_{p,\mathrm{pk}}$ as influenced by RIsland environmental variables.

Top left: north (0°), top right: east (90°), bottom right: south (180°), bottom left: west (270°). Summer (red) and winter (blue) depth-averaged propagation distances over sediments of coarse (0.5 **ϕ**, dotted lines), medium (1.5 **ϕ**, dashed lines), and fine (2.5 **ϕ**, solid lines) sand. Water depth at the source position was approximately 35 m.
µPa = micropascal; **ϕ** = grain size; dB = decibel; km = kilometer; $L_{p,\mathrm{pk}}$ = peak sound pressure level; re = with reference to; RIsland = Rhode Island site.

The $L_{p,\mathrm{rms}}$ values for RIsland as a function of range, season, and sediment grain size were plotted for each cardinal direction (**Figure 6-12**). The sensitivity of $L_{p,\mathrm{pk}}$ to the environment is consistent with the L_E results, with the order of importance (high to low) being bathymetry, season, and grain size.

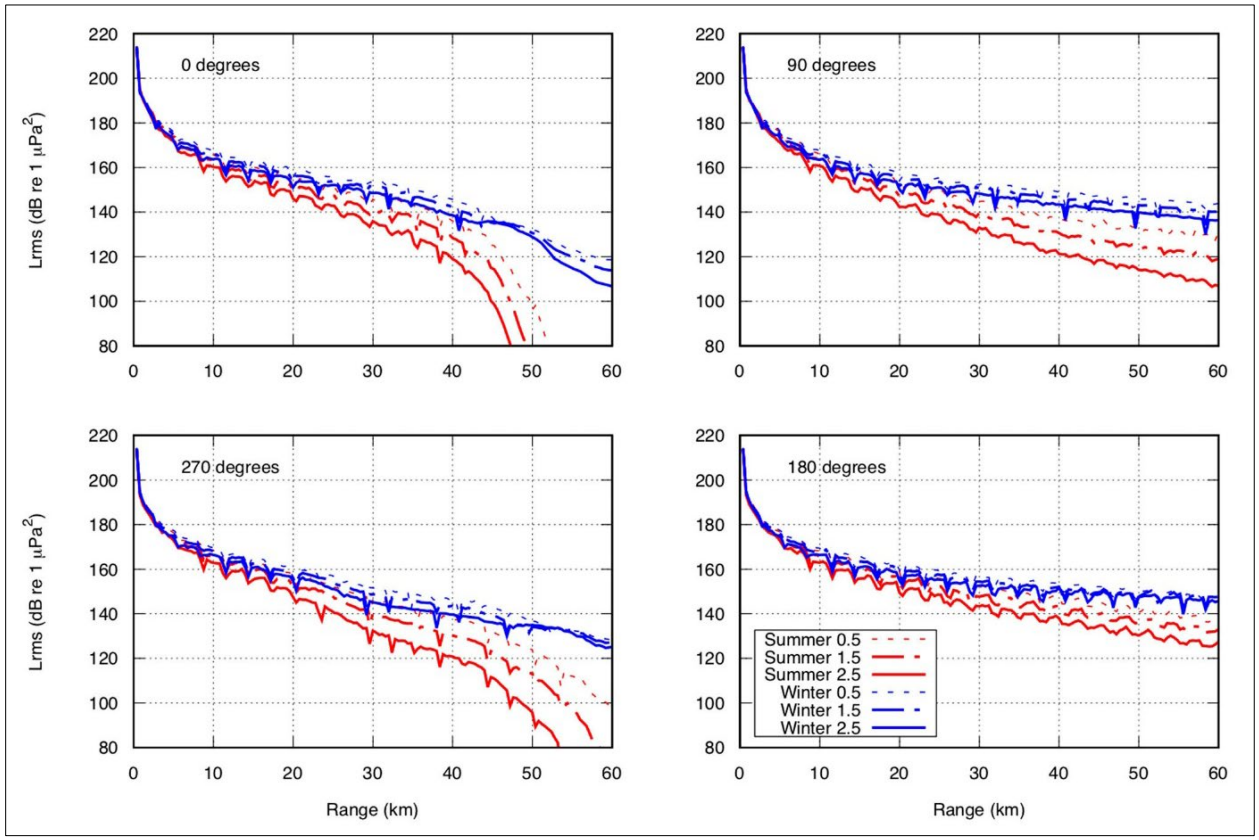

Figure 6-12. $L_{p,\mathrm{rms}}$ as influenced by RIsland environmental variables
Top left: north (0°), top right: east (90°), bottom right: south (180°), bottom left: west (270°). Summer (red) and winter (blue) depth-averaged propagation distances over sediments of coarse (0.5 **ϕ**, dotted lines), medium (1.5 **ϕ**, dashed lines), and fine (2.5 **ϕ**, solid lines) sand. Water depth at the source position was approximately 35 m.
µPa = micropascal; **ϕ** = grain size; dB = decibel; km = kilometer; $L_{p,\mathrm{rms}}$ = root-mean-square sound pressure level; re = with reference to; RIsland = Rhode Island site.

The L_E values for VAbeach as a function of range, season, and sediment grain size were plotted for each cardinal direction (**Figure 6-13**). The L_E values for VAbeach are markedly higher than for RIsland, showing the combined effect of water depth and SSP. This improved propagation at VAbeach is demonstrated by the substantially larger impact volume results relative to RIsland. RIsland has a downward refracting profile in a deeper water column. In the winter, VAbeach has an isovelocity from a uniform SSP, but its slight downward refracting SSP during the summer is truncated due to its shallower depth, effectively damping the refraction effect. This isovelocity at VAbeach also could be due to the more southern location, the proximity of the Gulf Stream, or better mixing by surface winds in shallow water. More regionally, the coastal counter current from the north creating a rougher sea combined with river runoff from the Chesapeake may lead to higher mixing than the more sheltered RIsland. This would contribute to the VAbeach isovelocity state throughout all seasons. Within the first 20 km, there were no large differences between the resulting ranges for L_E at RIsland and VAbeach. The acoustic sensitivity to

bathymetry is visible when comparing the four cardinal directions. As water depth decreases, there is more acoustic energy loss, particularly to the south (180°). There is much less seasonal variability in the VAbeach results than in the RIsland results, which may be due, in part, to less severe winters in Virginia and the influence of the Gulf Stream that reduce the impact of air temperature on surface water temperature. Differences due to sediment grain size are noticeable during summer due to more seafloor interactions caused by the warmer surface waters but are nearly negligible during winter. At both sites, the L_E with soft sediment (2.5 **ϕ**, fine sand) is approximately 5 dB lower than the corresponding hard sediment (0.5 **ϕ**, coarse sand) values beyond 20 km. At VAbeach, the west (270°) direction runs aground at a range of 44 km (**Figure 6-3**).

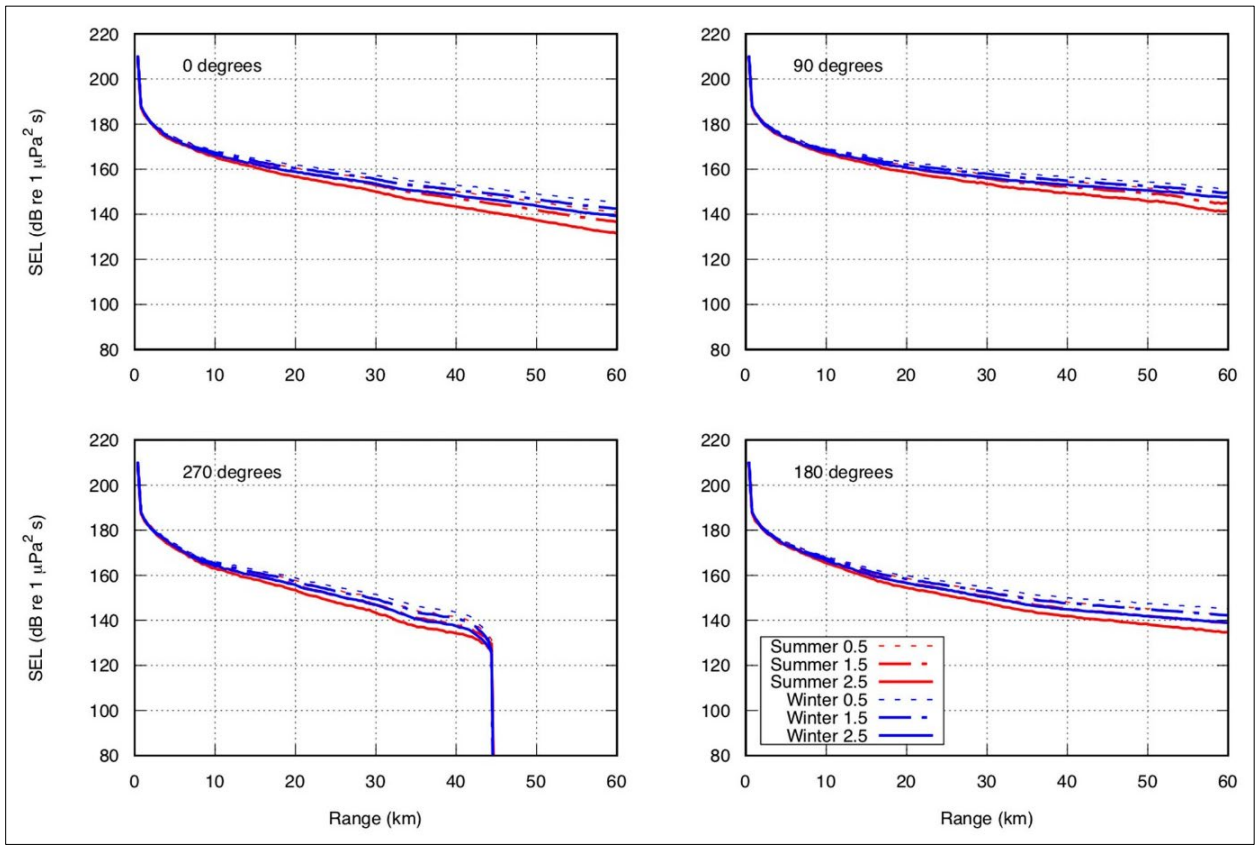

Figure 6-13. Single strike SEL as influenced by VAbeach environmental variables.
Top left: north (0°), top right: east (90°), bottom right: south (180°), bottom left: west (270°). Summer (red) and winter (blue) depth-averaged propagation distances over sediments of coarse (0.5 **ϕ**, dotted lines), medium (1.5 **ϕ**, dashed lines), and fine (2.5 **ϕ**, solid lines) sand. Water depth at the source position was approximately 24 m. Data at 270° were truncated at 45 km to avoid numerical instabilities of the model output in very shallow water. µPa = micropascal; **ϕ** = grain size; dB = decibel; km = kilometer; re = with reference to; s = second; SEL = L_E = sound exposure level; VAbeach = Virginia Beach site.

The $L_{p,\mathrm{pk}}$ values for VAbeach as a function of range, season, and sediment grain size were plotted for each cardinal direction (**Figure 6-14**). The sensitivity of $L_{p,\mathrm{pk}}$ to the environment is consistent with the L_E results, with the order of importance (high to low) being bathymetry, season, and grain size.

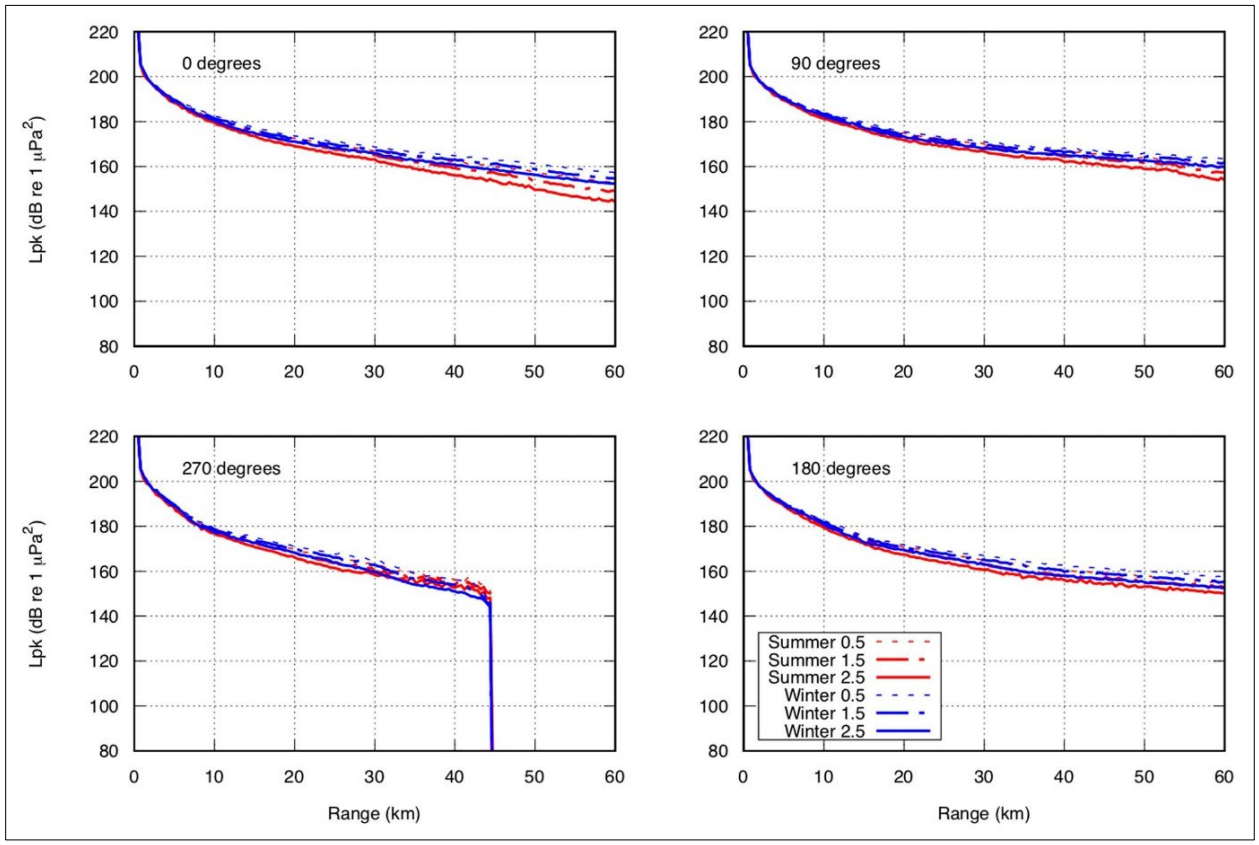

Figure 6-14. $L_{p,\mathrm{pk}}$ as influenced by VAbeach environmental variables.

Top left: north (0°), top right: east (90°), bottom right: south (180°), bottom left: west (270°). Summer (red) and winter (blue) depth-averaged propagation distances over sediments of coarse (0.5 **ϕ**, dotted lines), medium (1.5 **ϕ**, dashed lines), and fine (2.5 **ϕ**, solid lines) sand. Water depth at the source position was approximately 24 m. Data at 270° were truncated at 45 km to avoid numerical instabilities of the model output in very shallow water. µPa = micropascal; **ϕ** = grain size; dB = decibel; km = kilometer; $L_{p,\mathrm{pk}}$ = peak sound pressure level; re = with reference to; VAbeach = Virginia Beach site.

The $L_{p,\mathrm{rms}}$ values for VAbeach as a function of range, season, and sediment grain size were plotted for each cardinal direction (**Figure 6-15**). The sensitivity of $L_{p,\mathrm{pk}}$ to the environment is consistent with the L_E results, with the order of importance (high to low) being bathymetry, season, and grain size.

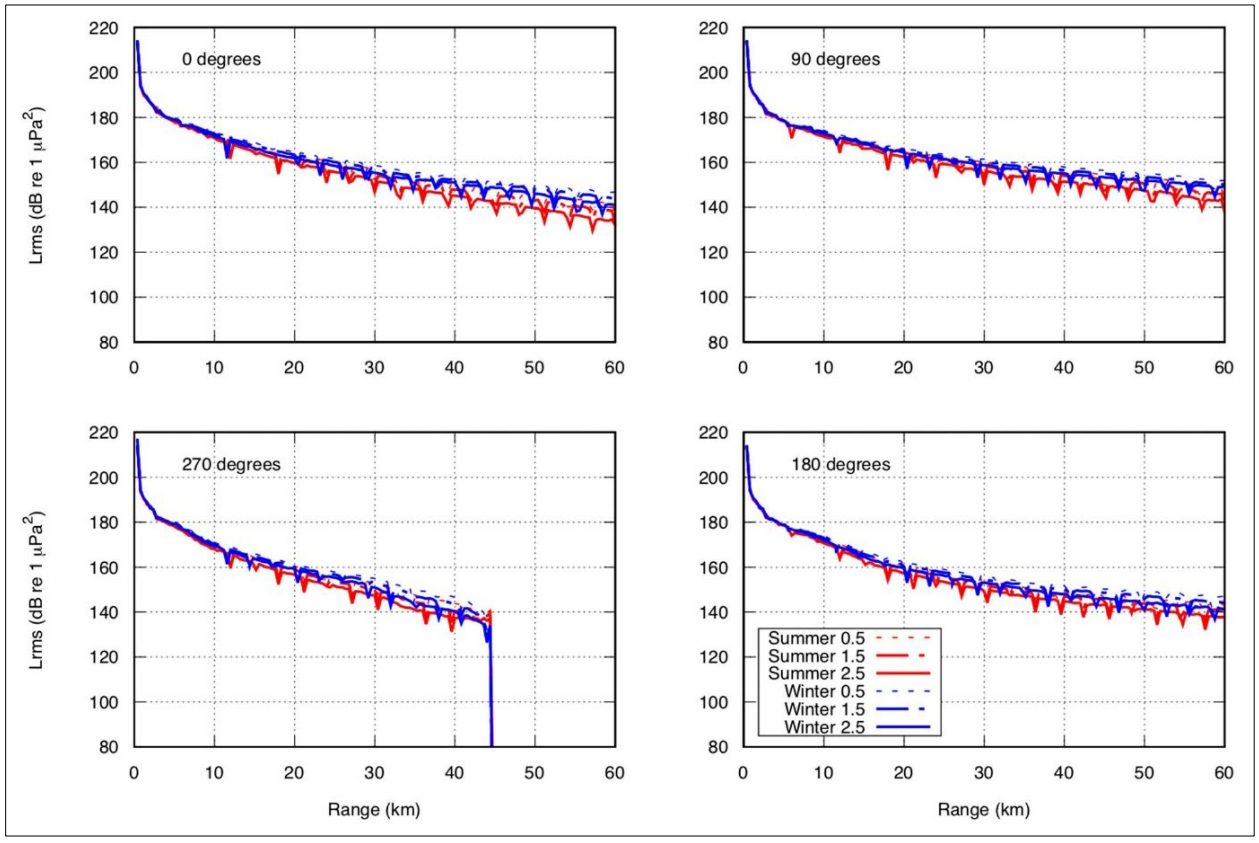

Figure 6-15. $L_{p,\mathrm{rms}}$ as influenced by VAbeach environmental variables.
Top left: north (0°), top right: east (90°), bottom right: south (180°), bottom left: west (270°). Summer (red) and winter (blue) depth-averaged propagation distances over sediments of coarse (0.5 **ϕ**, dotted lines), medium (1.5 **ϕ**, dashed lines), and fine (2.5 **ϕ**, solid lines) sand. Water depth at the source position was approximately 24 m. Data at 270° were truncated at 45 km to avoid numerical instabilities of the model output in very shallow water. µPa = micropascal; **ϕ** = grain size; dB = decibel; km = kilometer; $L_{p,\mathrm{rms}}$ = root-mean-square sound pressure level; re = with reference to; VAbeach = Virginia Beach site.

6.2.5 Statistical Characteristics

The environmental variables with the largest influence were determined by calculating the average vector values of the depth-averaged acoustic metrics (L_E, $L_{p,\mathrm{pk}}$, and $L_{p,\mathrm{rms}}$) in **Figures 6-10** to **6-15**, for three grain sizes, four bearings, and two seasons at each site. The mean and median for each acoustic metric provided averages that indicated a normal distribution, but neither provided an indication of the spread in the distribution. A large spread exists in the acoustic metrics at long ranges because, in bearings toward the direction of land, the water becomes very shallow. The standard deviation and interquartile range were used as statistical measures of this spread. For statistical comparison, acoustic metric means are presented in **Figures 6-16** and **6-19**, medians in **Figures 6-17** and **6-20**, and interquartile ranges for $L_E$in

Figures 6-18 and **6-21**. General trends in how means and medians can be used to understand the influence of different environmental parameters on sound propagation between two sites are discussed below.

Site selection was a proxy for water column depth. RIsland (35 m) was 11 m deeper than VAbeach (24 m) and farther from the continental shelf edge. When comparing the means (**Figures 6-13** and **6-16**) and medians (**Figures 6-17** and **6-20**), it is notable that the shallower VAbeach retained more sound energy overall than the deeper RIsland. The one exception towards the south is discussed in the bearing parameter subsection. The more pronounced case of summer to the north is discussed in subsequent parameter subsections. In general, the depth of the pile-driving site on its own does not sufficiently indicate how well sound will propagate in all directions from it, as site specificity/bathymetry needs to be considered.

Season was a proxy for SSP. When comparing the summer and winter means (**Figures 6-16** and **6-19**) and medians (**Figures 6-17** and **6-20**), it is notable that for all situations considered, the winter SSPs retained more sound energy than the summer SSPs, which was expected at LFs. (At HFs, effects of surface scattering were not modeled, as it might have increased TL in winter.)

Grain size was a proxy for sediment type. When comparing coarse, medium, and fine sediment means (**Figures 6-16** and **6-19**) and medians (**Figures 6-17** and **6-20**), the situations involving coarse (0.5 **ϕ**) sediments retained more sound energy than those involving fine (2.5 **ϕ**) sediments. This trend was more pronounced in summer SSPs along bathymetries that rapidly became shallow. In summary, finer sediments absorbed more sound energy than coarse sediments, especially during the summer.

Bearing was a proxy for bathymetry. When comparing the four cardinal directions of the means (**Figures 6-16** and **6-19**) and medians (**Figures 6-17** and **6-20**), the shallowing water columns lost more sound energy. At RIsland, the bearings from shallowest to deepest are north, west, east, and south (**Figure 6-2**). Sound energy attenuated most towards the north bearing with rapid shallowing, followed by west, east, and south (**Figures 6-16** and **6-19**). At VAbeach, the order of bearings from shallowest to deepest are west, north, south, and east (**Figure 6-3**). However, neither the means nor the medians followed the same bathymetrical influence as RIsland. This is likely because VAbeach is farther from land and generally flatter, so bathymetry has less of an influence overall.

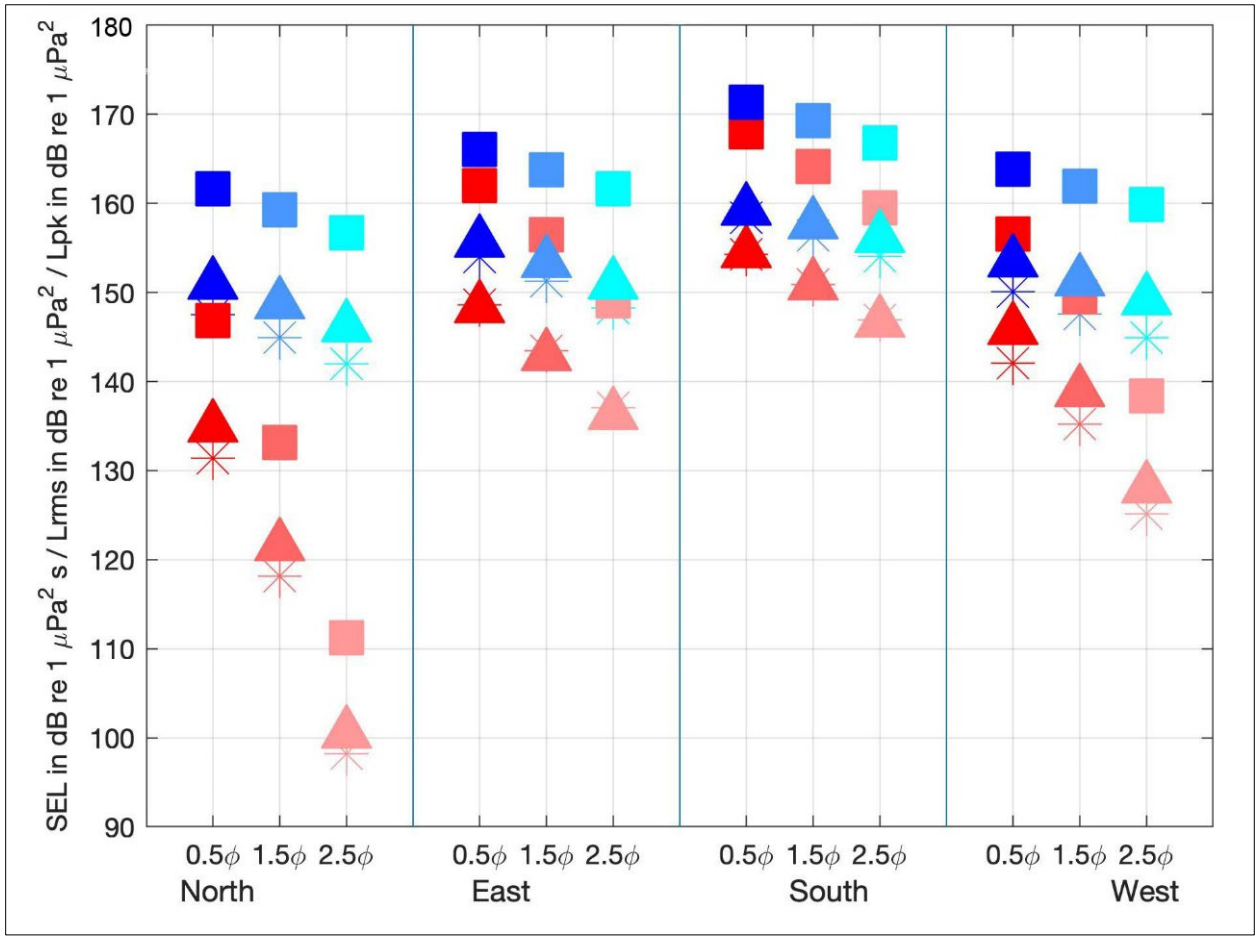

Figure 6-16. Mean acoustic metric values at RIsland.

Panels left to right: bearings of north (0°), east (90°), south (180°), and west (270°) during winter (blues) and summer (reds). Means of SEL (asterisks), $L_{p,\mathrm{rms}}$ (triangles), and $L_{p,\mathrm{pk}}$ (squares) for grain sizes 0.5 **ϕ** (dark shade), 1.5 **ϕ** (moderate shade), and 2.5 **ϕ** (light shade). For the west direction, vectors were truncated at 45 km to avoid numerical instabilities of the model output in very shallow water. µPa = micropascal; **ϕ** = grain size; dB = decibel; km = kilometer; $L_{p,\mathrm{pk}}$ = peak sound pressure level; $L_{p,\mathrm{rms}}$ = root-mean-square sound pressure level; re = with reference to; RIsland = Rhode Island site; s = second; SEL = L_E = sound exposure level.

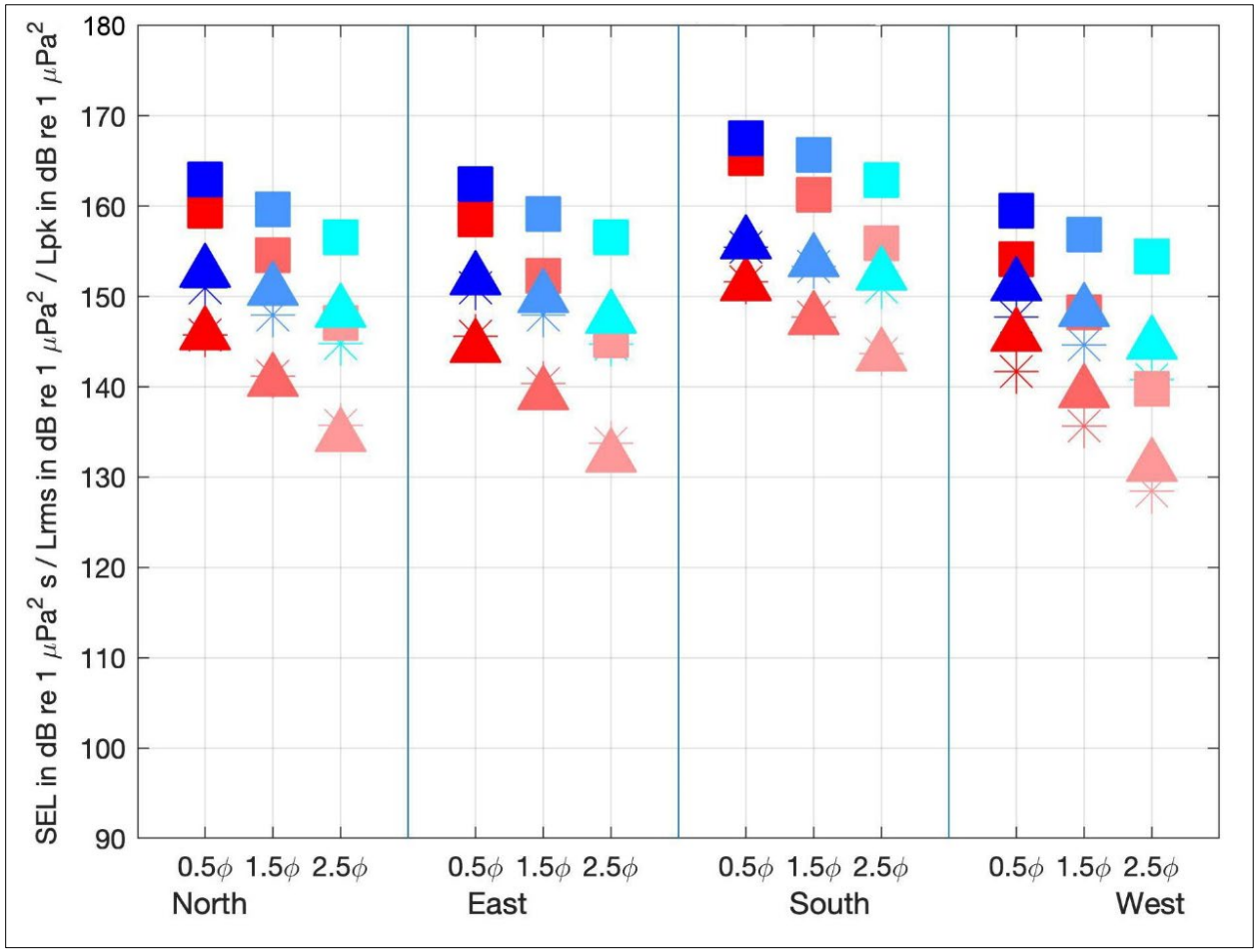

Figure 6-17. Median acoustic metric values at RIsland.
Panels left to right: four bearings of north (0°), east (90°), south (180°), and west (270°) during winter (blues) and summer (reds). Medians of SEL (asterisks), $L_{p,\mathrm{rms}}$ (triangles), and $L_{p,\mathrm{pk}}$ (squares) for grain sizes 0.5 **ϕ** (dark shade), 1.5 **ϕ** (moderate shade), and 2.5 **ϕ** (light shade). For the west direction, vectors were truncated at 45 km to avoid numerical instabilities of the model output in very shallow water. µPa = micropascal; **ϕ** = grain size; dB = decibel; km = kilometer; $L_{p,\mathrm{pk}}$ = peak sound pressure level; $L_{p,\mathrm{rms}}$ = root-mean-square sound pressure level; re = with reference to; RIsland = Rhode Island site; s = second; SEL = L_E = sound exposure level.

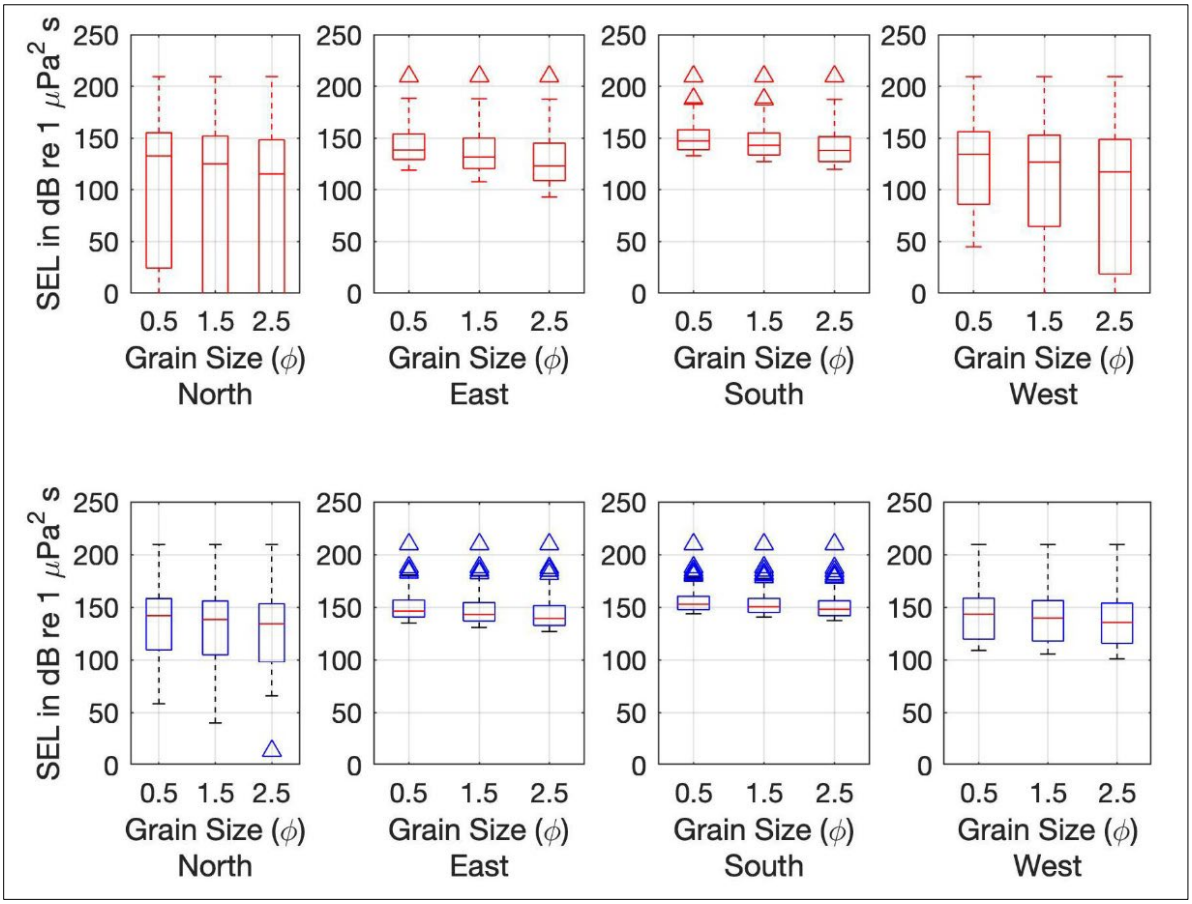

Figure 6-18. Percentiles of unweighted single strike SEL at RIsland.
During summer (red, top panels) and winter (blue, bottom panels). Quartile $L_{E,ss}$ distributions presented as box and whisker plots of 25th (bottom of box), median (red middle bar inside each box), and 75th (top of box) and extreme values (triangles) for four bearings (left to right): north (0°), east (90°), south (180°), and west (270°), and three grain sizes, smallest to largest. µPa = micropascal dB = decibel; re = with reference to; RIsland = Rhode Island site; s = second; SEL = L_E = sound exposure level.

Identifying the largest differences between the means and medians of the metrics across parameters and sorting them from most to least influential suggested the site parameter (water column depth proxy) had the largest influence compared to the other three parameters. However, the site parameter also could be accounting for proximity to land. The environmental sensitivity models may be driven more by how close a site is to shore than by the water depth at the precise pile location. Had the two sites been farther from shore, that propagation likely would have been more strongly influenced by water depth. If there existed bathymetry similarly complex to RIsland farther from land, then bathymetry would drive the sound propagation more than the nearest coastline. Because of the depths where piles are safe to drive into the seafloor, it is more likely those sites will exist close to shore where bathymetry is more likely to be complicated and the coastline can act as a physical barrier to sound.

If using only the difference in acoustic means to rank parameter influence within a single site, environmental factors influence acoustic propagation differently. For RIsland, bearing (bathymetry) was the most influential parameter, then season (SSP), and finally grain size (sediment type). For VAbeach, bearing (bathymetry) was the most influential parameter (slightly), while grain size (sediment type) and

season (SSP) exhibited nearly the same influence on sound propagation. In summary, the shallower, flatter water column exhibited less predictable influence on sound propagation compared to the deeper water column.

If using only the difference in acoustic medians to rank parameter influence within a single site, bearing (bathymetry), season (SSP), and grain size (sediment) had roughly the same effect on propagation at RIsland. At VAbeach, bearing (bathymetry) was slightly more influential than the equally ranked season (SSP) and grain size (sediment), though season was slightly more influential at higher grain sizes. In summary, using medians of the acoustic metrics to represent the influence of environmental factors on propagation illustrates bathymetry, sediment type, and the SSP all are impactful factors but not to the same degree as when using the means of the acoustic metrics.

Despite season being a proxy for the SSP, the static state of the SSP was not the most influential in terms of sound propagating through a water column while interacting with boundary conditions. This is because it is the change in SSP, not in the absolute water temperature, that matters. All three metrics captured some of these variations, but the $L_{p,\mathrm{pk}}$ metric was the most common indicator for comparing the means and the level of influence across and between parameters and their magnitudes.

Comparing means and medians gave different rankings of environmental parameter influence on sound propagation, particularly at RIsland; therefore, the interquartile ranges and extreme values are presented (as box and whisker plots) in L_E (**Figures 6-18** and **6-21**) for both sites. The L_E metric is the most robust as it represents the majority of acoustic criteria. The interquartile ranges are presented to provide insight on differences across the entire distribution. The interquartile results illustrate how the medians are more robust (less affected by outliers) than the means. While the medians are similar to one another across the environmental parameters, the spreads are quite different. However, they are in the same order as the means in terms of most to least influential. The larger spreads for RIsland versus VAbeach correspond with site being the most influential parameter (**Figures 6-18** and **6-21**). The second most influential parameter was bearing, especially between north and west versus east and south, followed by season, then grain size (**Figures 6-18** and **6-21**).

The influence of parameters on acoustic propagation follows consistent trends between RIsland and VAbeach (e.g., better propagation towards deeper water, with harder sediments, and at LF in winter). Even though RIsland (35 m) was 45% deeper than VAbeach (24 m), the impact volumes rarely were 45% the size of each other (the only close comparison was RIsland's impact volume being 47% the size of VAbeach's for LF cetaceans' mean PTS) (**Section 6.3**).

Most pile-driving sites will not occur in water deeper than 50 m, but variation in sound propagation exists across water columns from 0 to 50 m deep. For identical propagation conditions, a change of 50% in water depth should change the impact volume by 50%. Relative to the depths at RIsland and VAbeach, the following water depths between 0 and 50 m are 50% deeper (or 33% shallower) than each other: 5, 7, 11, 16, 23, 34, and 50 m. (This is similar to the Fibonacci sequence of …5, 8, 13, 21, 34, and 50 found throughout the natural world.) RIsland actually was 45% deeper than VAbeach but resulted in impact volume differences exceeding 50%. Thus, water depth is not the only explanatory variable for impact volume size, surrounding bathymetry and propagation conditions also play a role.

Because the contributions of each environmental parameter could be site-specific, it is advisable to repeat the propagation modeling procedure at each pile-driving site. Acoustic propagation at different sites likely

experiences a different ranking of environmental parameter influence when a site has deeper water (approximately 55 m), different oceanographic conditions (e.g., not in a major coastal current system), greater seasonal contrast (i.e., at higher latitudes), or is farther from shore (approximately 50 km), to name a few examples. Numerical quantifications of what makes a site deeper or farther from shore is discussed in **Section 8**. Parameter influence is site- and season-specific. A tentative overall ranking, based on an unweighted L_E and on the specific sites considered along the U.S. Atlantic Coast (RIsland and VAbeach), is bearing relative to shallowing water, grain size, and season (SSP). The influence of environmental parameters on the holistic impact volumes was calculated and analyzed and is presented in **Sections 6.4.2.1** to **6.4.3.7**. These impact volumes provide a more robust perspective of the environmental influences than can be deduced by investigating effects on each acoustic metric independently.

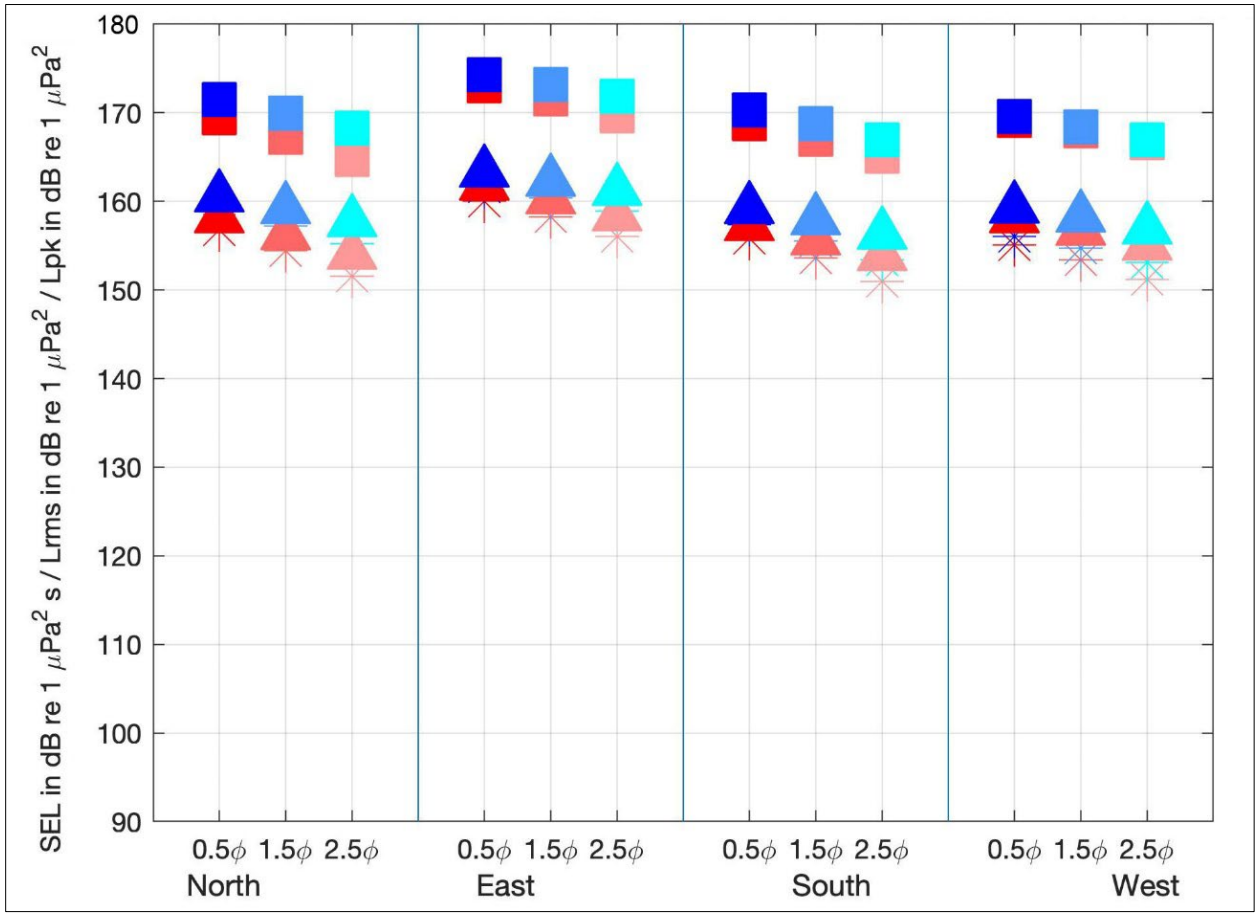

Figure 6-19. Mean acoustic metric values at VAbeach.
Panels left to right: four bearings of north (0°), east (90°), south (180°), and west (270°) during winter (blues) and summer (reds). Means of SEL (asterisks), $L_{p,\mathrm{rms}}$ (triangles), and $L_{p,\mathrm{pk}}$ (squares) for grain sizes 0.5 **ϕ** (dark shade), 1.5 **ϕ** (moderate shade), and 2.5 **ϕ** (light shade). For the west direction, vectors were truncated at 45 km to avoid numerical instabilities of the model output in very shallow water. µPa = micropascal; **ϕ** = grain size; dB = decibel; km = kilometer; $L_{p,\mathrm{pk}}$= peak sound pressure level; $L_{p,\mathrm{rms}}$ = root-mean-square sound pressure level; re = with reference to; s = second; SEL = L_E = sound exposure level; VAbeach = Virginia Beach site.

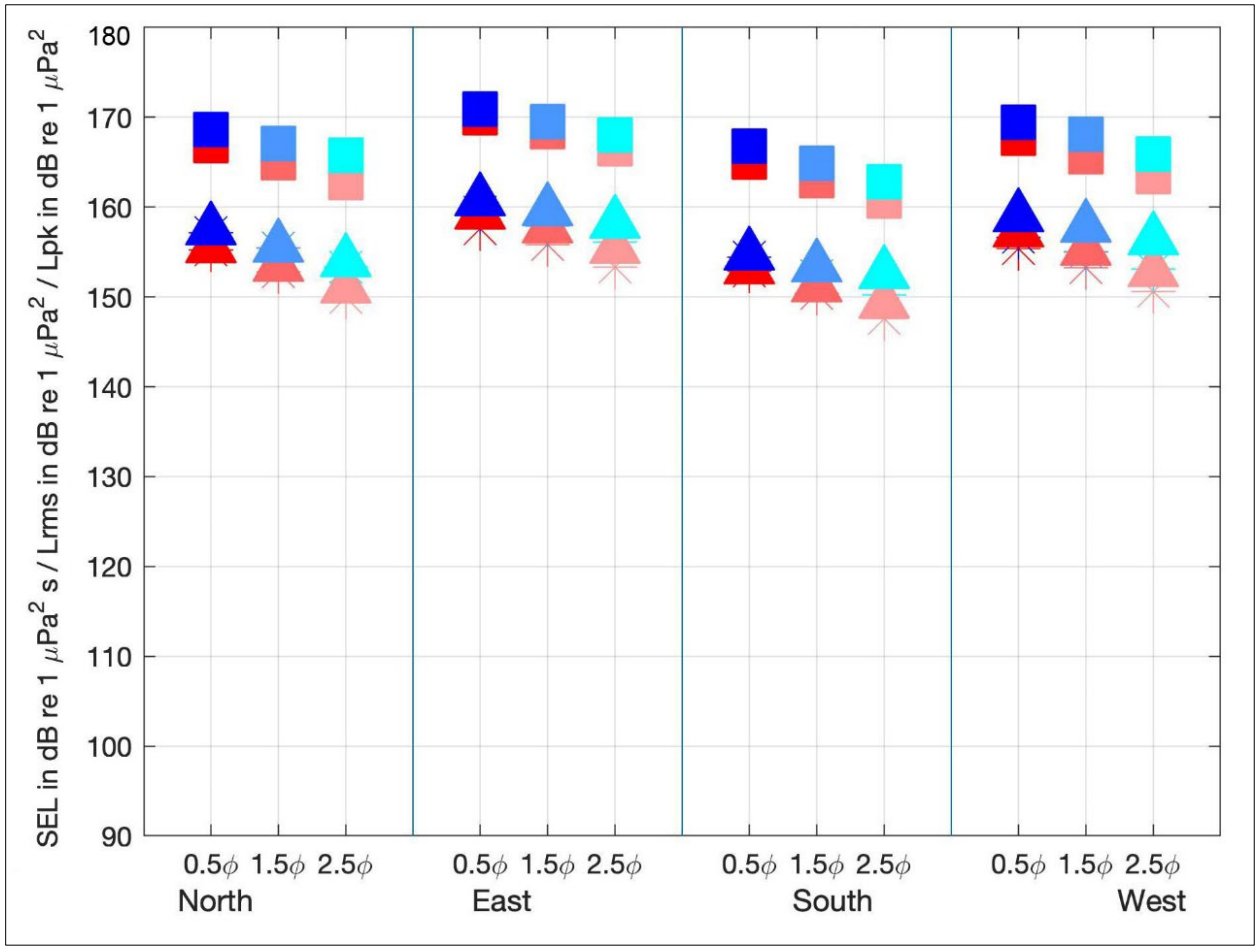

Figure 6-20. Median acoustic metric values at VAbeach.
Panels left to right: four bearings of north (0°), east (90°), south (180°), and west (270°) during winter (blues) and summer (reds). Medians of SEL (asterisks), $L_{p,\mathrm{pk}}$ (squares), and $L_{p,\mathrm{rms}}$ (triangles) for grain sizes 0.5 **ϕ** (dark shade), 1.5 **ϕ** (moderate shade), and 2.5 **ϕ** (light shade). For the west direction, vectors were truncated at 45 km to avoid numerical instabilities of the model output in very shallow water. µPa = micropascal; **ϕ** = grain size; dB = decibel; km = kilometer; $L_{p,\mathrm{pk}}$= peak sound pressure level; $L_{p,\mathrm{rms}}$ = root-mean-square sound pressure level; re = with reference to; s = second; SEL = L_E = sound exposure level; VAbeach = Virginia Beach site;.

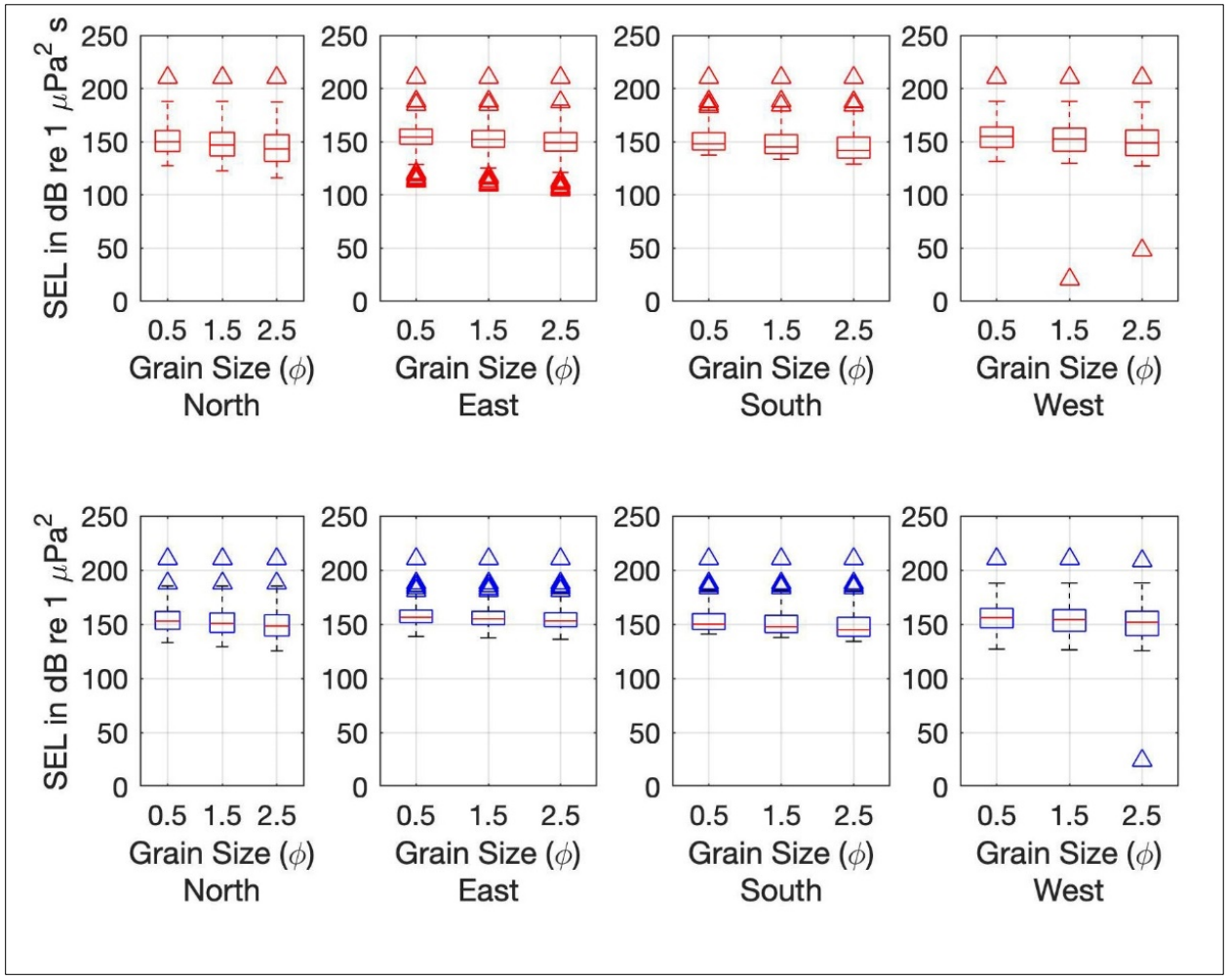

Figure 6-21. Percentiles of unweighted single strike SEL at VAbeach.

During summer (red, top panels) and winter (blue, bottom panels). Quartile $L_{E,\mathrm{ss}}$ distributions presented as box and whisker plots of 25th (bottom of box), median (red middle bar inside each box), and 75th (top of box) and extreme values (triangles) for four bearings (left to right): north (0°), east (90°), south (180°), and west (270°) and three grain sizes, smallest to largest. µPa = micropascal; dB = decibel; re = with reference to; SEL = L_E = sound exposure level; VAbeach = Virginia Beach site.

6.2.6 Sound Exposure Level Results as Plan View Plots

The metrics (means, medians, and percentiles) presented required high-resolution in frequency (0.5 Hz spacing) and therefore were computed only in the four cardinal directions. If only the $L_E$were computed, then the frequency spacing could be larger (10 Hz). The plan view (720 radials) unweighted L_E, averaged across depth, was computed and is presented in **Figures 6-22** and **6-23** for both sites. Color-coded contours align with values of PTS and TTS $L_{E,\mathrm{w,24h}}$ risk thresholds for LF cetaceans. A surrounding green contour is plotted for all L_E values above the $L_{E,\mathrm{w,24h}}$ noise floor for LF cetaceans calculated from a quieter Arctic soundscape example quantified by Martin et al. (2019). The Chukchi Sea soundscape was chosen as a comparison because it was quieter than other alternatives available and was considered free of man-made sounds (Martin et al., 2019).

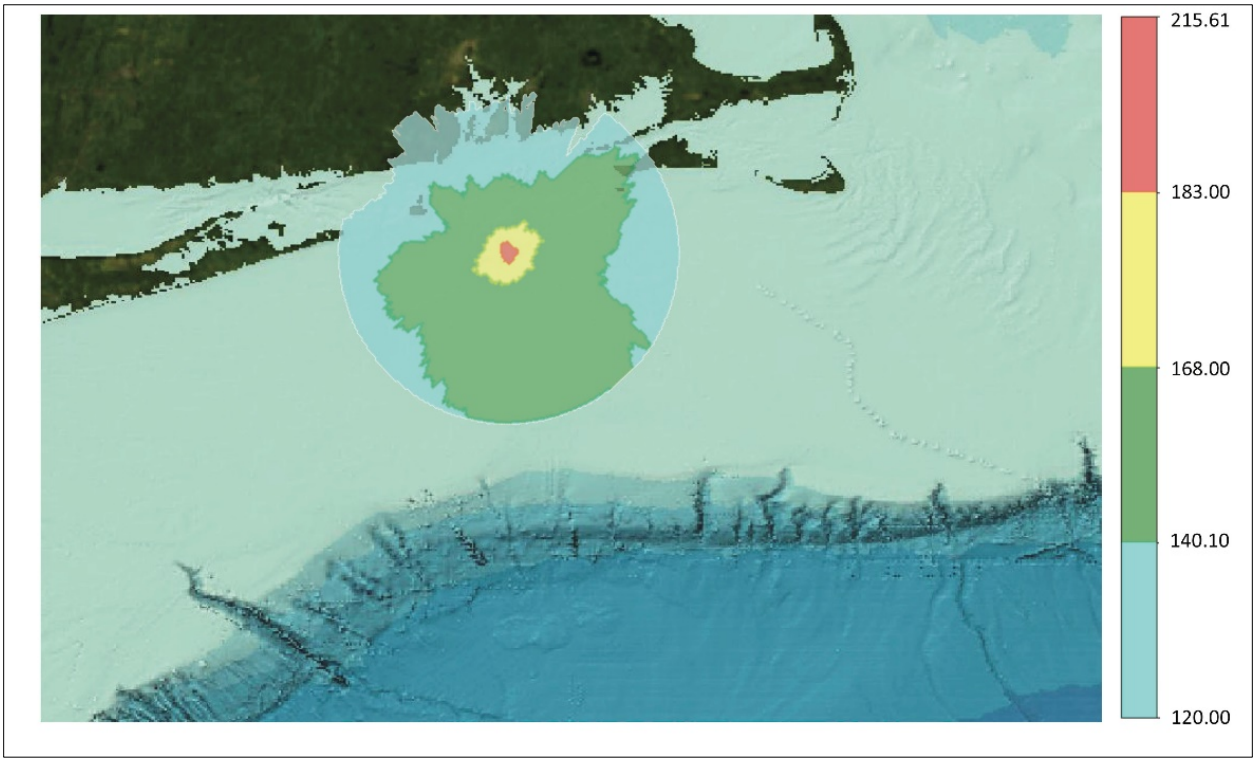

Figure 6-22. Plan view of the depth-averaged, low-frequency $SEL_{w,24h}$ at RIsland.
Cyan: 60-km radius modeled range, region below Chukchi Sea measured noise floor per Martin et al. (2019 and pers. comm.); green: region below TTS risk threshold; yellow: region below PTS risk threshold; red: region above PTS risk threshold. Color scale units are in dB re 1 µPa^2 s. µPa = micropascal; dB = decibel; km = kilometer; $L_{E,\mathrm{w,24h}}$ = weighted 24-hour sound exposure level; PTS = permanent threshold shift; re = with reference to; RIsland = Rhode Island site; s = second; SEL = L_E = sound exposure level; TTS = temporary threshold shift.

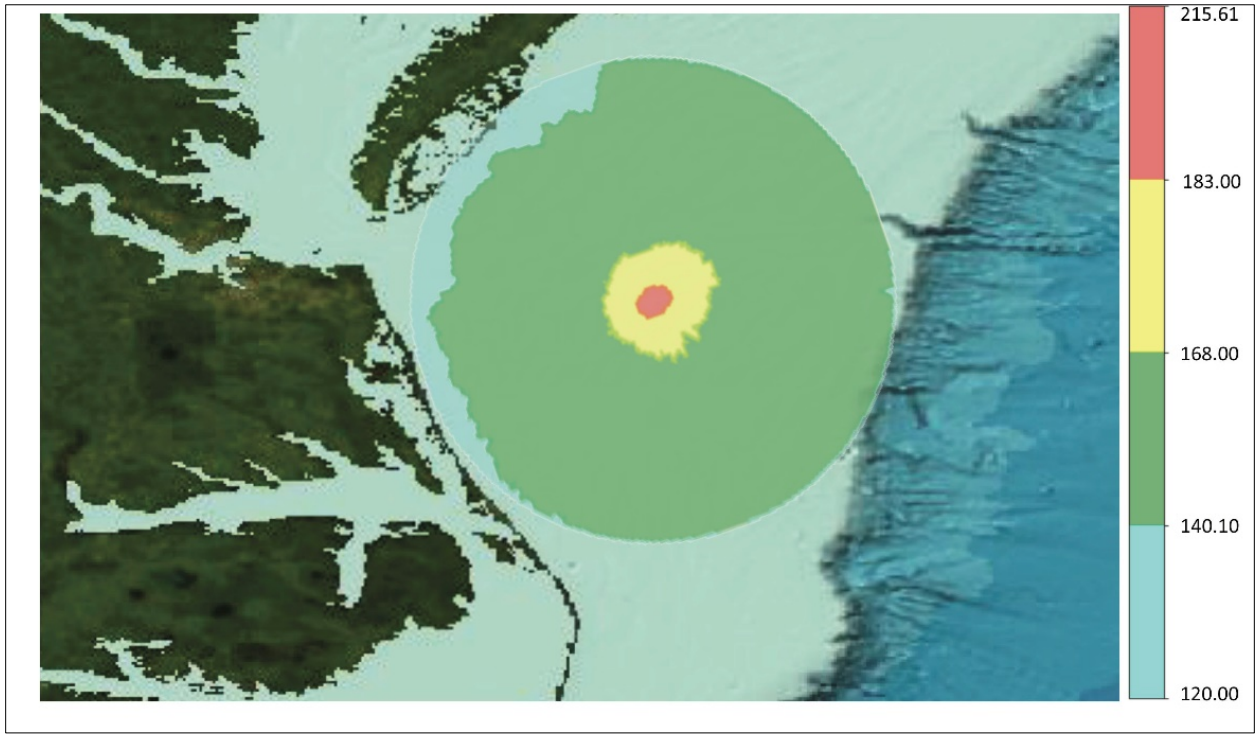

Figure 6-23. Plan view of the depth-averaged, low-frequency weighted, $SEL_{w,24h}$ at VAbeach.
Cyan: 60-km radius modeled range, region below Chukchi Sea measured noise floor per Martin et al. (2019 and pers. comm.); green: region below TTS threshold; yellow: region below PTS threshold; red: region above PTS threshold. Color scale units are in dB re 1 μPa^2 s. μPa = micropascal; dB = decibel; $L_{E,\mathrm{w,24h}}$ = weighted 24-hour sound exposure level; PTS = permanent threshold shift; re = with reference to; s = second; SEL = L_E = sound exposure level; TTS = temporary threshold shift; VAbeach = Virginia Beach.

6.3 Impact Volumes

6.3.1 Applying Dual Impact Criteria

Using the modeled ranges to the L_E, $L_{p,\mathrm{rms}}$, and $L_{p,\mathrm{pk}}$ threshold values, impact volumes were calculated for all effect criteria listed in **Section 1.5**. Specifically, criteria for the following 10 species groups were considered:

- Four groups of marine mammals specified by NMFS (2018): LF cetaceans, MF cetaceans, HF cetaceans, and phocid pinnipeds underwater;
- Three groups of fishes specified by Popper et al. (2014): without swim bladder, with swim bladder involved in hearing, and with swim bladder not involved in hearing;
- Two size classes of fishes specified by GARFO (2016): fish mass greater or less than 2 grams; and
- Sea turtles.

Impact volumes were determined using the computations across the four cardinal directions. Each range/depth cell of the computation represents a volume equivalent to range spacing (20 m) × depth spacing (1 m) × range (in m) × bearing sector (90°). All pixels that exceeded the specific

threshold value were counted to reach the total impact volume. Dual impact criteria were implemented by computing the impact volume for each of the criteria separately.

6.3.2 Impact Volumes for Marine Mammals

Prior to presenting the methodology and results of the impact volume computation variability across sites and animal groups, the received levels were compared from the combined FE/PE model and the observations made at the Gemini wind farm. The modeled Gemini site was an isovelocity SSP on a flat silt-sand seafloor 24 m deep. The recordings were made at ranges of 732 m, 7.017 km, 31.8 km, and 65.7 km from the pile. The unweighted decidecade band L_E for each range from the Gemini observations and RIsland (24 m deep) during winter (nearly isovelocity) are shown in **Figure 6-24**. The model was calibrated to match the Gemini result at 732 m.

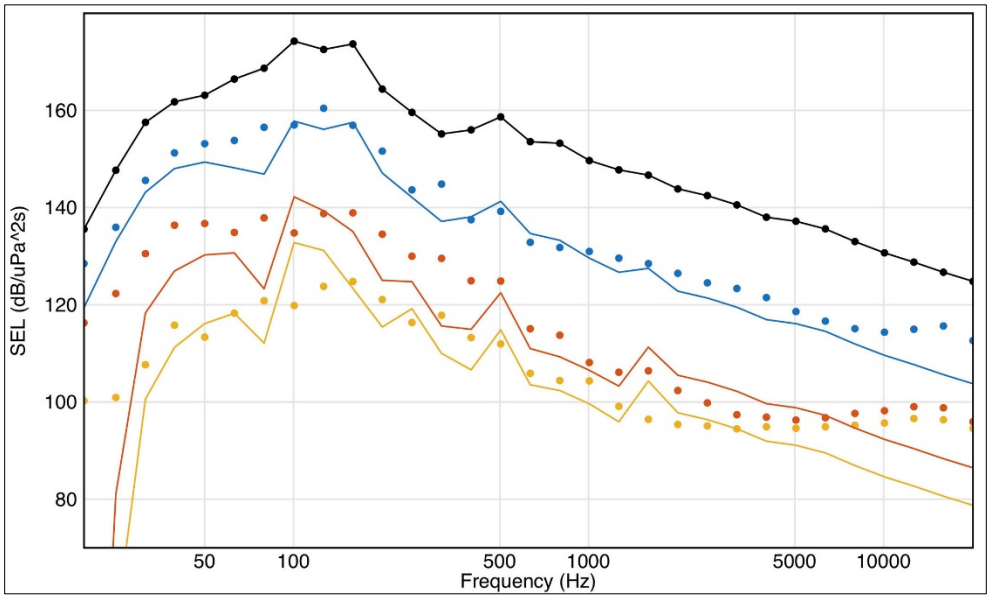

Figure 6-24. Comparison of unweighted single strike SEL in decidecade bands for Gemini U8-pile measurements and RIsland model predictions.

RIsland (lines) winter model and Gemini U8 pile measurements (dots) for four ranges from the pile: 0.7 km (black), 7 km (blue), 32 km (red), and 65 km (yellow). µPa = micropascal; dB = decibel; Hz = hertz; km = kilometer; m = meter; RIsland = Rhode Island site; s = second; SEL = L_E = sound exposure level.

The propagation model results are consistent with the Gemini observations, with a few differences. The most notable difference was that the Gemini measurements at long ranges showed considerable energy in the band above 3 kHz. Sound at these frequencies are not expected to propagate long distances; therefore, the L_E numbers in these bands very likely were dominated by ambient noise. The observed differences at very low frequencies (20 and 25 Hz) likely are due to propagation differences in the deep sediment. RIsland does appear to be more lossy than the Gemini site, which likely is due to its slightly softer seafloor (0.5 $\boldsymbol{\phi}$ for RIsland compared with 0.0 $\boldsymbol{\phi}$ for Gemini).

In order to set expectations for the impact ranges (and subsequent volumes), the observed Gemini $L_{E,w}$ values were investigated for HF and LF cetaceans. For these two cetacean hearing groups, the expected ranges for TTS were approximately 3 km and 15 km, respectively, based on the Gemini measurements.

As described below, there are significant differences between the impact volumes for a single strike and those for a 24-hour period.

Computed impact volumes are presented in cubic kilometers (km^3). One cubic kilometer is 10^9 (one billion) cubic meters. For these sites (assuming a nominal water depth of 31 m as the height of a cylinder), impact volumes of 0.01, 1.0, and 100 km^3 correspond to impact ranges from the pile (the cylindrical radii) of approximately 320 m, 3.2 km, and 32 km, respectively. An impact volume less than $1 \cdot 10^{-4}$ km^3 has a cylindrical area with a radius less than 32 m. This can be visualized as two blue whales fitting nose to tail in the impact volume. To facilitate visual interpretation in **Tables 6-1** to **6-12**, the cubic kilometer impact range results are color coded by radius length (and cylindrical volume) as green, <32 m ($<1 \cdot 10^{-4}$ km^3); yellow, 32 to 320 m ($<1 \cdot 10^{-4}$ to 0.01 km^3); orange, 320 m to 3.2 km (0.01 to 1.0 km^3); red, 3.2 to 32 km (1.0 to 100 km^3); and purple, >32 km (>100 km^3). Impact volumes involving L_E were calculated using the full frequency range of 17 Hz to 20 kHz. Impact volumes involving $L_{p,\mathrm{pk}}$ and $L_{p,\mathrm{rms}}$ were calculated using the limited frequency range of 17.5 to 2,238.5 Hz because these metrics are unweighted and therefore unaffected by contributions from HF energy.

6.3.2.1 Impulsive Signals, PTS Onset, $L_{E,\mathrm{w},24\mathrm{h}}$ for Marine Mammals

Impact volumes were calculated for PTS onset using $L_{E,\mathrm{w},24\mathrm{h}}$ thresholds. Recall that up to 3,500 strikes could occur in any one 24-hour period and that all strikes would contribute equally to the total sound exposure. These assumptions result in the equation for the single-strike threshold as $L_{E,\mathrm{ss,PTS}} = L_{E,24\mathrm{h,PTS}}$ - $10\log_{10}(3{,}500)$ dB. A practical example for LF cetaceans, the corresponding PTS single-strike threshold becomes $L_{E,\mathrm{ss,PTS}}$ = 183 dB – 35.4 dB = 147.6 dB. The $L_{E,\mathrm{w},24\mathrm{h}}$ thresholds and their respective impact volumes are shown in **Table 6-1**, which is color-coded to aid in visualization of impact volumes.

Table 6-1. Marine mammal PTS $L_{E,\mathrm{w},24\mathrm{h}}$ impact volumes.

Marine Mammal PTS $L_{E,\mathrm{w},24\mathrm{h}}$						
Thresholds[a] (dB re 1 µPa² s)			183	185	155	185
Site	**Season**	**Grain size (ϕ)**	**Low-frequency cetacean (km³)**	**Mid-frequency cetacean (km³)**	**High-frequency cetacean (km³)**	**Phocid pinniped, underwater (km³)**
VAbeach	Summer	0.5	64.20	0.0019	0.63	0.0015
VAbeach	Summer	1.5	48.36	0.0016	0.55	0.0014
VAbeach	Summer	2.5	34.27	0.0015	0.48	0.0013
VAbeach	Winter	0.5	88.95	0.0022	0.68	0.0016
VAbeach	Winter	1.5	65.84	0.0019	0.60	0.0015
VAbeach	Winter	2.5	51.01	0.0019	0.52	0.0015
RIsland	Summer	0.5	31.38	0.0001	0.17	0.0004
RIsland	Summer	1.5	20.14	0.0001	0.12	0.0004
RIsland	Summer	2.5	12.53	0.0001	0.06	0.0004
RIsland	Winter	0.5	47.20	0.0009	1.78	0.0008
RIsland	Winter	1.5	32.75	0.0007	1.07	0.0006
RIsland	Winter	2.5	21.25	0.0005	0.57	0.0005
VAbeach	Mean	--	58.77	0.0018	0.58	0.0015
VAbeach	Median	--	64.20	0.0019	0.60	0.0015
VAbeach	Std. Dev.	--	17.12	0.0002	0.07	0.0001
RIsland	Mean	--	27.54	0.0004	0.63	0.0005
RIsland	Median	--	31.38	0.0005	0.57	0.0005
RIsland	Std. Dev.	--	11.17	0.0003	0.62	0.0001

-- = not applicable; µPa = micropascal; dB = decibel; km = kilometer; m = meter; PTS = permanent threshold shift; re = with reference to; RIsland = Rhode Island site; $SEL_{w,24h}$ = $L_{E,\mathrm{w},24\mathrm{h}}$ = weighted, 24-hour sound exposure level; s = second; Std. Dev. = standard deviation; VAbeach = Virginia Beach site.
Volumes defined as: green = <0.032 km³, yellow = 0.032 to 0.32 km³; orange = 0.32 to 3.2 km³; red = 3.2 to 32 km³; purple = >32 km³.
a - National Marine Fisheries Service (2018).

The extent to which these impact volumes were influenced by grain size, SSP, and water depth are illustrated in **Figure 6-25**, which displays the impact volumes at both sites during both seasons and assumes sound energy is radiated into the deepening water to the east. The predicted impact volumes are larger and vary more at VAbeach. At both sites, impact volumes are larger during winter than during summer. Regardless of site and season, impact volumes always are smaller with finer grain sizes.

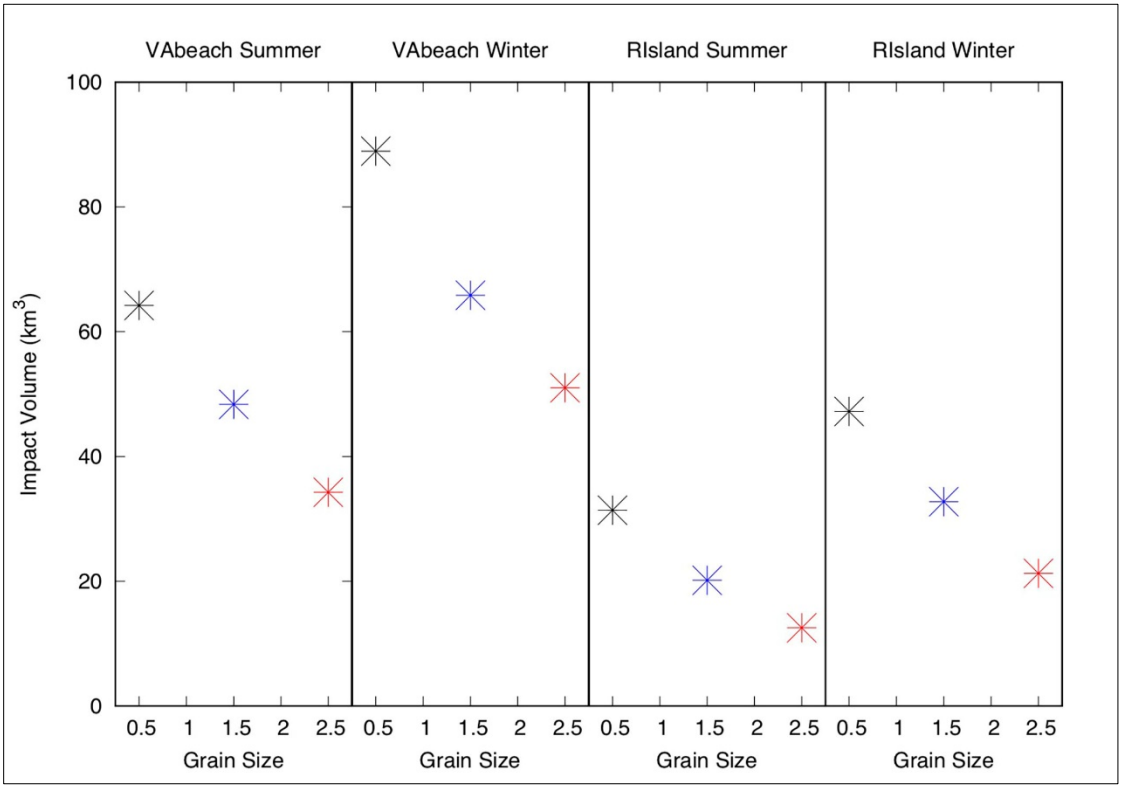

Figure 6-25. Environmental influence on impact volumes for low-frequency cetacean PTS, weighted, $SEL_{w,24h}$.

The $L_{E,w,24h}$ = $SEL_{w,24h}$ PTS threshold = 183 dB re 1 µPa^2 s, and provided basis for impact volumes, which are based on 3,500 strikes in 24 hours. µPa = micropascal; **ϕ** = grain size dB = decibel; km^3 = cubic kilometer; $L_{E,w,24h}$ = weighted 24-hour sound exposure level; PTS = permanent threshold shift; re = with reference to; RIsland = Rhode Island site; SEL = L_E = sound exposure level; VAbeach = Virginia Beach site.

6.3.2.2 Impulsive Signals, PTS Onset, $L_{p,pk}$ for Marine Mammals

The impact volume for PTS for all marine mammal groups was calculated using an $L_{p,pk}$ threshold (**Table 6-2**). In all impact volume tables, impact range radii less than 32 m were truncated and listed as $<1 \cdot 10^{-4}$ km^3 because of a lack of range resolution in the acoustic model prediction. The $L_{p,pk}$ impact volumes are smaller than the L_E impact volumes, so according to the dual criteria application, the impact volumes are determined by the larger L_E volumes in **Table 6-1**. The $L_{p,pk}$ impact volumes (and more generally, the smaller volumes for all dual criteria) are presented without color-coding.

Table 6-2. Marine mammal PTS onset $L_{p,\mathrm{pk}}$ impact volumes

Marine Mammal PTS $L_{p,\mathrm{pk}}$						
Thresholds[a] (dB re 1 µPa)			219	230	202	218
Site	**Season**	**Grain size (ϕ)**	**Low-frequency cetacean (km^3)**	**Mid-frequency cetacean (km^3)**	**High-frequency cetacean (km^3)**	**Phocid pinniped, underwater (km^3)**
VAbeach	Summer	0.5	0.000153	$<1{\cdot}10^{-4}$	0.0811	0.000235
VAbeach	Summer	1.5	0.000150	$<1{\cdot}10^{-4}$	0.0785	0.000230
VAbeach	Summer	2.5	0.000151	$<1{\cdot}10^{-4}$	0.0727	0.000214
VAbeach	Winter	0.5	0.000122	$<1{\cdot}10^{-4}$	0.0862	0.000166
VAbeach	Winter	1.5	0.000122	$<1{\cdot}10^{-4}$	0.0823	0.000157
VAbeach	Winter	2.5	0.000113	$<1{\cdot}10^{-4}$	0.0776	0.000168
RIsland	Summer	0.5	0.000161	$<1{\cdot}10^{-4}$	0.0592	0.000268
RIsland	Summer	1.5	0.000153	$<1{\cdot}10^{-4}$	0.0471	0.000272
RIsland	Summer	2.5	0.000163	$<1{\cdot}10^{-4}$	0.0359	0.000245
RIsland	Winter	0.5	0.000173	$<1{\cdot}10^{-4}$	0.0691	0.000232
RIsland	Winter	1.5	0.000172	$<1{\cdot}10^{-4}$	0.0581	0.000231
RIsland	Winter	2.5	0.000172	$<1{\cdot}10^{-4}$	0.0445	0.000222
VAbeach	Mean	--	0.000135	$<1{\cdot}10^{-4}$	0.0797	0.000195
VAbeach	Median	--	0.000150	$<1{\cdot}10^{-4}$	0.0811	0.000214
VAbeach	Std. Dev.	--	0.000016	--	0.0042	$3.198{\cdot}10^{-5}$
RIsland	Mean	--	0.000165	$<1{\cdot}10^{-4}$	0.0523	0.000245
RIsland	Median	--	0.000172	$<1{\cdot}10^{-4}$	0.0581	0.000245
RIsland	Std. Dev.	--	0.000007	--	0.0109	0.000019

-- = not applicable; µPa = micropascal; dB = decibel; km = kilometer; $L_{p,\mathrm{pk}}$ = peak sound pressure level; PTS = permanent threshold shift; re = with reference to; RIsland = Rhode Island site; Std. Dev. = standard deviation; VAbeach = Virginia Beach site.
a - National Marine Fisheries Service (2018).

The $L_{p,\mathrm{pk}}$ impact volumes followed the same trends as L_E for size, depending on the environmental parameters of site, season, and water column depth (**Figure 6-26**), but the details are unimportant because the larger impact volumes correspond to L_E (**Figure 6-25**), not $L_{p,\mathrm{pk}}$.

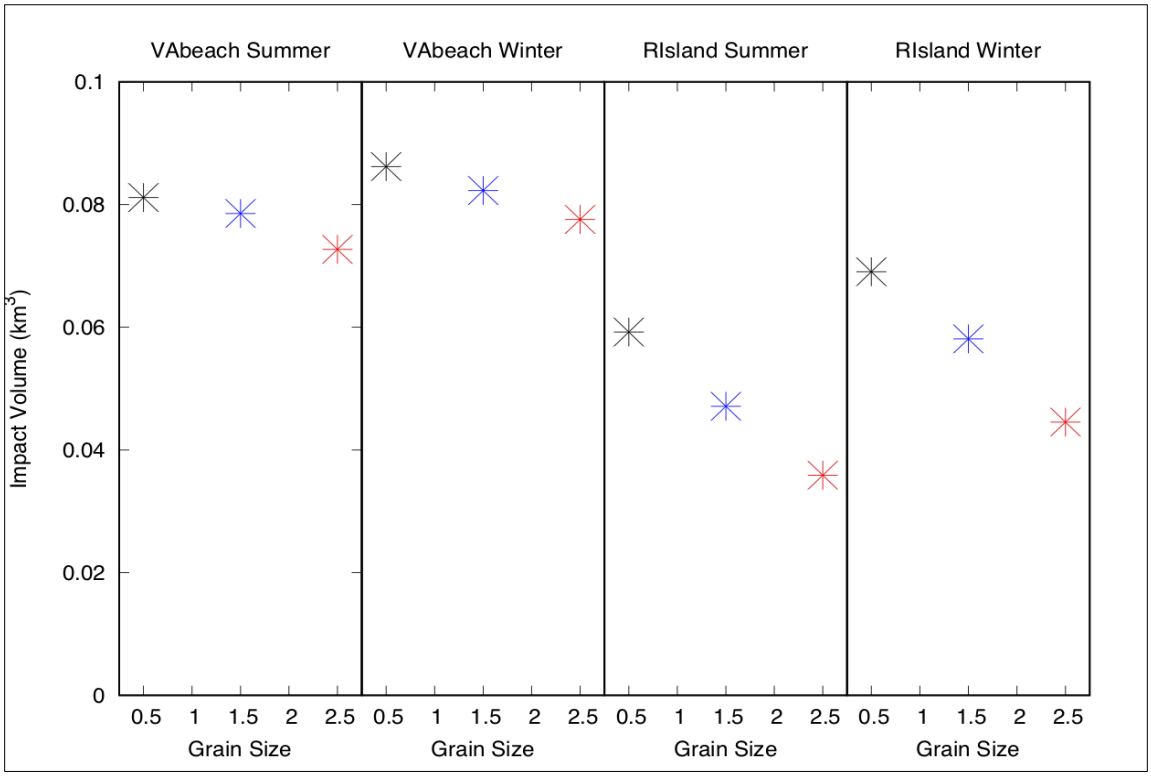

Figure 6-26. Environmental influence on impact volumes for high-frequency cetacean PTS, $L_{p,\mathrm{pk}}$.

The $L_{p,\mathrm{pk}}$ PTS threshold = 202 dB re 1 µPa, provided basis for impact volumes. µPa = micropascal; **ϕ** = grain size; dB = decibel; km^3 = cubic kilometer; $L_{p,\mathrm{pk}}$ = peak sound pressure level; PTS = permanent threshold shift; re = with reference to; RIsland = Rhode Island site; VAbeach = Virginia Beach site.

6.3.2.3 Impulsive Signals, TTS Onset, $L_{E,\mathrm{w},24\mathrm{h}}$ for Marine Mammals

For all marine mammal groups, the TTS impact volumes were calculated for L_E and $L_{p,\mathrm{pk}}$, as shown in **Tables 6-3** and **6-4**, respectively. As the TTS onset threshold is lower than PTS threshold, the TTS impact volumes were larger than PTS impact volumes. In many cases, the TTS impact volumes (**Table 6-3**) were at least three times larger than PTS impact volumes (**Table 6-1**). These assumptions result in the equation for the single-strike threshold as $L_{E,\mathrm{ss,TTS}} = L_{E,24\mathrm{h,TTS}} - 10\log(3{,}500)$ dB.
A practical example for HF cetaceans, the corresponding TTS single-strike threshold becomes $L_{E,\mathrm{ss,TTS}}$ = 140 dB – 35.4 dB = 104.6 dB.

Table 6-3. Marine mammal TTS $L_{E,w,24h}$ impact volumes

Marine Mammal TTS $L_{E,w,24h}$						
Thresholds[a] (dB re 1 µPa² s)			168	170	140	170
Site	**Season**	**Grain size (ϕ)**	**Low-frequency cetacean (km³)**	**Mid-frequency cetacean (km³)**	**High-frequency cetacean (km³)**	**Phocid pinniped, underwater (km³)**
VAbeach	Summer	0.5	267.8	0.028	32.63	0.239
VAbeach	Summer	1.5	238.8	0.025	24.15	0.215
VAbeach	Summer	2.5	188.2	0.021	21.73	0.189
VAbeach	Winter	0.5	281.6	0.030	31.65	0.253
VAbeach	Winter	1.5	269.6	0.027	23.42	0.229
VAbeach	Winter	2.5	246.4	0.023	21.08	0.204
RIsland	Summer	0.5	143.9	0.019	4.92	0.142
RIsland	Summer	1.5	94.5	0.012	2.84	0.112
RIsland	Summer	2.5	61.1	0.008	1.52	0.088
RIsland	Winter	0.5	263.7	0.150	27.15	0.222
RIsland	Winter	1.5	203.2	0.101	16.96	0.173
RIsland	Winter	2.5	158.0	0.058	9.37	0.122
VAbeach	Mean	--	248.8	0.026	25.78	0.222
VAbeach	Median	--	257.1	0.026	23.78	0.222
VAbeach	Std. Dev.	--	33.6	0.003	5.06	0.023
RIsland	Mean	--	154.1	0.058	10.52	0.143
RIsland	Median	--	151.0	0.038	7.33	0.132
RIsland	Std. Dev.	--	73.1	0.057	9.89	0.048

-- = not applicable; µPa = micropascal; dB = decibel; km = kilometer; $SEL_{w,24h}$ = $L_{E,w,24h}$ = weighted, 24-hour sound exposure level; re = with reference to; RIsland = Rhode Island site; s = second; Std. Dev. = standard deviation; TTS = temporary threshold shift; VAbeach = Virginia Beach site.
Volumes defined as: green = <0.032 km³, yellow = 0.032 to 0.32 km³; orange = 0.32 to 3.2 km³; red = 3.2 to 32 km³; purple = >32 km³ a - National Marine Fisheries Service (2018).

The environmental parameters (site, season, and grain size) had similar influence trends on impact volume for TTS compared to PTS. The shallower water columns, during winter, with hard sediments had the largest impact volumes (**Figure 6-27**).

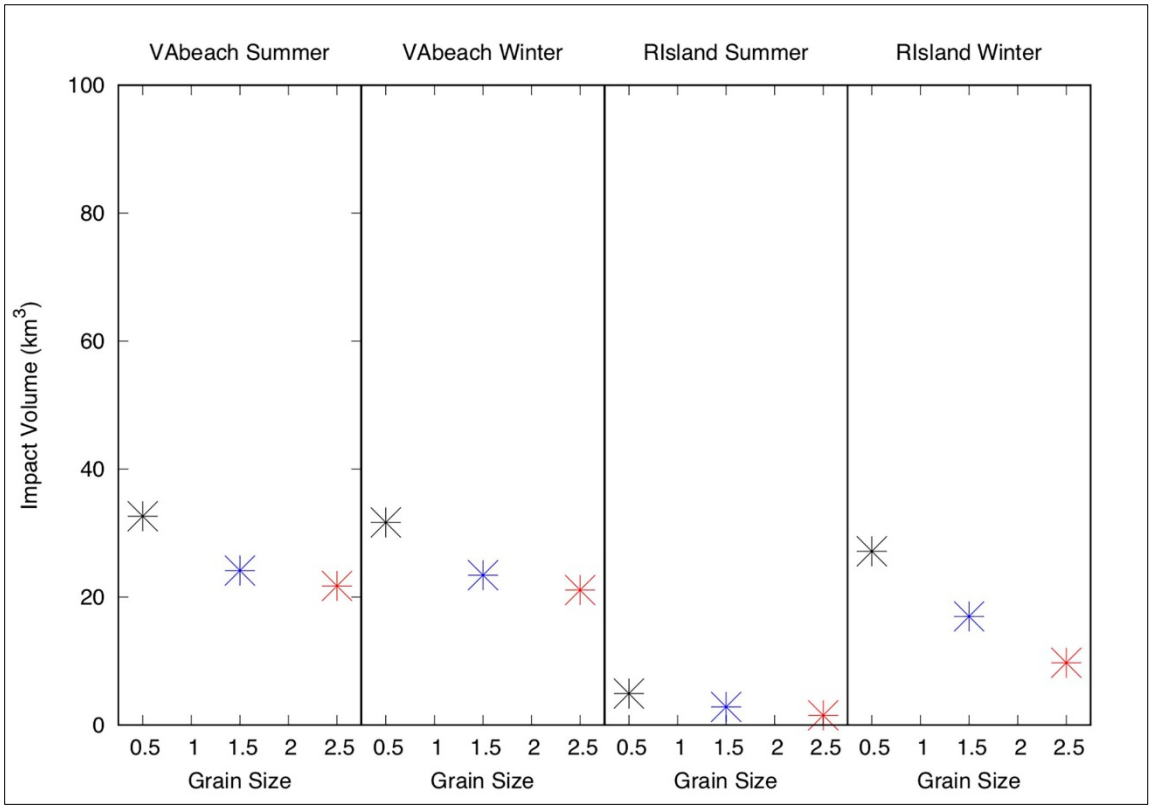

Figure 6-27. Environmental influence on impact volumes for high-frequency cetacean TTS weighted $SEL_{w,24h}$.

The $L_{E,w,24h}$ = $SEL_{w,24h}$ TTS threshold = 140 dB re 1 μPa^2 s, and provided basis for impact volumes, which are based on 3,500 strikes in 24 hours. μPa = micropascal; **ϕ** = grain size; dB = decibel; km^3 = cubic kilometer; $SEL_{w,24h}$ = $L_{E,w,24h}$ = weighted 24-hour sound exposure level; re = with reference to; RIsland = Rhode Island site; SEL = L_E = sound exposure level; TTS = temporary threshold shift; VAbeach = Virginia Beach site.

6.3.2.4 Impulsive Signals, TTS Onset, $L_{p,pk}$ for Marine Mammals

Compared with the PTS impact volumes, TTS impact volumes quantified by $L_{p,pk}$ had similar levels of influence from the environmental parameters (site, season, and water column depth) but were smaller (**Table 6-4**). For this situation, the standard deviation is not appropriate to report because of the lack of precision for impact ranges less than 32 m (i.e., volume $<1 \cdot 10^{-4}$ km^3). Because the volumes in **Table 6-4** are smaller than those in **Table 6-3**, the $L_{p,pk}$ volumes did not contribute to impact volume for TTS onset in marine mammals at either VAbeach or RIsland.

Table 6-4. Marine mammal TTS onset $L_{p,\mathrm{pk}}$ impact volumes.

Marine Mammal TTS Onset $L_{p,\mathrm{pk}}$						
Thresholds[a] (dB re 1 µPa)			213	224	196	212
Site	**Season**	**Grain size (ϕ)**	**Low-frequency cetacean (km^3)**	**Mid-frequency cetacean (km^3)**	**High-frequency cetacean (km^3)**	**Phocid pinniped, underwater (km^3)**
VAbeach	Summer	0.5	0.00146	$<1{\cdot}10^{-4}$	0.500	0.00222
VAbeach	Summer	1.5	0.00142	$<1{\cdot}10^{-4}$	0.468	0.00214
VAbeach	Summer	2.5	0.00134	$<1{\cdot}10^{-4}$	0.433	0.00201
VAbeach	Winter	0.5	0.00133	$<1{\cdot}10^{-4}$	0.563	0.00196
VAbeach	Winter	1.5	0.00128	$<1{\cdot}10^{-4}$	0.529	0.00185
VAbeach	Winter	2.5	0.00132	$<1{\cdot}10^{-4}$	0.492	0.00180
RIsland	Summer	0.5	0.00155	$<1{\cdot}10^{-4}$	0.307	0.00199
RIsland	Summer	1.5	0.00142	$<1{\cdot}10^{-4}$	0.240	0.00189
RIsland	Summer	2.5	0.00125	$<1{\cdot}10^{-4}$	0.177	0.00175
RIsland	Winter	0.5	0.00146	$<1{\cdot}10^{-4}$	0.389	0.00210
RIsland	Winter	1.5	0.00135	$<1{\cdot}10^{-4}$	0.309	0.00186
RIsland	Winter	2.5	0.00115	$<1{\cdot}10^{-4}$	0.229	0.00154
VAbeach	Mean	--	0.00135	$<1{\cdot}10^{-4}$	0.497	0.00200
VAbeach	Median	--	0.00133	$<1{\cdot}10^{-4}$	0.500	0.00201
VAbeach	Std. Dev.	--	0.00006	--	0.041	0.00015
RIsland	Mean	--	0.00136	$<1{\cdot}10^{-4}$	0.275	0.00185
RIsland	Median	--	0.00142	$<1{\cdot}10^{-4}$	0.307	0.00188
RIsland	Std. Dev.	--	0.00013	--	0.068	0.00018

-- = not applicable; µPa = micropascal; dB = decibel; km = kilometer; $L_{p,\mathrm{pk}}$= peak sound pressure level; re = with reference to; RIsland = Rhode Island site; Std. Dev. = standard deviation; TTS = temporary threshold shift; VAbeach = Virginia Beach site.
a - National Marine Fisheries Service (2018).

Table 6-4 does not have a corresponding figure showing environmental influence on impact volume because most of the ranges were less than 32 m, and dual criteria application states L_E would be followed for impact ranges instead of $L_{p,\mathrm{pk}}$.

6.3.2.5 Impulsive Signals, Behavior, $L_{p,\mathrm{rms}}$ for Marine Mammals

Table 6-5 shows the behavioral $L_{p,\mathrm{rms}}$ impact volumes to the 160 dB re 1 µPa threshold for the marine mammal groups. Of note are the differences between the sites; impact volumes were three times larger at VAbeach than at RIsland. Additionally, seasonality had a stronger influence at VAbeach compared to RIsland, which is visualized in **Figure 6-25**.

Table 6-5. Marine mammal behavioral $L_{p,\mathrm{rms}}$ impact volumes.

Marine Mammal Behavior $L_{p,\mathrm{rms}}$						
Thresholds[a,b] (dB re 1 µPa)			160	160	160	160
Site	**Season**	**Grain size (ϕ)**	**Low-frequency cetacean (km³)**	**Mid-frequency cetacean (km³)**	**High-frequency cetacean (km³)**	**Phocid pinniped, underwater (km³)**
VAbeach	Summer	0.5	49.93	49.93	49.93	49.93
VAbeach	Summer	1.5	40.26	40.26	40.26	40.27
VAbeach	Summer	2.5	31.98	31.98	31.98	31.98
VAbeach	Winter	0.5	60.80	60.80	60.80	60.81
VAbeach	Winter	1.5	51.51	51.51	51.51	51.51
VAbeach	Winter	2.5	42.77	42.77	42.77	42.77
RIsland	Summer	0.5	23.60	23.60	23.60	23.61
RIsland	Summer	1.5	15.68	15.68	15.68	15.68
RIsland	Summer	2.5	10.35	10.35	10.35	10.35
RIsland	Winter	0.5	36.42	36.42	36.42	36.42
RIsland	Winter	1.5	25.69	25.69	25.69	25.69
RIsland	Winter	2.5	17.79	17.79	17.79	17.79
VAbeach	Mean	--	46.21	46.21	46.21	46.21
VAbeach	Median	--	49.93	49.95	49.93	49.93
VAbeach	Std. Dev.	--	9.17	9.17	9.17	9.17
RIsland	Mean	--	21.59	21.59	21.59	21.59
RIsland	Median	--	23.61	23.61	23.61	23.60
RIsland	Std. Dev.	--	8.33	8.33	8.33	8.33

-- = not applicable; µPa = micropascal; dB = decibel; km = kilometer; $L_{p,\mathrm{rms}}$= root-mean-square sound pressure level; re = with reference to; RIsland = Rhode Island site; Std. Dev. = standard deviation; VAbeach = Virginia Beach site.
Volumes defined as: green = <0.032 km³, yellow = 0.032 to 0.32 km³; orange = 0.32 to 3.2 km³; red = 3.2 to 32 km³; purple = >32 km³ a - National Marine Fisheries Service (2018).
b - Federal Register (2005).

Comparing **Tables 6-1** and **6-5**, the predicted volumes for PTS in LF cetaceans at RIsland are larger than those for behavior at the same site. This is a combined consequence of the behavior and PTS criteria along with the exclusion of animal movement from the scope of this study. The behavior volume is determined by the rms sound pressure from a single hammer strike and does not change with the number of strikes. On the other hand, an animal is assumed stationary during the entire PTS volume, which is determined by the *cumulative* sound exposure from multiple strikes at a fixed position. The PTS volume therefore increases indefinitely with the number of strikes and ultimately exceeds the behavior volume once the number of strikes is large enough for $L_{E,\mathrm{w},24\mathrm{h}}$ to exceed the PTS threshold at the behavior range.

For the behavioral thresholds, the largest to smallest impact volumes ranked from RIsland winter to RIsland summer, VAbeach winter, and VAbeach summer, as occurred for the PTS and TTS (**Figure 6-28**).

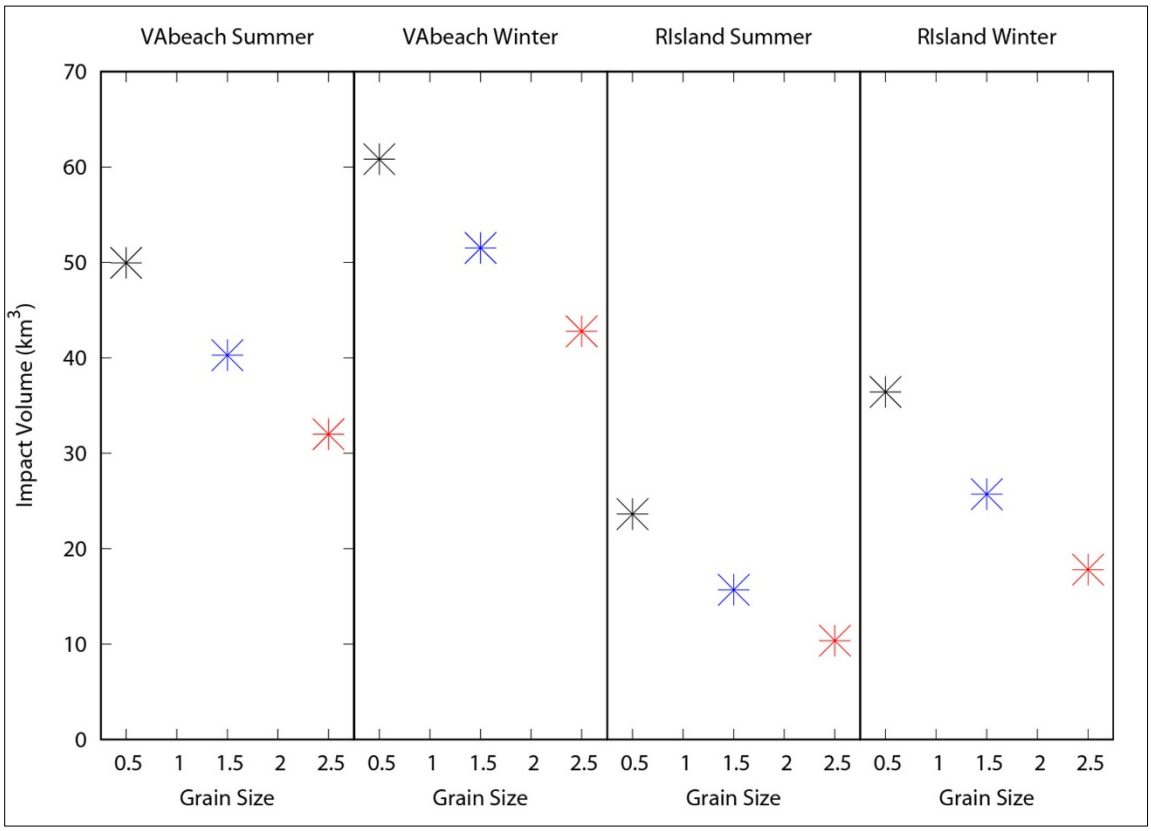

Figure 6-28. Environmental influence on impact volumes for cetacean behavioral, unweighted $L_{p,\mathrm{rms}}$.

The $L_{p,rms}$ behavioral threshold = 160 dB re 1 µPa and provided basis for impact volumes. Panels left to right: VAbeach summer, VAbeach winter, RIsland summer, and RIsland winter by grain size, 0.5 (black), 1.5 (blue), and 2.5 **ϕ** (red). µPa = micropascal; **ϕ** = grain size; dB = decibel; km^3 = cubic kilometer; $L_{p,\mathrm{rms}}$ = root-mean-square sound pressure level; re = with reference to; RIsland = Rhode Island site; VAbeach = Virginia Beach site.

6.3.3 Impact Volumes for Fishes and Sea Turtles

6.3.3.1 Impulsive Signals, Recoverable Injury, $L_{E,\#960}$ for Fishes

The L_E recoverable injury impact volumes for fish groups are shown in **Table 6-6** and **Figure 6-29**. The assumed number of strikes in a 24-hour period being 3,500 strikes also was applied for fishes. The threshold for 3,500 strikes is assumed to be the same as for 960 strikes, on which the criteria are based ($L_{E,\#960}$). This is a precautionary approach because the cumulative L_E injury threshold is known to increase when the energy is spread over a greater number of strikes (Halvorsen et al., 2011, 2012a,b; Casper et al., 2017). The median impact volume for recoverable injury calculated in this way varied from 0.06 to 3.2 km^3 for VAbeach, and from 0.04 to 1.8 km^3 for RIsland. The largest was 3.7 km^3, for VAbeach in winter, with coarse sand.

Table 6-6. Fish recoverable Injury $L_{E,\#960}$ impact volumes.

Fishes Recoverable Injury ($L_{E,\#960}$)					
Thresholds[a] (dB re 1 µPa^2 s)			>216	203	203
Site	**Season**	**Grain size (ϕ)**	**Without swim bladder (km^3)**	**With swim bladder not involved in hearing (km^3)**	**With swim bladder involved in hearing (km^3)**
VAbeach	Summer	0.5	0.0579	3.28	3.28
VAbeach	Summer	1.5	0.0535	2.81	2.81
VAbeach	Summer	2.5	0.0458	2.33	2.33
VAbeach	Winter	0.5	0.0600	3.73	3.73
VAbeach	Winter	1.5	0.0569	3.22	3.22
VAbeach	Winter	2.5	0.0521	2.74	2.74
RIsland	Summer	0.5	0.0437	2.00	2.00
RIsland	Summer	1.5	0.0394	1.59	1.59
RIsland	Summer	2.5	0.0365	1.22	1.22
RIsland	Winter	0.5	0.0438	2.25	2.25
RIsland	Winter	1.5	0.0402	1.80	1.80
RIsland	Winter	2.5	0.0379	1.41	1.41
VAbeach	mean	--	0.0544	3.02	3.02
VAbeach	Median	--	0.0569	3.22	3.22
VAbeach	Std. Dev.	--	0.0047	0.45	0.45
RIsland	Mean	--	0.0402	1.71	1.71
RIsland	Median	--	0.0402	1.80	1.80
RIsland	Std. Dev.	--	0.0027	0.35	0.35

-- = not applicable; µPa = micropascal; dB = decibel; km = kilometer; SEL#960 = $L_{E,\#960}$ = 960-strike sound exposure level; re = with reference to; RIsland = Rhode Island site; s = second; Std. Dev. = standard deviation; VAbeach = Virginia Beach site. Volumes defined as: green = <0.032 km^3, yellow = 0.032 to 0.32 km^3; orange = 0.32 to 3.2 km^3; red = 3.2 to 32 km^3; purple = >32 km^3 a - Popper et al. (2014).

A comparison of the impact volumes over each environmental parameter of site, season, and sediment grain size are shown in **Figure 6-29**. There was a factor of 4 spread between the lowest and highest impact volume based on site, season, and sediment type.

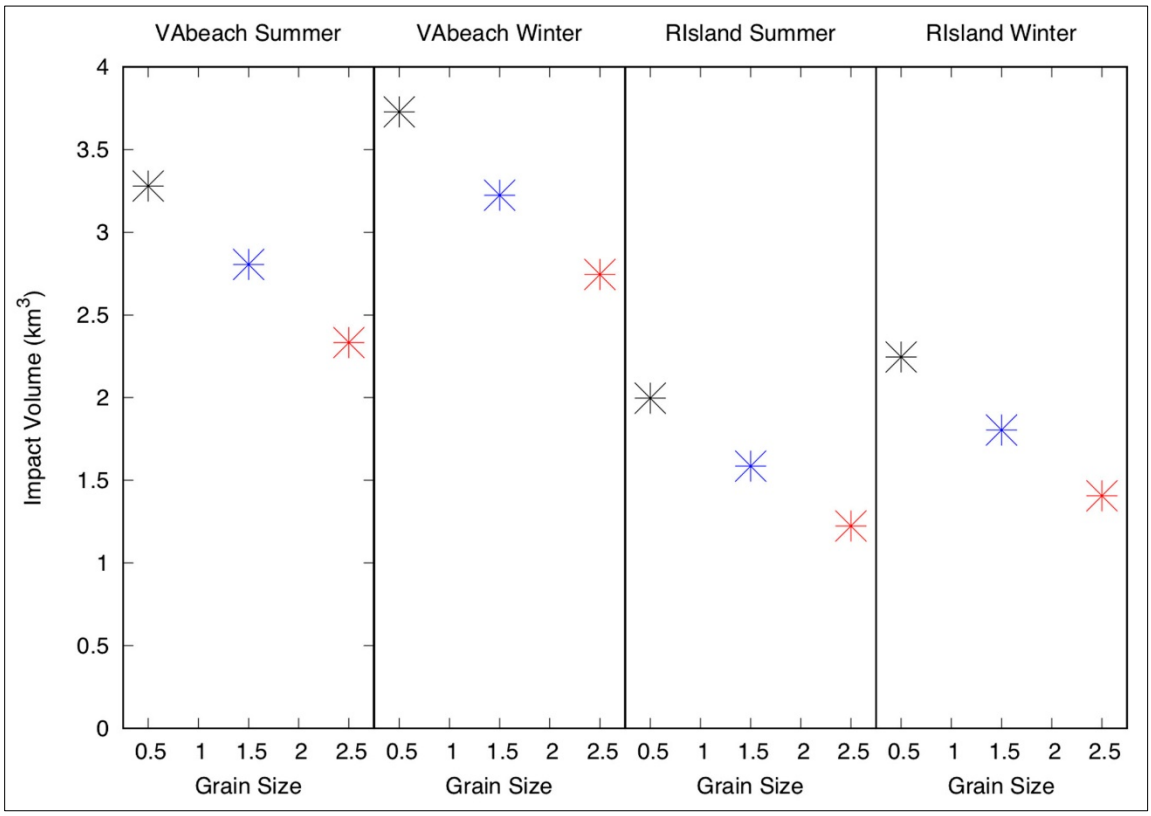

Figure 6-29. Environmental influence on impact volumes for fish with swim bladder, recoverable injury, unweighted 960-strike SEL ($SEL_{\#960}$).

The $L_{E,\#960}$ = $SEL_{\#960}$ recoverable injury thresholds are 203 and 216 dB re 1 µPa^2 s, and provided basis for impact volumes, which are based on 3,500 strikes in 24 hours. µPa = micropascal; **ϕ** = grain size; dB = decibel; km^3 = cubic kilometer; re = with reference to; RIsland = Rhode Island site; s = second; VAbeach = Virginia Beach site.

6.3.3.2 Impulsive Signals, Recoverable Injury, $L_{p,\mathrm{pk}}$ for Fishes

The $L_{p,\mathrm{pk}}$ recoverable injury impact volumes for fish groups are shown in **Table 6-7**. The volumes in **Table 6-7** are smaller than those in **Table 6-6** and therefore not color-coded.

Table 6-7. Fish recoverable injury $L_{p,\mathrm{pk}}$ impact volumes.

Fishes Recoverable Injury ($L_{p,\mathrm{pk}}$)					
Thresholds[a] (dB re 1 µPa)			>213	>207	>207
Site	**Season**	**Grain size (ϕ)**	**Without swim bladder (km^3)**	**With swim bladder not involved in hearing (km^3)**	**With swim bladder involved in hearing (km^3)**
VAbeach	Summer	0.5	0.00146	0.0133	0.0133
VAbeach	Summer	1.5	0.00142	0.0128	0.0128
VAbeach	Summer	2.5	0.00134	0.0122	0.0122
VAbeach	Winter	0.5	0.00134	0.0118	0.0118
VAbeach	Winter	1.5	0.00128	0.0119	0.0119
VAbeach	Winter	2.5	0.00132	0.0113	0.0113
RIsland	Summer	0.5	0.00155	0.0113	0.0113
RIsland	Summer	1.5	0.00142	0.0096	0.0097
RIsland	Summer	2.5	0.00125	0.0079	0.0079
RIsland	Winter	0.5	0.00146	0.0123	0.0124
RIsland	Winter	1.5	0.00136	0.0108	0.0108
RIsland	Winter	2.5	0.00116	0.0087	0.0088
VAbeach	Mean	--	0.00136	0.0122	0.0122
VAbeach	Median	--	0.00134	0.0121	0.0121
VAbeach	Std. Dev.	--	0.00006	0.0006	0.0007
RIsland	Mean	--	0.00137	0.0101	0.0101
RIsland	Median	--	0.00142	0.0108	0.0108
RIsland	Std. Dev.	--	0.00013	0.0015	0.0015

-- = not applicable; µPa = micropascal; dB = decibel; km = kilometer; $L_{p,\mathrm{pk}}$= peak sound pressure level; re = with reference to; RIsland = Rhode Island site; Std. Dev. = standard deviation; VAbeach = Virginia Beach site.
a - Popper et al. (2014).

6.3.3.3 Impulsive Signals, TTS, $L_{E,\#5}$ for Fishes

The L_E TTS impact volumes for fish groups are shown in **Table 6-8**. Here, the threshold for 3,500 strikes is assumed to be the same as for 5 strikes, on which the criteria are based. For fishes without a swim bladder, the TTS volumes would be much smaller because their threshold is "much greater" than 186 dB re 1 μPa^2 s (>>186). Therefore, the color-coding should be carefully considered as it incorrectly suggests that the impact volumes are just as large as for the other two columns of fishes with swim bladders.

Table 6-8. Fish TTS $L_{E,\#5}$ impact volumes.

Fishes TTS ($L_{E,\#5}$)					
Thresholds[a] (dB re 1 µPa^2 s)			>>186	>186	186
Site	**Season**	**Grain size (ϕ)**	**Without swim bladder (km^3)**	**With swim bladder not involved in hearing (km^3)**	**With swim bladder involved in hearing (km^3)**
VAbeach	Summer	0.5	88.5	88.5	88.5
VAbeach	Summer	1.5	65.1	65.1	65.1
VAbeach	Summer	2.5	47.4	47.4	47.4
VAbeach	Winter	0.5	126.7	126.7	126.7
VAbeach	Winter	1.5	96.7	96.7	96.7
VAbeach	Winter	2.5	71.2	71.2	71.2
RIsland	Summer	0.5	45.4	45.4	45.4
RIsland	Summer	1.5	30.6	30.6	30.6
RIsland	Summer	2.5	19.6	19.6	19.6
RIsland	Winter	0.5	73.5	73.5	73.5
RIsland	Winter	1.5	52.7	52.7	52.7
RIsland	Winter	2.5	36.8	36.8	36.8
VAbeach	Mean	--	82.6	82.6	82.6
VAbeach	Median	--	88.5	88.5	88.5
VAbeach	Std. Dev.	--	25.3	25.3	25.3
RIsland	Mean	--	43.1	43.1	43.1
RIsland	Median	--	45.4	45.4	45.4
RIsland	Std. Dev.	--	17.2	17.2	17.2

-- = not applicable; µPa = micropascal; dB = decibel; km = kilometer; SEL#5 = $L_{E,\#5}$ = 5-strike sound exposure level; re = with reference to; RIsland = Rhode Island site; s= second; Std. Dev. = standard deviation; TTS = temporary threshold shift; VAbeach = Virginia Beach site.
Volumes defined as: green = <0.032 km^3, yellow = 0.032 to 0.32 km^3; orange = 0.32 to 3.2 km^3; red = 3.2 to 32 km^3; purple = >32 km^3 a - Popper et al. (2014).

For fishes, the influence on the 5-strike L_E ($L_{E,\#5}$) TTS impact volumes were compared over the environmental parameters of site, season, and sediment grain size (**Figure 6-30**).

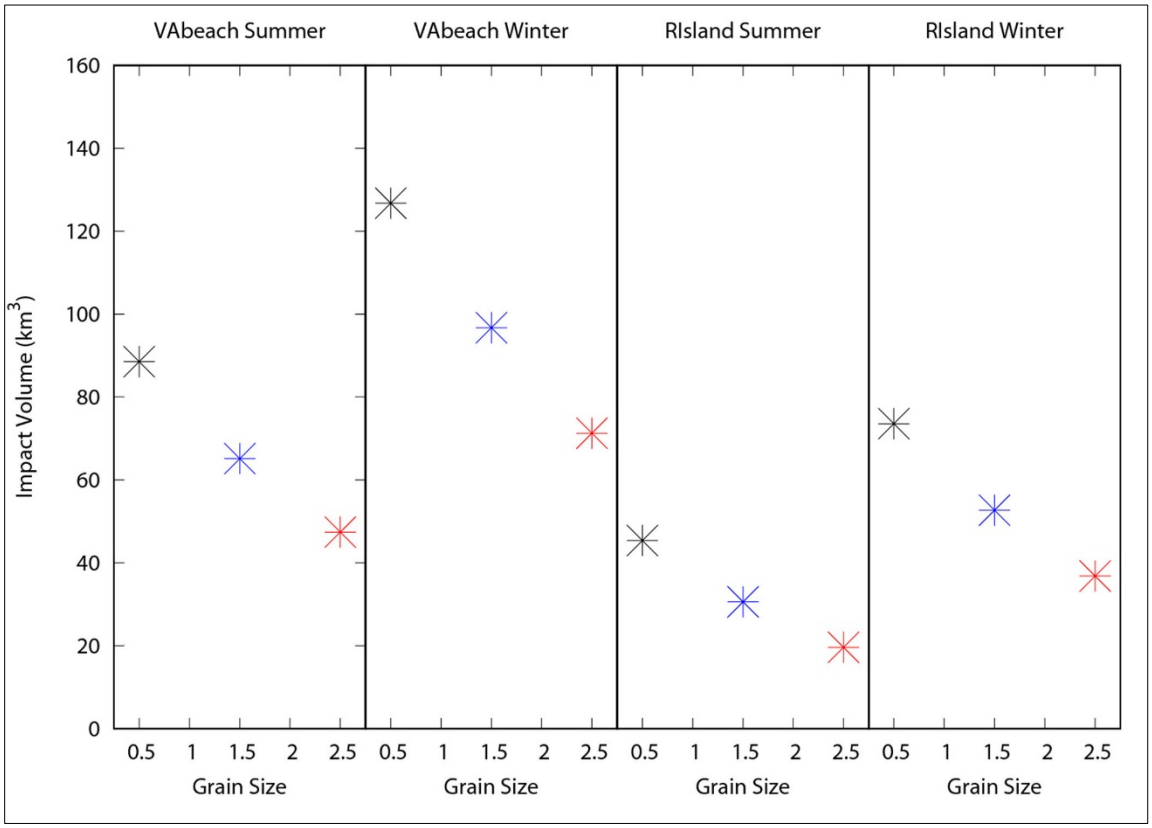

Figure 6-30. Environmental influence on impact volumes for fishes with swim bladder, unweighted 5-strike SEL (SEL$_{\#5}$) TTS.

The $L_{E,\#5}$ = SEL$_{\#5}$ TTS threshold is 186 dB re 1 µPa^2 s based on 5 strikes and provided basis for impact volumes. µPa = micropascal; **ϕ** = grain size; dB = decibel; km^3 = cubic kilometer; re = with reference to; RIsland = Rhode Island site; s = second; TTS = temporary threshold shift; VAbeach = Virginia Beach site.

6.3.3.4 Impulsive Signals, Injury, SEL$_{12h}$ for Fishes

The 12-hour L_E($L_{E,12h}$) injury impact volumes for small and large fish (Stadler and Woodbury, 2009; GARFO, 2016) are shown in **Table 6-9** and **Figure 6-31**. The median impact volume for injury calculated in this way varied from 76 to 130 km^3 for VAbeach, and from 40 to 63 km^3 for RIsland. Compared with the corresponding medians calculated for the Popper et al. (2014) criteria (**Table 6-9** versus **Table 6-6** and **Figure 6-31** versus **Figure 6**-29), on average the impact volumes of **Table 6-9** were 30x and 1,600x larger than those of **Table 6-6** for fishes with and without a swim bladder, respectively.

Table 6-9. Fish injury $L_{E,12h}$ impact volumes.

Fishes, Injury ($L_{E,12h}$)				
Thresholds[a,b] (dB re 1 µPa² s)			183	187
Site	**Season**	**Grain size (ϕ)**	**Small fish; mass <2 grams (km³)**	**Large fish; mass >2 grams (km³)**
VAbeach	Summer	0.5	133.7	75.9
VAbeach	Summer	1.5	97.2	57.6
VAbeach	Summer	2.5	68.5	40.8
VAbeach	Winter	0.5	189.4	109.9
VAbeach	Winter	1.5	144.7	82.3
VAbeach	Winter	2.5	111.3	60.8
RIsland	Summer	0.5	63.1	40.1
RIsland	Summer	1.5	43.3	26.8
RIsland	Summer	2.5	28.4	17.2
RIsland	Winter	0.5	113.8	63.2
RIsland	Winter	1.5	80.2	45.8
RIsland	Winter	2.5	55.1	31.6
VAbeach	Mean	--	124.1	71.2
VAbeach	Median	--	133.7	75.9
VAbeach	Std. Dev.	--	38.2	21.8
RIsland	Mean	--	64.0	37.5
RIsland	Median	--	63.1	40.1
RIsland	Std. Dev.	--	27.4	14.7

-- = not applicable; µPa = micropascal; dB = decibel; km = kilometer; SEL_{12h}= $L_{E,12h}$ = 12-hour sound exposure level; re = with reference to; RIsland = Rhode Island site; s = second; Std. Dev. = standard deviation; VAbeach = Virginia Beach site.
Volumes defined as: green = <0.032 km³, yellow = 0.032 to 0.32 km³; orange = 0.32 to 3.2 km³; red = 3.2 to 32 km³; purple = >32 km³ a - Stadler and Woodbury (2009).
b - Greater Atlantic Regional Fisheries Office (2016).

For fishes, the $L_{E,12\mathrm{h}}$ impact volumes were compared over the environmental parameters of site, season, and sediment grain size in **Figure 6-31**. The volume sizes followed the same trends from largest to smallest as those calculated for the marine mammal groups.

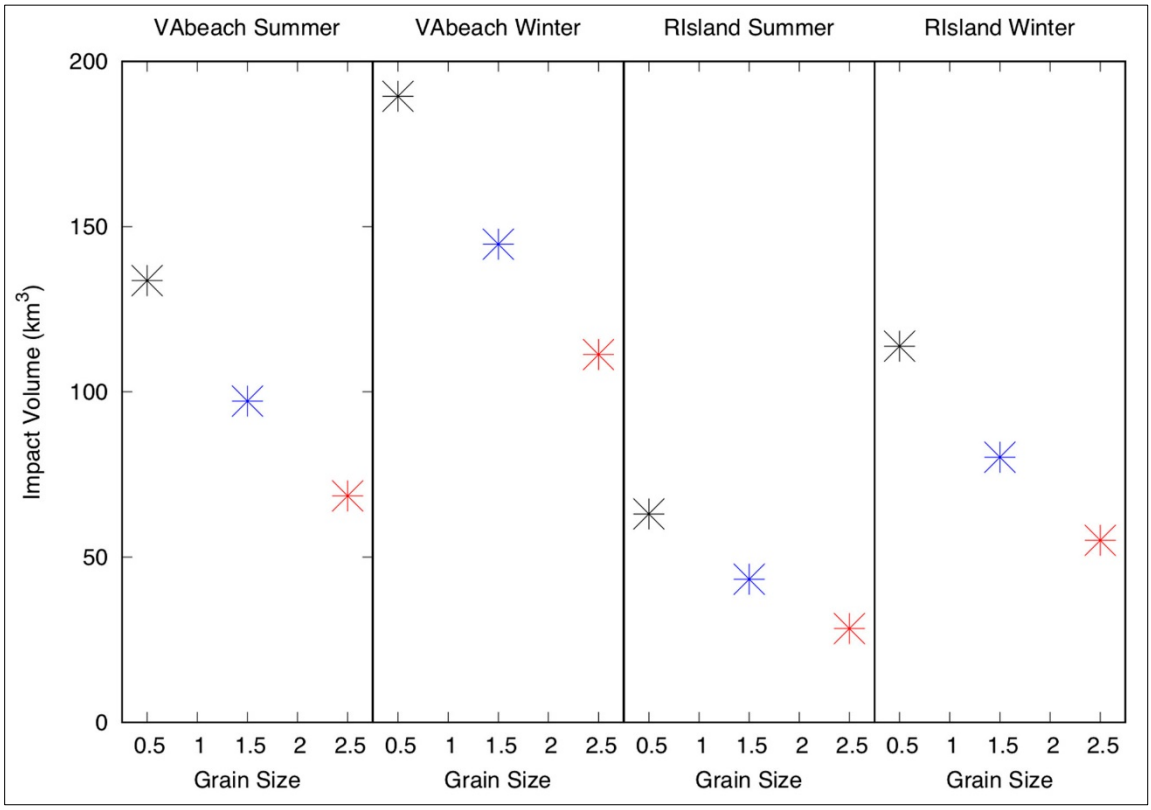

Figure 6-31. Environmental influence on impact volumes for small fishes unweighted 12-hour SEL (SEL_{12h}) injury.

The $L_{E,12\mathrm{h}}$ = SEL_{12h} injury threshold is 183 dB re 1 µPa^2 s for small fishes, and provided basis for impact volumes, which are calculated for 3,500 strikes in 24 hours. µPa = micropascal; **ϕ** = grain size; dB = decibel; km^3 = cubic kilometer; re = with reference to; RIsland = Rhode Island site; s = second; VAbeach = Virginia Beach site.

6.3.3.5 Impulsive Signals, Injury, $L_{p,\mathrm{pk}}$ for Fishes

The $L_{p,\mathrm{pk}}$ injury impact volumes for small (mass less than 2 grams) and large (mass greater than 2 grams) fishes are shown in **Table 6-10**. A comparison of the impact volumes for $L_{p,\mathrm{pk}}$ over site, season, and sediment grain size are shown in **Figure 6-32**. Because the volumes in **Table 6-10** are smaller than those from **Table 6-9**, when applying the criteria proposed by Stadler and Woodbury (2009), the $L_{p,\mathrm{pk}}$ volumes did not contribute to impact volume for injury in fishes at VAbeach or RIsland.

Table 6-10. Fish injury $L_{p,\mathrm{pk}}$ impact volumes.

Fishes, Injury ($L_{p,\mathrm{pk}}$)				
Thresholds[a] (dB re 1 µPa)			206	206
Site	**Season**	**Grain size (ϕ)**	**Small fish; mass <2 grams (km^3)**	**Large fish; mass >2 grams (km^3)**
VAbeach	Summer	0.5	0.0192	0.0192
VAbeach	Summer	1.5	0.0190	0.0190
VAbeach	Summer	2.5	0.0180	0.0180
VAbeach	Winter	0.5	0.0184	0.0184
VAbeach	Winter	1.5	0.0179	0.0179
VAbeach	Winter	2.5	0.0182	0.0182
RIsland	Summer	0.5	0.0158	0.0158
RIsland	Summer	1.5	0.0137	0.0137
RIsland	Summer	2.5	0.0113	0.0113
RIsland	Winter	0.5	0.0176	0.0176
RIsland	Winter	1.5	0.0153	0.0153
RIsland	Winter	2.5	0.0127	0.0127
VAbeach	Mean	--	0.01845	0.01845
VAbeach	Median	--	0.01836	0.01836
VAbeach	Std. Dev.	--	0.00048	0.00048
RIsland	Mean	--	0.01438	0.01438
RIsland	Median	--	0.01528	0.01528
RIsland	Std. Dev.	--	0.00206	0.00206

-- = not applicable; µPa = micropascal; dB = decibel; km = kilometer; $L_{p,\mathrm{pk}}$= peak sound pressure level; re = with reference to; RIsland = Rhode Island site; Std. Dev. = standard deviation; VAbeach = Virginia Beach site.
a - Stadler and Woodbury (2009).

The order of impact volumes for $L_{p,\mathrm{pk}}$ over site, season, and sediment grain size for small fish is the first to differ from the rest of the hearing groups, **Figure 6-32**. The impact volumes for these criteria show RIsland summer and winter sizes being very similar. This is because at the short ranges associated with crossing the $L_{p,\mathrm{pk}}$ thresholds, the difference in the propagation conditions is inconsequential. Both RIsland seasons are noticeably larger than both VAbeach seasons.

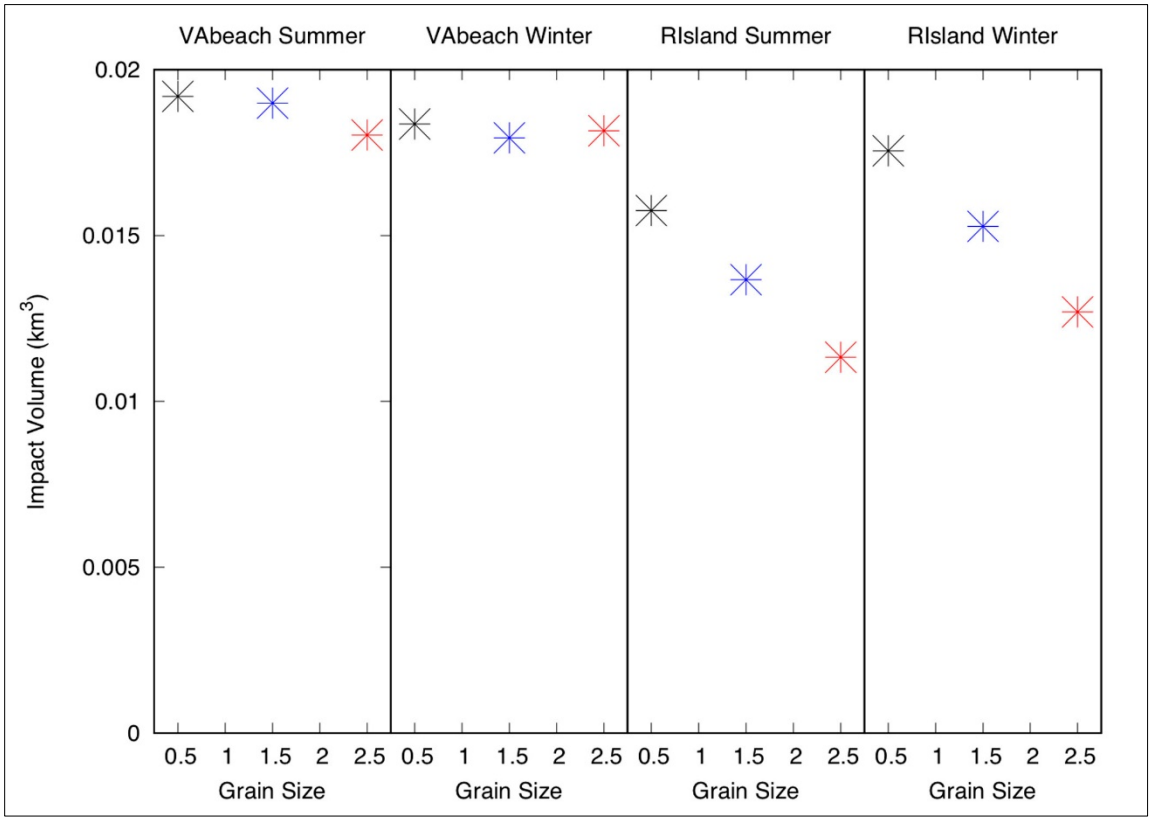

Figure 6-32. Environmental influence on impact volumes for small fish $L_{p,\mathrm{pk}}$ injury

The $L_{p,\mathrm{pk}}$ injury threshold is 206 dB re 1 µPa and provided basis for impact volumes. µPa = micropascal; **ϕ** = grain size; dB = decibel; km^3 = cubic kilometer; re = with reference to; RIsland = Rhode Island site; VAbeach = Virginia Beach site.

6.3.3.6 Impulsive signals, behavior, $L_{p,\mathrm{rms}}$ for Fishes

The $L_{p,\mathrm{rms}}$ behavioral impact volumes for small (mass less than 2 grams) and large (mass greater than 2 grams) fishes are shown in **Table 6-11**. A comparison of the impact volumes for $L_{p,\mathrm{rms}}$ over site, season, and sediment grain size are shown in **Figure 6-33**.

Table 6-11. Fish behavioral $L_{p,\mathrm{rms}}$ impact volumes.

Fishes, Behavior ($L_{p,\mathrm{rms}}$)				
Thresholds[a] (dB re 1 µPa)			150	150
Site	**Season**	**Grain size (ϕ)**	**Small fish; mass <2 grams (km^3)**	**Large fish; mass >2 grams (km^3)**
VAbeach	Summer	0.5	164.5	164.5
VAbeach	Summer	1.5	129.9	129.9
VAbeach	Summer	2.5	100.2	100.2
VAbeach	Winter	0.5	221.2	221.2
VAbeach	Winter	1.5	184.1	184.1
VAbeach	Winter	2.5	151.5	151.5
RIsland	Summer	0.5	72.8	72.8
RIsland	Summer	1.5	49.9	49.9
RIsland	Summer	2.5	33.0	33.0
RIsland	Winter	0.5	146.8	146.8
RIsland	Winter	1.5	108.7	108.7
RIsland	Winter	2.5	78.3	78.3
VAbeach	Mean	--	158.6	158.6
VAbeach	Median	--	164.5	164.5
VAbeach	Std. Dev.	--	38.5	38.5
RIsland	Mean	--	81.6	81.6
RIsland	Median	--	78.3	78.3
RIsland	Std. Dev.	--	37.5	37.5

-- = not applicable; µPa = micropascal; dB = decibel; km = kilometer; $L_{p,\mathrm{rms}}$= root-mean-square sound pressure level; re = with reference to; RIsland = Rhode Island site; Std. Dev. = standard deviation; VAbeach = Virginia Beach site.
Volumes defined as: green = <0.032 km^3, yellow = 0.032 to 0.32 km^3; orange = 0.32 to 3.2 km^3; red = 3.2 to 32 km^3; purple = >32 km^3 a - Greater Atlantic Regional Fisheries Office (2016).

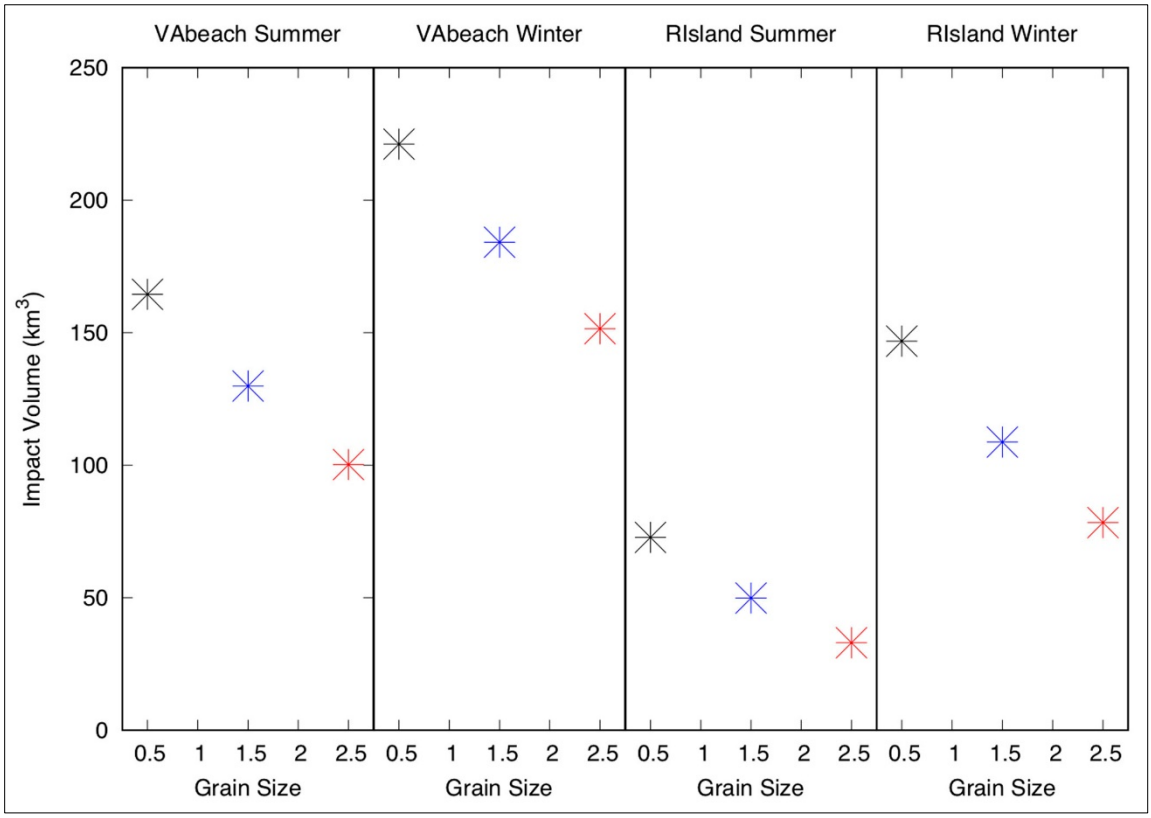

Figure 6-33. Environmental influence on impact volumes for small fish unweighted $L_{p,\mathrm{rms}}$ behavioral.

The $L_{p,\mathrm{rms}}$ behavioral threshold is 150 dB re 1 µPa and provided basis for impact volumes. µPa = micropascal; **ϕ** = grain size; dB = decibel; km^3 = cubic kilometer; re = with reference to; RIsland = Rhode Island site; VAbeach = Virginia Beach site.

6.3.3.7 Impulsive Signals, Mortal Injury, Physiological, and Behavior Volumes for Sea Turtles

The impact volumes for sea turtles based on various single-strike metrics are shown in **Table 6-12**, following the four acoustic criteria categories put forth by Popper et al. (2014) and GARFO (2016). The volumes in the $L_{p,\mathrm{pk}}$ column are smaller than those in the $L_{E,12\mathrm{h}}$ column and therefore not color-coded.

Table 6-12. Sea turtle mortal injury $L_{E,12h}$, physiological $L_{p,pk}$, and behavioral $L_{p,rms}$ impact volumes.

Sea turtles, Multiple metrics						
Thresholds (mixed metrics)			210[a]	>207[a]	180[b]	166[b]
Site	**Season**	**Grain size (ϕ)**	**Mortal Injury $L_{E,12h}$ (dB re 1 µPa² s, unweighted) (km³)**	**Mortal Injury $L_{p,pk}$ (dB re 1 µPa, unweighted) (km³)**	**Physiological $L_{p,rms}$ (dB re 1 µPa, unweighted) (km³)**	**Behavior $L_{p,rms}$ (dB re 1 µPa unweighted) (km³)**
VAbeach	Summer	0.5	5.41	0.0133	1.369	21.14
VAbeach	Summer	1.5	4.73	0.0129	1.248	17.90
VAbeach	Summer	2.5	4.08	0.0122	1.152	14.93
VAbeach	Winter	0.5	6.27	0.0118	1.572	25.03
VAbeach	Winter	1.5	5.54	0.0119	1.459	21.39
VAbeach	Winter	2.5	4.85	0.0113	1.365	18.15
RIsland	Summer	0.5	2.26	0.0113	0.744	9.55
RIsland	Summer	1.5	1.62	0.0097	0.625	6.65
RIsland	Summer	2.5	1.07	0.0079	0.528	4.35
RIsland	Winter	0.5	2.61	0.0124	0.807	12.82
RIsland	Winter	1.5	2.01	0.0108	0.666	9.07
RIsland	Winter	2.5	1.39	0.0088	0.556	6.36
VAbeach	Mean	--	5.15	0.0122	1.36	19.76
VAbeach	Median	--	5.41	0.0122	1.37	21.14
VAbeach	Std. Dev.	--	0.69	0.0007	0.14	3.21
RIsland	Mean	--	1.82	0.0101	0.65	8.13
RIsland	Median	--	2.01	0.0108	0.67	9.07
RIsland	Std. Dev.	--	0.52	0.0015	0.10	2.72

-- = not applicable; µPa = micropascal; dB = decibel; km = kilometer; $L_{p,pk}$= peak sound pressure level; $L_{p,rms}$= root-mean-square sound pressure level; PTS = permanent threshold shift; SEL_{12h} = $L_{E,12h}$ = 12-hour sound exposure level; re = with reference to; RIsland = Rhode Island site; s = second; Std. Dev. = standard deviation; VAbeach = Virginia Beach site. Volumes defined as: green = <0.032 km³, yellow = 0.032 to 0.32 km³; orange = 0.32 to 3.2 km³; red = 3.2 to 32 km³; purple = >32 km³ a - Popper et al. (2014).
b - Greater Atlantic Regional Fisheries Office (2016).

The $L_{p,rms}$ behavioral impact volumes for a single strike over the environmental parameters of site, season, and sediment grain size are compared in **Figure 6-34**.

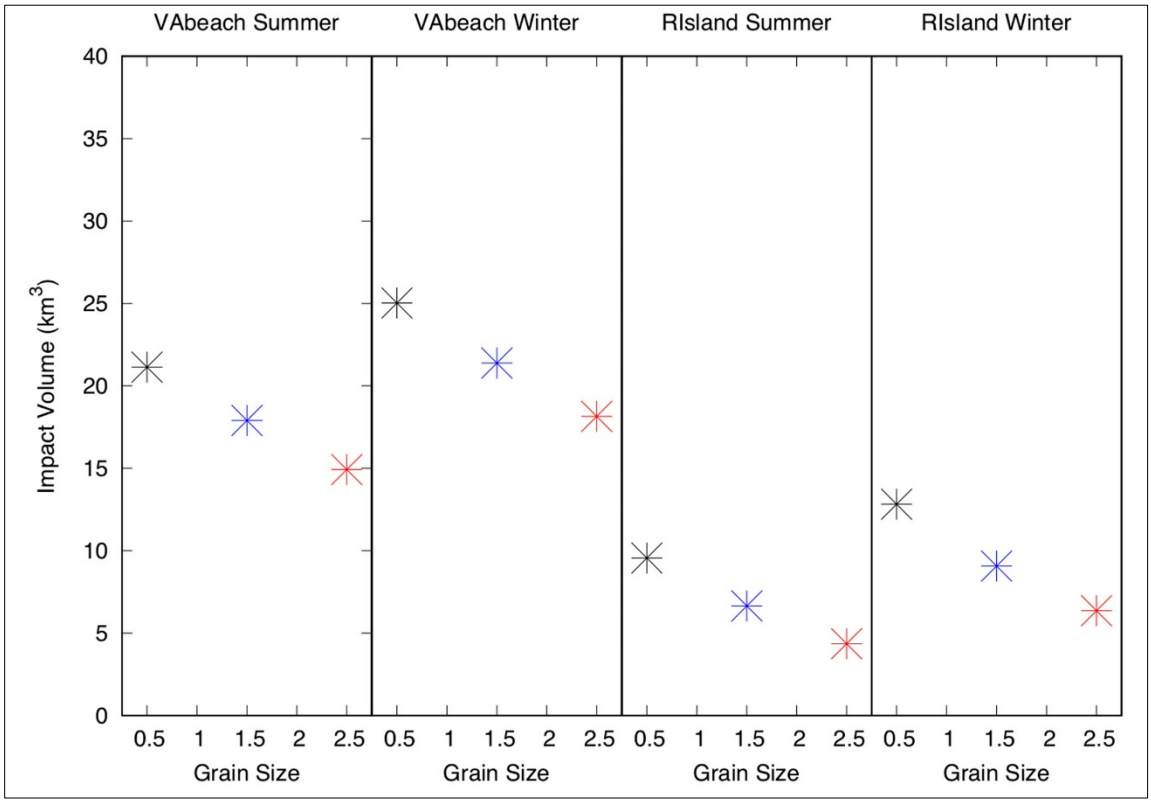

Figure 6-34. Environmental influence on impact volumes for sea turtles unweighted $L_{p,\mathrm{rms}}$ behavioral.

The $L_{p,\mathrm{rms}}$ behavioral threshold is 166 dB re 1 µPa and provided basis for impact volumes. µPa = micropascal; **ϕ** = grain size; dB = decibel; km^3 = cubic kilometer; re = with reference to; RIsland = Rhode Island site; VAbeach = Virginia Beach site.

6.3.4 Impact Versus Vibratory Piles

The primary focus of this work was the impact pile, which has an impact strike at the top of the pile and transmits a traveling pressure wave into the pile. This wave travels back and forth along the pile several times, each pass radiating into the water column. Much of this radiated energy goes into the Mach cone, which enters the water at an angle determined by the ratio of the sound speed in the metal pile and the sound speed in the water. Signals from impact pile driving were treated as impulsive, regardless of the distance from the source. The time spread for all signals and all sites is on the order of 2 seconds or less, even for ranges of 60 km. This means that a pile struck every 3 seconds or more will be received as a discrete pulse of energy.

For a vibratory pile, no hammer directly hits the top of a pile and there is no coherent traveling wave down the pile. It is this coherent acoustic structure of the impact strike on a pile that leads to bands of energy at specific angles that radiate into the seafloor, as evidenced in **Figure 6-35**. To model the vibratory pile, the same acoustic field generated 5 m from the pile was used in the FE model, but the phases of each frequency and depth component were randomized. The randomization of the phases

destroys the coherent nature of the propagating wave but maintains the physics of the sound in the pile and the water. No publicly available measured data were available to compare the vibratory pile with the impact pile, so it was assumed they have the same L_E (pressure squared) at each depth and frequency. This is a considerable assumption, based on the requirement that the same amount of work must be done to insert a pile into the seafloor whether by hitting it or shaking it. Note that when computing L_E, the integration time has not been specified.

A comparison of the decidecade band (band index 3: 1,778.279 to 2,238.721 Hz) L_E for the impact and vibratory pile at RIsland during winter is shown in **Figure 6-35**. The coherent energy from the Mach cone is clearly visible in the upper panel, and it radiates out to nearly 2 km. The vibratory pile has no such coherent wave, and in fact has energy entering the water column at all vertical angles. The energy leaving the pile at short range (total L_E for an integration time of 1 second, and at 3 m range from the pile axis) is the same for both models. The impact pile (top panel) shows the coherent multi-path resulting from the sound traveling from the impact through the pile into the water. This energy interacts with the seafloor and surface repeatedly to 2 km. For the vibratory pile, this coherent field is eliminated and the sound enters the water column at all angles, including much higher ones that are rapidly attenuated.

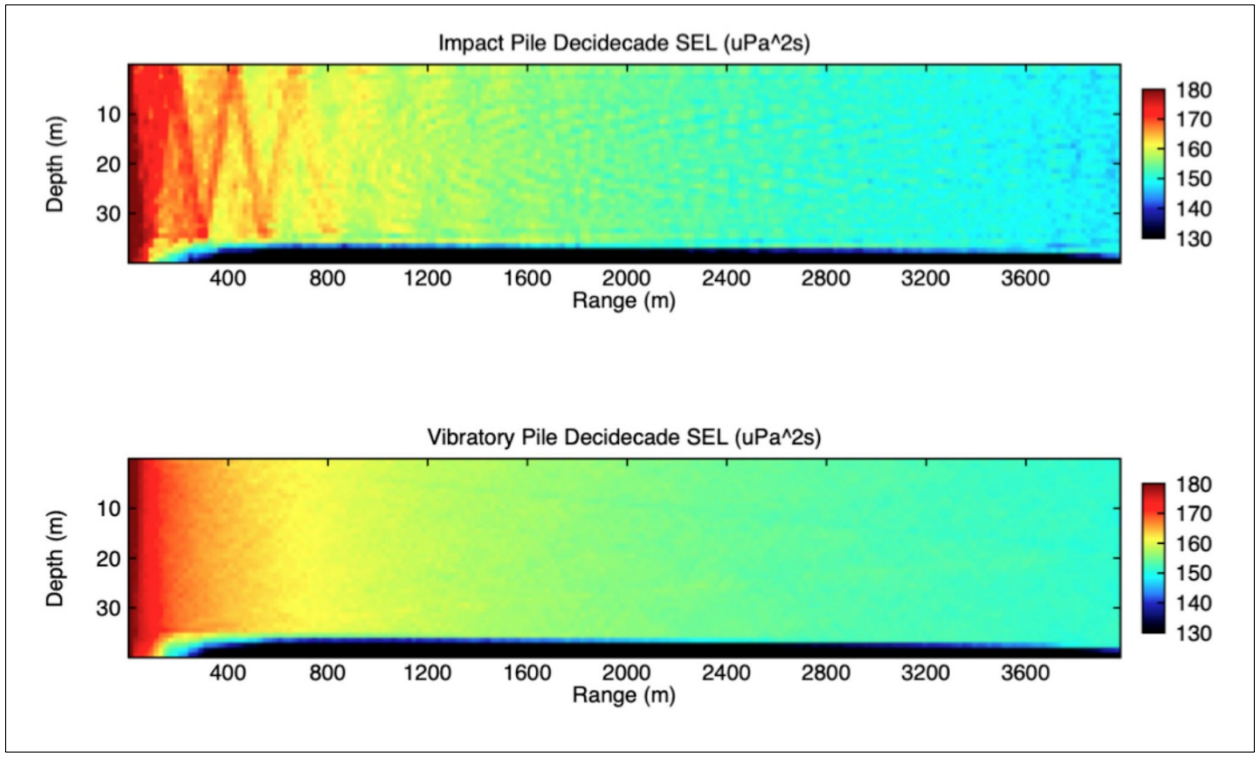

Figure 6-35. Modeled impact (top) and vibratory (bottom) pile comparison.
The piles were modeled in the decidecade band (band index 3: 1778 to 2239 Hz) for unweighted, single-strike sound exposure level ($L_{E,ss}$) at RIsland during winter. The $L_{E,ss}$ is in dB re 1 µPa^2 s. µPa = micropascal; dB = decibel; m = meter; re = with reference to; RIsland = Rhode Island site; s = second.

The unweighted, depth-averaged $L_{E,ss}$ was computed for the impact and vibratory piles for RIsland north (0°) and east (90°), shown in **Figures 6-36** and **6-37**, respectively.

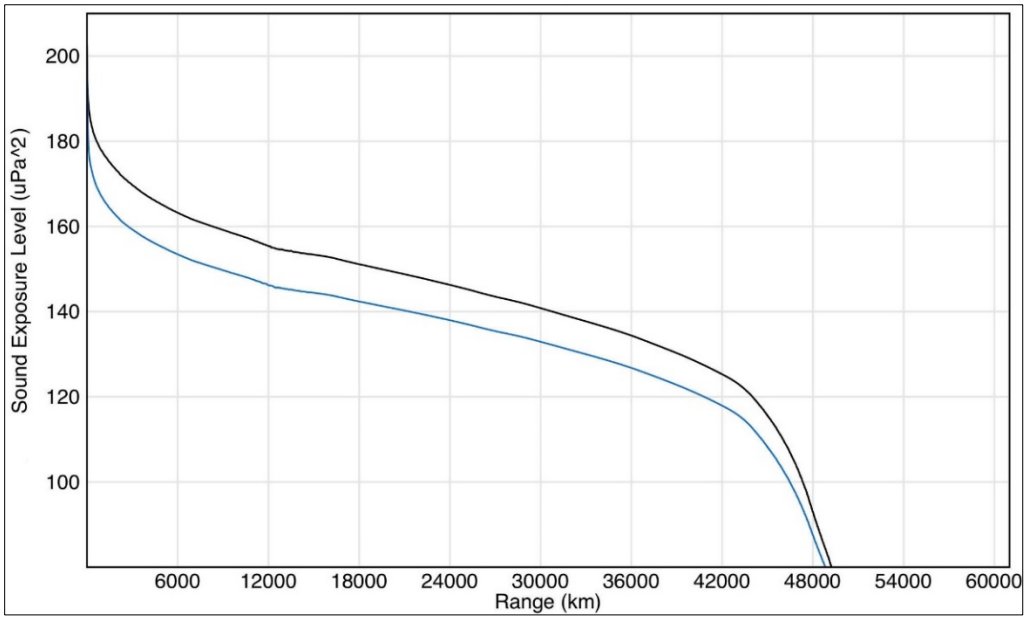

Figure 6-36. Modeled impact (black) and vibratory (blue) pile comparison of unweighted, single strike SEL, bearing north.

The piles were modeled in the decidecade band (band index 3: 1,778 to 2,239 Hz) for SEL_{ss} at RIsland during summer, bearing north (0°). The $L_{E,ss}$ = SEL_{ss} is in dB re 1 μPa^2 s. The sound exposure was integrated over a time duration of 1 second. µPa = micropascal; dB = decibel; km = kilometer; re = with reference to; RIsland = Rhode Island site; s = second.

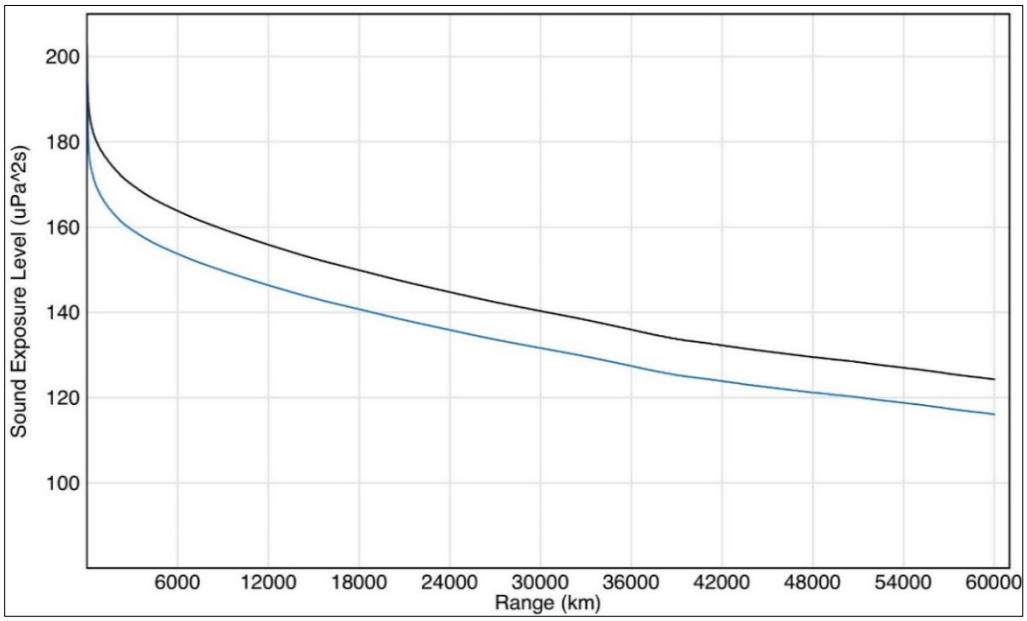

Figure 6-37. Modeled impact (black) and vibratory (blue) pile comparison of unweighted, single strike SEL bearing east.

The piles were modeled in the decidecade band (band index 3: 1,778 to 2,239 Hz) for $L_{E,ss}$ = SEL_{ss} at RIsland during summer, bearing east (90°). The SEL_{ss} is in dB re 1 μPa^2 s. The sound exposure was integrated over a time duration of 1 second. µPa = micropascal; dB = decibel; km = kilometer; re = with reference to; RIsland = Rhode Island site; s = second.

The unweighted, depth-averaged $L_{p,\mathrm{pk}}$ was computed for the impact and vibratory piles for RIsland north (0°) and east (90°), shown in **Figures 6-38** and **6-39**, respectively.

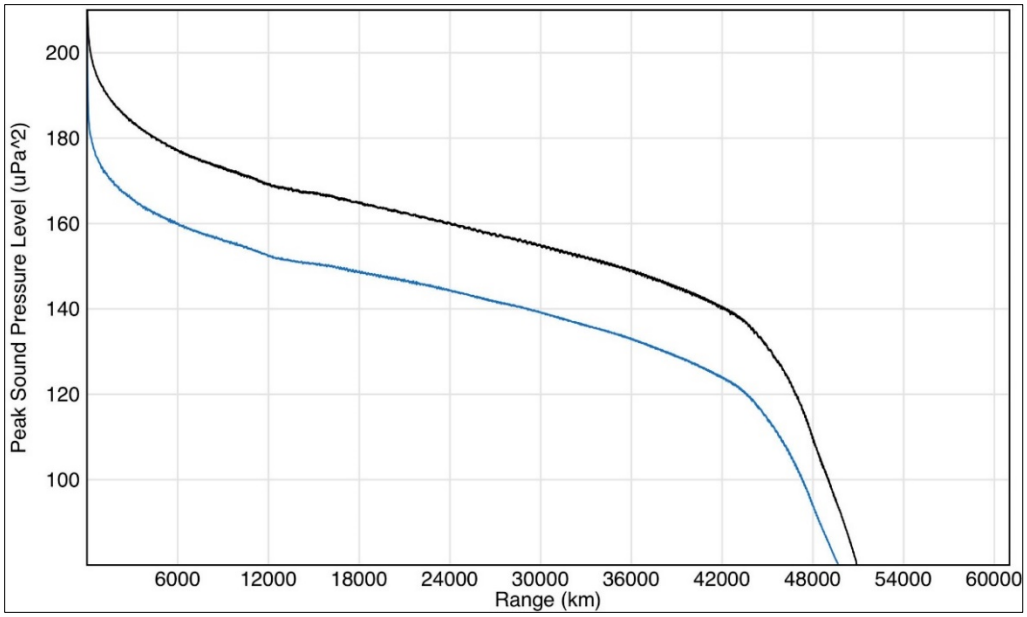

Figure 6-38. Modeled impact (black) and vibratory (blue) pile comparison of $L_{p,\mathrm{pk}}$, bearing north.
The piles were modeled in the decidecade band (band index 3: 1,778 to 2,239 Hz) for $L_{p,\mathrm{pk}}$ at RIsland during summer, bearing north (0°) where the seafloor shallows at 48 km. The $L_{p,\mathrm{pk}}$ is in dB re 1 µPa^2 s. µPa = micropascal; dB = decibel; km = kilometer; re = with reference to; RIsland = Rhode Island site; s = second.

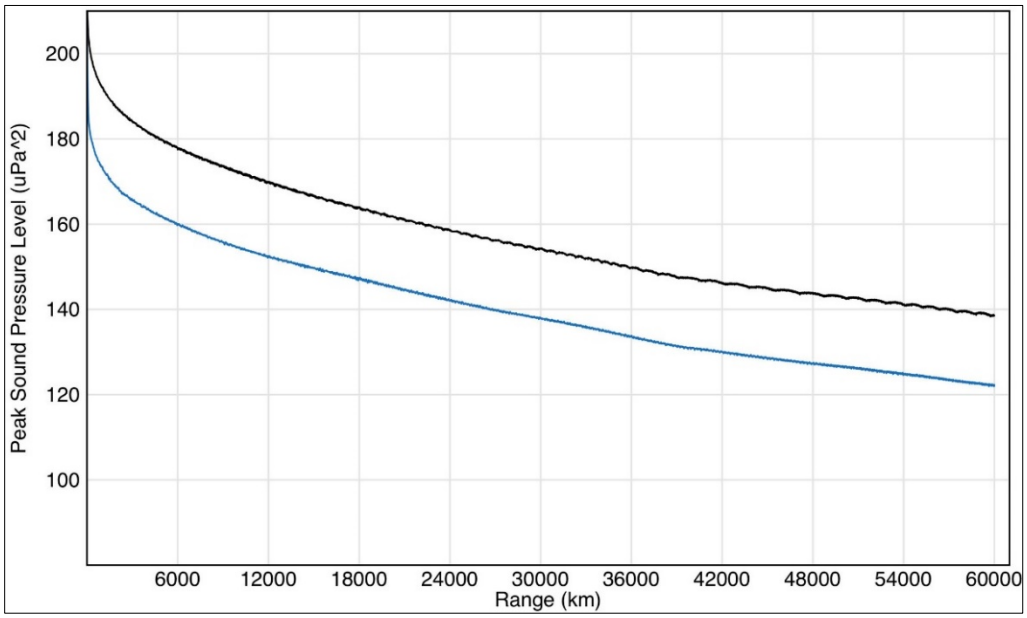

Figure 6-39. Modeled impact (black) and vibratory (blue) pile comparison of $L_{p,\mathrm{pk}}$, bearing east.
The piles were modeled in the decidecade band (band index 3: 1,778 to 2,239 Hz) for $L_{p,\mathrm{pk}}$ at RIsland during summer, bearing east (90°). The $L_{E,ss}$ = SEL$_{ss}$ is in dB re 1 µPa^2 s. µPa = micropascal; dB = decibel; km = kilometer; re = with reference to; RIsland = Rhode Island site; s = second.

6.4 Sensitivity Study Conclusions

The validated FE/PE model was used to compute the sound pressure time series (and subsequent) L_E, $L_{p,\mathrm{pk}}$, and $L_{p,\mathrm{rms}}$ metrics. Model sensitivity to environmental parameters was evaluated across season (SSP), site, bearing (range-dependent bathymetry), and grain size (sediment type). To investigate the overall sensitivity of impact volumes from the environment, the impact volumes were computed based on acoustic criteria. The introduction of energy above 2 kHz leads to impact volumes exceeding those that might be expected from LF energy alone. Regardless of size, impact volumes at both sites varied noticeably with season, sediment type, and bathymetry. How the relative contributions of these parameters occur at any pile-driving site, therefore, is unknown and creates a need to model multiple sites individually. How much an impact volume was shaped like a circular cylinder versus an amoeboid depended greatly on proximity to shore and bathymetry.

As a proxy for water depth and oceanography, two sites off the U.S. Atlantic Coast, RIsland and VAbeach, were chosen for the modeling study. The environmental variable with the greatest impact on acoustic propagation, and therefore on impact volume, was the site and, more specifically, the bathymetry. RIsland was closer to land than VAbeach, leading to differences of 40 dB at ranges beyond 20 km due to variability in water depth. Changes in sediment type were the next largest influence on impact volume, particularly in summer when warm surface waters led to increased refraction towards the seafloor and thus more absorption of sound into the seafloor. The environmental driver with less impact was season (SSP), with better propagation in winter than in summer, which led to higher received levels at all ranges and, therefore, larger impact volumes in winter. The effect of modeling sea surface scattering, though outside the project scope, would have been to decrease the predicted impact volumes, especially for MF and HF cetaceans in the winter.

There was substantial variability in the impact volumes, varying for marine mammals between 0.0001 km^3 (PTS in MF cetaceans; **Table 6-1**) and 282 km^3 (TTS in LF cetaceans; **Table 6-3**). In fishes, based on GARFO (2016) the impact volumes varied between 17 km^3 (injury, large fish; **Table 6-9**) and 221 km^3 (behavior, any fish; **Table 6-11**). For comparison, application of the Popper et al. (2014) guidelines resulted in volumes between 0.04 km^3 (recoverable injury, fishes with no swim bladder; **Table 6-6**) and 127 km^3 (TTS, fishes with a swim bladder involved in hearing; **Table 6-8**). In sea turtles, the spread was between 0.5 km^3 (physiological; **Table 6-12**) and 25 km^3 (behavior; **Table 6-12**).

For fishes, the calculated median impact volumes for recoverable injury based on the criteria of Popper et al. (2014) varied from 0.06 to 3.2 km^3 for VAbeach, and from 0.04 to 1.8 km^3 for RIsland (**Table 6-6**). The calculated median impact volumes for injury based on the criteria of Stadler and Woodbury (2009) varied from 76 to 130 km^3 for VAbeach, and from 40 to 63 km^3 for RIsland (**Table 6-9**). On average the impact volumes of **Table 6-9** were 30x and 1,600x larger than those of **Table 6-6** for fishes with and without a swim bladder, respectively.

For marine mammals, fishes, and sea turtles, the largest impact volumes were predicted at VAbeach in winter with coarse sand (0.5 $\boldsymbol{\phi}$). Whereas, the smallest impact volumes were predicted at RIsland with fine sand (2.5 $\boldsymbol{\phi}$). For fishes and sea turtles, the smallest impact volumes always occurred in summer; for marine mammals the impact volumes in winter were slightly larger than during the summer at VAbeach (**Figures 6-22** to **6-24**).

The largest predicted impact volumes were for TTS in LF cetaceans (282 km^3; **Table 6-3**) and behavior in small or large fish 221 km^3; **Table 6-11**), both at VAbeach in summer with coarse sand (0.5 **ϕ**). For these impacts, the predicted impact volumes for summer and fine sand decrease by 33% to 55% at VAbeach and by 77% to 78% at RIsland relative to those for winter and coarse sand.

At RIsland, season and grain size each led, on average, to a 45% reduction separately and a 77% reduction when combined. In other words, for both LF cetacean TTS and fish behavior, predicted impact volumes at RIsland were more than four times larger for coarse sand in winter than for fine sand in summer. The impact volume for RIsland in summer with fine sand (i.e., changing site, season, and grain size) was just 33 km^3, only 12% of the impact volume relative to VAbeach in winter with coarse sand (**Table 6-3**).

At VAbeach, the trend was similar, but the percentage differences were consistently smaller. The combined reduction of predicted impact volume for fine sand in summer relative to coarse sand in winter was 33% for LF cetacean TTS and 55% for fish behavior. The effect of grain size only (12% and 32%) was larger than for season only (5% and 26%).

Propagation has been shown to vary across season and grain size, and the impact volumes for each animal group also showed variability. For example, when considering sensitivity of impact volume to grain size and season, TTS impact volumes for LF cetaceans had a standard deviation of 73 km^3 at RIsland (**Table 6-3**). Multiple factors create a variety of propagation differences at a single site, so it would constitute good practice to acoustically model each site separately, in lieu of assuming another pile-driving site accurately represents environmental influences of SSP, range-dependent bathymetry, and sediment types.

The sensitivity studies showed a constant and reasonable trend for both predicted acoustic propagation modeling and predicted impact volumes that matched the expected physics of the two study scenarios (RIsland and VAbeach) for the following ranges of critical acoustic parameters: 34 m and 24 m at the pile, respectively; winter and summer SSPs; and sediment grain size from coarse to fine sediment. This indicates the reliability of the algorithm for the entire range of parameter values considered, which is a realistic representation for the U.S. Atlantic Coast.

Most pile-driving sites are not expected to occur in water deeper than 50 m, but variation in sound propagation exists across water columns from 0 to 50 m deep. For identical propagation conditions, a change of 50% in water depth should change the impact volume by 50%. To avoid changes in impact volume exceeding 50%, new models would be needed for sites that are 50% deeper (or 33% shallower) than each other (i.e., 5, 7, 11, 16, 23, 34 or 50 m deep) (This sequence is similar to the Fibonacci sequence of …5, 8, 13, 21, 34, and 50.)

7 Overall Conclusions

This section summarizes the overall conclusions of this report. Specifically, conclusions for DCSiE (**Section 3**), the model verification and validation results (**Section 5**), and the sensitivity study (**Section 6**)

7.1 Damped Cylindrical Spreading in Excel

A recently developed DCS model permits extrapolation of acoustic metrics from L_E based on physical principles, leading to an improved understanding and prediction of the propagation mechanism in the first few kilometers from the pile. The form of TL in DCS is $10\log_{10}\frac{r}{r_1}$ dB + $\alpha(r - r_1)$, which performs well out to 5-6 km for the measurements and test scenarios available.

DCS enables estimation of L_E at ranges that satisfy $\alpha r < 20$ dB. For ranges that do not satisfy this inequality, the DCS model is expected to overestimate TL and underestimate L_E. Therefore, it remains necessary to supplement the DCS model with an alternative method at long ranges, where the field appears to follow a power law instead of an exponential decay. **Figure 3-5** suggests the possibility of extrapolating for $\alpha r > 20$ dB using the PSLM with F between 25 and 45 (based empirically), although caution is warranted and validation is needed for this untested approach. In **Section 3.5.1**, extrapolation using F = 25 was recommended as a precautionary approach.

While systematic validation of the empirical correlations for $L_{p,\mathrm{pk}}$ and $L_{p,\mathrm{rms}}$ to L_E is needed, extrapolation of L_E to estimates of $L_{p,\mathrm{pk}}$ and $L_{p,\mathrm{rms}}$ may be permitted. In this way, impact assessments involving the metrics L_E, $L_{p,\mathrm{pk}}$, and $L_{p,\mathrm{rms}}$ can be carried out based on a single measurement of L_E near the pile, without requiring measurements of $L_{p,\mathrm{pk}}$ or $L_{p,\mathrm{rms}}$.

Conversion from L_E to $L_{p,\mathrm{pk}}$ (and $L_{p,\mathrm{rms}}$) remains an empirical correlation and is limited to the range of parameters (water depth, sediment type, hammer energy, and pile diameter) considered during the regression analysis. Therefore, the approach described in this project is applicable, but the values are site specific. A validation of the recommended method at a suitable U.S. site, though outside this project's scope, is needed to test the accuracy of the predictions of L_E, $L_{p,\mathrm{pk}}$, and $L_{p,\mathrm{rms}}$. A validation study likely would lead to improved understanding of the observed correlations and the possibility of further improvement.

Finally, the concept of $L_{p,\mathrm{eff}}$ was introduced alongside $L_{p,90\%}$ as an alternative metric to represent $L_{p,\mathrm{rms}}$. Both $L_{p,\mathrm{eff}}$ and $L_{p,90\%}$ are measures of the $L_{p,\mathrm{rms}}$, but they are calculated in different ways. Using $L_{p,\mathrm{eff}}$ leads to stronger (more robust) correlations with L_E than does using $L_{p,90\%}$. Therefore, the $L_{p,\mathrm{eff}}$ metric is suggested as a supplement to $L_{p,90\%}$.

7.2 Model Verification and Validation Methods

7.2.1 Verification

To address the issue of sound radiation from pile driving, an FE model was used to generate the sound field close to the pile. This model handles the complexity of the hammer strike on a large solid object

penetrating the seafloor and the transfer function from the pile to the sea. This sound field was matched to a PE propagation model, and the pile signals were propagated out to distances of interest. Using this combination of models (FE/PE), the results from the COMPILE I workshop were successfully reproduced, which verified the approach used for this project.

7.2.2 Validation

When validating the combined FE/PE model prediction by comparing it to measurements from construction of the Gemini wind farm (ITAP, 2015b), differences were identified. To address these differences, a layered sediment was introduced. With sediment layering included, validation was carried out against two Gemini pile measurements: U8 and Z2. To get good agreement, a simple inversion for the seafloor was performed, and the sediment was determined to be a fine sand (0.0 **ϕ**), which is slightly softer than the 0.5 **ϕ** used as the softest sediment in the U.S. Atlantic continental shelf region for this study.

For U8, good agreement occurred at all frequencies above approximately 30 Hz. Frequencies lower than 30 Hz did not contribute substantially to the broadband L_E, even before frequency weighting. After weighting, they were negligible. The level of the model at 3 m from the pile axis was chosen to match the L_E U8 measurements at 732 m. The agreement between these predictions and the U8 measurements at ranges 7, 32, and 62 km was excellent at all frequencies.

For Z2, at 3 m from the pile axis of symmetry, the L_E spectrum was assumed to be the same as for U8. Under this assumption, the same LF (<30 Hz) discrepancies as with U8 were identified, but these were unimportant as they did not contribute substantially to the broadband L_E.

7.3 Sensitivity Study

The validated FE/PE model was used to compute the sound pressure time series (and subsequent) L_E, $L_{p,\mathrm{pk}}$, and $L_{p,\mathrm{rms}}$ metrics at two representative sites for pile driving along the U.S. Atlantic Coast. The model's sensitivity was evaluated across four environmental parameters: site (depth), season (SSP), sediment type (grain size), and bearing (range-dependent bathymetry). To investigate the overall sensitivity of impact volumes from the environment, the impact volumes were computed based on previously published acoustic criteria for PTS, TTS, and behavioral categories.

The environmental variable with the greatest impact on acoustic propagation, and thereby on impact volume, was site (water column depth), which inherently incorporated general bathymetry characteristics not completely represented in the bearing parameter. RIsland was 45% deeper than VAbeach but resulted in most impact volume differences exceeding 50%. Therefore, water depth is not the only explanatory variable for impact volume size because surrounding bathymetry and propagation conditions also play a role.

RIsland was closer to land than VAbeach, leading to differences of 40 dB at ranges beyond 20 km due largely to variability in water depth. Change in sediment type was the next largest influence on impact volume. The environmental driver with the least impact was season (SSP). Better propagation occurs in the winter than in the summer because warm surface waters lead to a refraction of the sound waves towards the seafloor where more absorption can occur, especially with softer sediments. In general,

higher received levels, and therefore larger impact volumes, occurred in colder waters over harder sediments. Including sea surface scattering in the model, though outside the project scope, would have caused a decrease in the predicted impact volumes, especially for MF and HF cetaceans in the winter.

For marine mammals, fishes, and sea turtles, the largest impact volumes always were predicted at VAbeach in winter with coarse sand (0.5 **ϕ**) except when values for 0.5 **ϕ** and 1.5 **ϕ** at VAbeach in the summer were slightly larger (**Figure 6-29**). The smallest impact volumes always were predicted at RIsland in summer with fine sand (2.5 **ϕ**).

There was substantial variability in the impact volumes, varying for marine mammals between 0.0001 km^3 (PTS in MF cetaceans; **Table 6-1**) and 282 km^3 (TTS in LF cetaceans; **Table 6-3**). This largest predicted impact volume (282 km^3) occurred at VAbeach in winter with coarse sand (0.5 **ϕ**). In fishes, the impact volumes varied between 17 km^3 (injury, large fish; **Table 6-9**) and 221 km^3 (behavior, any fish; **Table 6-11**) (GARFO, 2016). For comparison, application of the Popper et al. (2014) guidelines resulted in volumes between 0.04 km^3 (recoverable injury, fishes with no swim bladder; **Table 6-6**) and 127 km^3 (TTS, fishes with a swim bladder involved in hearing; **Table 6-8**). In sea turtles, the spread was between 0.5 km^3 (physiological; **Table 6-12**) and 25 km^3 (behavior; **Table 6-12**).

For fishes, the median impact volumes for recoverable injury calculated using the criteria of Popper et al. (2014) varied from 0.06 to 3.2 km^3 for VAbeach, and from 0.04 to 1.8 km^3 for RIsland (**Table 6-6**). The median impact volumes for injury calculated using the criteria of Stadler and Woodbury (2009) varied from 76 to 130 km^3 for VAbeach, and from 40 to 63 km^3 for RIsland (**Table 6-9**). On average the impact volumes of **Table 6-9** were 30x and 1,600x larger than those of **Table 6-6** for fishes with and without a swim bladder, respectively.

The largest predicted impact volumes were for TTS in LF cetaceans (282 km^3; **Table 6-3**) and behavior in small or large fish (221 km^3; **Table 6-11**), both at VAbeach in summer with coarse sand (0.5 **ϕ**). For these impacts, the predicted impact volumes for summer and fine sand decreased by 33% to 55% at VAbeach and by 77% to 78% at RIsland, relative to those for winter and coarse sand.

At RIsland, season and grain size each led, on average, to a 45% reduction separately and a 77% reduction when combined. In other words, for LF cetacean TTS and fish behavior, predicted impact volumes at RIsland were more than four times larger for coarse sand in winter than for fine sand in summer. The impact volume for RIsland in summer with fine sand (i.e., changing site, season, and grain size) was just 33 km^3, only 12% of the impact volume at VAbeach in winter with coarse sand (**Table 6-3**).

At VAbeach, the trend was similar, but the percentage differences were consistently smaller. The combined reduction of predicted impact volume for fine sand in summer relative to coarse sand in winter was 33% for LF cetacean TTS and 55% for fish behavior. The effect of grain size only (12% and 32%) was larger than for season only (5% and 26%).

Propagation has been shown to vary across season and grain size, and the impact volumes for each animal group also showed variability. For example, when considering sensitivity of impact volume to grain size and season, TTS impact volumes for LF cetaceans had a standard deviation of 73 km^3 at RIsland (**Table 6-3**). Multiple factors create a variety of propagation differences at a single site, so it would constitute good practice to acoustically model each site separately, in lieu of assuming another

pile-driving site accurately represents environmental influences of SSP, range-dependent bathymetry, and sediment types.

The sensitivity study showed a constant and reasonable trend for both predicted acoustic propagation modeling and predicted impact volumes. These trends matched the expected physics of the two study sites (RIsland and VAbeach) for the ranges of acoustic environmental parameters employed. This indicates the reliability of the PE/FE model algorithm used in this study and suggests it should perform just as well across similar sites that are typical for the U.S. Atlantic Coast (i.e., have similar bathymetries, sediment types, and distances to land).

8 Recommendations for Practical Application of Sensitivity Results

To help understand and apply recommendations based on the results and findings of this study, an example narrative scenario is provided. Consider 10 piles being driven for a wind farm off the coast of Atlantic City, New Jersey. The piles will be placed 2 km apart in a straight line going west to east, starting at 39.44448° N, 73.88525° W in a water depth of 30 m during March. Also assume the same specific starter field (based on a pile size and forcing function, among other parameters) that was used for this project applies to the following example scenario. The following suggestions aim to provide a clearer explanation of how the sensitivity results could be applied.

Prior to applying the impact volume and sensitivity results to new sites, the reader should be reminded of two limiting facts from this study. First, this study was focused on environmental variability and therefore a single type of pile (with a total energy L_E set to match the Gemini U8 pile) was used. For a different size pile, the total energy in the water will be different and this needs to be measured or modeled in some way. The second point is that this study was for vertical piles. A tilted pile is significantly different, leading to strong azimuthal dependence on the sound exposure levels.

First, any site that has a 50% depth difference should be modeled separately: at 5, 7, 11, 16, 23, 34, and 50 m depths. For the example Atlantic City site, the depths moving in 2-km increments west to east from the starting point above are: 30, 31, 31, 30, 32, 33, 33, 33, 33, and 35 m deep. All the sites fall well within 50% of RIsland at 35 m and can be represented by that model.

Second, if a pile-driving site occurs between Rhode Island and Virginia Beach (with similar environmental parameters), then the winter and summer models results should suffice. The example Atlantic City site is closer to RIsland, and if it were to occur in March, the RIsland winter model could represent the example piles without need for additional new model calculations. (More generally, sites north of RIsland and south of VAbeach should be modeled again for the month of proposed pile driving. This is because sites farther north may be colder for more months of the year and tend to have more winter-like propagation environments than modeled by RIsland, while sites farther south may be warmer for more months of the year and tend to follow more summer-like propagation environments than modeled by VAbeach.)

Third, when a pile-driving site occurs in an area with similar sediment types as VAbeach and RIsland, it would be well represented by this study's results. For the purposes of this example, it could be assumed that USGS data indicate a sediment grain size of 1.5 ϕ at the Atlantic City example site. This would fall within grain sizes modeled in this project and not require additional models.

Fourth, the closest distance from shore to the easternmost pile-driving site is 32 km. This means, for all 10 piles, the closest distances to shore would be 32, 34, 36, 38, 40, 42, 44, 46, 48, and 50 km. Sites at least 15 km closer to or farther from shore than the sites in this study (i.e., closest distances of 11, 41, 71, 86, etc. km to shore) would require new model runs. The fifth and sixth piles in the line at the Atlantic City example site fall on either side of the 41 km recommendation. Therefore, a new model would be needed at either the fifth or sixth pile site.

Given these four recommendations for assessing the environmental sensitivity on impact volumes at the Atlantic City example site, 9 of the 10 piles could be represented by the models presented in this project. In general, if a pile site differs by more than 50% in depth, more than 1.0 **ϕ** in grain size, seasons north of Rhode Island or south of Virginia Beach, or intervals of 15 km farther away or closer to shore, then new models should be generated during the month of proposed activity to appropriately model the acoustic propagation and understand how sound may travel through the environment.

9 Bibliography

Ainslie MA. 2005. Effect of wind-generated bubbles on fixed range acoustic attenuation in shallow water at 1–4 kHz. Journal of the Acoustical Society of America 118(6):3,513-3,523.

Ainslie MA 2010. Principles of sonar performance modeling. Springer-Verlag Heidelberg. 723 pp.

Ainslie MA. 2015. A century of sonar: Planetary oceanography, underwater noise monitoring, and the terminology of underwater sound. Acoustics Today 11:12-19.

Ainslie MA, de Jong CA, Robinson SP, and Lepper PA. 2012. What is the source level of pile-driving noise in water?, pp. 445-448. In: AN Popper and A Hawkins (eds.), The Effects of Noise on Aquatic Life. Springer, New York, NY.

Ainslie MA, Dahl P, and de Jong CA. 2014. Practical spreading laws: The snakes and ladders of shallow water acoustics, pp. 22-27. In: Proceedings of the 2nd International Conference and Exhibition on Underwater Acoustics. Rhodes, Greece.

Bachman RT. 1985. Acoustic and physical property relationships in marine sediment. Journal of the Acoustical Society of America 78(2):616-621.

Bachman RT, Schey PW, Booth NO, and Ryan FJ. 1996. Geoacoustic databases for matched-field processing: Preliminary results in shallow water off San Diego, California. Journal of the Acoustical Society of America 99(4):2,077-2,085.

Bellmann MA, Gündert S, and Remmers P. 2016. Offshore measurement campaign 3 (OMK3) for the project BORA at the offshore-wind farm *Borkum Riffgrund 1*. Technical report (2016). 147 pp.

Berenger JP. 1994. A perfectly matched layer for the absorption of electromagnetic waves. Journal of Computational Physics 114(2):185-200.

Binnerts B, de Jong CA, Ainslie MA, Nijhof M, Müller R, and Jansen E. 2016. Validation of the Aquarius models for prediction of marine pile driving sound. TNO 2016 R11338. October 2016.

Borger T, Broszeit S, Ahtiainen H, Atkins JP, Burdon D, Luisetti T, and Uyarra MC. 2016. Assessing Costs and Benefits of Measures to Achieve Good Environmental Status in European Regional Seas: Challenges, Opportunities, and Lessons Learnt. Frontiers in Marine Science 3.

Brekhovskikh L. 1980. Waves in layered media (Vol. 16). Academic, New York.

Burdic WS. 1991. Underwater Acoustic System Analysis. Prentice Hall, Englewood Cliffs, NJ. 222 pp.

California Department of Transportation (Caltrans). 2015. Technical Guidance for Assessment and Mitigation of the Hydroacoustic Effects of Pile Driving on Fish. Report No. CTHWANP-RT-15-306.01.01. November 2015. Accessed 16 October 2019 at: https://dot.ca.gov/-/media/dot-media/programs/environmental-analysis/documents/bio-tech-guidance-hydroacoustic-effects-110215-a11y.pdf.

Casper BM, Popper AN, Matthews F, Carlson TJ, and Halvorsen MB. 2012. Recovery of barotrauma injuries in Chinook salmon, *Oncorhynchus tshawytscha* from exposure to pile driving sound. PlosONE 7(6):e39593.

Casper BM, Halvorsen MB, Matthews F, Carlson TJ, and Popper AN. 2013. Recovery of barotrauma injuries resulting from exposure to pile driving sound in two sizes of hybrid striped bass. PlosONE 8(9):e73844.

Casper BM, Halvorsen MB, Carlson TJ, and Popper AN. 2017. Onset of barotrauma injuries related to number of pile driving strike exposures in hybrid striped bass. Journal of the Acoustical Society of America 141(6):4,380-4,387.

Collins MD. 1993. A split-step Padé solution for the parabolic equation method. Journal of the Acoustical Society of America 93(4):1,736-1,742.

Collins MD. 1996. User's Guide for RAM Version 1.0 and 1.0p. Naval Research Laboratory, Washington, D.C. 14 pp.

COMPILE. 2014. COMPILE workshop problem description, Case 1: Generic pile (v07, 14 April 2014).

Dahl, PH, Reinhall PG, and Farrell DM. 2012. Transmission loss and range, depth scales associated with impact pile driving. In: 11th European Conference on Underwater Acoustics.

Dahl PH, de Jong CA, and Popper AN. 2015. The underwater sound field from impact pile driving and its potential effects on marine life. Acoustics Today 2(11):18-25.

Davidsen JG, Dong H, Linné M, Andersson MH, Piper A, Prystay TS, and Sjursen AD. 2019. Effects of sound exposure from a seismic airgun on heart rate, acceleration and depth use in free-swimming Atlantic cod and saithe. Conservation Physiology 7(1):coz020.

de Jong K, Amorim MCP, Fonseca PJ, Fox CJ, and Heubel KU. 2018. Noise can affect acoustic communication and subsequent spawning success in fish. Environmental Pollution 237:814-823.

Farcas A, Thompson PM, and Merchant ND. 2016. Underwater noise modelling for environmental impact assessment. Environmental Impact Assessment Review 57:114-122.

Federal Register. 2005. NOAA. ID 060804F. Endangered Fish and Wildlife, Notice of Intent to Prepare an EIS 70(7):1871-1875.

Fisheries Hydroacoustic Working Group (FHWG). 2008. Agreement in Principle for Interim Criteria for Injury to Fish from Pile Driving Activities, June 12, 2008, Fisheries Hydroacoustics Working Group, Vancouver, Canada. Accessed 16 October 2019 at: https://dot.ca.gov/-/media/dot-media/programs/environmental-analysis/documents/bio-fhwg-criteria-agree-a11y.pdf.

Frankignoul C, de Coetlogon G, Joyce TM, and Dong S. 2000. Gulf Stream variability and ocean-atmosphere interactions. Journal of Physical Oceanography 31:3,516-3,529.

Greater Atlantic Regional Fisheries Office (GARFO). 2016. Acoustic Tool: Analyzing the effects of pile driving on ESA-listed species in the Greater Atlantic Region, Excel spreadsheet. U.S. Department of Commerce, National Oceanic and Atmospheric Administration, National Marine Fisheries Services. Accessed 1 May 2018 at: http://www.greateratlantic.fisheries.noaa.gov/protected/section7/guidance/consultation/index.html.

Halvorsen MB, Casper BM, Woodley CM, Carlson TJ, and Popper AN. 2011. Predicting and mitigating hydroacoustic impacts on fish from pile installations. NCHRP Research Results Digest 363, Project 25-28, National Cooperative Highway Research Program. Transportation Research Board, National Academy of Sciences, Washington, D.C. 26 pp. Accessed 16 October 2019 at: http://onlinepubs.trb.org/onlinepubs/nchrp/nchrp_rrd_363.pdf.

Halvorsen MB, Casper BM, Woodley CM, Carlson TJ, and Popper AN. 2012a. Threshold for onset of injury in Chinook salmon from exposure to impulsive pile driving sounds. PlosONE 7(6):e38968.

Halvorsen MB, Casper BM, Matthews F, Carlson TJ, and Popper AN. 2012b. Effects of exposure to pile-driving sounds on the lake sturgeon, Nile tilapia and hogchoker. Proceedings of the Royal Society B: Biological Sciences 279:4,705-4,714.

Hamilton EL. 1980. Geoacoustic modeling of the sea floor. Journal of the Acoustical Society of America 68(5):1,313-1,340.

Hamilton EL, and Bachman RT. 1982. Sound velocity and related properties of marine sediments. Journal of the Acoustical Society of America 72(6):1,891-1,904.

Hawkins AD and Popper AN. 2016. A sound approach to assessing the impact of underwater noise on marine fishes and invertebrates. ICES Journal of Marine Science: Journal du Conseil, fsw205.

Hawkins AD, Pembroke AE, and Popper AN. 2015. Information gaps in understanding the effects of noise on fishes and invertebrates. Reviews in Fish Biology and Fisheries 25(1):39-64.

Higgs DM and Humphrey SR. 2019. Passive acoustic monitoring shows no effect of anthropogenic noise on acoustic communication in the invasive round goby (*Neogobius melanostomus*). Freshwater Biology.

IHC Merwede. 2015. IHC Hydrohammer Pile driving equipment, IHC Merwede. Accessed 16 October 2019 at: http://greenglobalgroup3g.com/images/sampledata/parks/landscape/IHCHydrohammerOffshore.pdf.

Institut für technische und angewandte Physik (ITAP). 2014. Offshore measurement campaign 1 (OMK1) for the project BORA at the offshore-wind farm *Bard Offshore 1*, Version 7, Project Number: 1924-12-bm.

Institut für technische und angewandte Physik (ITAP). 2015a. Offshore Wind Farm *Eneco Luchterduinen*, Ecological monitoring of underwater noise during piling at Offshore Wind Farm *Eneco Luchterduinen*, Version 5, Project Number: 2322-14-bel.

Institut für technische und angewandte Physik (ITAP). 2015b. Offshore Wind Farm *Gemini*, Ecological monitoring of underwater noise during piling at Offshore Wind Farm *Gemini*, Version 1, Project Number: 2571-15.

Institut für technische und angewandte Physik (ITAP). 2015c. Offshore measurement campaign 3 (OMK3) for the project BORA at the offshore-offshore-wind farm *Borkum Riffgrund 01*, Version 2, Project Number: 2271-14-bel.

Institut für technische und angewandte Physik (ITAP). 2015d. Offshore measurement campaign 2 (OMK2) for the project BORA at the offshore-offshore-wind farm *Global Tech I*, Version 4, Project Number: 2162-13-bel.

International Organization for Standardization (ISO). 2017. ISO 18405 Underwater Acoustics – Terminology. International Organization for Standardization, Geneva, Switzerland. 62 pp.

Jensen F, Kuperman W, Porter M, and Schmidt H. 1994. Computational Ocean Acoustics. New York: Springer.

Lippert S, Nijhof M, Lippert T, Wilkes D, Gavrilov A, Heitmann K, Ruhnau M, von Estorff O, Schäfke A, Schäfer I, Ehrlich J, MacGillivray A, Park Y, Seong W, Ainslie MA, de Jong C, Wood M, Wang L, and Theobald P. 2014. COMPILE I results for SEL and Lpk. Case_1_Result_collection_SEL_SPLpeak.xlsx. Excel spreadsheet.

Lippert S, Nijhof M, Lippert T, Wilkes D, Gavrilov A, Heitmann K, Ruhnau M, von Estorff O, Schäfke A, Schäfer I, Ehrlich J, MacGillivray A, Park Y, Seong W, Ainslie MA, de Jong C, Wood M, Wang L, and Theobald P. 2016. COMPILE-A Generic Benchmark Case for Predictions of Marine Pile-Driving Noise. IEEE Journal of Oceanic Engineering 41(4):1,061-1,071.

Lippert T, Galindo-Romero M, Gavrilov AN, and von Estorff O. 2015. Empirical estimation of peak pressure level from sound exposure level. Part II: Offshore impact pile driving noise. Journal of the Acoustical Society of America 138(3):EL287-EL292.

Lippert T, Ainslie MA, and von Estorff O. 2018. Pile driving acoustics made simple: Damped cylindrical spreading model. Journal of the Acoustical Society of America 143(1):310-317.

Lucke K, Scowcroft G, Winter HV, Knowlton C, Lam FPA, Hawkins A, and Popper AN. 2016. International harmonization of approaches to define underwater noise exposure criteria and needs of the international regulatory community. In: Proceedings of Meetings on Acoustics 4ENAL. Acoustical Society of America 27(1):070010..

Lurton X. 2002. An Introduction to Underwater Acoustics: Principles and Applications. Springer Science and Business Media.

Martin SB, Morris C, Bröker K, and O'Neill C. 2019. Sound exposure level as a metric for analyzing and managing underwater soundscapes. Journal of the Acoustical Society of America 146(1):135-149.

National Marine Fisheries Services (NMFS). 2012a. Guidance Document: Sound Propagation Modeling to Characterize Pile Driving Sounds Relevant to Marine Mammals, NOAA memo, January 31, 2012.

National Marine Fisheries Services (NMFS). 2012b. Pile Driving Calculations, Excel spreadsheet. Accessed 25 July 2016 at: http://www.dot.ca.gov/hq/env/bio/fisheries_bioacoustics.htm. Spreadsheet accessed at: http://www.dot.ca.gov/hq/env/bio/files/NMFS%20Pile%20Driving%20Calculations.xls.

National Marine Fisheries Service (NMFS). 2018a. 2018 Revisions to: Technical Guidance for Assessing the Effects of Anthropogenic Sound on Marine Mammal Hearing (Version 2.0): Underwater Thresholds for Onset of Permanent and Temporary Threshold Shifts. U.S. Department of Commerce, National Oceanic and Atmospheric Administration. NOAA Technical Memorandum NMFS-OPR-59. 167 pp. Accessed 16 October 2019 at: https://www.fisheries.noaa.gov/resource/document/technical-guidance-assessing-effects-anthropogenic-sound-marine-mammal.

National Marine Fisheries Service (NMFS). 2018b. User spreadsheet tool (optional) excel, Version 2.0 (2018), companion to: NMFS 2018 Revisions to: Technical Guidance for Assessing the Effects of Anthropogenic Sound on Marine Mammal Hearing (Version 2.0): Underwater Thresholds for Onset of Permanent and Temporary Threshold Shifts. U.S. Department of Commerce, National Oceanic and Atmospheric Administration. NOAA excel sheet. Accessed 16 October 2019 at: https://www.fisheries.noaa.gov/national/marine-mammal-protection/marine-mammal-acoustic-technical-guidance.

Popper AN, Smith ME, Cott PA, Hanna BW, MacGillivray AO, Austin ME, and Mann DA. 2005. Effects of exposure to seismic airgun use on hearing of three fish species. Journal of the Acoustical Society of America 117(6):3958-3971.

Popper AN, Hawkins AD, Fay RR, Mann DA, Bartol S, Carlson TJ, Coombs S, Ellison WT, Gentry RL, Halvorsen MB, Løkkeborg S, Rogers PH, Southall BL, Zeddies DG, and Tavolga WN. 2014. Sound Exposure Guidelines for Fishes and Sea Turtles. Springer Briefs in Oceanography. ANSI-Accredited Standards Committee S3/SC1.4 TR-2014.

Porter MB. 2011. The BELLHOP Manual and User's Guide, Preliminary Draft. Accessed 16 October 2019 at: http://oalib.hlsresearch.com.

Reinhall PG and Dahl PH. 2011. Underwater Mach wave radiation from impact pile driving: theory and observation. Journal Acoustical Society of America 130(3):1,209-1,216.

Roberts L, Cheesman S, Elliott M, and Breithaupt T. 2016a. Sensitivity of *Pagurus bernhardu*s (L.) to substrate-borne vibration and anthropogenic noise. Journal of Experimental Marine Biology and Ecology 474:185-194.

Roberts L, Pérez-Domínguez R, and Elliott M. 2016b. Use of baited remote underwater video (BRUV) and motion analysis for studying the impacts of underwater noise upon free ranging fish and implications for marine energy management. Marine Pollution Bulletin 112(1):75-85.

Sabet SS, Neo YY, and Slabbekoorn H. 2015. The effect of temporal variation in sound exposure on swimming and foraging behaviour of captive zebrafish. Animal Behaviour 107:49-60.

Stadler JH and Woodbury DP. 2009. Assessing the effects to fishes from pile driving: Application of new hydroacoustic criteria, inter-noise. 23-26 August 2009. Ottawa, Canada.

Taormina B, Bald J, Want A, Thouzeau G, Lejart M, Desroy N, and Carlier A. 2018. A review of potential impacts of submarine power cables on the marine environment: Knowledge gaps, recommendations and future directions. Renewable and Sustainable Energy Reviews 96:380-391.

Tindle CT. 1983. Ray calculations with beam displacement. Journal of the Acoustical Society of America 73(5):1,581-1,586.

Weinberg H. 1975. Application of ray theory to acoustic propagation in horizontally stratified oceans. Journal of the Acoustical Society of America 58(1):97-109.

Weston DE. 1976. Propagation in water with uniform sound velocity but variable-depth lossy bottom. Journal of Sound and Vibration 47(4):473-483.

Weston DE and Ching PA. 1989. Wind effects in shallow-water acoustic transmission. Journal of the Acoustical Society of America 86(4):1,530-1,545.

Westwood EK and Tindle CT. 1987. Shallow water time-series simulation using ray theory. Journal of the Acoustical Society of America 81(6):1,752-1,761.

Williams SJ, Arsenault MA, Buczkowski BJ, Reid JA, Flocks J, Kulp MA, Penland S, and Jenkins CJ. 2007. Surficial sediment character of the Louisiana offshore continental shelf region: a GIS compilation. Open-File Report 2006-1195. United States Geological Survey, Reston, VA.

Zampolli M, Malm N, and Tesei A. 2008. Improved Perfectly Matched Layers for Acoustic Radiation and Scattering Problems. In: Proceedings of the COMSOL Conference 2008. Hannover.

Zampolli M, Nijhof MJ, de Jong CA, Ainslie MA, Jansen EH, and Quesson BA. 2013. Validation of finite element computations for the quantitative prediction of underwater noise from impact pile driving. Journal of the Acoustical Society of America 133(1):72-81.

Zhou JX, Zhang XZ, and Knobles DP. 2009. Low-frequency geoacoustic model for the effective properties of sandy seabottoms. Journal of the Acoustical Society of America 125(5):2,847-2,866.

Appendix A: Definitions

Zero-to-peak and peak-to-peak sound pressure level

The zero-to-peak sound pressure level ($L_{p,\mathrm{pk}}$) is

$$L_{p,\mathrm{pk}} \equiv 10 \log_{10} \frac{p_{\mathrm{pk}}^2}{p_0^2} \text{ dB} \qquad \textit{Equation A.1}$$

The peak-to-peak sound pressure level is not defined by ISO (2017). Lucke et al. (2009) defines this quantity as

$$L_{p,\mathrm{pk-pk}} \equiv 10 \log_{10} \frac{p_{\mathrm{pk-pk}}^2}{p_0^2} \text{ dB} \qquad \textit{Equation A.2}$$

This definition is used by Lippert et al. (2015).

Effective signal duration:

The effective signal duration is a robust measure of signal duration used in signal processing (Burdic, 1991). It is defined (**Figure A-1**) in terms of the complex envelope (**Figure A-2**) of the analytic signal (**Figure A-3**).

3.5.1.3
effective signal duration

τ_{eff}

square of the integral with respect to time of $|\mu(t)|^2$ divided by the integral with respect to time of $|\mu(t)|^4$, where $\mu(t)$ is the **complex envelope** (3.5.1.2) of the **sound pressure** (3.1.2.1)

Note 1 to entry: In formula form, $\tau_{\mathrm{eff}} = \dfrac{\left[\int_{-\infty}^{+\infty} |\mu(t)|^2 \, \mathrm{d}t\right]^2}{\int_{-\infty}^{+\infty} |\mu(t)|^4 \, \mathrm{d}t}$.

Note 2 to entry: Effective signal duration is expressed in seconds (s).

Note 3 to entry: Effective signal duration is a property of a transient signal.

Note 4 to entry: The magnitude of the complex envelope is equal to the magnitude of the **analytic signal** (3.5.1.1).
[SOURCE: Reference [24]]

Figure A-1. Definition of effective signal duration in terms of complex envelope (From: ISO 18405:2017).

3.5.1.2
complex envelope
μ
product of the **analytic signal** (3.5.1.1), $q(t)$, and the exponential function of the product of the constant $-2\pi i$, a constant frequency, f_0, and the time, t

Note 1 to entry: Complex envelope is a function of time, which may be indicated by means of an argument t, as in $\mu(t)$, where μ is complex envelope and t is time.

Note 2 to entry: In formula form, $\mu(t) = q(t)\exp(-2\pi i f_0 t)$.

Note 3 to entry: If $q(t)$ is the analytic signal of the **sound pressure** (3.1.2.1), the complex envelope is expressed in pascals (Pa).

Note 4 to entry: For a narrowband signal, the quantity f_0 is typically the centre frequency of that signal.

Figure A-2. Definition of complex envelope in terms of analytic signal (From: ISO 18405:2017).

3.5.1.1
analytic signal
q
complex quantity whose real part is equal to the **signal** (3.1.5.8), $p(t)$, and whose imaginary part is equal to the Hilbert transform of $p(t)$

Note 1 to entry: Analytic signal is a function of time, which may be indicated by means of an argument t, as in $q(t)$, where q is analytic signal and t is time.

Note 2 to entry: In formula form, the analytic signal, $q(t)$, of a signal, $p(t)$, is given by $q(t) = p(t) + i\,h(t)$, where $h(t)$ is the Hilbert transform of $p(t)$.

Note 3 to entry: If the signal, $p(t)$, is **sound pressure** (3.1.2.1), the analytic signal is expressed in pascals (Pa).

Figure A-3. Definition of analytic signal in terms of sound pressure (From: ISO 18405:2017).

References

Burdic, WS. 1991. Underwater acoustic system analysis. Prentice Hall, Englewood Cliffs, NJ.

ISO. 2017. ISO 18405:2017 Underwater Acoustics – Terminology. Geneva, Switzerland.

Lippert, T, M Galindo-Romero, AN Gavrilov, and O von Estorff. 2015. Empirical estimation of peak pressure level from sound exposure level. Part II: Offshore impact pile driving noise. The Journal of the Acoustical Society of America 138(3):EL287-EL292.

Lucke, K, Siebert, U, Lepper, PA, Blanchet, MA. 2009. Temporary shift in masked hearing thresholds in a harbor porpoise (*Phocoena phocoena*) after exposure to seismic airgun stimuli. Journal of the Acoustical Society of America. 125(6):4060-4070. DOI: 10.1121/1.3117443.

Appendix B: Extracting Aggregated Quantities for the Hammer Strikes

For pressure trace segments (between t_{start} and t_{end}), the following quantities are determined:

- integration time $t_{\text{end}} - t_{\text{start}}$
- t_5, such that $\int_{t_{\text{start}}}^{t_5} p^2 \, \mathrm{d}t = 0.05 \int_{t_{\text{start}}}^{t_{\text{end}}} p^2 \, \mathrm{d}t$
- t_{95}, such that $\int_{t_{\text{start}}}^{t_{95}} p^2 \, \mathrm{d}t = 0.95 \int_{t_{\text{start}}}^{t_{\text{end}}} p^2 \, \mathrm{d}t$
- 90% sound exposure: $E_{90} = \int_{t_5}^{t_{95}} p^2 \, \mathrm{d}t$
- rms sound pressure: $p_{\text{rms}} = \sqrt{E_{90}/(t_{95} - t_5)}$
- sound exposure level (L_E): $L_E = 10 \log_{10}(E_{90}/(0.9\, p_0^2\, 1s)$ dB
- zero-to-peak sound pressure level: $L_{p,\text{pk}} = 10 \log_{10}(\max(p^2)/p_0^2)$ dB
- rms sound pressure level: $L_{\text{rms,90\%}} = 10 \log_{10}(p_{\text{rms}}^2/\, p_0^2)$ dB

Finally, the kurtosis β was calculated, according to ISO 18405:2017, §3.1.5.5:

$$\beta = \mu_4/\mu_2^2, \text{ where } \mu_n = \frac{1}{t_{\text{end}} - t_{\text{start}}} \int_{t_{\text{start}}}^{t_{\text{end}}} (p(t) - \bar{p})^n \, \mathrm{d}t, \text{ so}$$

$$\beta = \frac{\frac{1}{t_{\text{end}} - t_{\text{start}}} \int_{t_{\text{start}}}^{t_{\text{end}}} (p(t) - \bar{p})^4 \, \mathrm{d}t}{\left(\frac{1}{t_{\text{end}} - t_{\text{start}}} \int_{t_{\text{start}}}^{t_{\text{end}}} (p(t) - \bar{p})^2 \, \mathrm{d}t\right)^2} = \frac{\overline{(p(t) - \bar{p})^4}}{\left(\overline{(p(t) - \bar{p})^2}\right)^2} \qquad \textit{Equation B-1}$$

References

ISO. 2017. ISO 18405:2017 Underwater Acoustics – Terminology. Geneva, Switzerland.

Appendix C: Borkum Riffgrund 1 Measurements

The values shown in **Table C-1** were used to obtain the circles in **Figure 5-18**. Specifically, power averages were calculated over the two hydrophone positions (2 m and 10 m above the seafloor) of the median L_E (SEL50 [dB] columns) and of $L_{p,\mathrm{pk}}$ (LPeak [dB] columns).

Table C-1. Borkum Riffgrund 1 measurements from ITAP (2015; Section 12.1.2, translated into English).

Measurement position	Distance (m)	Hydrophone 2 m height above ground				Hydrophone 10 m height above ground				
		SEL90 (dB)	SEL50 (dB)	SEL5 (dB)	LPeak (dB)	SEL90 (dB)	SEL50 (dB)	SEL5 (dB)	LPeak (dB)	Pile strikes
MPS1	726	172	174	174	199	173	173	175	199	1859
MPS2	1,509	169	171	171	192	168	170	170	192	1853
MPS3	783	172	173	174	198	172	174	174	197	1503
MPS4	288	180	182	182	209	179	180	180	208	1859
MPS5	234	178	180	180	207	180	182	182	209	1859
MPS6	499	176	178	178	201	174	176	177	200	1860
MPS7	738	173	174	175	198	173	174	175	197	1859
MPS8	1491	170	171	172	193	169	171	171	192	1856
MPS9	1992	167	169	169	190	172	174	174	195	1859
MPS10	2487	165	167	167	186	165	166	166	186	1859
MPS11	2985	164	165	166	185	164	165	166	184	1859
MPS12	4057	160	162	162	181	161	162	163	182	1859
MPS13	4991	158	160	160	177	no measurable data				
MPS14	66	189	190	190	216	187	189	189	215	1859
MPS15	93	190	191	191	217	186	187	188	215	1859
MPS16	70	189	190	191	217	187	188	189	217	1858
MPS17	30	no measurable data				no measurable data				
MPS18	28	193	193	195	221	189	190	191	218	576

dB = decibel; LPeak = $L_{p,pk}$ or peak sound pressure level; SEL = sound exposure level; SEL90 = 90% exceedance level (10th percentile sound exposure level); SEL50 = 50th percentile sound exposure level (median); SEL5 = 5% exceedance level (95th percentile sound exposure level).

References

Institut für technische und angewandte Physik (ITAP). 2015. Offshore measurement campaign 3 (OMK3) for the project BORA at the offshore-offshore-wind farm *Borkum Riffgrund 01*, Version 2, Project Number: 2271-14-bel.

Department of the Interior (DOI)

The Department of the Interior protects and manages the Nation's natural resources and cultural heritage; provides scientific and other information about those resources; and honors the Nation's trust responsibilities or special commitments to American Indians, Alaska Natives, and affiliated island communities.

Bureau of Ocean Energy Management (BOEM)

The mission of the Bureau of Ocean Energy Management is to manage development of U.S. Outer Continental Shelf energy and mineral resources in an environmentally and economically responsible way.

BOEM Environmental Studies Program

The mission of the Environmental Studies Program is to provide the information needed to predict, assess, and manage impacts from offshore energy and marine mineral exploration, development, and production activities on human, marine, and coastal environments. The proposal, selection, research, review, collaboration, production, and dissemination of each of BOEM's Environmental Studies follows the DOI Code of Scientific and Scholarly Conduct, in support of a culture of scientific and professional integrity, as set out in the DOI Departmental Manual (305 DM 3).